Simple device to measure the macular pigment optical density in vivo

National University of Ireland, Galway

Ollscoil na hÉireann, Gaillimh

Andrew O'Brien

Supervised by Professor Chris Dainty

An Grúpa Optaic Feidimí
Ollscoil na hÉireann, Gaillimh

A thesis submitted in partial fulfillment of the requirements for the degree of Doctor of Philosophy and the Diploma of the National University of Ireland, Galway

June 2008

Contents

List of Figures

List of Tables

Acknowledgements

This thesis has benefited from the insights and direction of several people mentioned here and probably many others I may have unintentionally overlooked for which I apologise.

Firstly I would like to thank my supervisor Prof Chris Dainty for his patience, trust and guidance throughout the project. His inherent respect and time for all students is an invaluable asset in a teacher and is one of the more worthy lessons I have learned and benefitted from over the past 4 years. I am also indebted to members of the Applied Optics group for their help and willingness to assist, both in a scientific nature and more entertaining matters. In particular thank you Sasha and David Lara for your priceless help and advice. Thank you Emer for all your help in finding missing forms, which seem to disappear in the ether of University bureaucracy and Conor for endless and welcome discussion on rugby and various you-tube excursions. Thank you to the Physics workshop and to Conor McBrierty from the electronics workshop for your help not only during the PhD but during my time as an undergraduate.

I would like to acknowledge my father Eugene, who died during the project and who's bravery and unfaltering humor truly belied his illness and was a constant inspiration in terms of confronting and over coming any obstacle. I would like to thank my sister Thelma and her future husband Johnny for keeping my feet on the ground. Thank you to my great friends Gus, Mikey, Eoin, Elaine, Bernie and Eimhin for their laughter and ability to gain unrivaled pleasure from any embarrassment that may befall me, your loyalty won't be forgotten. Prea thank you for everything, I believe your name should have a place on the front of this thesis, as you have being there for every broken beam splitter, scratched lens, incompatible camera driver, unknown reflections, blown LED, bugs in the software and the subsequent fall out from these and many other frustrations. Your presence, love and ability to help me see beyond the problem has truly being invaluable and your sacrifice will never be forgotten.

Finally this thesis and the work it represents is dedicated to my mother Mary and step-father John, who's constant support has made this possible and without whom I would not be thinking about Physics nevermind writing my PhD thesis.

Go a raibh míle maith agaibh.
Andrew O'Brien
Room AO107b, Galway, June 08.

Abstract

Growing interest in the macular pigment (MP) may be attributed to its possible correlation to the debilitating ocular disease of Age Related Macular Degeneration (AMD). Within the western world, the possibility of preventing the onset of this disease by modification of MP levels, is an attractive strategy for retaining adequate vision among the aging population.

Various clinical studies attempt to establish the correlation between MP levels and AMD. Further investigations attempt to demonstrate the possibility of modification of MP levels by lifestyle adjustment, examine various risk factors pertaining to low levels of MP and establish conclusively the exact role of this yellow pigment. The common problem of these studies is the method employed for the measurement of MP levels *in vivo*. The inherent deficiencies with the devices employed in determining MP levels, may result in ambiguity over many of the conclusions reached.

In this thesis the design and construction of a simple imaging device to measure MP optical density (MPOD) is presented, and its attempts to confront the frailties of previous devices will be discussed. The combination of three different techniques in one dedicated device, presents the opportunity to choose which technique to utilise, depending on the subject under examination. This strategy also allows for internal calibration and comparison of results. We suggest that a successful device should produce consistent, accurate and rapid results, while retaining the distinction of ease of use, portability, inexpensive to produce and comfortable for the subject. Its versatility should allow both for a clinical screening application, as well as establishing the physiological role of the MP in a laboratory based environment.

This thesis will discuss the macular pigment, its inferred role and potential importance to sustained vision in old age. The design and assembly of a simple device to measure the pigment will be presented, and will attempt to present to the reader the ideas and reasons for its construction. Results will be presented in both the testing of the device and the measurement of a cross section of subjects. Future work, and possible amendments to the current system will also be discussed, with the objective of producing a more robust, more consistent easy to use system that can produce more rapidly an accurate examination of the the macular pigment optical density.

Chapter 1

Human vision and the macular pigment

1.1 Introduction

The physiology of the human eye has both intrigued and captivated humankind for at least a millennium, from Aristotle's somewhat flawed perspective of the visual process in the 4th century BC, to Decartes eventual explanation of image formation on the retina in the 17th century. Thomas Young's novel experiments on accommodation in the 19th century [1], to Helmholtz and Gullstrand [2], and their investigation of the influence of the imaging optics on wavefront behaviour in the eye, has both enhanced our knowledge of the mechanics of the human visual system and intensified our curiosity and subsequent requirement of more progressive investigation methods. More recent developments in advanced optical techniques such as optical coherence tomography (OCT), scanning laser ophthalmoscope (SLO) and continuing development of adaptive optics, further builds on previous research and demonstrates our indefatigable curiosity in the biological and physical behaviour of the eye. Continued research into vision, perceptual psychology and visual neuroscience has provided us with a far improved understanding of the visual process and a hunger for a complete knowledge of its performance. The more that is revealed, the more that we appreciate the human eye as a complex anatomical device, that remarkably demonstrates the architectural wonders of the human body. This thesis examines just one aspect of the complex physiology of the eye, namely the macular pigment. The macular pigment is located exclusively in the macular region of the retina (see figure 1.6(a)), and its presence and role in this very important area of the retina remains unresolved.

Investigation of the pigment reveals an extensive history of study, dating back to Buzzi [3], who in 1782 documented a yellow colour in the centre of the retina. Home [4] in 1798, published the first literature review on the macular yellow spot, while independently Sommering [5] in 1799, described the spot as pale in older people compared to that in younger subjects. Contention continued regarding the significance of the spot, as Home concluded that the spot is the outcome of the postmortem process and has no significance for the living eye. As a result of his dissections of various animal retinas, Home also noticed that apart from primates, that the spot was absent from other specimens. Essentially this yellow spot was exclusive to primate specimens, humans and simians. Interest in the

spot manifested again in 1851, when Helmholtz [2] introduced his revolutionary ophthalmoscope, which allowed for *in vivo* observation of the human retina. The yellow macular spot was now visible in living subjects, and while Maxwell [6] noted absorption of short wavelength light by the spot and Schultze [7] hypothesised that the spot functioned as some form of filter to reduce chromatic effects, it was not until 1945 that George Wald [8] provided a more accomplished account of the pigment. Wald established that the pigment absorbed light between the wavelengths 430nm and 490nm, with maximum absorption taking place at 465nm. Importantly he demonstrated that the absorption spectrum of the pigment was characteristic of that of the xanthophyll lutein, illustrated in figure 1.1. Wald also noted that the spectrum of the pigment, extracted from human retinas, agreed quite well with the visual estimate of the macular pigment derived from the differences in the log sensitivity of peripheral and foveal cones.
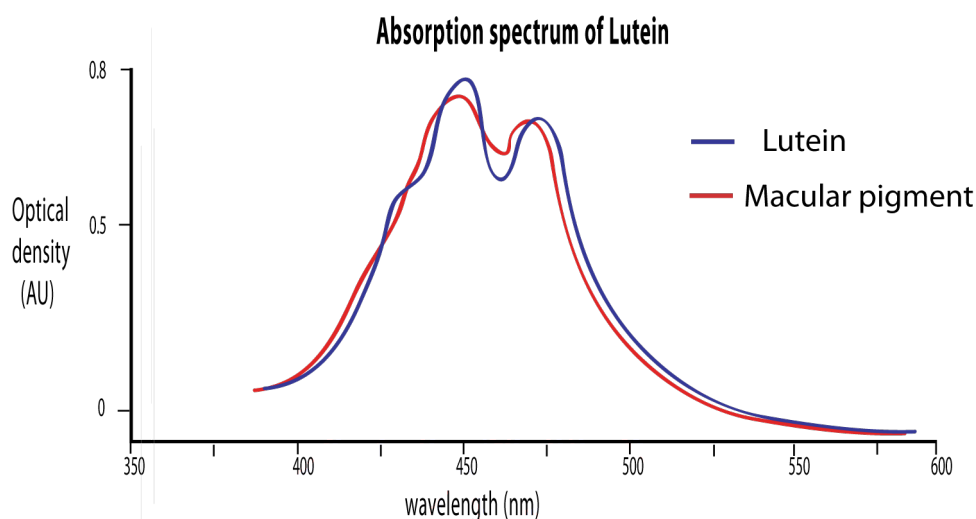
Figure 1.1: Absorption spectrum of lutein as measured by Wald [8] compared to macular pigment absorption spectrum as measured *ex vivo* by Brown (taken from data in [9])

In 1988, using high performance liquid chromatographic (HPLC), Bone and Landrum identified that there was actually two xanthophylls present in the macula, lutein and zeaxanthin [10]. Chapter two will examine the characteristics of the macular pigment in a more complete manner.

The remainder of **Chapter one** investigates the imaging optics of the eye and outlines the structure of the retina. The intention is to present the difficulties of imaging the retina, and the challenge and considerations of dealing with real subjects, due both to unwanted corneal reflections, imperfections of the eye and various abilities of potential subjects.

Chapter two examines the pigment and introduces the characteristics, location and possible role. The debilitating disease of age related macular degeneration (AMD) will be discussed, while the growing interest in the macular pigment will be explained due to it's inferred correlation this age related disease.

Chapter three presents the numerous methods and devices currently employed to measure the macula pigment optical density. The advantages and disadvantages of the various devices employing the various techniques will be highlighted, while the strategy for a complete device will be presented.

Chapter four introduces the system hardware and explains the function and need for the various components. An explanation and full investigation of all the optical components will be presented. The independent control of the system via an 8051 μ-controller will be justified, and a full investigation of the relevant features of the 8051 will be examined.

Chapter five explains the implementation of the software written to measure the macula pigment optical density. The full assembly language code is included in the appendix and a sufficient explanation of its design is highlighted in this chapter. Due to size constraints of the thesis, the full Labview code is not included, however some of the key features are explained in this chapter. The strategy of an independent control system will be presented and rationalised, and the software for the control and analysis of acquired data will be presented.

Chapter six presents preliminary results from the interface software, and results from the data analysis of acquired images. Results of testing the system using specifically designed targets, as well as results from real eyes will be presented. A small study comparing the results of this device with the results of an established device for a small sample of subjects, is also be presented.

Chapter seven includes an overall conclusion as well as suggested amendments and improvements for the device. This chapter aims at refining the bench prototype in order to produce an attractive commercially viable product.

1.2 Human optical system

In order to achieve an adequate understanding of acquiring information from the retina objectively, an overview of the refractive elements anterior to the retina will be examined. An investigation of these elements, will highlight the limitations and challenges encountered in order to obtain satisfactory retinal information. A simple schematic of the human eye is shown in figure 1.2 exhibiting, the major contributors and limiting components, to attaining adequate working images of the retina.

1.2.1 Refractive elements

This section will examine the main contributors in forming an image on the retina. Specifically the cornea and the lens. The problem of on-axis reflections from these two elements will also be briefly outlined.
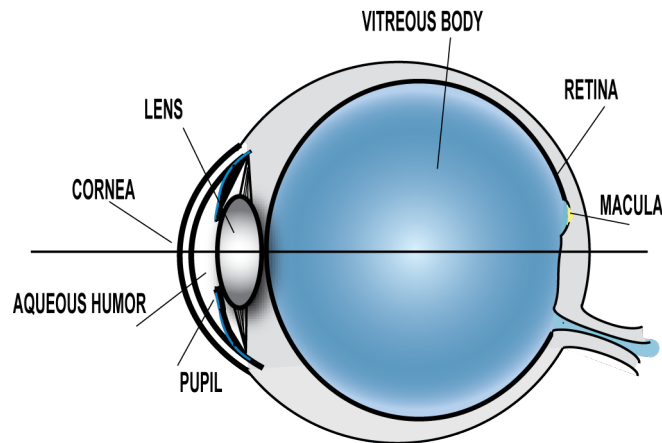
Figure 1.2: Simple schematic of human eye illustrating the primary refractive elements anterior to the retina.

Cornea

When light is incident upon the eye the first and strongest refractive element it encounters is the cornea[1]. The cornea consists of an outer layer of epithelial cells, which are continuously renewed. The interaction between these surface cells and that of the tear film produce a smooth optical surface which refracts the incident light [11]. It is mechanically strong and transparent. Approximately 200 collagen fibre layers crisscross the cornea in different directions and this is where its strength originates from. The arrangement of the fibers not only provides strength and transparency to the cornea but the gaps between the major layers act as probable pathways for white blood cell migration, if any injury or infection were to occur [11].

Lens

The lens is a specialised epithelial tissue that is responsible, together with the cornea, for producing a focussed image on the retina. Essentially the function of the lens is to fine tune the overall refractive power of the eye. This tuning is possible due to the adjustable nature of the lens. The focusing power resides in the unusually high protein content of the lens. The protein concentration may reach as much as 50% in some parts of the lens [11]. This high concentration increases the refractive index above that of water and so explains the lens ability to refract light even though it is surrounded by the *aqueous humor*[2]. For a young subject the change in optical power can be up to 15 diopters [12]. This amplitude of accommodation declines dramatically with age.

On-axis reflections

The primary method of imaging the retina is to sufficiently illuminate the retina, and image any reflected light. This requires a method of getting light into the retina. While it is possible to illuminate the retina in the IR through the sclera [13], for most purposes

---

[1]Power $\approx$ 45 diopters.

[2]refractive index $\approx$ 1.33

illumination is through the pupil. When light encounters an object, the light will be either be scattered, transmitted, absorbed or reflected, or combination of all four. As illustrated in figure 1.3, on axis illumination through the pupil will produce on axis reflection from the cornea and lens (light is also transmitted, scattered and absorbed). These reflections are detrimental when imaging the retina, as the light reflected from the fundus is orders of magnitude less than that reflected from the optics.
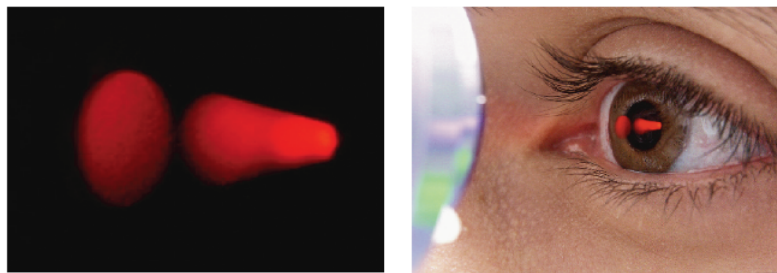
Figure 1.3: Illustration of scatter from the air-cornea interface and aquaeous-lens interface indicating the presence of strong reflection due to on-axis illumination. Image produced by Alfredo Dubra [14].

Various methods exist to combat this reflection, such as off-axis illumination, imaging through a hole drilled in a mirror[3], and creating a corneal mask to block these reflections. The method utilised will depend on the required retinal information, and/or design restrictions of the device.

Other factors restrict the amount of information available from *in vivo* imaging of the eye. These include various aberrations induced by the cornea and lens, aberrations in the imaging device (see chapter 4), any ocular diseases[4], and fundamentally the diffraction limit dictated by the pupil. Further investigation of these factors are beyond the overall interest of this thesis, and in regards to the resolution requirements for this device, do not impose a detrimental role.

1.3   The retina

When light passes through the cornea, the aqueous humor, the lens and the vitreous humor (see figure 1.2), it is focused onto the retinal photoreceptors. As can be seen from figure 1.4, light must pass through a number of retinal layers of nerve fibers, nerve cells and blood vessels before reaching the photoreceptors. These retinal layers are transparent (aside from the blood vessels) due to the small size of their elements and their tight packing arrangement.

There is a total of 8 distinct layers that must be passed before reaching the photoreceptors. The retina is divided into two main zones, the foveal area and the parafoveal region. The

---

[3]Hole conjugated to pupil of eye

[4]for example Cataract, which will produce more scatter, and as with all imaging devices will be detrimental in acquiring accurate retinal information.
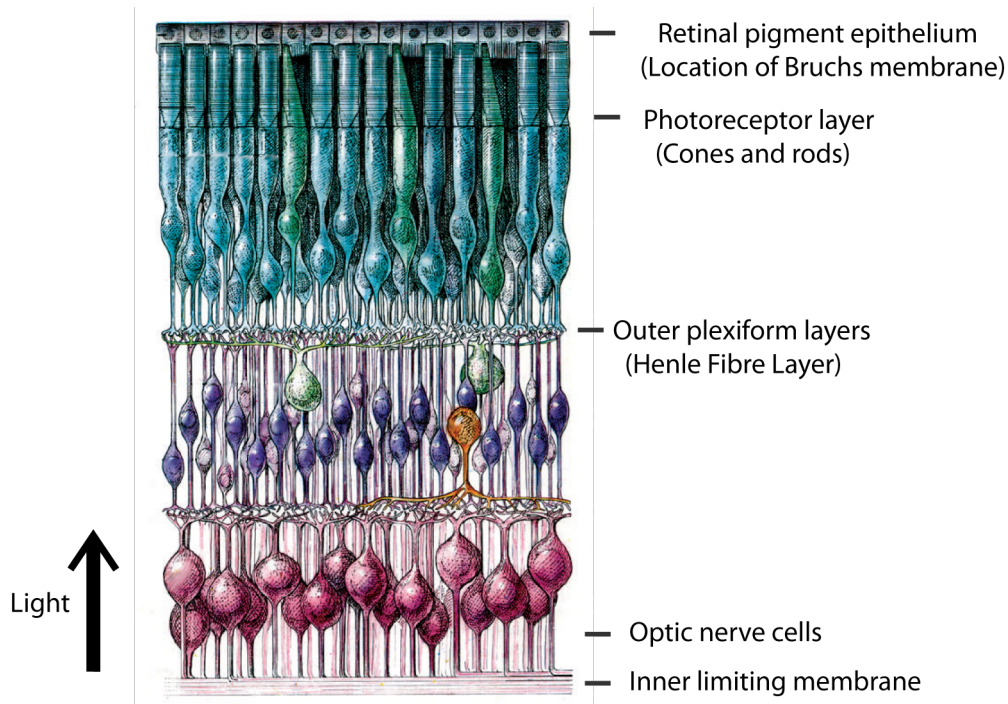
Figure 1.4: Illustration of retina displaying its multilayered nature. Light travels from the bottom to the top of diagram passing through the numerous transparent layers. The different colours are for the purpose of clarity only. Adapted from [15].

central foveal region is distinguished by it's characteristic fovel pit, and is approximately 5° in diameter. This is a depression which can be seen in the cross section of the retina and is caused by the radial displacement of outer plexiform layer to the optic nerve cells [11]. The parafoveal region is defined as any region outside the central 5°, particularly in this project the parafoveal region is taken from 7° outwards.

1.3.1 The photoreceptors

Photoreceptor cells are a specialised family of neurons found in the eye's retina, each characteristically identified by its spectral absorption. The four distinct spectral characteristics of the 3 types of cone photoreceptor and the single type of rod photoreceptor, can be seen in figure 1.5.

In a process known as phototransduction, the photoreceptor absorbs photons from the visual field and subsequently signals this information to neurons through a change in its membrane potential. The design of the photoreceptor is essentially in two parts, the outer segment which is adapted for collecting light and the inner segment adapted to transmit it (see figure 1.6(b)). As mentioned previously, each photoreceptor type can be characterised by it's wavelength sensitivity, and as such this information will be used by the visual system to form a complete representation of the visual world. The two distinct families of photoreceptor present on the human retina, the rods and the cones, serve an unique and different purpose, which will be briefly outlined in the following sections. The

17
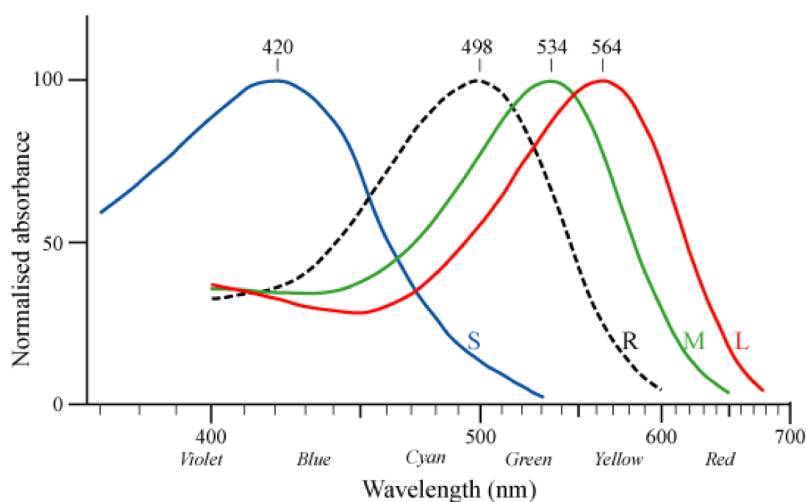
Figure 1.5: Photoreceptor types and their spectral responses. Adapted from results from [16]. The 3 cone types are S, M, and L (short, medium, long respectively in reference to their peak wavelength absorption) while the rod type is R.

optic nerve contains no photoreceptors and thus gives rise to its pseudonym, the blind spot.

Rods

The rods are located more in the peripheral area of the retina and rod vision is very sensitive achromatic[5] vision. They are by far the most common photoreceptor across the retina, with approximately 140 million present [11]. The light sensitivity of rod cells can be up to a 1,000 times that of cone cells. The rods are responsible primarily for scoptic, low flux vision[6]. All rods contain the same rhodopsin, which when exposed to light, undergoes a process known as phototransduction, which is perceived as vision[7]. Hundreds or thousands of rod cells are combined and transmitted to the visual cortex through a single bipolar cell, connected in turn to a singe ganglion cell leading to the brain. This results in a reduction of visual resolution (compared to the resolution from the cone receptor population, as each individual cone cell is connected to a bipolar cell) but greatly increases the rods sensitivity to light. The rods sensitivity to light is also a consequence to its reaction to incident light. Rod cells respond more slowly to light than cone cells, stimuli received by rod cells are integrated over about 100 milliseconds. This slower integration time makes rods more sensitive to light, however it also means that their ability to sense temporal changes, such as quickly flickering stimuli, is less accurate than that of cones[8] [17]. Rhodopsin takes approximately 30 minutes to regenerate fully in humans [11].

---

[5]Not the same as monochromatic as rod activation is not response to colour of the light.

[6]Essentially night vision, luminance levels of 10^{-2} to 10^{-6} cdm^{-2}

[7]Activation of a photoreceptor cell is actually a hyperpolarization (inhibition) of the cell.

[8]Accounts for lower CFF values in the peripheral retina(see later chapters for a more complete description of CFF)
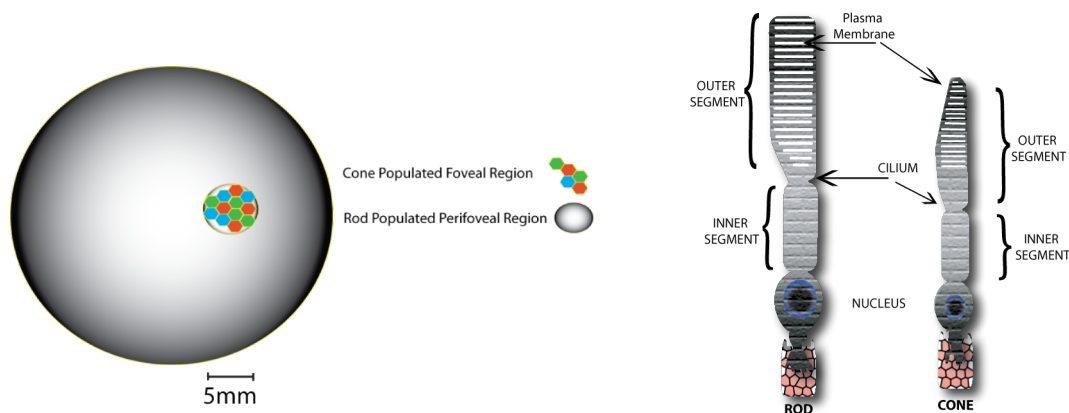
(a) Simple schematic of rod and cone distribution across the retina

(b) Schematic of rod and cone photoreceptor

Figure 1.6: Illustration of rod and cone distribution on the retina and schematic of the rod and cone photoreceptor. Cones can also appear in the peripheral area of the retina but the largest accumulation is in the macular region.

Cones

The cones are located primarily in the foveal area of the retina and number approximately 7 million[9]. Due to their tight mosaic style packing the cones account for high visual acuity. Cone cells can be classified as three different types, defined by their peak spectral response (see figure 1.5). The different cones distinguish from each other due to the different opsins they contain. Cone cells sensitive to green and red light predominate the central foveal area with a complete absence of blue sensitive cells [10]. The highest abundance of blue cones can be found on the slopes of the foveal pit and are quite unevenly spaced compared to that of the red and green spacing. The reduction in blue cones may be due to the presence of the macular pigment in this area. Agreement is still not reached about the exact distributions of these cells but numbers around 10% to 15% of the cones are blue, 50% to 54% are green[11] and 33% to 35% are red sensitive. However these figures are highly subject dependent. Cones operate primarily in the photopic region of light intensity[12].

As one will notice from figure 1.6(a) the cones, although vitally important to maintaining adequate vision, constitute a relatively small area on the retina. The macular pigment is also located primarily in this area of the retina[13], and as such it may be inferred that this

---

[9]Cones can also be found in the peripheral retina, but by far the largest accumulation of cones is in the fovea.

[10]May be due to presence of blue absorbing macular pigment peaking in the central fovea

[11]Peak output of the sun is in the green part of the spectrum

[12]Luminance levels of 1 to 10^6 cdm^{-2}

[13]Largest accumulation of MP is in the macular region, however traces of the pigment have being found

pigment, for some reason is associated with these important photosensitive cells. The role of the pigment will be dealt with in more detail in chapter 2.

Henle's fibre layer

Henle's fibre layer consists of the foveal portion of the outer plexiform layer of the retina. The layer is composed of elongated inner processes of foveal cones and rods which radiate away from the foveal pit. In the central retina, the cones have oblique axons displacing their cell bodies from their synaptic pedicles in the outer plexiform layer (OPL). These oblique axons with accompanying Muller cell processes form a pale-staining fibrous-looking area known as the Henle fibre layer [11].

The layer is essentially where the photoreceptors connect with their bipolar cells. Interest in this layer for this project is due to the presence of the macular pigment in the axons of the photoreceptors in this layer. As is evident from figure 1.4, this layer is located anterior to the cones, therefore light entering from the pupil traverses this layer before reaching the photo sensitive cells. Henle's fibre layer is absent in peripheral retina.

1.3.2 Retinal pigment epithelium

The retinal pigment epithelium (RPE) is the pigmented cell layer just outside the neurosensory retina that nourishes retinal visual cells, and is firmly attached to the underlying choroid and overlying retinal visual cells. This layer essentially supports, and maintains the functions of the photoreceptor outer segments. The RPE also plays a central role in retinal physiology by forming the outer blood-retinal barrier[14]. Although encouraging progress has been made with RPE transplantation, it remains unclear how to restore RPE-retinal interactions or re-establish a blood-retinal barrier [18].

When viewed from the outer surface, the photoreceptor outer segments are smooth and hexagonal in shape. When seen in section, each cell consists of an outer non-pigmented part containing a large oval nucleus and an inner pigmented portion which extends as a series of straight thread-like processes between the rods, this being especially the case when the eye is exposed to light. The RPE is involved in the phagocytosis of the outer segment of photoreceptor cells and it is also involved in the vitamin A cycle where it isomerizes all trans retinol to 11-cis retinal[11] (initiates the visual process). The RPE itself is multilayered and holds some interest in relation to this project.

Bruch's membrane

Current studies on age related macular degeneration suggest that Bruch's membrane could have a key role, and as such requires far more study. The membrane itself is multilayered (5 distinct layers), and stretches from the optic disc to the ora serrata[15] [11].

---

in almost all tissues of the eye.

[14]The blood-retinal barrier consists of cells that are joined tightly together in order to prevent certain substances from entering the tissue of the retina (bacteria) and allowing other substances (oxygen).

[15]The ora serrata is the serrated junction between the retina and the ciliary body

Bruch's membrane thickens with age, and as a result the transport of metabolites can be slowed. This may lead to the formation of drusen in age-related macular degeneration. Further to this, there is also a build up of deposits on and within the membrane. Inflammatory and neovascular mediators can then invite choroidal vessels to grow into and beyond the fragmented membrane. This neovascular membrane destroys the architecture of the outer retina and leads to sudden loss of central vision.

The primary interest in regards to this project with Bruch's membrane is the presence of the aging pigment lipofuscin in this particular area of the retina. It's presence can be exploited to measure the macular pigment optical density.

1.3.3 RPE lipofuscin

Lipofuscin present as brown pigment granules composed of lipid-containing residues of lysosomal digestion. Lipofuscin exhibits autofluorescence and its presence in Bruchs membrane can be exploited to measure the MPOD. Lipofuscin is normally associated with age, and commonly referred to as the aging pigment. However, the accumulation of lipofuscin in the RPE can also be linked with many retinal disorders, such as Stargardts's disease, Best's macular dystrophy and cone-rod dystrophy [19].
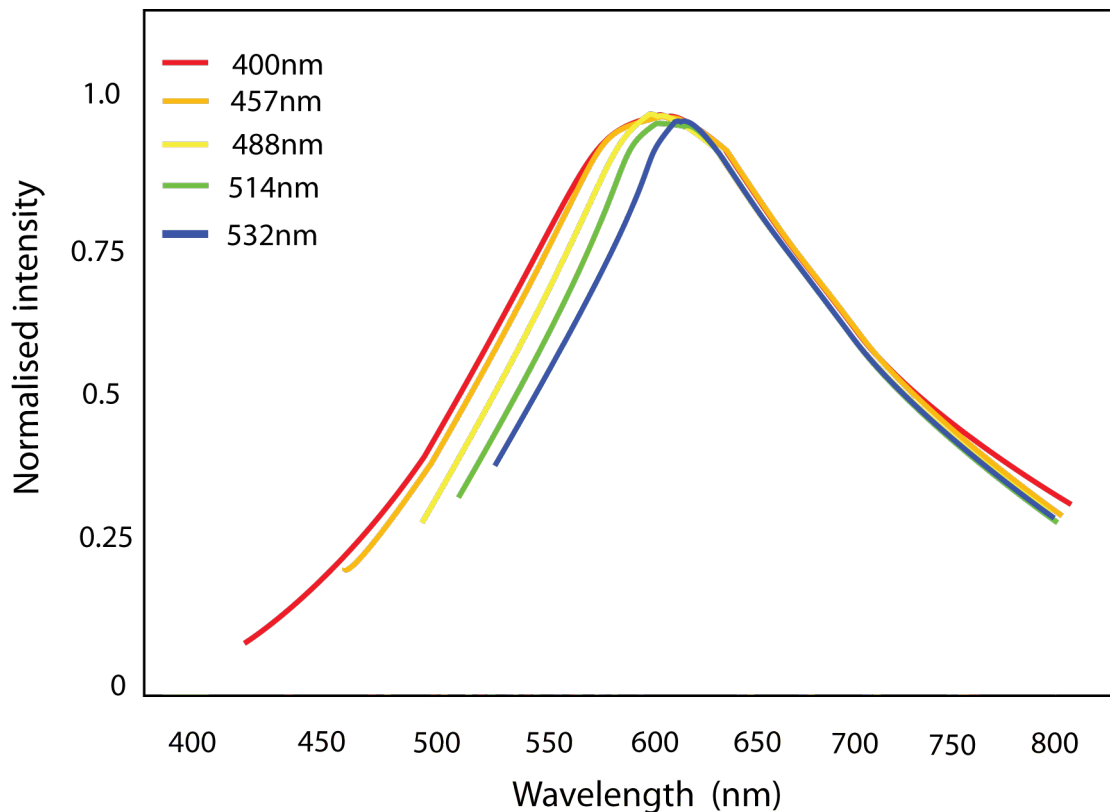
Figure 1.7: Illustration of lipofuscin fluorescence for a number of excitation wavelengths. The graph is adapted from Haralampus-Grynaviski *et al* [20].

Ben-Shabat *et al* suggest that the deposition of lipofuscin occurs largely as a consequence of the phagocytotic burden placed on the RPE cell [21], the presumption being that lipofuscin accumulates due to the failure of lysosomal enzymes to degrade components of the ingested outer segments of photoreceptors (by-product of disc renewal). Feeney-Burns *et al* have demonstrated that the content of lipofuscin is notable in subjects as young as 20 and that by the age of 80 that 20% of the area of an RPE cell in the central retina is occupied by lipofuscin [22]. The connection was also made that the levels of lipofuscin in the RPE are also topographically correlated with histopathological indicators of AMD [22]. The primary interest of lipofuscin, in regards to this project, is its ability to demonstrate auto-fluoresecence. Figure 1.7 displays the fluorescence of lipofuscin for a number of exciting wavelengths.

The backbone of this PhD project is to develop a simple device to measure the macular pigment optical density *in vivo*, both accurately and rapidly, with patient comfort a priority. This should enable large scale population studies to be carried out using the device, and various hypotheses in regard to the pigments role within the retina may be established.

Chapter 2

The Macular Pigment

This chapter details the characteristics of the macular pigment (MP). The location and chemical orientation of the pigment and it's overall distribution across the retina will be examined. The origins and unique attributes of the pigment will be presented, while its relation to age related macular degeneration (AMD), the leading cause of blindness in the western world, will be discussed.
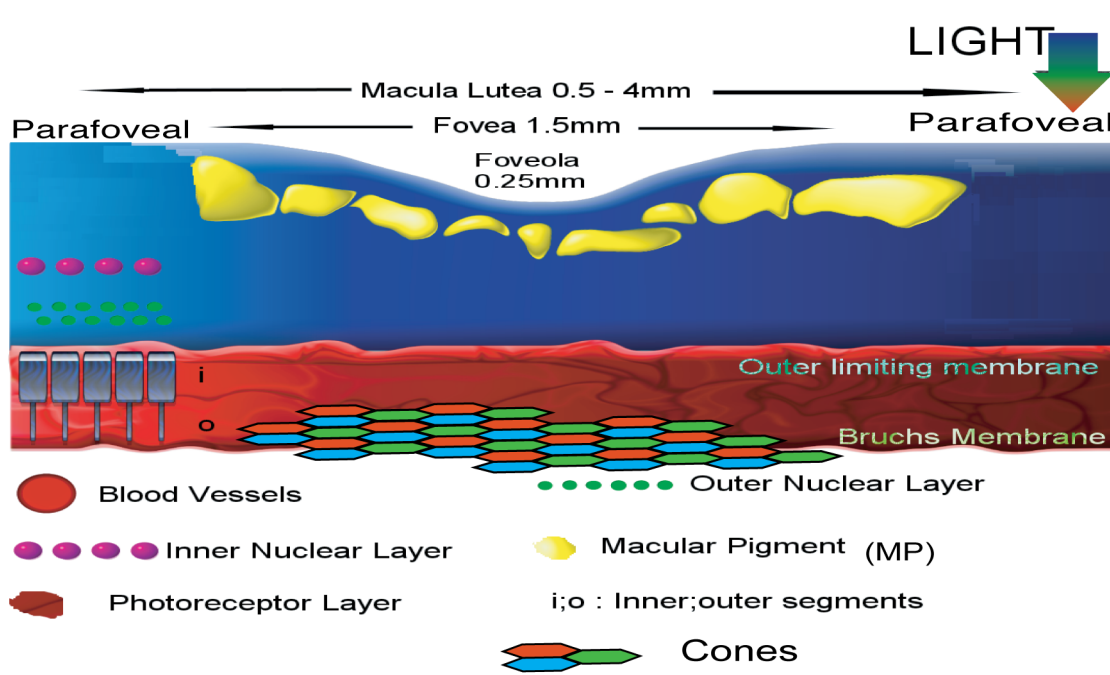
Figure 2.1: Simple view of the macula region

2.1 Lutein and Zeaxanthin

The macula lutea literally translates from Latin as yellow spot. This pigmentation in the foveal region is due to the accumulation of the carotenoids lutein and zeaxanthin (see figure 2.1). These dihydroxy-carotenoids or xanthophylls are more commonly found in

leafy plants and account for the rich pigment in their leafs[1]. Bone and Landrum using high performance liquid chromatographic characterised the pigment and confirmed the presence of the two xanthophylls; they also revealed a different ratio of lutein to zeaxanthin between the central fovea and more parafoveal regions, with zeaxanthin dominating the central area while lutein was more plentiful in the parafoveal region [10]. Subsequent studies by Bone *et al* identified *meso*-zeaxanthin, a stereo-isomer of zeaxanthin, as an important constituent of the macula pigment [23]. The chemical structure of the two primary carotenoids found in the macular region can be seen in figure 2.2

(a) Lutein
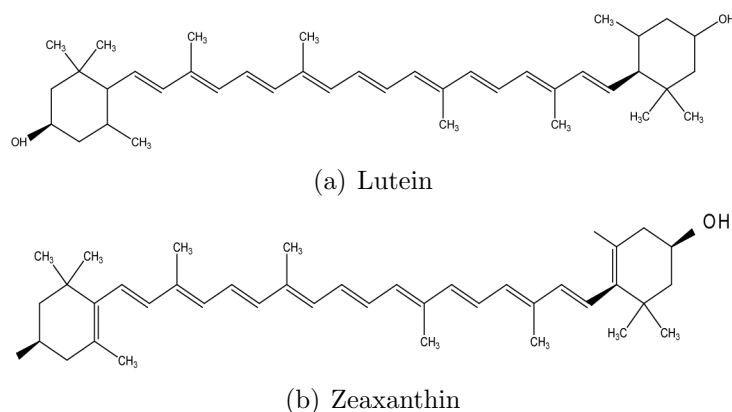
(b) Zeaxanthin

Figure 2.2: Chemical structure of the two main carotenoids that constitute the macula pigment

2.1.1 Pigment characteristics

Lutein and zeaxanthin are isomeric carotenoids that differ chemically from each other in very subtle ways [24] (See figure 2.2). In order to gain an appreciation of the individual function of each of the carotenoids these differences will be briefly examined. The origins of the pigment will be examined first, followed by a deeper investigation into the nature of the pigment, which may give further indication of its role within the human retina.

Origins of carotenoids

Lutein and zeaxanthin are not synthesised within the body, consequently the macula pigment (MP) is entirely supplied by dietary intake. As mentioned in chapter 1, Wald originally identified the MP as having the spectral properties of the xanthophyll lutein, which originates in the leaves of green plants. As a result, it may be inferred that the development of MP exclusively in primates may be explained by their dietary patterns.

Sommerburg *et al* [25] used HPLC[2] to analyse the content of lutein and zeaxanthin in commonly consumed fruits and vegetables (see appendix A). The two foods that have the highest amount of lutein are spinach and kale. The best sources of zeaxanthin are

---

[1]Seen as orange and brown in colour. Noticeable during autumn when leaves no longer contain chlorophyll

[2]High performance liquid chromatography

egg yolks, corn, orange peppers and orange juice. Khachik *et al* analysed the carotenoid concentration in human plasma, and how the concentration is influenced by diet [26]. In a study by Malinow *et al*, it was demonstrated that primates fed on a carotenoid free diet had no detectable macular pigmentation [27] while numerous studies, among them Bone *et al* and Hammond *et al*, exhibited that levels of MP in humans can be raised by dietary supplementation[3] [28, 29]. Once ingested, serum levels of carotenoids are affected by multiple factors including body fat, oxidative stress, gender, among others [30]. However it must be noted that the fundamental procedure of incorporation of the carotenoids into the retinal tissues is still relatively poorly understood.

Spectral absorption of the macular pigment

The ability of the carotenoids to absorb light is due to their chemical constitution, particularly the presence of a conjugated polyene chain (See figure 2.2). The absorption spectrum of the carotenoids depends on the extent of conjugation in the polyene chain [31]. Lutein and zeaxanthin both possess a polyene chain consisting of nine conjugated double bonds which results in a maximum absorbtion of 445nm and 451nm respectively. The small disparity in the maximum absorbtion of the two carotenoids may be due to the small disparity in the chemical structure of the two carotenoids. Lutein and zeaxanthin are constitutional isomers and differ in the position of a double bond in one of the ionone rings. The differences arise due to interactions of the double bonds in the β-ionone rings with the polyene chain. Figure 2.3 shows the absorption spectrum for the pigment (L+Z).
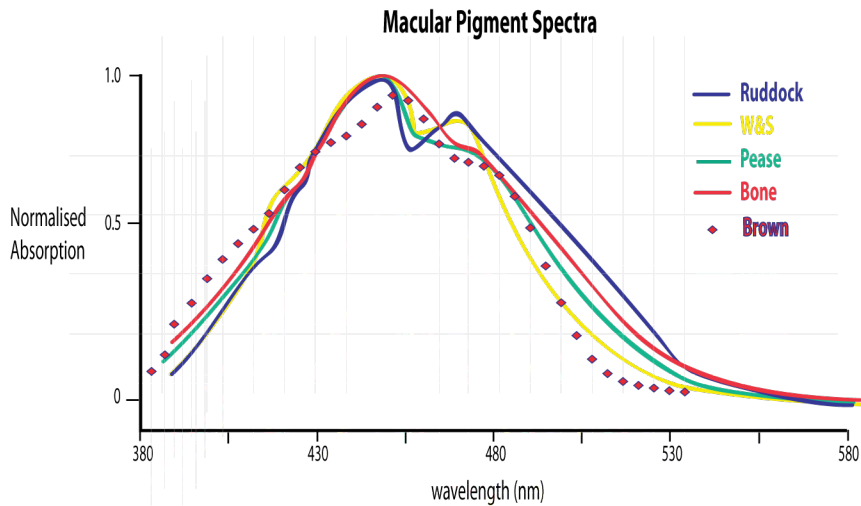
Figure 2.3: Normalised absorbtion spectrum of the MP as measured by Ruddock [32], Wyszecki and Stiles [33], Pease *et al* [34], Bone *et al* [35] and Brown (taken from data in [9]). The subtle differences in absorption up to 500nm may be due to the different techniques used by the different examiners i.e Brown et al used *ex vivo* measurements on excised eyes, while the remaining examiners employed various *in vivo* techniques. Differences after 500nm accounted for in later text.

---

[3]MP levels measured using heterochromatic flicker photometry. Debate remains over the accuracy of this method due to its subjective nature.

It should be noted that figure 2.3 shows there is noticeable differences in the absorption spectrum beyond 500nm. The production of a standard absorption curve would be very welcome but this itself harbours difficulties. Perhaps the differences between the curves arises from differing combinations of L and Z concentrations. If so, the method of Bone *et al* may be more representative of a precise absorption spectrum, as it represents the most likely combination of L and Z. In saying that, relative concentrations of L and Z varies with the individual due to diet, gender, BMI[4] etc [36]. Further differences may arise in disparities between individual levels of oxidation products of L and Z. These variances may perturb further the spectral absorption due to the overall macular pigmentation.

As a result subjects with the same absorption at 460nm may have different absorption at different wavelengths, due to individual proportions of the constituents of MP [37]. Therefore, it may be impossible to reach a overall agreement for a complete spectral identification of the macula pigment.

Reactive oxygen intermediates

A free radical is a highly chemically reactive atom, molecule or molecular fragment with a free or unpaired electron. Along with peroxides and singlet oxygens these form what are known as reactive oxygen intermediates (ROIs). ROIs form as a natural byproduct of the normal metabolism of oxygen and have important roles in cell signaling. However due to their highly reactive state ROIs can cause tissue damage, generally referred to as oxidative stress. Generally speaking, oxidative stress is caused by an imbalance between the production of reactive oxygen and a biological system's ability to readily detoxify the reactive intermediates or easily repair the resulting damage.

Unfortunately due to the physiology of the retina, it is an ideal region for the production for ROIs. This is due to its high consumption of oxygen, its high exposure to to large quantities of solar radiation, its wealth of chromophores and its continual process of phagocytosis by the RPE [38]. In fact the retina is the most metabolically active tissue in the body and the photoreceptor layer is maintained at a high oxygen tension. Also the presence of a high concentration of polyunsaturated fatty acid in the outer segments of the photoreceptor layer [39], which are very readily oxidised, contrive to make the retina a breeding ground for ROIs. The carotenoids as a family, particularly Lycopene and β-carotene, have well documented antioxidant properties.

2.1.2 A protective role for the macular pigment

As referred to earlier, ROIs, and consequently retinal cell and photoreceptor damage, are not just produced from the internal metabolic mechanism but also from external processes, namely photic damage. This is the damage caused by exposure to incident and consequent absorbed light. The damaging effects of exposure to short wavelength light was established by Ham *et al* in 1978 [40]. RPE cell death was demonstrated in rhesus monkey retinas after prolonged exposure to short-wavelength light. Ham also reported

---

[4]Body mass index.

that, depending on exposure duration, the power required to obtain this photochemical damage, was 70-1000 times lower for light of 441nm than for infrared light of 1064nm[5]. Mechanisms of photoreceptor damage by light in eyes has being investigated by Noell *et al* [41] and Faktorovich *et al* [42]. Since the lens absorbs practically all wavelengths less than 400nm, the most damaging wavelength incident on the retina is that of visible blue light (approximately 430nm - 490nm). It therefore seems logical to propose an evolutionary development of macular pigment for the protection of the retina, as the MP absorbs maximally in the blue range of the spectrum (see figure 2.3). If blue light cannot reach these highly oxidised polyunsaturated fats in the photoreceptor outer segments, then there is an reduced risk of the production of ROIs and consequently photochemically induced cell damage.

The macular pigment has also being linked a process outside that of the protection of the retinal cells. The hypothesis is the improvement of visual acuity and image contrast by reducing chromatic aberration[6] [43, 44].

2.2   Location of the pigment

The exact location of the macula pigment molecules within the Henle fibre layer is not known. However, observations of the pigment using polarised light reveals that the pigment is highly organised, and that the retinal structure provides the pigment with a preferential, rather than random, alignment [45]. The main evidence for this is the entopical phenomenon known as Haidinger's brushes.

2.2.1   Haidinger's brushes

The phenomenon of Haidinger's brushes was first described by Austrian physicist Wilhelm Karl von Haidinger in 1844 [46]. The phenomenon is evidence of the ability of the human eye to perceive polarised light. Figure 2.4 is a simulated appearance of Haidinger's brush for vertically polarized light[7][8]. The brush, which appears in the centre of the visual field, is consistent with the size of the macular region. Due to its perceived location, and the fact that it has colour implies that the cones and/or the macula pigment are involved in its formation. The brush is invisible in the red, a region outside the absorption of the macula pigment (see fig 2.3).

In 1866, H. von Helmoltz related the effect of Haidinger's brush to the dichroism of the retinal pigment [47]. A more detailed explanation was provided by Krinsky *et al* [31] who suggest that the dichroic behaviour of the pigment is attributed to the linear nature of the conjugated polyene chain of carotenoid molecules (see figure 2.2(a)). Further to this Bone *et al* [48] demonstrated the dichroic properties of lutein.

---

[5]Exposure durations from 1 to 1000secs
[6]Due to its absorption of short wavelength light
[7]The size and intensity exaggerated for clarity
[8]The orientation of the figure is perpendicular to the electric field vector of the light

Figure 2.4: Simulated version of Haidinger's brushes. The scale of the brushes is consistent with the size of the macular region (5mm) and its colour further suggests the use of the cones and possible contribution of the macular pigment in its perception.

Assuming that the phenomenon is possible due to the dichroic nature of the pigment, a certain arrangement of the carotenoids is required. Blue light is maximally absorbed by the pigment when the electric field vector is parallel to the conjugated polyene chain of the carotenoid molecules and minimally when it is perpendicular [49]. In addition to this, each carotenoid molecule must be aligned perpendicular to a line connecting it to the centre of the fovea. In such an arrangement, the molecules are placed perpendicular to the Henle fibers that run in radial directions outward from the centre of the fovea. Retention of the carotenoids transversely within the membranes of these fibers is one possible arrangement that is consistent with Haidinger's Brushes [48].

Krinsky *et al* [31] have provided another hypothesis which states that the carotenoids are protein bound within the photoreceptor nerve axon. For the brushes to be perceived, the proteins would have to be correctly orientated, so that the carotenoids were held at 90° to the axis of the nerve axon. Interestingly the protein tublin, which is found in abundance in the Henle fibre layer [11] is a likely candidate. Also on binding with this particular protein, lutein exhibits a shift in its absorption maximum to 460nm, which is accepted as the maximum absorption by the pigment measured *in vivo*.

The exact arrangement of the carotenoids in the living eye remains unresolved, and further studies are required. The contribution due to the birefringence of the cone's outer layer and the slight birefringence[9] of the cornea should also be examined.

2.2.2   Spatial profile of the pigment

Traditionally, when a subject's macular pigment level is measured, the figure that is quoted is that of the macular pigment optical density averaged over a 1 degree area of the retina. The ability to measure the spatial profile of the macular pigment is limited by the measuring device and until recently has being largely ignored.
Haegertrom-Portnoy [52] suggests that adults preferentially retain sensitivity to the blue

---

[9]However, this birefringence is nearly zero across the whole cornea because the relative orientation of the fibres of any two adjacent lamellae is more or less random[50]
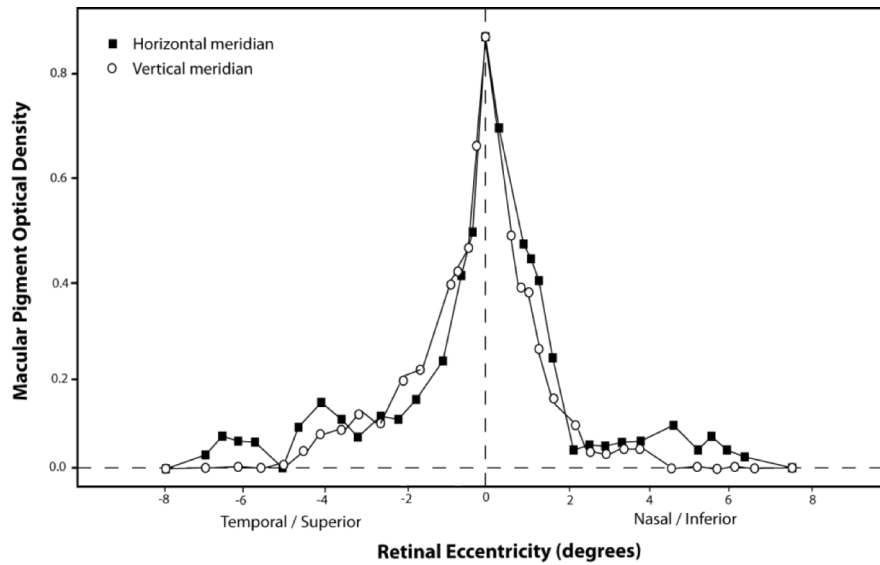
Figure 2.5: MPOD distribution measured for a single subject measured by Hammond *et al* [51]. The close relationship between the two curves suggests that the MPOD along the two meridians (for this subject) is symmetrical in nature. (Graph adapted from [51])

end of the visual spectrum. Early stages in the development of age related macula degeneration (AMD) can be characterised by a deterioration in short-wave length sensitivity. This may suggest that differences in MP spatial profiles could contribute to differences in the spatial extent of visual loss in AMD[10] patients [51]. For this possible link to AMD, and to attain a value for the entire macular pigment present on the retina, the ability to measure a distribution profile is essential.

2.3 Age related macula degeneration

Age related diseases are a growing public health concern due to a significant portion of the population now living longer than ever before. Among the elderly population the leading liability to their sustained vision is that of Age Related Macular Degeneration (AMD)[11]. The underlying pathogenesis of this debilitating disease is still not fully understood and consequently the treatment options, once the disease has established itself, are very limited. Therefore the key to combating the disease is early detection or prevention of the disease. Early presence of the disease may be indicated by the presence of Drusen[12] in bruch's membrane (layer of retina adjacent to the retina pigment epithelium layer, see figure 1.4) and certain steps can be taken which may prevent further damage to the retina (see below). The use of Amsler's grid is a simple technique to identify any deformation of

---

[10]Age related macular degeneration

[11]Cataract also affects a large portion of the population but unlike AMD, can be reversed by replacing the damaged lens.

[12]Drusen alone do not usually cause vision loss. In fact, uncertainty remains about the exact relationship between drusen and AMD. However an increase in the size or number of drusen raises a person's risk of developing either advanced dry AMD or wet AMD.

the macular region and can indicate the onset of the disease. The most attractive strategy in the combat of AMD is that of prevention.

2.3.1   Forms of AMD

AMD is classified as either wet (neovascular) or dry (non-neovascular), each of which are outlined briefly in the following sections. Figure 2.6 illustrates the effect each of these forms of the disease has on the retina. The two forms of AMD will be outlined briefly in the following sections.

(a) Advanced dry AMD   (b) Advanced wet AMD
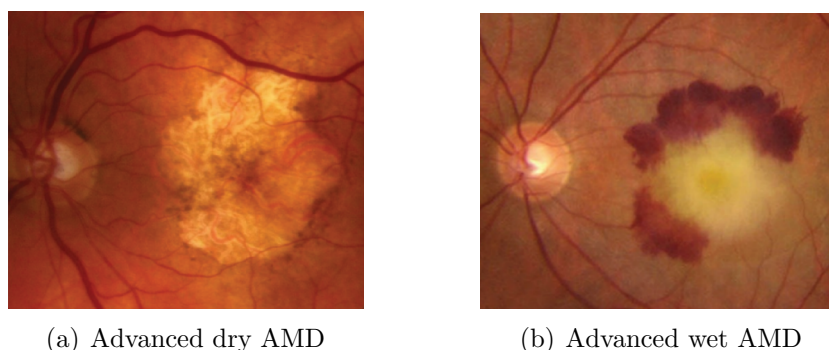
Figure 2.6: The effect of advanced AMD on the retina (a) displays advanced case of dry AMD illustrating extensive retinal atrophy/thinning at the macula while (b) displays advanced wet AMD showing central sub retinal elevation with fibrosis, fluid and surrounding sub retinal haemorrhage consistent with sub foveal choroidal neovascular membrane (CNVM). Images from the Thames Valley Macular Group.

Non-neovascular AMD

The majority of patients diagnosed with AMD suffer from the dry form of the disease. When an an retinal image of a patient is obtained, it is quite evident that the central macular has become distorted, pigmented, or most commonly thinned (see figure 2.6(a)). The technology for retinal transplants as of yet is not possible, therefore with dry AMD, once the retina has become damaged, it cannot be replaced. The progression of the disease is quite slow, consequently patients slowly lose the function of their central vision, and in fact many patients retain most of their vision. In general, patients with dry macular degeneration do not go blind, though they can have poor central vision. As outlined earlier the development of Drusen in Bruch's membrane may predispose to macular degeneration and in particular the dry form of this disease.

There is at the moment no effective cure for dry AMD but if detected at the initial or intermediate stage further advancement of the disease can be delayed. AREDS[13] study results (National Eye Institute) released in 2001, involving more than 3,600 people, suggest that antioxidant vitamins (vitamin A, vitamin C and vitamin E) can help slow down

---

[13]The Age-Related Eye Disease Study (AREDS) is a major clinical trial sponsored by the National Eye Institute, one of the US government's National Institutes of Health.

the progression of dry AMD. Several treatments for delaying dry AMD, and preventing it's development into wet AMD, are in the experimental stage.

Neovascular AMD

Unfortunately for approximately 15% of AMD sufferers, they will be diagnosed with the more serious wet form of macular degeneration. Wet AMD can be characterised by fats, fluid, and, or red blood cells beneath the retina. Patients can develop abnormal blood vessels beneath their retina, which can leak under and into the macula. This is known as a choroidal neovascular membrane (CNVM). The leaked blood and fluid will eventually form a scar in the macula (see figure 2.6(b)). Since this scar occurs in the center of vision, it creates a black or gray spot in the vision called a scotoma. Patients with wet macular degeneration usually have multiple episodes of new blood vessel formation. This can cause several episodes of leakage and bleeding into the macula. Therefore, any treatment that does not confront the underlying cause of this new blood vessel formation and leakage will only provide temporary help for most patients. Treatments for wet AMD include both the relative un-invasive[14] subscription of specific medication and invasive laser techniques. Both remedies share the same objective, that is to stop the growth of new blood vessels, and thus avoid any further leakage and scarring.

Laser treatments include Argon or Diode Focal Laser Treatment (DFLT) and the newer technique of Photodyanamic therapy (PDT). The technique of Argon or DFLT requires a specially focussing contact lens which aids in the accuracy of the destruction of the leaky blood vessels. The benefit of this treatment is that it can prevent further degeneration of the macula. However, the technique is not completely effective in targeting just the damaged cells and consequently many healthy cells will be destroyed in the procedure. The treatment is more effective for patients whose symptoms have being identified at an early stage, however Laser treatment is only useful in about 10% of patients. In the PDT technique, a light-sensitive chemical dye is injected into the bloodstream and is utilised to highlight the blood vessels that are growing abnormally. A low energy laser causes a reaction within the chemical dye, which destroys the leaking blood vessels, without damaging the healthy macular tissue. Multiple treatments are usually required and the success of the procedure again is dependent on early identification of the disease [53].

There are encouraging results from clinical trials of a medication to treat neovascular AMD [54]. The drug attacks VEGF (vascular endothelial growth factor), a protein which promotes the growth of blood vessels, and as such halts the progression of the disease. A number of similar drugs are under investigation. RhuFab, is an antiangiogenic drug that is injected into the eye in order to stop the growth of blood vessels. MACUGEN is the first VEGF therapy shown to help reduce the risk of vision loss in all neovascular age-related macular degeneration [55].

Drugs like RhuFab and MACUGEN might also be used after other treatments like PDT in hopes of reducing the need for repeated laser treatments.

---

[14]Most techniques require direct administration into the affected area, i.e. injection of drugs into the retina

2.3.2 Macular pigment and AMD

The two biggest risk factors for developing AMD is age and an advanced presence of the disease in the fellow eye. Certain risk factors involved in developing AMD can be controlled while others cannot. Those risk factors which cannot be modified include gender, family history, iris colour and hyperopia. Risk factors which may be controlled include physical inactivity, hypertension, smoking, excessive alcohol consumption, low dietary and blood carotenoids and excessive lifetime exposure to sunlight [38]. The exact effect of ammending any of these risk factors remain inconclusive, and debate exists regarding all the above putative risk factors.

Risk of developing AMD and average daily intake of L and Z
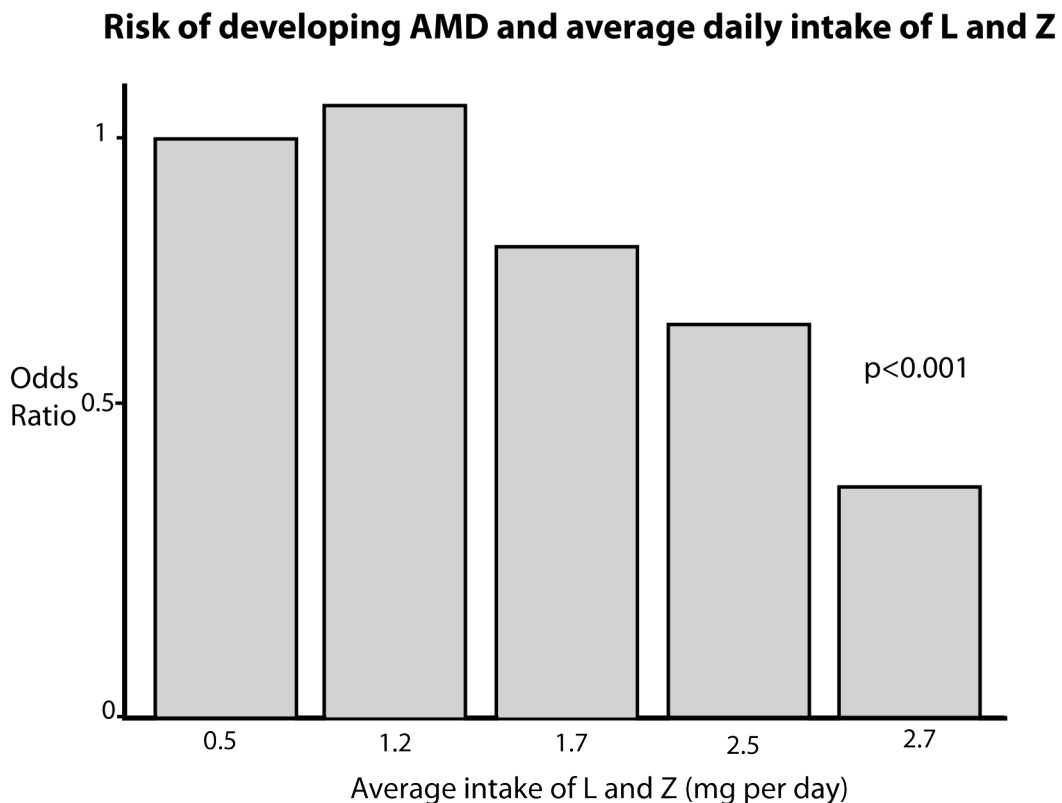
Figure 2.7: Studies suggest that the risk of AMD decreases significantly as the average dietary intake of lutein and zeaxanthin increase from approximately 1.5 mg per day to approximately 5.7 mg per day. Adapted from [56]

Several epidemiological studies have associated frequent consumption of foods containing lutein and zeaxanthin, and high plasma levels of zeaxanthin and lutein, with a reduction in risk for AMD. A study by Landrum et al [57], revealed that when excised eyes of 12 normal subjects were compared with those of 48 eyes suffering AMD, that the average lutein and zeaxanthin concentrations were approximately 30% lower in the retinas of AMD patients than in the healthy control group. Seddon et al [56] have shown in a later paper from the same study group that the relative risk for AMD is approximately 60% lower in subjects consuming 5.7 mg of lutein and zeaxanthin per day. These results can be seen in table 2.7[15].

---

[15]**Odds ratio** : The ratio of the odds of having the target disorder in the experimental group relative

A case-control investigation published in 1993 by the Eye Disease Case-Control (EDCC) Study Group [58] compared the antioxidant status and the progress of age-related macular degeneration in a population of 356 subjects with a specific form of AMD compared to 520 control subjects. They were able to show a statistically significant inverse relationship between plasma levels of zeaxanthin and lutein and the risk of developing AMD.

Hammond *et al* [29] have conducted a number of different studies investigating the levels of MPOD as a function of the previous risk factors, each in in isolation. All these studies revealed a lower MPOD for the groups at risk, compared with a control group. This result, coupled with the MPs known role as an antioxidant, the macula's predisposition for promoting oxidative stress, and significantly Beatty's hypothesis that oxidative stress plays a major role in the pathogenesis of AMD [59], may indicate the MP may have a role in protecting the macula from the onset of developing AMD.

---

to the odds in favour of having the target disorder in the control group.

Chapter 3

Techniques for the measurement of macular pigment optical density *in vivo.*

This chapter is dedicated to the current techniques employed in estimating the macula pigment optical density (MPOD) *in vivo*. Both subjective and objective techniques are discussed, and the intention is to highlight impartially the advantages and disadvantages of each individual method. While greater emphasis will be applied to the techniques utilised in this project, the intention is not to demonstrate any bias towards any specific technique.

3.1   Subjective techniques

The presence of the macular pigment (MP) on the retina consequently influences visual perception, primarily due to its absorption, and thus attenuation of blue light, anterior to the photo-sensitive cones. Psychophysical approaches to measuring the MPOD are technically relatively straightforward, and accounts for these methods being the most popular and commercially successful procedures to date. However, the inherent difficulty with these methods is that the detection system is the subject being measured. Therefore, an understanding of the task is required by the subject, as well as the mandatory dexterity to successfully accomplish the measurement, both accurately and consistently. While an appropriate design of the system can aid in achieving more accurate and consistent results, the fundamental limit to the success of the technique is subject dependent. Two of the most popular subjective techniques are outlined in the following sections, colour matching and the subjective technique employed in this project, heterochromatic flicker photometry (HCFP).

3.1.1   Colour matching

The method measuring the macular pigment optical density (MPOD) by the mechanism of colour matching was pioneered in 1963 by Ruddock *et al* [32, 60] and later developed by Moreland *et al* in 1978 [61]. In this technique the subject is presented with

three adjustable monochromatic light stimuli, and must attempt to match the energy of these three adjustable stimuli, to that of a single monochromatic test stimulus. The wavelength of the green test stimulus is outside the absorption spectrum of the macular pigment (MP)[1] and therefore undergoes no perceived luminance change due to any absorption by the pigment. The three adjustable stimuli produces differential absorption by the MP, dependent on its wavelength i.e. blue will produce more of an effect than green. As a result more blue will be needed for a colour match at the foveal region compared to that at a more eccentric location. Depending on the individual stimuli, a full spectral characterisation of the MP can be achieved when colour matches are performed at various different wavelengths [32]. Dedicated equipment and more efficient methods have being established by Moreland [61]. While attaining the spectral profile of the pigment is scientifically interesting, for the rapid estimate of its optical density the use of three test stimuli is not necessary. The ability to calculate spatial profiles of the pigment has still not being implemented using this method, nor has any differing methods for adjustment of the stimuli, which may aid in the matching of the stimuli. Inaccuracies regarding the influence of absorption by the cones, or rods have not been considered. This method can be more time consuming and technically more difficult to implement than its counterpart, the heterochromatic flicker photometry method.

3.1.2 Heterochromatic flicker photometry (HCFP)

Similar to the colour matching technique, heterochromatic flicker photometry (HCFP) is essentially a psychophysical technique to measure the macular pigment optical density (MPOD). The presence of the macular pigment (MP) affects the perceived luminance of blue light in the foveal region, compared to more eccentric locations [62]. The principle of the HCFP technique is that the subject is presented with a blue light (close to the spectral optical density peak of the MP) which alternates with a green light (outside the absorption spectrum of the MP).
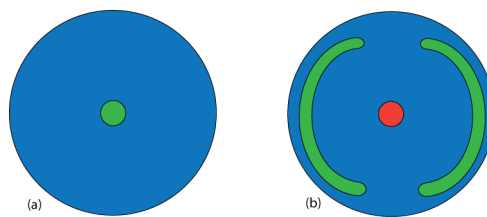
Figure 3.1: Illustration of the subject view for (a) foveal and (b) parafoveal measurements for the Mellerio device [63].

The subject, whilst viewing this alternate flicking between the two different colours, adjusts the intensity of the blue until the perceived flicker is minimised (minimum flicker point). An accurate measurement of the macular pigment optical density (MPOD) requires computation and accurate identification of the minimum flicker point, both on the foveal region and in the parafoveal region. The log ratio of the blue intensity and green intensity, for the foveal flicker point to that of the parafovel flicker point, results

---

[1]See figure 2.3

in the MPOD. There exist definite disadvantages with this technique. Due to its subjective nature, the primary difficulty is identifying correctly, accurately and consistently the minimum flicker point. This decision can be made easier for the subject using different techniques.

One device which utilises the HCFP technique is the Maculometer developed by Mellerio *et al* [63]. The frequency of flicker in the Mellerio device is fixed (13 Hz for parafovel field, 18 Hz for foveal field) and cannot be adjusted. These frequency values are chosen so to be above both the critical flicker fusion (CFF) threshold for rods and also that of the cones. However, these static values can lead to errors, because like all neural structures, the retinal cells experience changes in regards to neural processing speeds [64]. Peters *et al* suggest that the age-related breakdown of myelination may contribute to this slowing of conduction rate of neural axons [64] and this may account for the variation in CFF values for different subjects. Wooten *et al* [65] have addressed the problem by allowing the flickering frequency to be adjusted. This is done by measuring the critical flicker fusion (CFF) threshold over a certain area on the retina. This allows greater accuracy for finding the minimum flicker point, as when this point is reached (perceived green luminance and perceived blue luminance are equal), no perceived flicker is discerned. The Maculometer may also suffer from noise in the measurements, for subjects with low levels of macular pigment. This may be due to the MPOD calculations not correcting for the spectral spread of the flickering stimuli, noise in the electronics, errors in calculation of calibration relationships to convert DVM^2 readings to luminance^3 values or accounting appropriately for lens fluorescence.

Another feature of Wooten's device is the ability to adjust the stimulus level in a normal mode, or in a yoked manner. The yoked adjustment method means as blue intensity is increased by a certain amount, the green intensity is automatically decreased by the same amount. This has the effect that any differences in perceived luminance between the two stimuli is more noticeable, relative to when the perceived luminance is the equal. Normal mode means that as one stimulus remains at a constant intensity, the intensity of the other stimulus is adjusted. In spite of its improvements this device still retains some disadvantages. The system electronics for the control of the device are heavy and bulky. The design of the adjustment console allows for subject 'learning' of the minimum flicker point i.e. since each end point of the dial is clearly defined, a subject can learn his/her position for a reading, and can repeat this position for all readings.

The success of a subjective technique itself depends on a cooperative, alert subject fully aware of the tasks required. The Wooten device is not very portable and analysis of the measurement is carried out on an external program, on a different platform. Again, a device which is not fully inclusive, and contains all required adjustments and calculations on a single platform/terminal can lead to errors and is certainly more time consuming. Other devices which implement the flicker technique will not be discussed here. A more detailed comparison of the two flicker devices described in this thesis can be found at [66].

---

^{2}Digital Volt Meter

^{3}The photometric equivalent of radiance. Luminance is obtained by integrating spectral radiance weighted by luminous efficiency over the visible spectrum. Units are candela per meter squared.

In this particular project, the calculation of the MPOD is based on Delori's analysis [9] and is outlined in the following equations. The values of λ_1 and λ_2 are stated for the peak output wavelength for the blue and green LEDs respectively, employed in this project. The equations cited assume that all the light perceived by the subject has being affected by the MP, so for the foveal (F)[4] and the parafoveal (P) sites, the luminance match is given by:

$$I_F(\lambda_1)10^{-D_F(\lambda_1)}S_F(\lambda_1) \;\; = \;\; I_F(\lambda_2)10^{-D_F(\lambda_2)}S_F(\lambda_2)$$

$$I_P(\lambda_1)10^{-D_p(\lambda_1)}S_p(\lambda_1) \;\; = \;\; I_P(\lambda_2)10^{-D_P(\lambda_2)}S_p(\lambda_2) \tag{3.1}$$

where I_F and I_P represent the minimum flicker radiant powers at the fovea and the parafoveal regions respectively, while S_F and S_P represent the photoreceptor sensitivities at these two sites. Since the wavelength λ_2 is outside the absorption of the MP, this should be unaffected by the MP present in the foveal region. Therefore, the radiant power at the fovea $I_F(\lambda_2)$ should equal the radiant power at the parafovea $I_P(\lambda_2)$.

$$I_F(\lambda_2) \cong I_P(\lambda_2)$$

Assuming this and taking the log difference between both locations one obtains equation 3.2;

$$D_{flick}(\lambda_1) - D_{flick}(\lambda_2) = \log \frac{I_P(\lambda_1)}{I_F(\lambda_1)} + \left[\log \frac{S_P(\lambda_2)}{S_P(\lambda_1)} - \log \frac{S_F(\lambda_2)}{S_F(\lambda_1)}\right] \tag{3.2}$$

where $D_{flick}(\lambda)$ represents the density difference between the fovea and parafoveal location, for the specific wavelength i.e.

$$D_{flick}(\lambda_1) \;\; = \;\; D_F(\lambda_1) - D_P(\lambda_1)$$

$$D_{flick}(\lambda_2) \;\; = \;\; D_F(\lambda_2) - D_P(\lambda_2)$$

The macular pigment optical density can be expressed as a function of its maximum absorption at 460nm. $D_{flick}(460)$ is a function of the density difference $D_{flick}(\lambda)$ and that of the corresponding extinction coefficient[5] for the specific wavelength λ. Specifically, this is found by applying Beer's law for both wavelengths utilised in this project, and is shown in equations 3.3 and 3.4.

$$D_{flick}(\lambda_1) = K_{mp}(\lambda_1)D_{flick}(460) \tag{3.3}$$

$$D_{flick}(\lambda_2) = K_{mp}(\lambda_2)D_{flick}(460) \tag{3.4}$$

---

[4]This project takes a number of different location readings in the foveal region. For simplicity, these readings will be referred to just as the foveal readings.

[5]These are calculated using known data obtained from excised retinas.

Assuming that selective chromatic adaption and frequency of flicker (measured CFF) are sufficient to suppress the influence of the blue cones, that the proportion of green and red cones are comparable in the foveal and parafoveal regions, interference of the rods are minimal and self-screening is negligible [9], then the density of MP as measured by the flicker technique $D_{flick}(460)$ is given by[6] equation 5.14.

$$D_{flick}(460) = \frac{-1}{K_{mp}(\lambda_1) - K_{mp}(\lambda_2)} \times \left[\log \frac{I_P(\lambda_1)}{I_F(\lambda_1)} \right] \qquad (3.5)$$

3.2 Objective techniques

Objective techniques employed for the measurement of macular pigment optical density (MPOD), have distinct advantages over subjective techniques. The primary advantage is that objective methods require minimal comprehension from the subject. The fundamental requirement is an ability to fixate for a short period of time. However since retinal information is achieved by reflection/fluorescence, the subject's pupil is dilated in order to achieve adequate quality retinal data, and thus minimise the subject's measurement time in the device. Accurate alignment of the subject, in order to achieve this adequate retinal information, can be difficult. However various procedures can be implemented to minimise the difficulty and ensure accurate and more consistent alignment of the subject. Each of the techniques have their own inherent advantages, for example due to their greater accumulation of the aging pigment lipofuscin, auto-fluorescence (AF) may suit older subjects, while younger subjects, which would have clearer less opaque lens and cornea, may be more suited to the reflectance (RE) technique. An overview of the two objective techniques employed in this project will be outlined in the following sections, while for the case of completeness another popular objective technique will also be outlined, and a case made for it's omission from this device will be presented.

3.2.1 Auto-fluorescence (AF)

The auto-fluorescence technique takes advantage of the fluorophore lipofuscin. Lipofuscin is located in Bruchs' membrane (within the retinal pigment epithelium, see figure 1.4), posterior to the macular pigment (MP). The fluorophore is excited using the two wavelengths, green and blue, and its fluorescence detected at a longer wavelength (approx. 710 nm, outside the absorption range of the pigment). The macular pigment optical density (MPOD) can be calculated from this method, due to the fact that the exciting blue light will be attenuated before reaching the fluorophore, thus less exciting light will reach the lipofuscin, and consequently less emission from the lipofuscin will be detected.

To apply this method certain techniques have been established. The technique of a bi-wavelength, bi-location measurement is utilised in this project and has evolved from the following mathematical examination of the method. This technique is essentially based on Wald's original observations [8] and has being adapted from Delori's work [9]. If one assumes that the only absorption is by the macular pigment, and the only detected

---

[6]Please note that lens fluorescence is not considered and may influence the macular pigment reading.

fluorescence is from the RPE lipofuscin then, the detected AF intensity at an emission wavelength λ, for excitation wavelength Λ is given by equation 3.6

$$I_F(\Lambda, \lambda) = I_0(\Lambda)10^{-D_F(\Lambda)}F_F(\Lambda)S(\lambda) \tag{3.6}$$

where $I_0(\Lambda)$ is the intensity of the uniform illumination light at an energy Λ, $D_F(\Lambda)$ is the optical density of the MP for Λ, $F_F(\Lambda)$ is the fluorescence efficiency of the lipofuscin for Λ and $S(\lambda)$ is the sensitivity of the detection system for the emission wavelength λ. Since the measured fluorescence light $\lambda = 710$ nm, which is well outside the absorption of the MP, then the macular pigment optical density $D_F(\Lambda)$, is proportional to the amount of MP present on the retina.

Equation 3.6 can be simplified by taking another measurement on a different area of the retina. Simply this area of the retina can be seen as reference location, and can be used to negate the influence of the intensity of the light on the retina and the sensitivity of the detection system. These two factors can be difficult to measure as they depend on absorption of the cornea and lens[7], and instrument characteristics. If we chose the reference retinal location to be devoid of any pigment, specifically the parafovel region[8], and find the ratio of the autofluorescence for both sites (applying equation 3.6 to foveal (F) and parafoveal (P) location) then,

$$\frac{I_F(\Lambda, \lambda)}{I_P(\Lambda, \lambda)} = \frac{I_0(\Lambda)10^{-D_F(\lambda)}}{I_0(\Lambda)10^{-D_P(\lambda)}}\frac{F_F(\Lambda)}{F_P(\Lambda)}\frac{S(\lambda)}{S(\lambda)} \tag{3.7}$$

As outlined for the subjective technique, the optical density of the MP is traditionally expressed as a function of it's maximum absorption at 460nm. Applying Beer's law it is possible to express the density $D(\lambda)$ as a function of the density difference at 460nm and of the corresponding extinction coefficient. Thus,

$$D(\lambda) = K_{mp}(\Lambda)D(460) \tag{3.8}$$

where $K_{mp}(\Lambda)$ is the known extinction coefficient for the MP at Λ relative to the extinction coefficient of the MP at its maximum absorption at 460nm. In order to find the absorption of the pigment we obtain the log of equation 3.7, also eliminating $I_0(\Lambda)$ and $S(\lambda)$ and including the extinction coefficient we obtain equation 3.9.

$$D_{AF}(460) = \frac{1}{K_{mp}(\Lambda)} \times \left[\log\frac{I_P(\Lambda)}{I_F(\Lambda)} - \log\frac{F_P(\Lambda)}{F_F(\Lambda)}\right] \tag{3.9}$$

where $D_{AF}(460) = D_F(460) - D_P(460)$, the optical density difference between the foveal location F, and the reference parafoveal location P. However, the problem with equation 3.9 is that the latter term in the brackets, the fluorescence efficiency ratio $F_P(\Lambda)/F_F(\Lambda)$, is unknown and realistically cannot be easily calculated. In order to eliminate this term

---

[7]These factors cannot easily be clearly defined for all subjects.
[8]Approximately 7° eccentricity.

we use the two wavelength method as pioneered by Delori *et al* [9]. The two wavelengths used are one maximally absorbed by the MP, Λ_1 and one outside the absorption spectrum of the pigment, Λ_2. Assuming that the ratio of the fluorescence efficiencies $F_P(\Lambda)/F_F(\Lambda)$, is constant and wavelength independent for all retinal locations, then this allows for the elimination of this fluorescence efficiency ratio. Rewriting equation 3.9 to include the two wavelengths, applying the previous assumption, followed by subtraction rearrangment we obtain equation 3.10.

$$D_{AF}(460) = \frac{1}{K_{mp}(\Lambda_1) - K_{mp}(\Lambda_2)} \times \left[\log \frac{I_P(\Lambda_1)}{I_P(\Lambda_2)} - \log \frac{I_F(\Lambda_1)}{I_F(\Lambda_2)} \right] \qquad (3.10)$$

This equation assumes that the excitation spectrum at the parafoveal region must be proportional to the excitation spectrum at the fovea. In other words, the amount of lipofuscin can vary across the field but the composition of lipofuscin (composed of several fluorophores) is assumed to remain constant.

The graph in figure 3.2 is adapted from results obtained by Delori. This represents the fluorescence at the fovea and peripheral area of the retina, as well as the emission spectrum, for a single subject, over a $2°$ area on the retina. Figure 3.3(b) displays the emission spectrum for lipofuscin for a number of different excitation wavelengths. Comparison of readings on the macular (pigment present) and on the parafoveal region (no pigment present) results in a value for a single pass measurement of the MPOD. However, the success of this method relies on the fact that all detected fluorescence is influenced just by the MP and that the concentration of lipofuscin is constant across the retina. Similar to the reflectance technique, devices employed to implement AF measurements are adapted high-end ophthalmic devices. Again many disadvantages are inherent with utilising a non-dedicated device for the measurements. These include cost, difficult to use, time to adapt a non-dedicated instrument, among others.

The emission signal is very low so very bright excitation light is required, or alternatively relatively long exposure times. These two factors can add to patient discomfort. Success of this technique can be more difficult to achieve in young subjects, since they possess far less lipofuscin than older subjects, and as a result the already weak emission signal will be of far less intensity. The auto-fluorescence technique for measuring the MPOD is a single pass measurement i.e. the detected light on the measuring camera passes through the MP once. Since lipofuscin is an end waste product, it may be of interest to investigate whether it always shows the same fluorescent properties.

3.2.2   Reflectance (RE)

The reflectance (RE) method for the measurement of macular pigment optical density (MPOD) utilises the spectral absorption properties of the pigment. An area of the retina is illuminated in blue, and separately in green, and an image of each is obtained. Information acquired from the fovea (pigment present) and the parafovea (no pigment present) can then be used to, essentially self calibrate the system, and calculate the MPOD (see
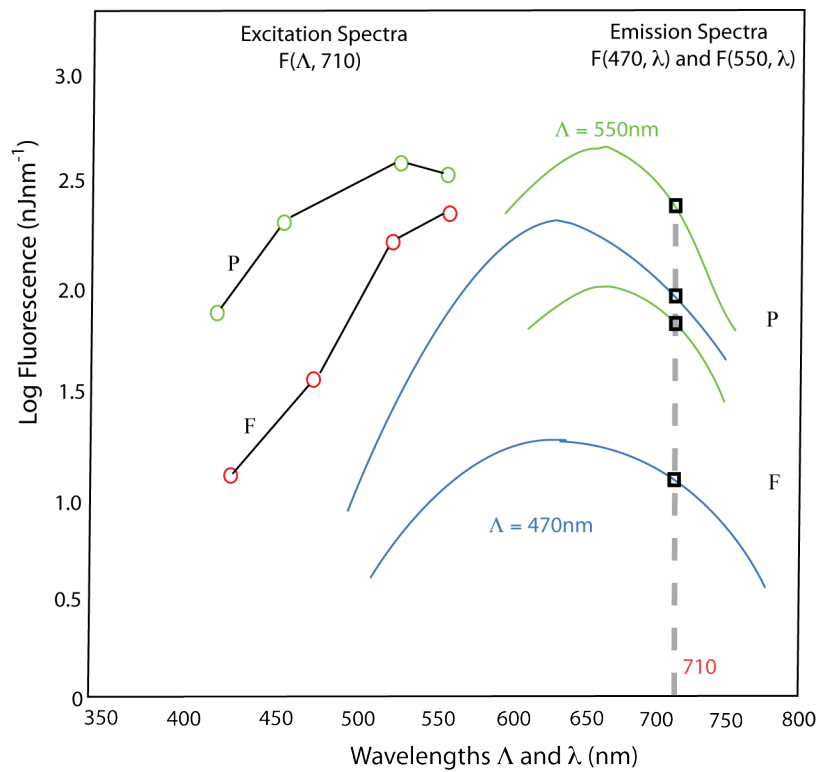
Figure 3.2: Illustration of fluorescence excitation (measured at 710nm) and emission spectra (for 470nm and 550nm excitation) measured at the fovea and parafovea for a single subject. The graph is adapted from results gathered by Delori *et al* [9].

equation 3.12). An area of at least 7° is required to provide foveal and parafoveal information. Due to its absorption characteristics, the macular pigment (MP) will absorb the blue light, while the green light will be relatively unaffected.

(a) Test target to measure

(b) Blue image of test target (a)

(c) Green image of test target (a)

(d) Difference image between blue and green
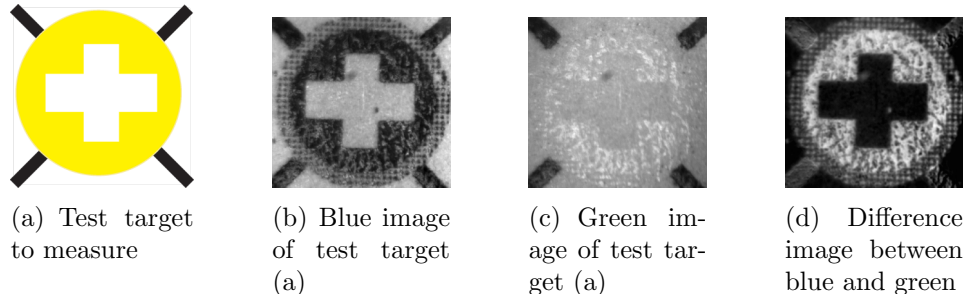
Figure 3.3: Illustration of 12-bit grayscale reflectance images of target (a) under (b) blue illumination,(c) green illumination and their corresponding difference image (d) (Images (b), (c) and (d) are real images produced by the system built for this thesis, and calculated by application of equation 3.12).

Figure 3.3 displays a green image and blue image of the yellow target, and the difference image between the blue and green image. For a gray scale image, the greater the absorption the darker the corresponding area of the image, or alternatively in the difference image, the brighter the image area the greater the difference between the images in question[9]. As is evident from figure 3.3, the distribution of the pigment, as well as the peak MPOD, can be calculated from the reflectance method.

Similar to the derivation of the auto-fluorescence technique the reflectance equation follows the same logic and procedure. The intensity of the reflected light $I_F(\lambda)$ for a illumination wavelength (λ) is given by equation 3.11.

$$I_F(\lambda) = I_0(\lambda)10^{-D_F(\lambda)}R_F(\lambda)S(\lambda) \qquad (3.11)$$

Again this equation contains a number of unknown and difficult to calculate parameters, namely the intensity of the illuminating light on the retina $I_0(\lambda)$, the sensitivity of the imaging system to the illuminating light $S(\lambda)$ and the reflectance of layers located posteriorly to the pigment layer $R_F(\lambda)$. Following the same logic as previously outlined in the AF technique, these parameters can essentially be cancelled out by examining two areas on the retina, the foveal (pigment present) and the parafoveal (no pigment present). If the MPOD is stated as a function of its maximum absorption at 460nm, by including the relative extinction coefficient, apply the use of two different wavelengths at two different locations on the retina then equation 3.11 can be simplified to equation 3.12 which can be used to calculate the MPOD.

---

[9]The quality of the image is limited by the resolution of the printer used to create the image, and also the quality of the paper the image is printed on.

$$D_{RE}(460) = \frac{0.5}{K_{mp}(\lambda_1) - K_{mp}(\lambda_2)} \times \left[\log \frac{I_P(\lambda_1)}{I_F(\lambda_1)} - \log \frac{I_P(\lambda_2)}{I_F(\lambda_2)} \right] \qquad (3.12)$$

The wavelengths λ_1 and λ_2 represent the values at which maximum and minimum absorption by the pigment takes place, I_P is parafoveal reflectances and I_F are the foveal reflectances. K_{mp} represents the extinction coefficients for both wavelengths employed, λ_1 and λ_2. The equation is taken from a paper by Delori *et al* where the robustness of the equation was examined and deemed sufficient [9]. Reflectance measurements can be described as a double pass measurement, and this is the reason for the 0.5 in equation 3.12. The equation can be used to produce a difference image between the blue and green images, essentially weighted by the absorption characteristics of the MP.

The problem with devices implementing the reflectance technique, is that they are usually adapted high end imaging instruments (e.g. an adapted scanning laser ophthalmoscope). The analysis software would be separate from the imaging acquisition software and each reading would be difficult and time consuming to carry out, and not too comfortable for the subject. Due to the nature of these devices, this adapted approach is time consuming, expensive, and not very portable.

Delori *et al* have also examined the influence of lens scatter and hard drusen on the reflectance and auto fluorescence equations and found these factors to be negligible [9].

3.2.3 Raman spectroscopy

This method of measuring the macular pigment (MP) is based on the phenomena known as Raman scattering. Raman scattering occurs when photons interact with molecules in such a way that energy is either gained or lost (inelastic scattering), as a result the scattered photons are shifted in frequency. Figure 3.4 illustrates the comparison between Rayleigh scatter (elastic scatter, no energy loss after interaction) and that of Raman scatter. Although both Stokes (shift towards lower energies) and anti-Stokes (shift towards higher energies) constitutes Raman shift, only the Stokes shift is considered, due to its greater intensity. Spectroscopy based on Raman scattering is a powerful technique for identifying individual chemical concentrations of the macular pigment carotenoids.

Raman spectroscopy can be used as a noninvasive *in vivo* optical technique to measure the concentration of the carotenoid pigments, lutein (L) and zeaxanthin (Z), in the macular region. As mentioned previously the two macular carotenoids are found to absorb in the blue spectral range. By use of blue-green laser excitation, clearly distinguishable carotenoid Raman spectra superimposed on a fluorescence background can be obtained. By use of resonant molecular excitation in the visible (using an Argon laser), the Raman signals from the single- and double-bond stretch vibrations of the π-conjugated molecule's carbon background can be measured (See figure 2.2 for L and Z chemical structure). The Raman signal is linearly related to the carotenoid content [67].

Gellermann *et al* have performed numerous studies employing the Raman method [67, 68]. Again there are problems with this particular technique. The optical setup is quite
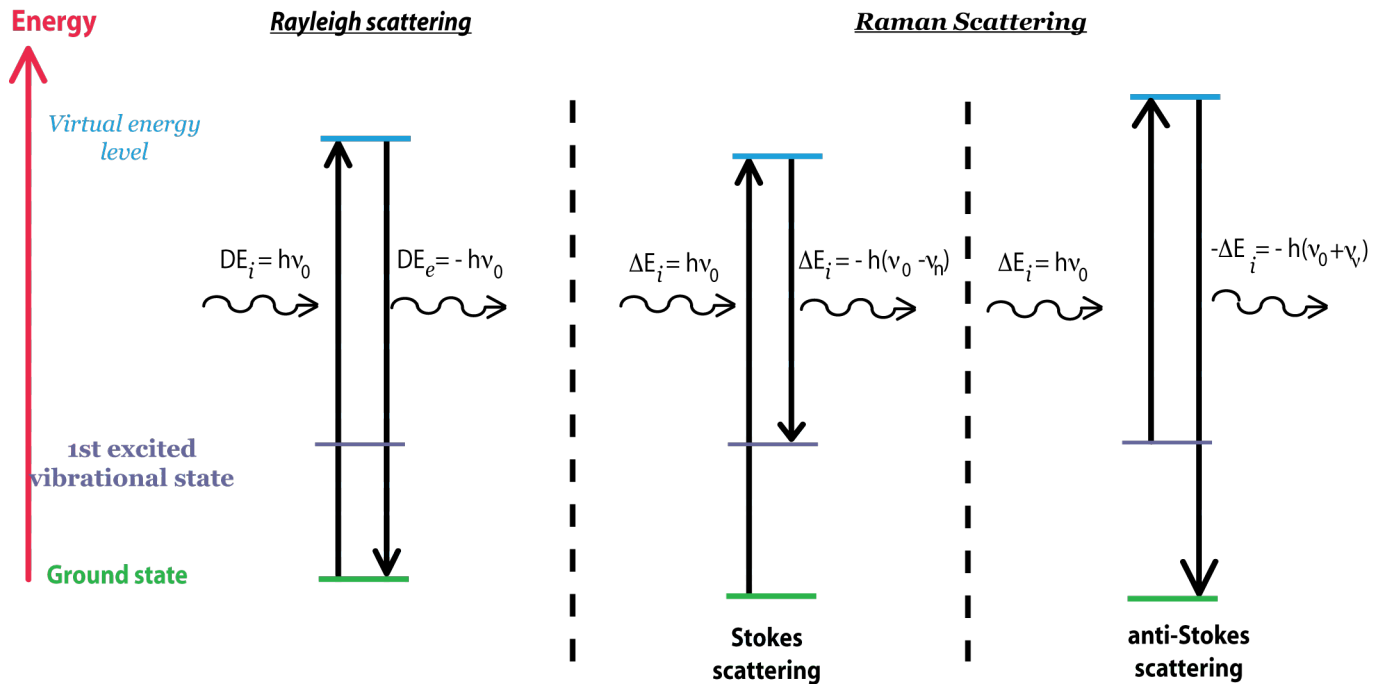
Figure 3.4: Comparison of Rayleigh and Raman scattering. Due to its greater intensity, only Stokes shift is considered in measurement of the macular pigment.

complex and in order to achieve appropriate resonance of the pigment carotenoids a large laser is required[10]. Pupil dilation is also necessary. As a result the device is not easy to use, patient comfort is not a priority, and the device is not very portable. These features combine to make the Raman technique not a attractive solution for rapid and simple measurements of the macular pigment. The complexity of the technique has accounted for its omission from this particular device.

3.2.4 Techniques utilised in this project

As outlined in this chapter, there's a number of different techniques for the measurement of the MPOD *in vivo*. Each technique has its own advantages and disadvantages, both in the measurement of the MPOD and the implementation of the technique in an instrument.

For this particular project, the techniques that were chosen were reflection (RE), auto-fluorescence (AF) and heterochromatic flicker photometry (HCFP). The reflection technique was chosen primarily due to its objective nature and ease of implementation in a real world instrument. It was initially envisaged, that to implement the auto-fluorescence technique very little modification to the reflectance set-up (addition of red filter, increase intensity of illumination light) would be required. For this reason, it was concluded that this new instrument would benefit from this additional objective technique. The most popular technique for the measurement of the MPOD is the subjective technique of heterochromatic flicker photometry. For this reason it was decided to design an instrument

---

[10]Modern lasers may reduce the size of the device, however no such setup has yet being constructed.

that could also achieve a measurement of the MPOD using this established technique. Chapter 4 and chapter 5 will outline various methods to increase the reliability of the subjective technique.

The methods of colour matching and Raman spectroscopy were discounted due to its unreliability and difficulty in implementing.

Chapter 4

Device Hardware

The hardware prerequisites for the successful measurement of the macular pigment optical density (MPOD) *in vivo* are a good optical design, an appropriate control system and an accurate method for analysis of acquired data. Figure 4.1 illustrates the strategy employed for the control of the electronics, and consequently the optical setup. System control refers to an appropriate strategy to coordinate LED, filter wheel and camera activity. Dynamic and independent control over the LED operation, data acquisition and image analysis, should also be available from a single intuitive user interface.
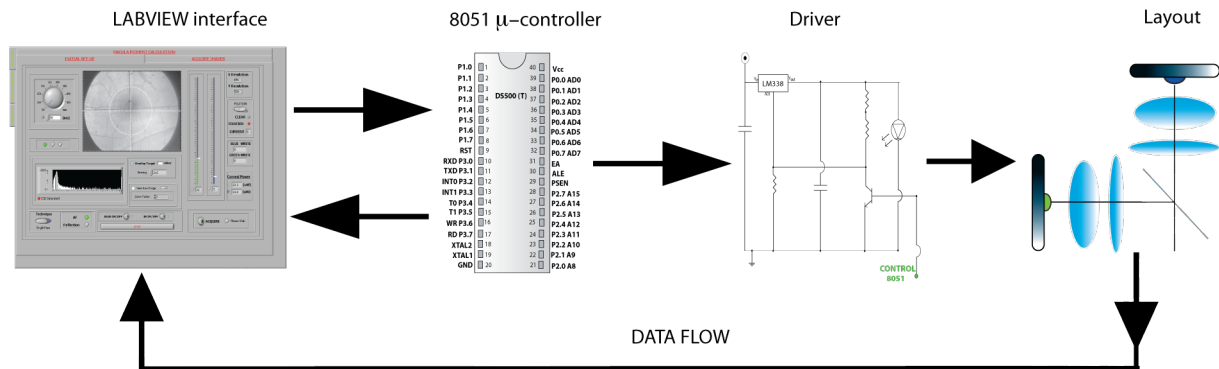
Figure 4.1: The key to successful operation is an accurate and sufficient communication strategy between the interface (Labview platform) and the control system (μ-controller). The control of data flow is governed by the method of handshaking. This mutual acknowledgment of data transfer enables all the desired modes (i.e. green LED adjust, blue LED adjust, filter wheel adjust, exposure adjust etc.) to be independently and easily adaptable from a single terminal.

In the following sections, a description of the hardware highlighted in figure 4.1 will be presented. The design of the components, the features of the hardware, and the strategy implemented to ensure successful and consistent measurement of the MPOD, via appropriate interplay between the highlighted components, will be outlined. Detail of the software and control of data flow will be explained in the next chapter. Selected sections for application of ethical approval can be seen in the appendix[1].

---

[1]Full document not included due to size constraints. The sections selected are deemed to be the more relevant sections in regards safety considerations.

4.1 Optical set-up

The objective of the optical design in this device is to provide a light-efficient device that is capable of calculating the macular pigment optical density (MPOD) *in vivo*, using three different techniques, reflectance, autofluorescence, heterochromatic flicker photometry (HCFP). The transition between the three techniques should require minimum effort, while maintaining high accuracy and consistency in the measurement of the MPOD. The device should be optically simple, portable and robust, while maintaining comfort for the patient and providing an intuitive, easy to use system for the examiner. A schematic of the optical set-up and a photograph of the system can be seen in figure 4.3.
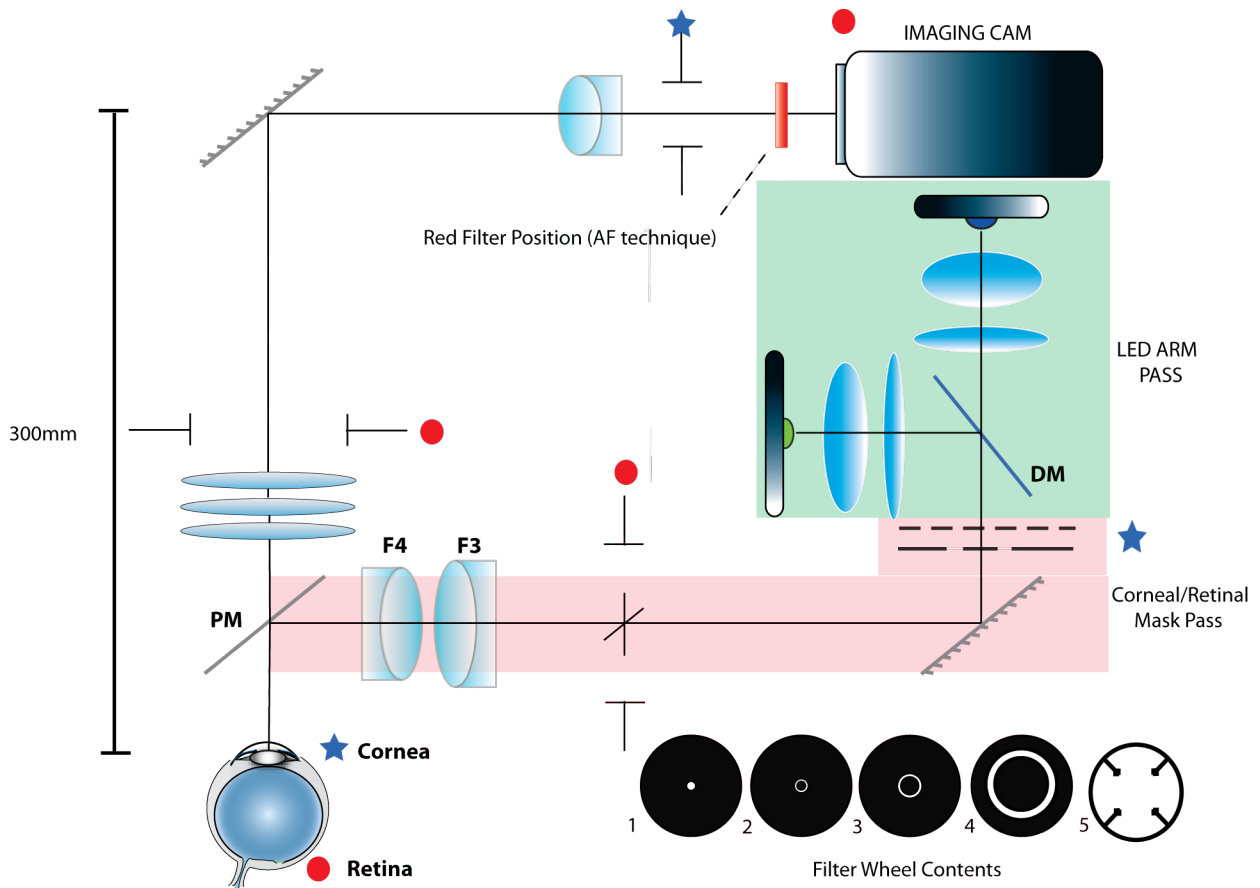
Figure 4.2: Schematic of the optical layout for the measurement of macular pigment optical density (MPOD). The dimensions of the system are approximately 300mm × 250mm. The retinal (●) and corneal (★) planes throughout the system are identified.

The following sections will present each of the optical arms separately, and outline the dependence between the two. The two arms are the illumination arm (highlighted in figure 4.2) and the imaging arm. The illumination arm is distinguished by different highlighting into the LED arm pass and the corneal/retinal mask pass. The purpose of the LED arm pass is to efficiently illuminate the corneal mask, while the purpose of the corneal/retinal pass is to both image the corneal mask on the cornea, and to illuminate the desired area of the retina. The design of these two illumination sections are intimately related and

will be discussed further in the following sections.

(a) Side view of system.

(b) Top view of system displaying retinal and corneal conjugates
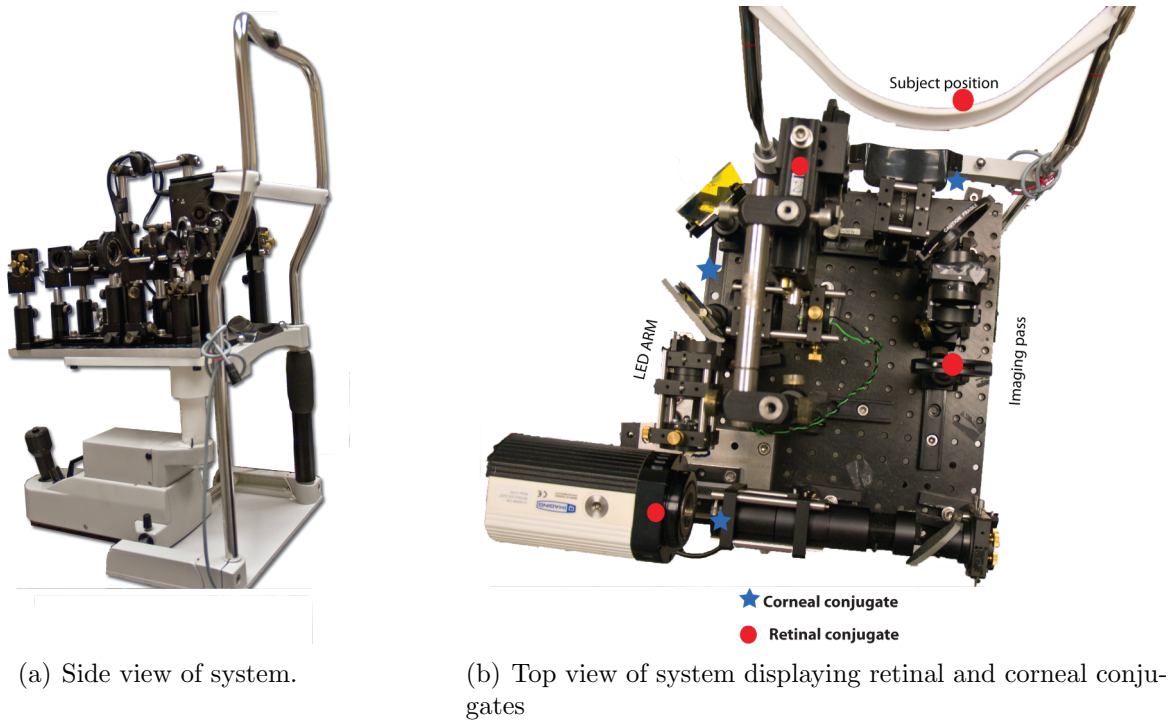
Figure 4.3: The device is mounted on an adjustable x-y mount (sourced from Zeiss). This allows for comfortable, rapid and accurate alignment of subjects.

The filter wheel is located in the corneal/retinal mask pass (retinal plane) and its contents are also shown in figure 4.2. This plane is adjustable for each subject, and also for each technique[2]. The system is folded using mirrors to produce a compact system which can be mounted on an adjustable base (figure 4.3). The location of each of the corneal and retinal planes are also highlighted in the diagram and can be used to trace the function and logic of the design of the device.

4.1.1 Illumination Arm

The success of the imaging arm of the system, depends on the illumination arm achieving certain requirements. In particular, an appropriate area of the retina must be uniformly illuminated and the problem of on-axis corneal reflections must be solved. In addition, the choice of beamsplitter, to direct light into the eye must be biased towards the imaging pass, and finally the design must contain a retinal plane within the illumination arm, which can be easily adaptable and manipulated.

Beamsplitters (Dichroic and Pellicle)

There are two beamsplitters employed in the illumination arm of the system, a pellicle beamsplitter and a dichroic beamsplitter. The pellicle beamsplitter will be initially de-

---

[2]Subjective technique requires no dilation therefore the eye will accommodate.

scribed (PM in figure 4.2).

The illumination pass and imaging pass of the system are intimately related but only share one common element. From figure 4.2, it is clear that this common element is the beamsplitter (PM), which reflects the illuminating light into the eye and allows the transmission of the subsequent reflected retinal light (or fluorescence light in the AF technique) into the imaging arm. The choice of this element is crucial and establishes restrictions on the design of both the imaging and illumination pass. Primarily the physical constraints of this element must be sufficient to fit into a small portable system. In addition, the optical performance of the element must be devoid of any secondary reflections, chromatic effects must be at a minimum, low dispersion is required and it must allow the maximum transmission of light back into the imaging arm (maximum information from the eye). A pellicle beamsplitter of 92 % transmission and 8 % reflection was therefore chosen. Figure 4.4(a) shows the spectral behavior of the element for both transmission and reflection.
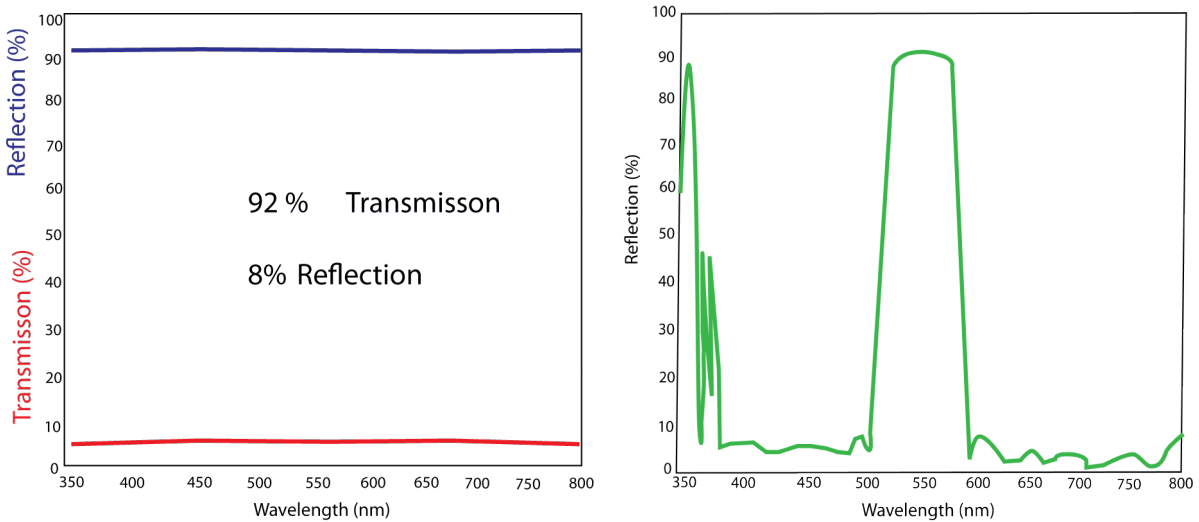
(a) Spectral behavior of the pellicle beamsplitter used in set up. Illumination pass has loss of 92%.

(b) Spectral behavior of green dichroic used in set up

Figure 4.4: Behaviour of beamsplitters used in the illumination pass of the system. Graphs adapted from the supplied datasheets for each of the elements.

The second beamsplitter used in the illumination pass is the dichroic beamsplitter (DM in figure 4.2). This accommodates a simple method to reflect the green light and transmit the blue light into the system. The spectral behaviour of the beamsplitter can be seen in figure 4.4(b). Figure 4.5 illustrates the effect of the dichroic on the power of the green LED. Priority in the choice of the element was minimum loss of power (over the spectral range employed) and the demostrated loss of approximately 10% is deemed sufficient.
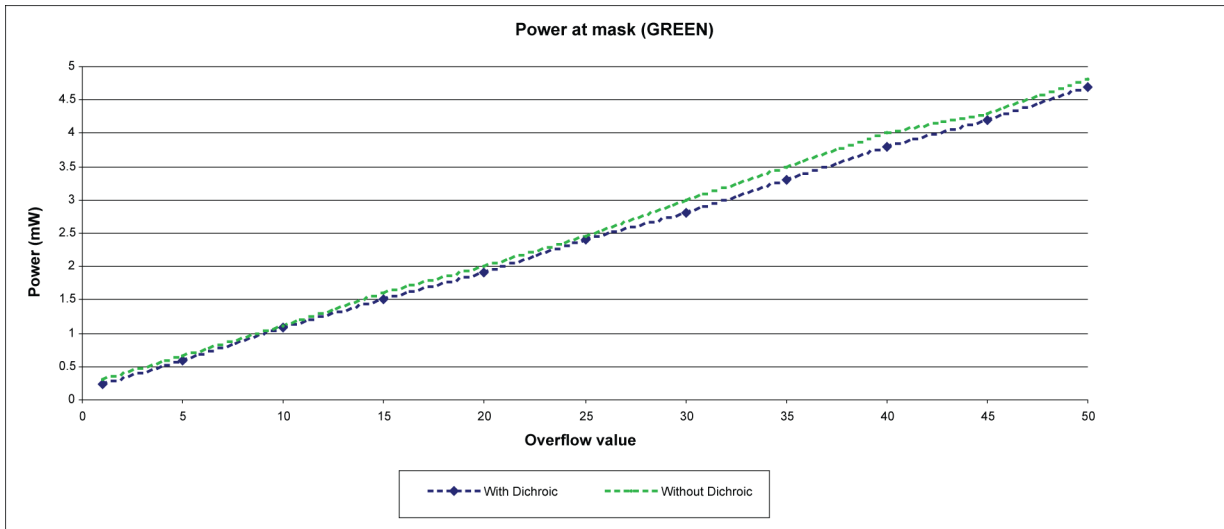
Figure 4.5: The graph illustrates the loss in power due to the dichroic in the system. The power is measured at the mask and illustrates approximately a 10% loss in power over the range of overflow values. These overflow values are the LED level chosen on the Labview interface and range from 0 to 50. This value is coded and sent to the 8051 and in combination with the off resistance produces the desired LED intensity. (In this case off resistance of 17Ω. See later sections for a more complete description)

Corneal mask and holographic diffuser (Restrictions on illumination area)

In order to combat the detrimental on-axis reflections, an image of the corneal mask is formed on the cornea (see figure 4.2 for corneal planes throughout the system).
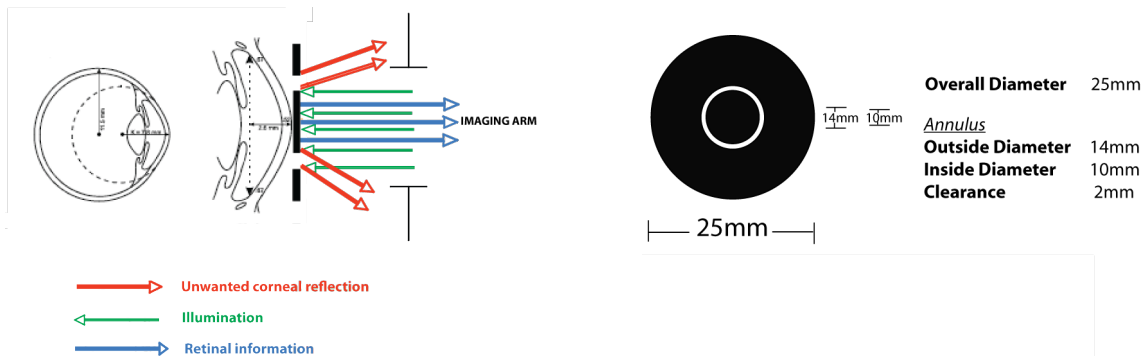
(a) Combating unwanted corneal reflections by imaging through central 3mm. (Further defined by corneal stop in the imaging arm. See figure 4.2)

(b) Corneal mask design. Dimensions for 2 to 1 magnification, ie 7mm pupil with 5mm obstruction. Imaging pupil determined by imaging arm design.

Figure 4.6: Design of mask to combat on axis corneal reflections

Figure 1.3 demonstrates such on axis reflections from the cornea and lens. The mask must also provide an efficient method for allowing the desired area of the retina to be homo-

geneously illuminated. The dimensions and position of the mask, within the illumination arm, is determined by the characteristics of the two doublets in the illumination arm, and the desired image dimensions. In the case of this particular project, the subjects pupil is 7mm in diameter[3], and the imaging pass extracts the retinal information through a 3mm pupil in the corneal plane.
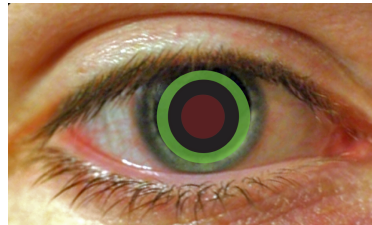
Figure 4.7: Corneal mask representation. Illumination of the retina is provided by the green area. This is 7mm in diameter. The central black obstruction combats the on axis reflections from the cornea (refer to figure 4.6(a). Imaging is provided through a central 3mm (represented by red above) which is defined by the corneal stop in the imaging pass (see figure 4.2)

X_1: Radius of desired illumination X_3: Required cone radius = $X_1 + X_2$ α = Cone angle to achieved desired illumination

X_2: Obstruction size d = Equivalent axial length (17mm for eye) $\alpha = 2*\tan^{-1}\left(X_3/d\right)$
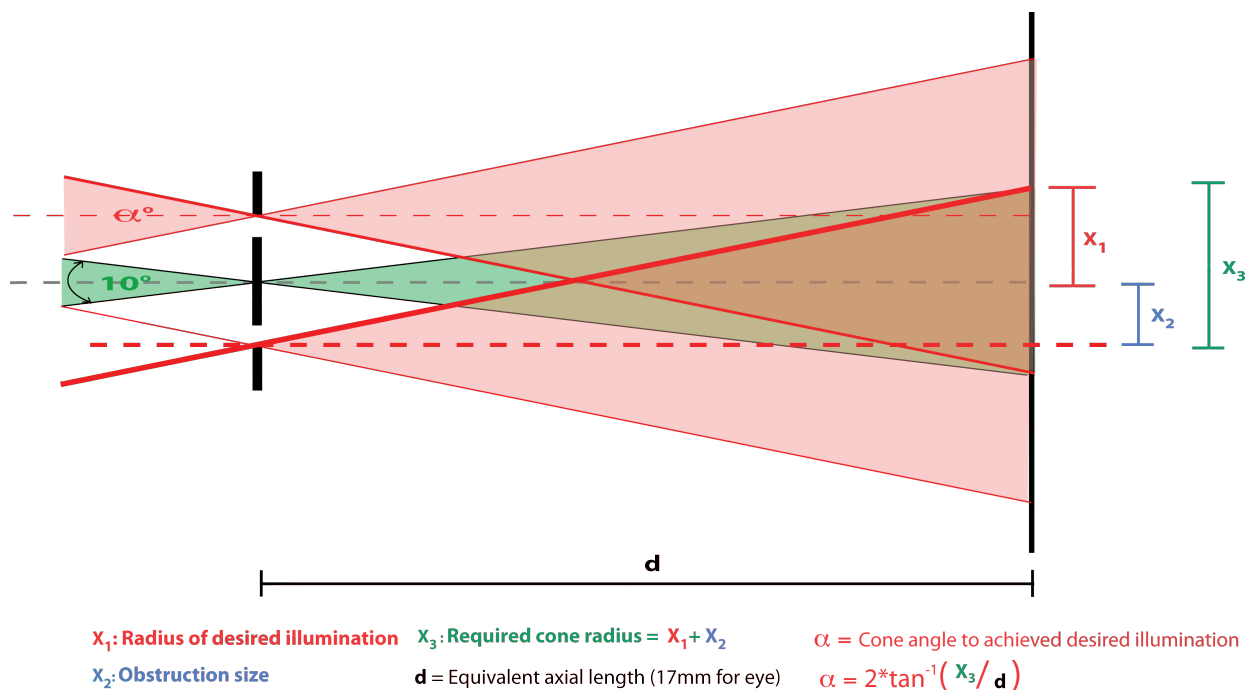
Figure 4.8: Restrictions imposed by use of central obstruction, on utilising on-axis illumination to achieve homogenous retinal illumination.

The pair of doublets provide a 2 to 1 magnification, (F3=160mm, F4=80mm, image formed 80 mm from F4 is half that of object dimensions. Object placed 160mm from

---

[3]Further investigation must be carried out in regards to older subjects and their ability to dilate to such diameters.

F3) which determines that the mask dimensions are 14mm outer ring, with 10mm inner obstruction. This results in a 7mm outer ring with a 5 mm inner obstruction at the cornea. This also allows for adequate imaging through the central 3mm of the pupil while removing the possibility of any potentially contaminating reflections from infiltrating the imaging pass.
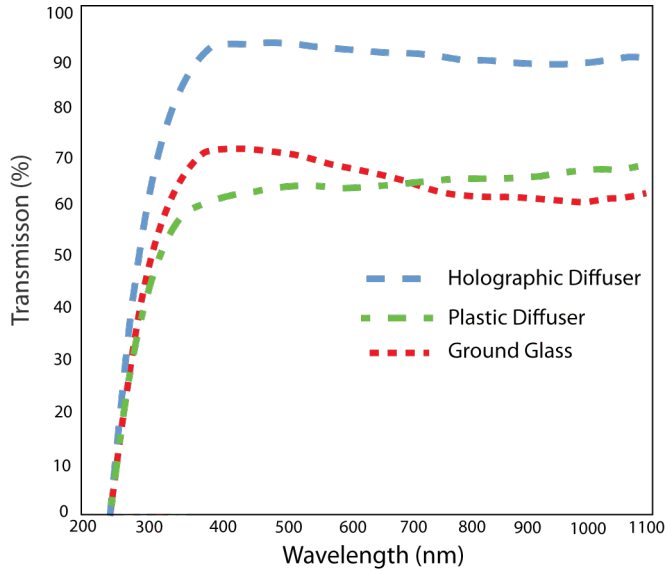
(a) Comparison of different diffusing materials. Adapted from Newport Optics catalog

(b) Photograph of the holographic diffuser used in the setup

Figure 4.9: A comparison of different diffusing elements illustrating the transmission of each and a photograph of the holographic diffuser used in the setup.

The characteristics of the two doublets not only determines the magnification, but consequently the beam convergence angles. Due to the central obstruction of the mask, this will also have an effect on the required beam angle to produce the requisite uniform retinal illumination area. Simply, to produce a 10° area, if there is no central obstruction, the entrance beam angle has to be 10°. However due to the central area being blocked the entrance angle required to produce an uniform illumination area of 10°, the entrance angle has to be at least 32 ° (see figure 4.8).

The choice of the holographic diffuser was made primarily due to its high transmission, and ability to somewhat shape the beam angle. The diffuser also has the task of destroying the image of the LED structures, which are formed on the diffuser, and consequently prevent any contamination of the cornea, and any unwanted artifacts being imaged on the retina. The diffusing element employed in this project is the 10° 25mm holographic diffuser. Due to the magnification of this pass, results in a diffused angle of at least 20° (if the incident light on the diffuser is collimated, however in this system the incident light is convergent, which results in greater angle of diffusion).

Luxeon LEDs (efficient LED illumination arm)

The choice of the illumination LED[4]s used in this project was due to their spectral characteristics, reliability and their high radiant power. As outlined in previous chapters, the techniques employed in this project required analysis of wavelengths maximally absorbed by the macula pigment (MP) and minimally absorbed.

Figure 4.10 illustrates the spectral content of the blue and green LED as measured in the lab with a spectrometer[5]. The absorption spectrum of the MP is included to illustrate the suitability of the LEDs to this specific task. Due to the choice of the pellicle beamsplitter (figure 4.4(a)), it was necessary to design a photo efficient illumination arm, with the minimum wastage of light before this beamsplitter. The illumination arm is divided into two sections, one section to deliver blue and green illumination of the corneal mask, and then the imaging of the mask on the cornea with consequent illumination of the desired area of the retina.
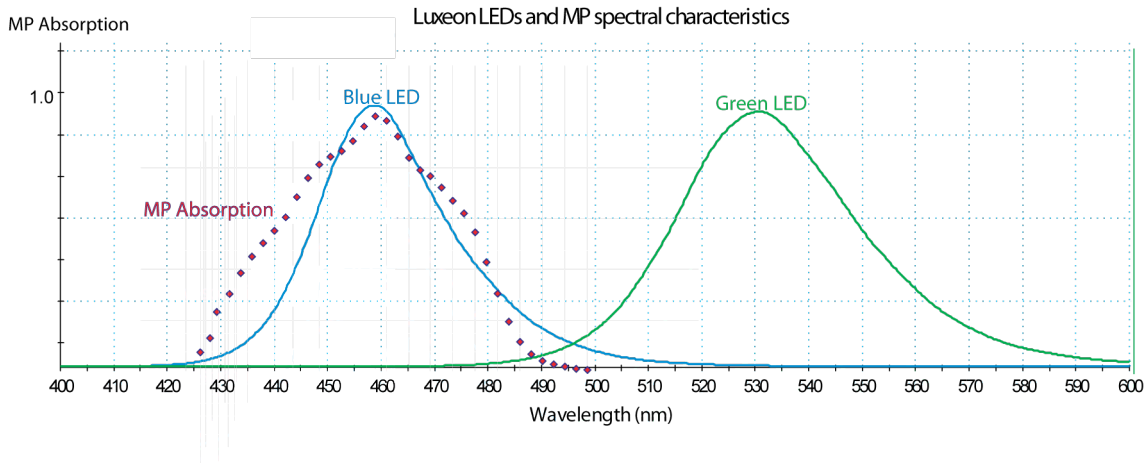
Figure 4.10: Luxeon LEDs spectral characteristics overlaying MP absorbance as calculated by Brown *et al*(Quoted in [9]) for blue (λ_1) and green (λ_2). The LEDs spectral distribution(overlap of green LED spectrum into the MP absorption and sprectral width of blue LED) are accounted for using extinction coefficients. See chapter 5 and figure 5.37 for complete explanation.

Figure 4.11 shows a schematic of the first section of the illumination pass. The dichroic[6] allows green and blue illumination of the diffuser[7] and mask. The choice of the two singlet lenses were due to the fact that image quality was not a priority and chromatic effects were not a consideration. The characteristics of the lenses were based on the LED attributes outlined in figure 4.12. The LEDs are the Luxeon V Star, green (LXHL-LM5C) and royal blue (LXHL-LR5C).

To avoid unnecessary wastage of light from the LEDs, the structure of the LED (Figure 4.12(a)) was imaged, and appropriately magnified, to uniformly illuminate the mask

---

[4]Light Emitting Diode
[5]Ocean Optics USB2000 Fiber Optic Spectrometer.
[6]See figure 4.4(b)
[7]See figure 4.9(a)
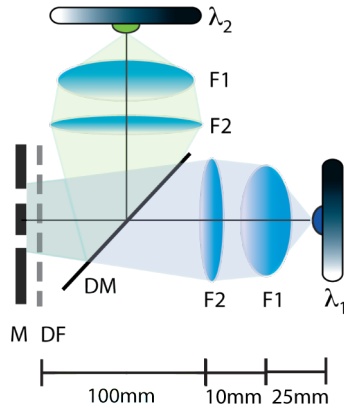
Figure 4.11: Design of LED illumination arm for efficient illumination of the mask. The two 30 mm diameter singlets F1 and F2 have focal length of 25mm, and 100mm respectively. DM is the dichroic mirror (see figure 4.4(b)), DF is the diffuser (see figure 4.9(a)) and M is the corneal mask (see figure 4.6(b)).

annulus (approximately 14mm). The diffuser not only destroys the image of the LED structure in the corneal conjugate (avoiding re-imaging on the retina) but also controls the entrance beam angle to attain uniform retinal illumination (see previous section and figure 4.8). As outlined in figure 4.12, the LED emitters emit light at an angle of approximately 80°. The dimensions of the emitting area are 3mm × 2mm, so in order to uniformly illuminate the mask area, a magnification of 5 is required. Due to constraints on lens focal lengths, and on system size a tradeoff of a magnification of 4 was reached. The beam divergence on the diffuser as a result is 20°.

(a) LED emitter array.

(b) Beam divergence from the Luxeon LEDs. Design of LED arm was based on a 80° emission angle.
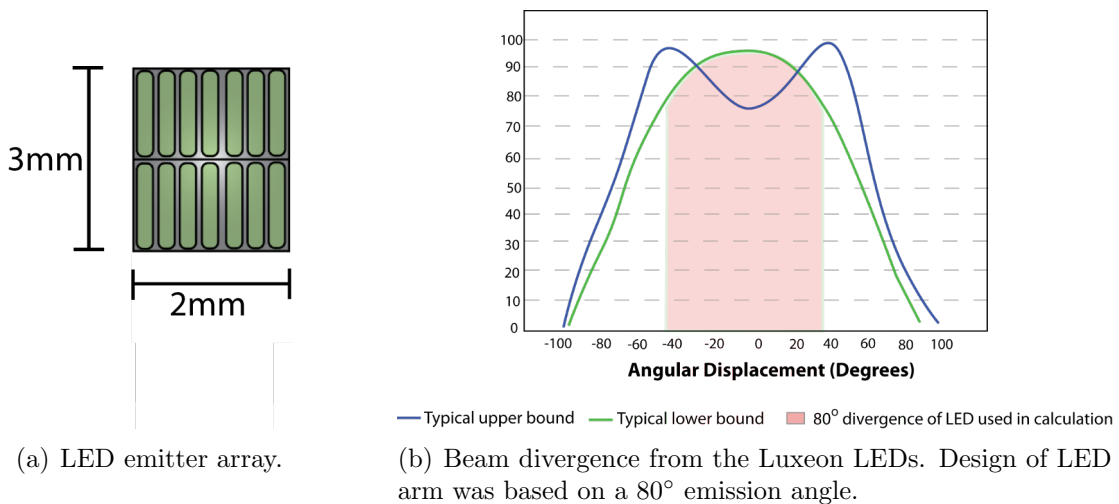
Figure 4.12: Characteristics to be considered in the design of the LED optical arm.

Filter wheel

The decision to include a motorised filter wheel in the device was made in order to avoid physically changing the retinal masks each time a different area of the retina was to be illuminated i.e for pigment distribution in the subjective technique, or displaying fixation target for objective techniques.

Filter wheel position	Target	Mode
1	0.5 degree (default)	HCFP
2	1 degree	HCFP
3	3 degrees	HCFP
4	Parafoveal (7 degrees)	HCFP
5	Fixation target	RE and AF
6	Clear	RE and AF

Table 4.1: Various targets and their position within the filter wheel

The filter wheel used in this project is the FW102 motorised filter wheel from Thorlabs. This particular element was chosen due to its capacity (can hold up to 6 filters of 25mm diameter), and its ability to be triggered via a TTL pulse. The operation of the filter wheel can be controlled by the 8051(via BNC cable), managed from the Labview interface (the code is outlined in the next chapter).

The filter wheel can hold 6 different masks, four for the flicker technique (four illumination areas on the retina, see table 4.1), 1 fixation target and 1 blank. The four designs for the flicker technique can be seen in figure 4.13. The effect of each of these masks is outline in chapter 6.
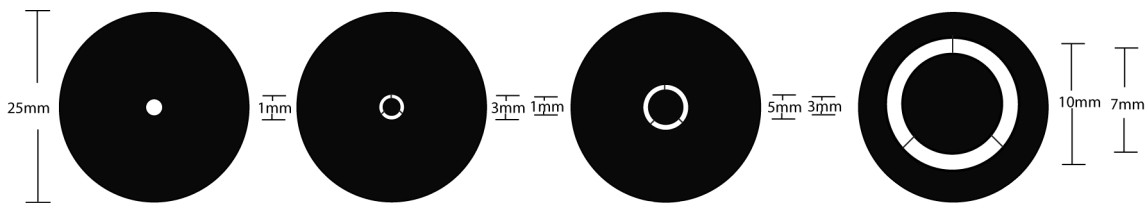
Figure 4.13: Design of retinal masks used for HCFP and fitted in filter wheel. Positions within the wheel are stated in table 5.5.

The filter wheel position can be altered either by a button on the filter wheel itself, or preferably by the external TTL pulse. The main electrical characteristics to be considered

when designing the TTL pulse are outlined in table 4.2. The next chapter will outline the design of the TTL pulse and will refer back to this table.

Parameter	Minimum Pulse width (ms)	Max Rate (pulses per s)	Power (V)
BNC Input trigger	1.0	0.5	-
Power at DC	-	-	5

Table 4.2: Primary characteristics to be considered when designing the TTL pulse.

4.1.2 Imaging Arm

This section will concentrate on the design of the imaging pass of the system (see figure 4.2). The primary concern when designing the imaging arm is for the system to be optically simple and as compact as possible[8] . The predominant portion of this section deals with an unfamiliar imaging design, incorporating a novel objective lens, which delivers quite adequate imaging performance while fulfilling the prerequisites of cost effectiveness, simplicity and considerations over system size. Examination of the remaining elements that constitute the imaging pass will also be discussed.

Objective lens

A number of factors determine and restrict the choice of objective lens[9] that can be utilised in the system. The primary consideration is that the lens is capable of imaging a retinal area of 10° through a pupil diameter of 3 mm (see figure 4.7). In addition, the image performance of this element must complement any other refractive elements in the imaging path (in this case the focusing doublet) and in combination, should produce an image quality which renders the software capable of measuring the macular pigment optical density (MPOD).

The working distance between the objective lens and the subject position is also a vital consideration, and must be comfortable for the subject, while remaining within the size restrictions of the system. The design of the illumination pass produces a pupil plane 60 mm from the pellicle beamsplitter, and is chosen to be the minimum distance that can comfortably accommodate all potential subjects. Due to the working distance and the desired imaging area on the retina the lens diameter required should be approximately 30 mm. This relatively large diameter lens may restrict the potential candidates freely available on the market and thus a cheaper, more general solution is required.
The lens choice due to availability and cost was between a doublet and a singlet. The system requires a certain magnification, dictated by the finite CCD chip dimensions, and is restricted to a certain size[10]. To achieve these goals, the objective lens is to have a focal

---

[8]Optically simple refers to constituting a small number of optical components, while size refers to fitting on 300 mm × 300 mm footprint

[9]See figure 4.2

[10]Fit on a breadboard approximately 300 mm × 300 mm.
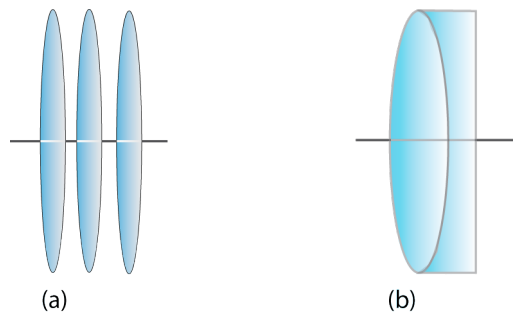
Figure 4.14: The two considerations for the objective lens of the system. A triplet consisting of three separate singlets or a doublet of equivalent power (doublet choice actually requires demagnifying stage consisting of an additional two doublets to produce intermediate image of sufficient quality across the full field (see figure 4.15)). Both options operate at approximately f/2

length of approximately 70 mm, which forms an intermediate image, which can be refocussed and demagnified by the focusing lens to achieve the desired image size in the image plane (CCD). A singlet of this power in isolation, would induce a detrimental amount of spherical aberration and field curvature in the intermediate image. In addition the lens would display insufficient chromatic behaviour[11] and subsequently the final images would be unusable.
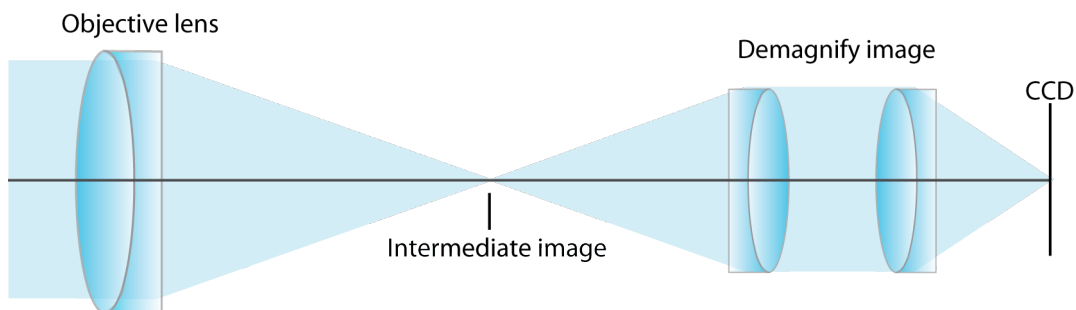
Figure 4.15: Alternate imaging design utilising a doublet objective lens and a two doublet demagnifying system.

An equivalent doublet in isolation, as in figure 4.15, would demonstrate similar behaviour (however there would be improvement to the chromatic correction but off axis performance would be greatly limited), and would require an additional doublet to account for these spherical and field curvature effects. While field curvature can be corrected by insertion of an additional refractive element (addition piece of glass designed to negate the original curvature) this does not correct astigmatism, and must be specifically manufactured to account for the curvature produced by the specific lens in the system. This 3 doublet imaging system, as illustrated in figure 4.15, is a common design for a fundus camera[69].

---

[11]For green (535nm) and blue (460nm) illumination wavelengths.

However, due to the magnification requirements of this system, this layout would greatly lengthen the overall path and subsequently exceeds the desired dimensions.

$$
\begin{aligned}
P_{power} &= \frac{1}{f_1} + \frac{1}{f_2} + \frac{1}{f_3} \\
F_{focal} &= \frac{1}{P_{power}}
\end{aligned}
\tag{4.1}
$$

Figure 4.14(a) illustrates simply the final design of the objective lens in the system. It is composed of three singlet lenses, each individually of focal length 200 mm, which gives an effective focal length of 67 mm (applying equation 4.1, thin lens equation for elements all in the same plane). Each lens is relatively low power lens and thus field curvature is dramatically reduced. In addition this combination provides very good off-axis performance, especially for astigmatism. Spherical aberration is quite low and of opposite sign to the focusing doublet in the system, and as a result complements this lens in terms of final image quality. The exit pupil is very near (26.6 mm) the back side of the focusing doublet which helps to obtain large beam overlap in the central part of the lens[12]. The overall system size is within the constraints and results in a compact, cheap, high performance system.

Focusing lens

The purpose of the focusing lens is to re-image the intermediate retinal image, formed by the objective lens, at the correct magnification determined by the CCD chip dimensions[13]. The behaviour of this lens should also compliment the performance of the objective lens, with the goal of producing a practical on the CCD.
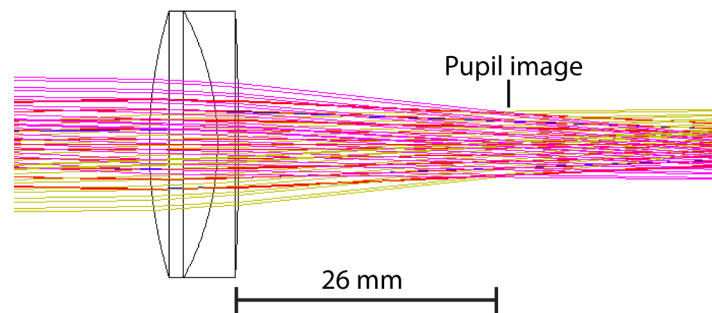
Figure 4.16: The exit pupil and the beam overlap in the focusing doublet as predicted by Zemax, for the two colours used in the device (represented by the differing colours in the illustration).

The focusing lens also forms an image of the corneal plane which presents an opportunity to insert a diaphragm to further define the imaging pupil, and thus improve the overall

---

[12]Doublet design is optimised to work on infinity, and gives best performance up to .75 of overall diameter.

[13]Approximately 6 mm in diameter.

quality of the final retinal image[14]. As mentioned previously, this pupil is formed very close to the doublet and thus provides very good beam overlap within the lens (formed within the optimal 0.75 of lens diameter), and as such is operating within the optimal design constraints of the lens. Figure 4.16 displays this beam overlay as predicted by Zemax[15] and the formation of the pupil image after the doublet.

As in the case for the objective lens, chromatic effects eliminate any possibly of using singlets in isolation, and thus the lens choice has to be a doublet.
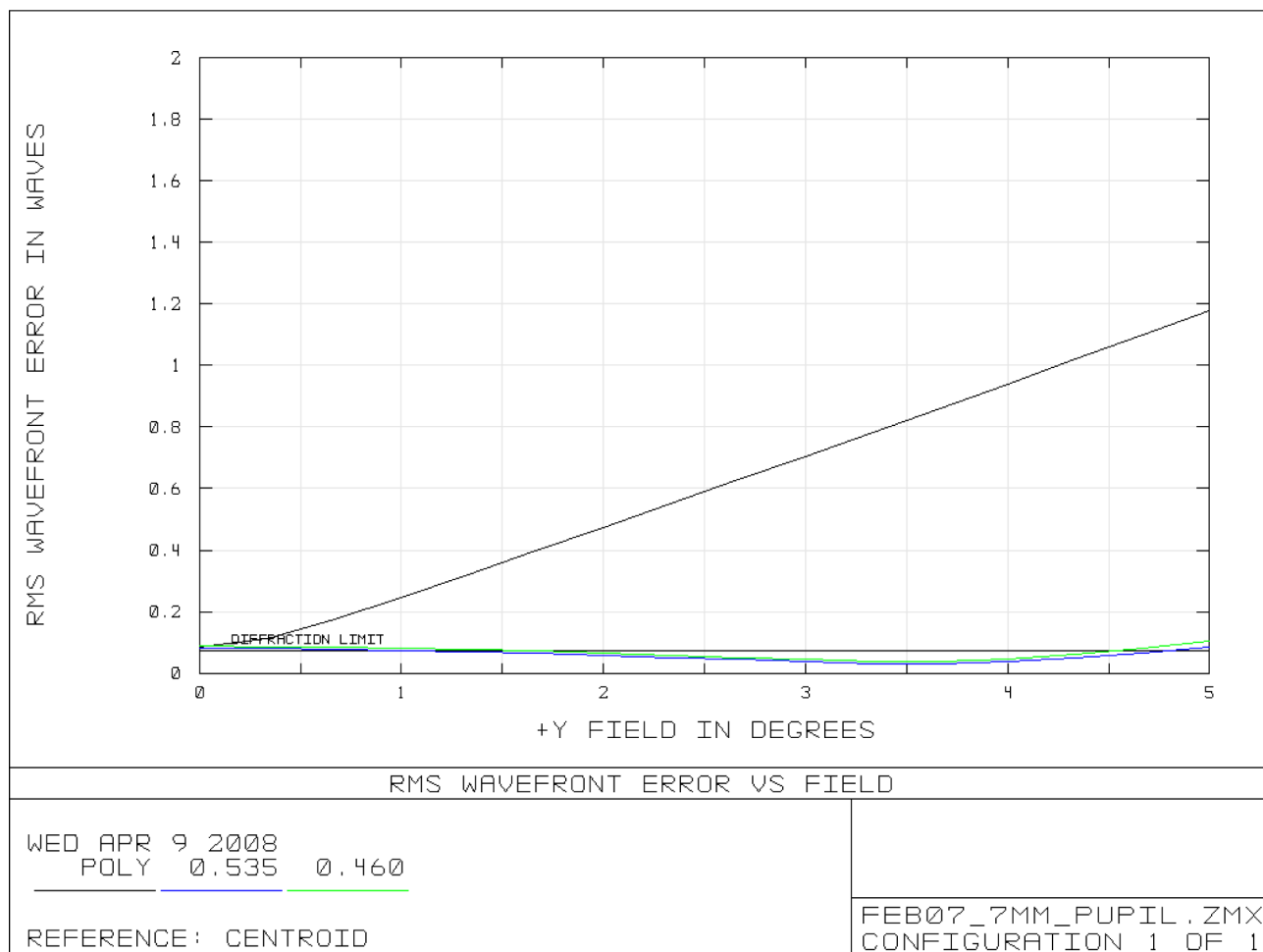
Figure 4.17: RMS vs field angle for the imaging system. The diffraction limit (not clear from graph but represents $\lambda/14$) is also included and displays that the system in theory, can perform at the diffraction limit. The polychromatic curve assumes both LEDs to be on at the same time which is not the case and so may be disregarded.

---

[14]Essentially improves contrast of image. Behaviour similar to that of a confocal setup.

[15]Zemax is a widely-used optical design program sold by Zemax Development Corporation of Bellevue, Washington (formerly Focus Software). It is used to design, optimize, and tolerance optical systems.

CCD sampling

Figure 4.17 is produced in Zemax and illustrates the RMS[16] wavefront error versus image field angle for the imaging arm of the system, for wavelengths 535 μm and 460 μm. The graph also includes the diffraction limited case and theoretically the imaging pass performance for operating at this fundamental limit[17]. Figure 4.18 displays the RMS radius (in μm) for the imaging arm, which essentially represents the FWHM[18] of the PSF of the system. This can also be stated as the maximum pixel size that can be used to sample the image, without any information loss taking place[19].
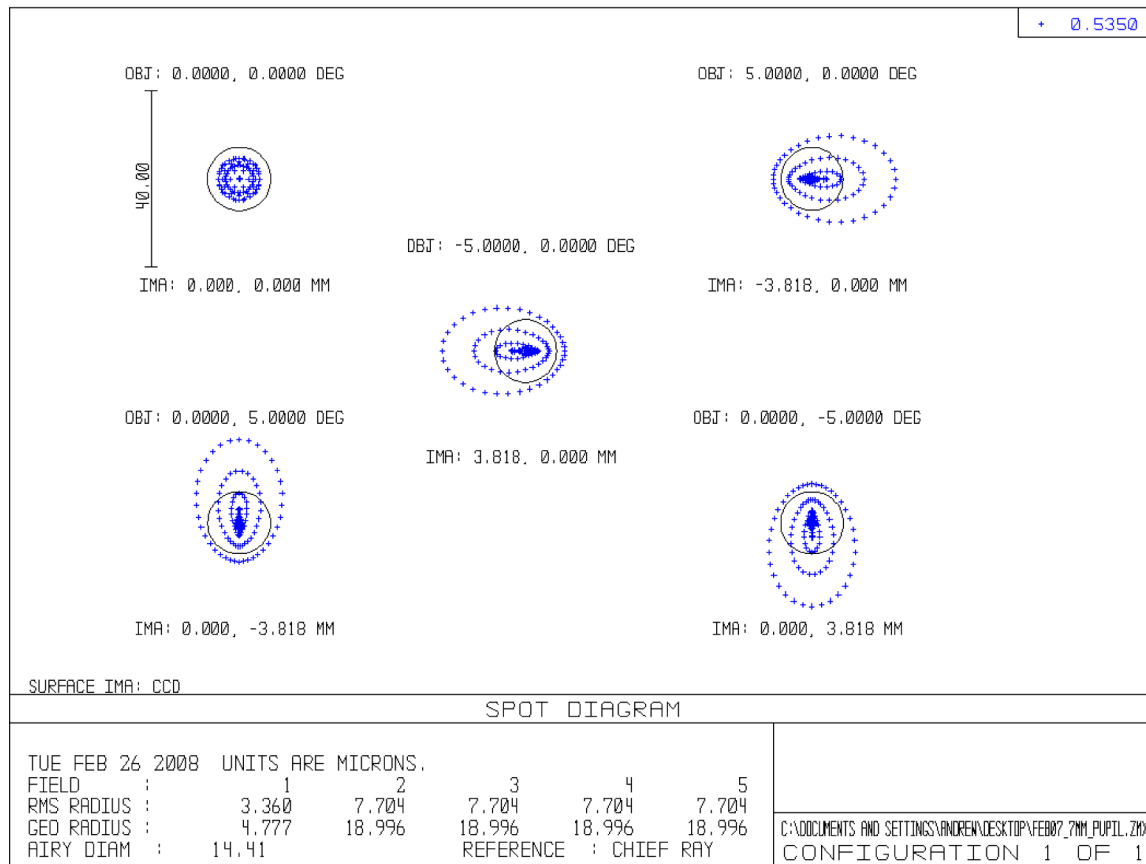
Figure 4.18: Theoretical performance of the imaging arm of the device as predicted from Zemax. The dark circle represents the Airy disk. The Airy diameter is 14.8 μm with an RMS error radius of approximately 7.7 μm. This is for 535 nm, a similar performance is achieved for 465 nm.

Due to the high performance of the system optics on-axis it can be said that the camera is under-sampling the image. For the off-axis imaging, slight aberrations are induced which

---

[16]Root mean square, for this case measured in waves

[17]This assumes perfect eye, however this is not the real world case and as such the system is not a perfect imaging device.

[18]Full width half max.

[19]RMS spot diameter requires 2 pixels per spot minima for sampling without any information loss occurring. Essentially Shannon's limit.

pushes the RMS error to 7.7 μm, which is above the pixel size of the camera (pixel size 6.75 μm) and as such is adequate sampling for the imaging arm. However the eye itself is far from aberration free and its characteristics from subject to subject will be unknown, and consequently cannot be corrected. Therefore the best strategy is to endeavor to make the system arm as optically good and sufficiently sampled to produce the best image of the imperfect eye. Fortunately the success of the device is not entirely dependent on high resolution imaging, but reflectance values, subsequently diffraction limited imaging is not required for the measurement of the macular pigment optical density.

Pupil alignment

Pupil alignment is vital in any device attempting to successfully image the retina. It is necessary to place the pupil in the correct position, in order to image the retina at the desired magnification and to make full use of the corneal mask, to combat unwanted cornel reflections . Previous designs of this device achieved proper alignment, using IR[20] LEDs to flood illuminate the cornea and an IR sensitive camera provides an appropriately magnified image of the pupil on an external monitor. The design required an IR dichroic to be placed in the imaging pass, to reflect the IR light to the IR sensitive camera. Since in the AF method the retinal information is acquired at approximately 710nm the dichroic affected this already low signal. Solutions to this problem included removing the dichroic when inserting the red filter for AF measurements, however, this was time consuming (required careful handling of the optics, i.e gloves to avoid contamination of the surfaces). This previous design also required the inclusion of further imaging optics to re-image the pupil and of course the requirement of the additional IR camera. These additional optics increased the size and complexity of the system.

The final solution was to remount the entire device on a Zeiss adjustable mount (see figure 4.3) and alignment was confirmed by both the examiner looking at the mask on the subjects pupil and the live view of the retina on the Labview interface, and adjusting the mount where appropriate. The removal of this IR pupil monitoring ensured that the imaging pass was as clean as possible, and the only elements present in the imaging pass were those essential for imaging the retina.

Imaging camera

The imaging camera used in the system is the retiga EXi from Q-imaging. The camera was chosen due to its high resolution (1360 X 1036), high quantum efficiency (70% at 500nm), spectral characteristic of the CCD chip (see figure 4.19), it's 12-bit digital read-out, availability of Labview VIs, and low readout noise (8e-). The camera is connected to the host computer via IEEE 1394 (firewire cable). This not only provides power to the camera, but allows a high bandwidth (40MBs^{-1} - 1394a; 80MBs^{-1} - 1394b) interface for rapid transfer of images.

In addition to this the ability to externally trigger the camera allowed a sophisticated method of synchronizing the camera to the system. The external trigger port is a 6-

---

[20]Infrared, approximately 900nm

pin miniature circular DIN connector, and due to this ports isolation from the cameras electronics an external power supply is required for successful operation.
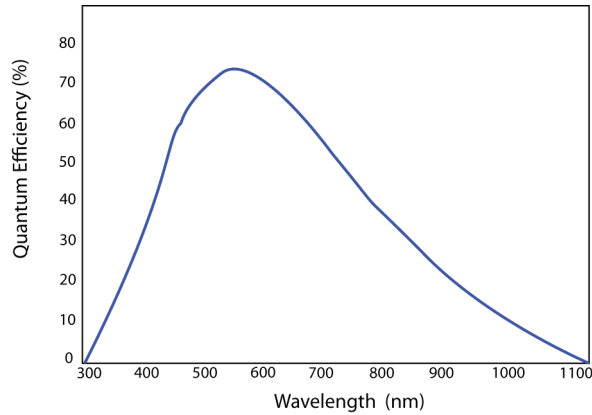
Figure 4.19: Spectral response of the ICX-285 progressive scan interline monochrome CCD chip used in the retiga EXi.

To trigger the camera a 5V TTL pulse must be delivered through the appropriate pin on the DIN connector. The electronics to power and control the triggering of the camera can be seen in figure 4.23

Red filter

The purpose of the red filter in the imaging pass is to detect the emission wavelength of the excited lipofuscin. The filter will block any reflected light from the green and blue exciting light and allow only the emission wavelength. Since the camera is not very sensitive in this range it is vital that the transmission in the desired wavelength is at a maximum, and to avoid contamination that the cut off is at a maximum. The filter used in this project is a red additive filter from Edmund optics, model number NT52-528. The typical transmittance curve is displayed in figure 4.20.
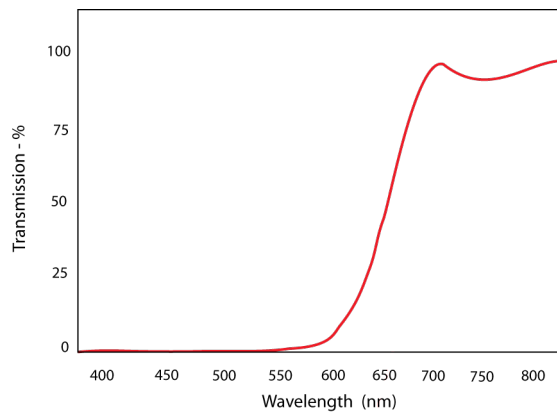
Figure 4.20: The performance of the red filter used in the system. Adapted from the specifications supplied by Edmund optics for the additive filter NT52-528.

4.1.3 System mount

Essential to rapid acquirement of sufficient quality images is the ease and speed at which the subject can be aligned in the system. The comfort of the subject must also be taken into consideration. For this reason the Zeiss adjustable mount was chosen. The mount has good x-y translation and limited but adjustable height control. The subject is sta-blilised by means of a chin and forehead rest and is of minimum discomfort to the subject.

The optical layout of the system is mounted on a modified Linos base. This base is connected onto the Zeiss device by means of a specifically designed mount. The mount is made from perspex, which is light but strong. The design is capable of holding at least 15 kg. This enables rapid and accurate alignment of a subject, for both eyes, while retaining comfort and portability. See the photograph of the system in figure 4.3 to see the fully mounted system.

4.2 System control

The control of the system refers to the controlling of the LED intensity, synchronisation of the LED flash and camera triggering, control of the IR LEDs and management of the filter wheel. An overview of the hardware required will be outlined in the following sections, while an overview of the software can be found in Chapter 5.

4.2.1 Micro-controller

The Dallas Ds5000 series microcontroller is utilised in this project, to manage and dictate the operation of the system. The package is a fully 8051 compatible 8-bit CMOS μ-controller. The DS5000 executes an instruction set which is object code compatible with the industry standard 8051 μ-controller. In particular, this project uses assembly code complied by TASM to achieve the desired output (see chapter 5 for more detail). A full list of the many features of the DS5000 can be examined in the appendix. For full pin out of the chip see figure 4.21(a).

On-board crystal (XTAL)

The speed at which the DS5000 operates is limited both by the physical constraints of the architecture of the chip itself and the speed of the on-board XTAL. The chip architecture limits the speed to 16MHz, so any XTAL operating at a faster rate is redundant. A number of differing XTAL speeds were tested and the eventual chip used in the project operates at 14.7456 MHz. This is the maximum available XTAL speed for this particular 8051 chip. However, as will be discussed in later sections, this limits certain aspects of the operation of the device. This limit is imposed by the fundamental limit of the duration of each clock count, which is dictated by the XTAL speed. This clock count is calculated as follows. Each machine cycle on the chip is timed by 12 XTAL pulse, therefore;

(a) PIN ASSIGNMENT DS5000

(b) SFRs Addresses (adapted from [70])

Figure 4.21: Pinout of the 8051 chip and schematic of memory allocation on the chip. The memory loctions are given in HEX.

$$XTAL = 14.7456 \text{ MHz}$$

$$1cy = \left(\frac{12}{XTAL}\right) \mu s$$

$$1cy = 0.8138 \ \mu s \tag{4.2}$$

This is the fundamental limit on the speed at which the chip operates, and dictates the operation of the on board timers on the chip and thus influences the behaviour of the baud rate and the implementation of PWM[21]. For example, each clock count takes 32 machine cycles. Therefore the time for one count of the timer is

$$1 \text{ count} = 32 \times 0.8138 \ \mu s$$

$$1 \text{ count} = 26 \ \mu s \tag{4.3}$$

This clock count directly influences the overflow time for the timers and thus influences and limits the baud rate and PWM period. This limit on the PWM period affects temporal resolution, brightness step and frequency of flicker of the LEDs. This will be examined in later sections and solutions to these imposed limits will be presented, and further future improvements will be outlined.

---

[21]Pulse width modulation, see later sections

4.2.2 Special function registers

The 8051 family of microcontrollers provides a distinct memory area for accessing Special Function Registers (SFRs). SFRs are used in the program to control timers, counters, serial I/Os, port I/Os, and peripherals. SFRs reside in a reserved area in memory, from address 0x80 to 0xFF, and can be accessed as bits, bytes, and words. Figure 4.21(b) provides a graphical representation of the 8051's SFRs, their names and addresses. A description of the SFRs used in this project is outlined below. The names of the SFR locations are defined in the register file. This register file can be seen in the appendix and an outline is provided in figure 5.10.

Bit	Name	Bit Address	Explanation of function
7	SM0	9Fh	Serial port mode bit 0
6	SM1	9Eh	Serial port mode bit 1
5	SM2	9Dh	Multiprocessor communications enable
4	REN	9Ch	Receive enable.
3	TB8	9Bh	Transmit bit 8
2	RB8	9Ah	Receive bit 8
1	TI	98h	Transmit flag.
0	RI	99h	Receive flag.

Table 4.3: SCON SFR

SCON SFR

One of the the powerful features of the 8051 is its integrated UART (Universal Asynchronous Receiver-Transmitter), also known as its serial port. Via the serial port, it becomes very easy to read and write values to the chip from some external source (in this particular case Labview). In order to successfully communicate between the two platforms, it is necessary to configure correctly the serial ports operation mode. This configuration is done using the **S**erial **CON**trol or SCON SFR. The SCON SFR controls the calculation method of baud rate of the serial port, whether the serial port is activated to transmit/receive data and also flags successful communication along the serial port. The SCON is bit-addressable and has an address[22] in memory of 98h. A table of the SCON addresses and function of each of its bits is can be seen in table 4.3[23].

TCON SFR

The **T**imer **CON**trol or TCON SFR is used to configure and customise the operation of the 8051's two on board timers. This SFR is bit addressable and is located at 88h in memory. The SFR is used to switch on or off each of the timers (timer0 and timer1) and

---

[22]All addresses in hex
[23]Based on table from [70]

flags whether a overflow has occurred. The overflow is vital in this project and is used to calculate the baud rate and implement pulse width modulation. These factors will be explained in later sections. See table 4.4[24].

Bit	Name	Bit Address	Explanation of function
7	TF1	8Fh	Timer1 overflow flag
6	TR1	8Eh	Timer1 Run
7	TF0	8Dh	Timer0 overflow flag
6	TR0	8Ch	Timer0 Run

Table 4.4: TCON SFR

TMOD SFR

The **T**imer **MOD**e or TMOD SFR is used to configure the mode of operation of the two timers. The different modes which the timers can operate are 16-bit timer, 8-bit autoreload timer, 13-bit timer or as two separate timers. TMOD is not bit addressable and is located at 89h in memory. Again this SFR is vital to the correct operation of the device in this project. A full overview of it's operation will be discussed in the software section in the chapter 5.

SBUF SFR

The **S**erial **BUF**fer is used to send out and receive data via the serial port. Any value written to SBUF will be transmitted through the serial ports TXD pin and likewise any received byte will be gathered through the serial ports RXD pin. Any data received or transmitted through SBUF is appropriately flagged on the SCON SFR (see table 4.3 or appendix).

IE SFR

The IE (interrupt enable) SFR is used to control the on board interrupts. These interrupts are the serial port interrupt (flagged when a byte is recieved, or ready to transmit) and a flag for each of the on board timers (timer0 and timer1, flagged when an overflow occurs, determined by timer mode set by TMOD). The implementation and use of this SFR can be seen in the next chapter.

PCON SFR

The **P**ower **CON**trol or PCON SFR is used to control the 8051's power control modes. However, in this project the PCON is used to effectively double the baud rate of the system. This is done by setting the PCON.7 bit high. The next chapter, Device software, will examine this process further.

---

[24]Only bits related to timers displayed

8051 output

Vital to the successful behaviour of the device is control of the output of the 8051 μ-controller. Control of each component ie green LED, blue LED, camera trigger etc is governed by appropiate control of the corresponding output port on the 8051 memory.

CAM TRIG (P2.0, $A0)
FILTER TRIG (P2.1, $A1)
IR LED (P2.4, $A4)
BLUE LED (P2.5, $A5)
GREEN LED (P2.7, $A7)
GROUND
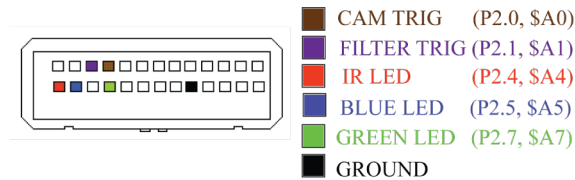
Figure 4.22: Pin-out control for 8051

The port used for this project is port 2, the output pins can be seen in figure 4.21(a). The various names assigned to the physical address in memory can be seen in the register file extract in figure 5.10. The output pins of the 8051 are connected to a serial connection and the pin out of such is shown in figure 4.22. The renamed and hex memory location is also displayed. The output from each of these pins is a 5V TTL pulse, the duration and frequency, thus the behaviour of the system, is controlled by the 8051 program.

This output pulse can be used to switch the BFY50 transistor and thus control the various elements in the system. The following section discusses the design of the driver electronics, the next stage in the control of the system.

4.3 Driver electronics

The driver electronics refers to the control board of the setup. This does not include the 8051 board, however its operation is dictated by the output of the 8051. In addition to this, the driver electronics incorporates a number of other factors essential to the successful operation of the device. These factors include power for the LEDs, power for the camera trigger, and to provide a mechanism to interpret and implement the appropriate control from the 8051 output. Figure 4.23 illustrates a schematic of the driver electronics, and its design and operation will be discussed in the following sections.

Luxeon LEDs driver

The primary component in the electronic set up is the two luxeon LEDs. The main concern when designing the electronics is to provide the optimum setup for efficient operation of these two high power LEDs.

The design must incorporate a method for switching the LEDs at high frequency, as well as providing the optimum setup for providing power to the LEDs, i.e. forward voltage of 6.7V, driving a current of 700mA, thus providing 5W (see equation 4.5) of electrical power to each of the LEDs (see figure 4.24).
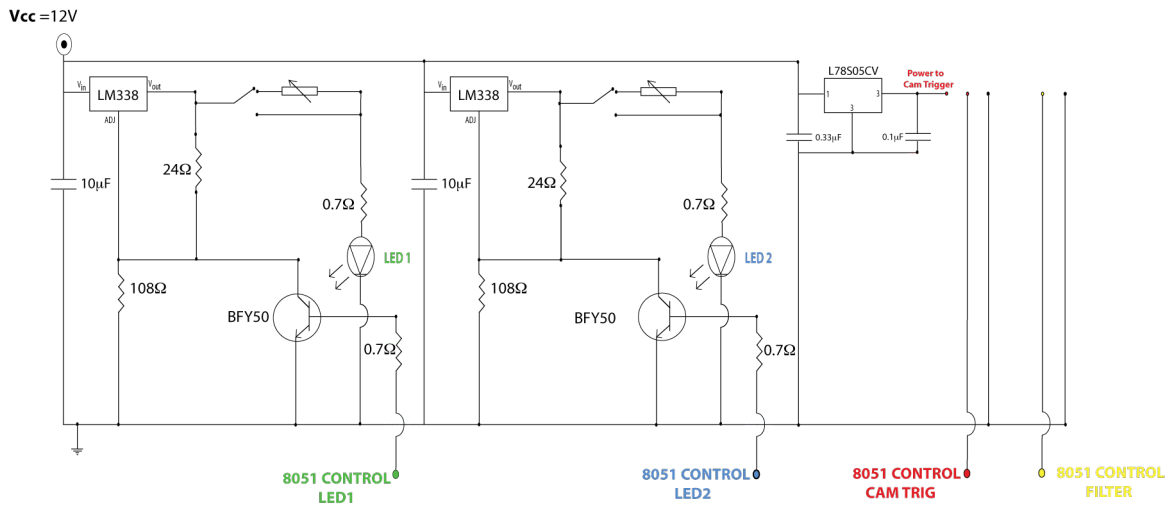
Figure 4.23: Schematic of the driver electronics used in project.

(a) Forward current in mA versus forward voltage in V

(b) Forward current in mA versus luminous flux
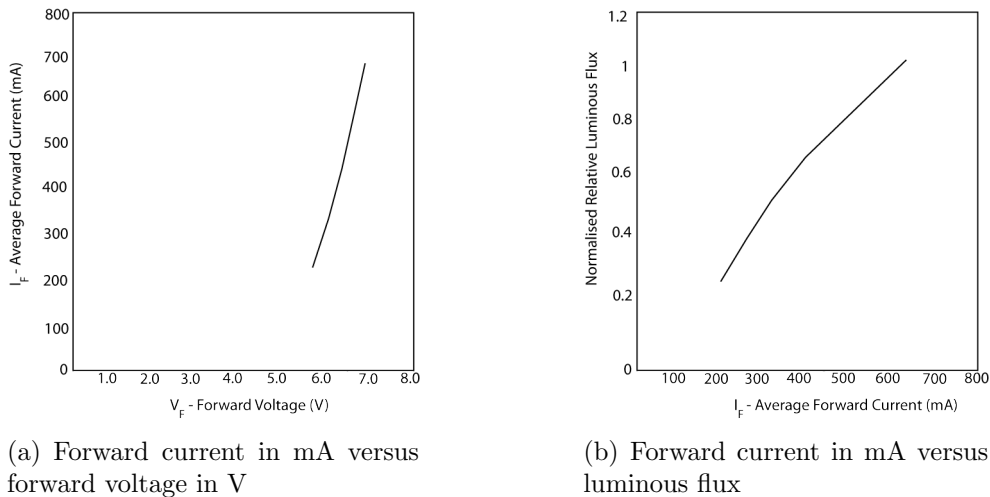
Figure 4.24: Electrical characteristics for the two LEDs utilised in the project. The values illustrated assumes a junction temperature across the LED of 25°C. The optimum performance for the LEDs is a forward voltage of 6.7V driving a current of 700mA. This ensures maximum efficiency and prolonged life for the LED.

Limiting the LED current

In order to protect the LED a current limiting resistor is required in series with the LED. The reason is due to the non-linear relationship between voltage across a diode and the current through a diode. This can lead to low voltages driving a large current and damaging the LED.

The linear relationship between current through, and voltage across a resistor, allows the opportunity to control the current in the circuit. Connecting the appropriate limiting resistor in series with the LED, ensures the characteristics of the circuit can be confidently
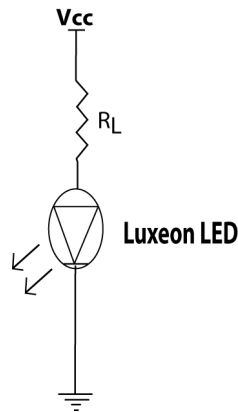
Figure 4.25: Current limiting resistor connected in series with the LED it is protecting.

defined and consequently the LED protected.

Equation 4.4 is a simple implication of Ohm's law and can be used to define the required resistance to deliver the desired current to the LED.

$$R_L = \frac{V_0 - V_R}{I} \qquad (4.4)$$

From figure 4.24 it is clear that the maximum forward current and forward voltage are 700mA (I) and 6.7V (V_R) respectively. Assuming $V_0 = 7$V, and applying the LED values to equation 4.4 gives a result for the limiting resistor (R_L) of 0.2 Ω. Even though the reistance is very low, the important factor is that its presence ensures linearity in the system between current and voltage, and thus protects the LED. Another consideration for the resistor choice is the power dissipated by the resistor. For this case the power is given by 4.5.

$$P = V \times I \qquad (4.5)$$

Applying the equation gives power across the resistor and the LED to be 0.14W and 5W respectively. Low power across the resistor avoids any excessive heating and consequent instability, however the high power across the LED does lead to heating, and accordingly a heat sink is required for optimum prolonged performance.

Importance of LED heat sink

The junction temperature of the LEDs has dramatic effects on the output radiant power of the LED. This is especially true for the green LED (see figure 4.26(a)). In order to avoid these temperature effects, it is necessary to build a heat sync to dissipate the excessive heat produced by the high power circuit.

Figure 4.26 displays the design of the heat sink for the two luxeon LEDs[25]. The piece is designed to fit in a xy adjustable Linos mounting[26]. The LED is mounted on the top and

---

[25]Design based on a suggested design by Luxeon, outlined in appropriate datasheets
[26]Ensures accurate alignment of the LED in the system, diameter of 25mm
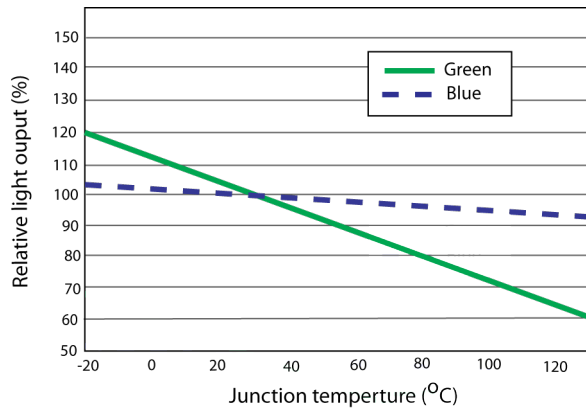
(a) The relative light output as a function of junction temperature for the green and blue luxeon LED. Graph adapted from datasheet for luxeon V LED.
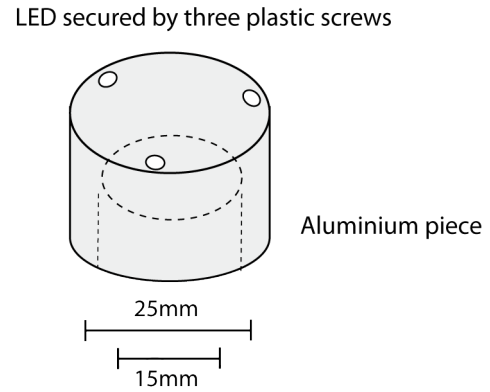
(b) Heat sink design for the luxeon V stars

Figure 4.26: The design of the heat sink utilised in this project, and the effects of temperature on the two different LEDs.

secured using 3 plastic screws. A conducting paste is applied before mounting to ensure maximum transfer of heat. A hole is drilled in the heat sink to aid in the conduction of heat away from the LED and into the environment.

While not all the heat will be removed, the majority will be conducted away from the LED. This ensures that a more predictable, efficient and prolonged LED performance can be achieved.

Voltage regulator (LM338)

A voltage regulator is used in the system in order to provide a constant voltage source (V_0) which is unaffected by any changes in the Vcc (main supply voltage). For this set-up specific criteria have to be met and for this reason the LM338 voltage regulator was chosen. The LM338 is a adjustable 3 terminal positive voltage regulator capable of driving up to 5A over a wide output voltage range (1.2V to 32V).

This voltage regulator is easy to use and requires only two resistors to to set the output voltage (V_0). The LM338 is designed as such, to deliver a nominal reference voltage (V_{ref}) of 1.25V, between the output and adjustment terminal. The reference voltage is impressed across the resistor R1 and since this voltage is constant, a constant current is present through the output resistor R2. The output voltage can be calculated from equation 4.6. The current I_{adj} is very small and the LM338 is designed to minimise this term, and make it very constant with line and load changes. This term can be ignored for most applications and is done so in this project. A capacitor can be placed across the input and ground and is used to provide improved output impedance and rejection of transients.

$$V_0 = V_{(ref)} \times \left(1 + \frac{R2}{R1}\right) + I_{adj} \times R2 \qquad (4.6)$$

70
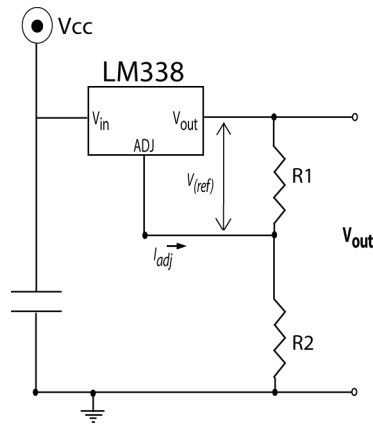
Figure 4.27: Voltage regulator set up

Clearly from equation 4.6 the output voltage depends on the ratio of the two resistors. However what is less clear is considerations over the actual values of the resistors, specifically power, and subsequent heating across the resistors. Larger resistances produce a larger voltage drop (for same current) and consequently more power (and heat) across the resistor. Heat produced in a circuit, and especially in a resistor produces instability in the circuit and should be avoided. For this reason care must be taken in the decision of the individual values of the resistors, to produce the desired resistance ratio.

Transistor (BFY50)

The transistor is used as a switch and implements any flashing of the LEDs, and controls the intensity (via pulse width modulation (PWM)) of the LEDs.

Parameter	Current (A)	Gain	T (ns)
I_C	1	-	-
Gain	-	30	-
Switch speed	-	-	100

Table 4.5: Selected characteristics of the BFY50 transistor

The operation of the transistor is dictated by the base current, and can be switched by applying the appropriate current on this pin. The 8051 output is connected to the appropriate transistor and can be used to control and coordinate the behaviour of the electronics associated with the particular transistor. The transistor chosen for this particular project is the BFY50. The BFY50 is a silicon planar epitaxial NPN transistor and was designed for general purpose linear and switching applications. The maximum collector current on the component is 1A (needs to handle 700mA for this project) and has a typical switching speed (rise time + all time) of 100ns. The gain, h_fe, has a typical value of 30 which is

used to calculate the current limiting resistor on the base[27]. Table 4.5 displays some of the characteristics of the transistor, operating under typical parameters.
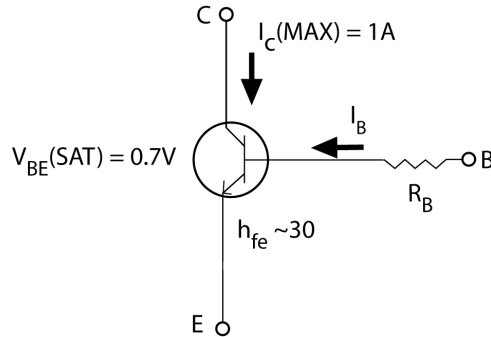
Figure 4.28: The NPN bipolar transistor (BFY50) utilised in the project.

The choice of R_B in figure 4.28 is calculated to deliver the optimum current at the base to saturate the transistor, and is based on the required collector current I_c and the gain of the transistor $h_f e$. The base current I_B is related to the collector current I_c as shown in equation 4.7.

$$I_B = \frac{I_c}{h_{fe}}$$

(4.7)

In order to saturate the transistor the minimum current required to deliver I_c is I_B. Therefore, to switch the transistor it is customary to apply at least twice the required current at the base. Applying Ohms law, the value of R_B is given by equation 4.8.

$$R_B = \frac{V_B \times h_{fe}}{2 \times I_c}$$

(4.8)

The inclusion of the transistor in the circuit will be outlined in a later section.

Potentiometer and SPDT switch

The addition of the option of a potentiometer is to offer the user the ability to operate the LEDs at its maximum potential, or alternatively limit the brightness, and essentially calibrate the system. The use of a switch in the system is due to the fact that the potentiometer still has some resistance even when it is at its minimum value.

The typical minimum resistance is approximately 1Ω, which would normally be negligible, however, in this case the limiting resistor is of a similar low value, so the decision to bypass the potentiometer was made. The SPDT (single pole double throw) switch allows swift and easy interchange between the two options. The potentiometer is a 1KΩ, multi-turn, linear, 3W potentiometer, which allows for sensitive adjustment of resistance values over a high power range. The ability to handle power up to 3W negates the possibility for the device to heat up and produce instability in the system. The addition of the potentiometer also effects the adjustment step in power of the LED. Essentially the larger the resistance

---

[27]For I_c = 1A, T_{case} = 25°
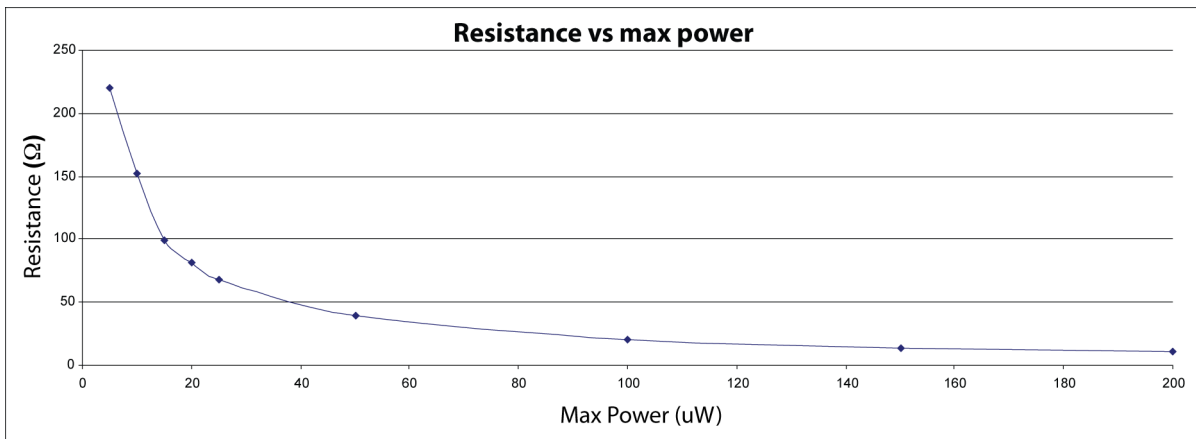
Figure 4.29: The effect of the potentiometer resistance value on the maximum power output of the LED as measured at the cornea.

the greater the power step between each labview command. The potentiometers can also be adjusted to match the light output of both LEDs, so the power of each are relatively equal at the cornea. The stated resistance is that of the off resistance, which is the measured resistance when the LED is off.

Actively LO triggered driver for Luxeon LED

Figure 4.30 illustrates the driver design used in this project. This is an active LO design. Current is delivered to the LED when a LO signal is outputted from the 8051.
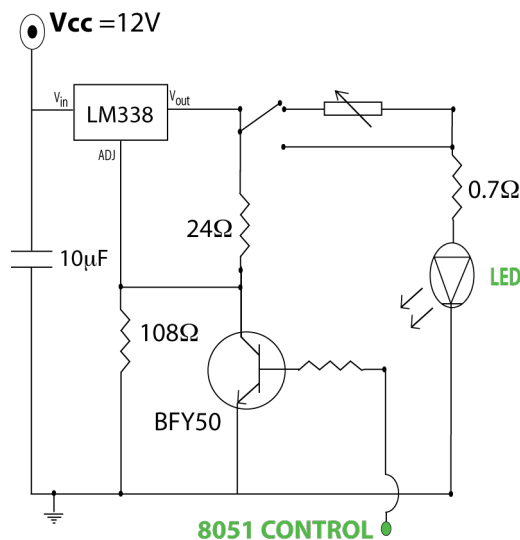
Figure 4.30: Electronic driver for the LED. This design limits the current and voltage to the maximum values outlined in figure 4.24. The design also provides a method to switch the LED at high frequencies as dictated by the 8051 output. The 8051 pinout can be seen in figure 4.22

An alternative active HI design was also considered but due to interference effects between the two transistors, and problems with actively grounding the signal delivered to each LED, resulted in the final active LO design. A drawback to the active LO design is the need for a voltage regulator for each LED and thus increases the amount of components in the design.

Triggering of camera

An important role of the electronics is to provide an accurate method to trigger the camera on each LED pulse. The camera used in this setup has the option of applying an external trigger pulse to expose the camera for the duration of the trigger pulse. In order to power the trigger a +5V voltage must be applied to the appropriate input pin (see figure 4.32 for complete pin out for the DIN connector).

Figure 4.31 illustrates the voltage regulator, the L78S05CV, employed to step down the V_{cc} to the required 5V. In contrast to the LM338, the L78S05CV is hard wired to deliver 5V so no external resistors are required.
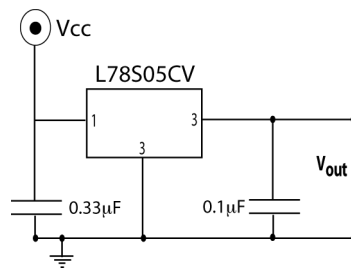
Figure 4.31: Voltage regulator to deliver 5V from potentially varying voltage source V_{cc} in order to power the trigger of the retiga camera.

The connector at the rear of the camera is a 6 pin miniature circular DIN receptacle, AMP 749265-1, while the mating connector is Singatron Enterprises part number 62000-6P. The pins for the miniature DIN (rear of the camera) can be seen in figure 4.32. Pin 1(+5VDC) and pin 4 (ground) must be connected for the trigger to be live, and pin 2 is connected to the cam trigger output pin (P2.1)of the 8051 (see figure 4.22).

This setup is fully incorporated into the driver electronics and can be examined in figure 4.23. The software to control the timing of the triggering will be presented in the next chapter. It should be noted for completion that there exists a 12 μ-second delay between the Trigger event and the beginning of the exposure period. This time frame is negligible for this particular project.

Triggering of the filter wheel

For completeness the triggering of the filter wheel must be mentioned. Power is supplied to the wheel from a source external to the device electronics. This is not an ideal situation and it would be preferable to supply the power to the wheel from the electronic board but
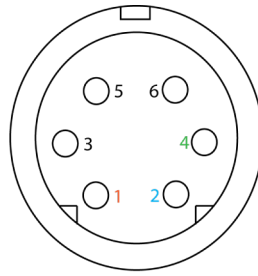
1 : +5VDC (Power for optocoupler trigger)
2 : TRIGGER (Active LOW trigger input)
3, 5, 6 : n/a for this project
4 : GROUND (Ground reference for optocoupler trigger)

Figure 4.32: Sync control connector (as seen from back of camera)

time constraints limited the implementation of this. However, the TTL pulse is supplied
from the electronic board, via coaxial cable, and its operation is dictated by the 8051
output. Construction of the appropriate TTL pulse duration will be discussed in the
following chapter.

Chapter 5

Device Software

Device software in this project refers to the interface design, data analysis software and system control software. The interface and analysis software is written in Labview, chosen both for its potential to offer an user friendly GUI[1], and its fulfillment of the technical requirements (speed, serial communication ability, compatibly with retiga imaging camera etc.). The objective of the interface is to present to the user an intuitive design which accommodates easy and rapid control over the entire system, and subsequently allows for the precise and swift measurement of subjects, for the various measurement techniques. Labview is also responsible for the analysis of the acquired data from the imaging camera. The analysis section of the software performs a number of post processing tasks on the acquired information, to obtain a result for the peak macular pigment optical density (MPOD), as well as a result for the distribution of the MPOD across the desired area of the retina.
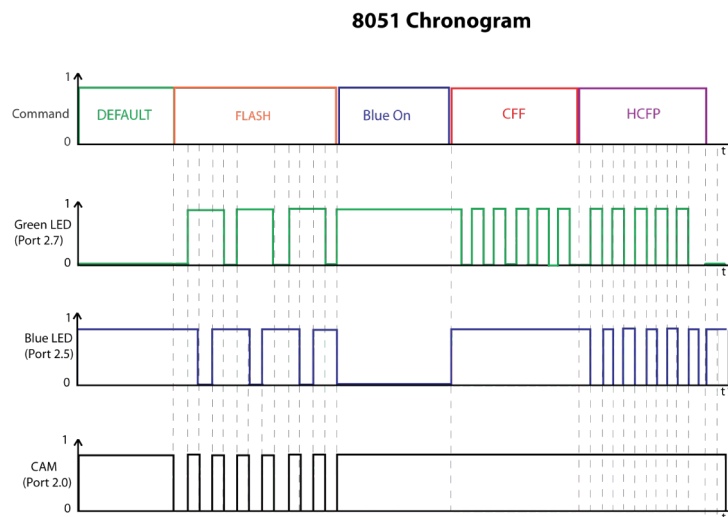
Figure 5.1: Simple chronograph illustrating the operation of the LED and camera activity for certain 8051 μ-controller modes. The graph illustrates active LO behaviour. The filter wheel operation and the method of pulse width modulation is not included for sake of clarity.

---

[1]Graphical user interface

Control of the system is primarily achieved by a 8051 μ-controller[2], the operation of such is coded in assembly language. The desired activity for the different modes is illustrated in figure 5.1. The interplay between the two platforms, the interface and μ-controller, ensures the successful operation of the device for the three measurement techniques.

The operation of the system is dictated entirely from the user interface, which ensures, after initial calibration, that no further external calibration or additional measurements are required. Figure 4.1 illustrates the flow of data, and the relationship between the various components of the system. The following sections endeavors to present the device software used in this project, for both platforms, and attempt to demonstrate the interplay and logic behind it's design in the most transparent and discernible manner. The intention is to present a near complete explanation of the software design, but to avoid a definite breakdown of all the features and potentially losing the interest of the reader[3]. Chapter 6 will present the results of the software, therefore the emphasis of this chapter will be on the implementation and thought behind its design.

5.1   System communication

The key to competently controlling the various system modes from a single terminal, is essentially the ability to communicate capably between Labview and the μ-controller. The communication strategy of handshaking is implemented to ensure valid data transfer between the two platforms, and is key both to the versatility of the system and the implementation of the different modes of the system.

Flagged BIT (S)	NAME	Function
B.7	DIMGREEN	Loads value of green LED intensity
B.6	FLASH	Sends command to flash LEDs (Imaging methods)
B.5	EXPOSURE	Controls LED and camera exposure (also flicker freq in HCFP)
B.4	DIMBLUE	Loads value of blue LED intensity
B.3	ALL OFF	Switch off both LEDs
B.2	BLUECON	Switches Blue LED ON/OFF, for saturating in HCFP
B.1	HCFP_FLICKER	Sends command to flicker LEDs (HCFP)
B.1 + B.2	Filter Wheel Adjust	Advance the Filter Wheel by one position
B.0	CFF_FLICKER	Flicker LED to measure the critical fusion of flicker for subject

Table 5.1: Different operation modes of 8051. The flagged bit refers to the initial byte send to the μ-controller. The system is MSB so B.7 is most significant bit HI i.e. 10000000

These functions or modes are outlined in table 5.1[4]. These different modes are determined

---

[2]See chapter 4 for hardware description.

[3]The complete code can be found in the appendix.

[4]Bold indicates second adjustment command required from Labview, i.e handshaking required

by sending an identifying byte[5] from Labview and waiting for the acknowledgment byte from the μ-controller, before sending the required information to alter the mode indicated by the initial byte. The method of handshaking essentially is mutual acknowledgment of data transfer between the two platforms.
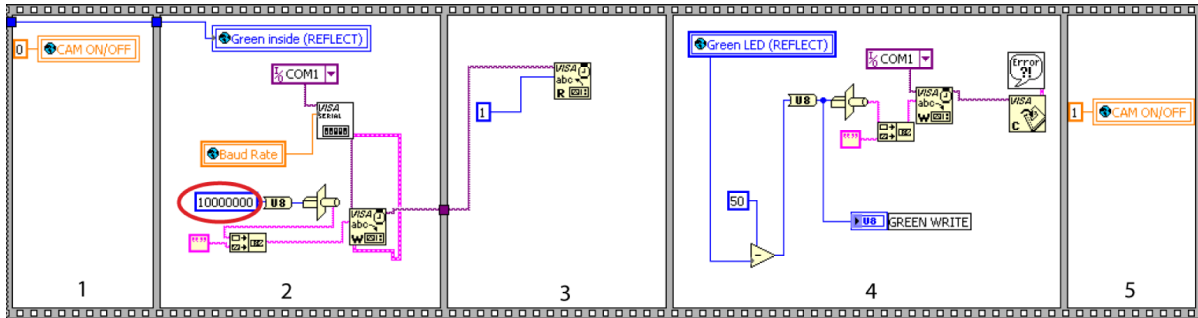
Figure 5.2: Example of labview code to adjust the Green LED intensity. The byte circle in red is the initial byte to define the mode for the 8051. The next panel waits for the acknowledgment bit from the 8051 to labview to indicate it is ready to receive the adjustment byte. Labview then sends the adjustment byte, which is saved as a global variable, in this particular example called *Green LED (REFLECT)* above. The content of the global variable is determined by user input on the interface.

Figure 5.2 displays the Labview code for adjusting the intensity of the green LED. Circled in red is the initial byte, which tells the μ-controller which mode to alter. Referring to table 5.1 one will notice that the HI bit is B.7. Labview waits for a response from the μ-controller, and then sends the control byte, which the μ-controller loads and uses to alter the appropriate mode, in this case the brightness of the green LED. The success of communication between the two platforms initially depends on correctly defining the baud rate for both systems. This will be outlined in the following sections.

5.1.1 Baud Rate

The baud rate is the rate at which data are transmitted, and received between compatible devices[6]. Each of the devices, in communication need to have an identical baud rate, i.e. transmitting device must transmit data at the same rate as the receiving device reads the data, otherwise the information is garbled and unusable. In order for successful communication between Labview and the 8051, both platforms must have the correct baud rate. In this section the initialisation of the baud rate for the 8051μ-controller and Labview will be presented.

Setting of Baud rate for the 8051 μ-controller

The setting of the baud rate for the 8051 μ-controller is achieved by the control software on the 8051, and thus written in assembly language. For this particular project,

---

[5]8-bit number

[6]Measured in bits per second (bps)

the desired baud rate is achieved by setting the 8051 timer[7] to overflow at a certain rate, which can be used to define the baud rate. In otherwords, on each occasion that the timer overflows (reaches a certain maximum value before resetting itself), an overflow event on that timer is flagged. By controlling the rate of this event flagging, a timing mechanism can be simulated, and consequently be utilised to define the desired baud rate.

Initially the 8051 must be correctly set up in order to achieve the correct rate. The initial factors that must be correctly defined are, the serial port control, the timing mode and the correct reload value that causes Timer1 to overflow at a frequency appropriate to generate the desired rate. The latter is calculated from equation 5.1, while the first two can be defined by manipulation of the respective SFRs[8].

SM0	SM1	Serial Mode	Explanation	Baud Rate
0	0	0	8-bit Shift Register	Oscillator/12
0	1	1	8-bit UART	Set by Timer 1
1	0	2	9-bit UART	Oscillator/32
1	1	3	9-bit UART	Set by Timer 1

Table 5.2: Configuration of the serial mode using the SCON SFR. This is used to define how the baud rate is calculated as well as the serial mode.

Communication between the μ-controller and Labview is via the serial port (RS232 cable), and therefore the mode of operation of the serial port must be correctly defined. This is achieved by loading the appropriate byte into the SCON SFR. Table 5.2 illustrates the various serial modes available, and their associated method for calculating the baud rate. Each mode can be selected by setting the appropriate bit of the SCON SFR. The serial port can run in 4 different modes of operation, with each mode also determining how the baud rate will be calculated. The desired mode for this project is 8-bit UART, with the baud mode determined by the behaviour of timer1. This is determined by SMO LO and SM1 HI, essentially the first two bits of the byte should be 01.

The next step is manipulation of timer1 in order to achieve the desired overflow rate. In this project, the mode of counting that is desired is 8-bit auto-reload mode. This means that timer1 will count from a initial value (TH1), increment at a rate depending on the chip speed, and overflow when it reaches 255 (0 to 255, 2^8 states), flagging the overflow event, reloading the initial value TH1 and repeating the process. The timer mode is set by loading the appropriate byte into the TCON SFR. Table 5.3 illustrates the available modes for timer1. Similar to setting the correct mode for the serial port control, the setting of the desired timer control is loading the appropriate byte into the TCON SFR. In the case of this project the first two bits of the byte should be 10.

---

[7]The 8051 has two timers. For the baud rate definition Timer1 is used.
[8]Special Function Registers (See chapter 4).

M0	M1	Timer Mode	Explanation
0	0	mode 0	13-bit counter
0	1	mode 1	16-bit counter
1	0	mode 2	8-bit counter with auto-reload
1	1	mode 3	two 8-bit counters

Table 5.3: Setting the timer mode using the TCON SFR.

The final step is to calculate the initial count value TH1. This depends on the crystal speed (XTAL), and the desired baud rate. Ideally the baud rate should be as high as possible, so data can be passed between the platform as quickly as possible. For the specific 8051 chip in this project (DS5000T) the architecture limits the maximum speed of the chip, essentially limits the usable XTAL speed. The maximum speed is 14.7456 MHz and, consequently the fastest baud rate possible is 12800bps. The following equations illustrates the calculation of the reload value TH1 to achieve, the desired overflow rate, and consequently the baud rate of 12800bps.

$$TH1 = 256 - \left(\frac{\frac{XTAL}{384}}{Baud} \right) \tag{5.1}$$

An attractive feature of the chip is the ability to effectively double the baud rate by manipulation of the PCON SFR. Essentially, if PCON.7[9] (SMOD) is set then the baud rate is effectively doubled so the equation now becomes;

$$TH1 = 256 - \left(\frac{\frac{XTAL}{192}}{Baud} \right) \tag{5.2}$$

Filling in for the known values, i.e. the desired baud rate, and the XTAL speed;

$$TH1 = 256 - \left(\frac{\frac{14.7456 \times 10^6}{192}}{12800} \right)$$

$$TH1 = 250 \tag{5.3}$$

Extracts from the assembly code can be seen in figure 5.3. These examples illustrate the loading of bytes into the various SFRs to setup the chip, for the desired baud rate. Figure 5.3(a) illustrates setting the serial mode to 1 and enabling the receive interrupt (essentially turning on serial communication). This figure also illustrates loading the initial

---

[9]See previous chapter

TH1 value with the appropriate value of 250 (FA in hex) to achieve the desired overflow rate. Figure 5.3(b) displays the initialisation of the timer mode, 8 bit timer, and the turning on of the on board timers, timer1 for baud rate calculations and timer0 for PWM (see later sections).

```
;Serial Port Comm set up (Baud Rate 12800bps) (when PCON.7 set)
;*********************************************************************************************
;
        MOV   SCON, #%01010000   ;mode1 (baud rate set by Timer1 overflow), recieve enable
        MOV   PCON, #080h        ;set PCON.7 to double baud rate
        MOV   TH1, #0FAh         ;Timer1 overflow sets baud rate to 12800

;*********************************************************************************************
;
```

(a) Loading TH1 and setting SMOD

```
;Timer set up

;*********************************************************************************************
;
        MOV   TMOD, #%00100000    ;set timer to mode0 (8bit with 5 bit prescaler)
        SETB  TR1                 ;turn on timer1
        SETB  TR0                 ;turn on timer0
        SETB ET0

;*********************************************************************************************
;
```

(b) Setting Timer mode

Figure 5.3: Setting up the baud correct baud rate

This sets up the 8051 μ-controller to operate at a baud rate of 12800 bps. For successful communication with the interface terminal, Labview must be set up to operate also at this baud rate.

Setting of Baud rate for Labview

Since Labview is a higher level programming language than assembly language, it would be envisaged that the method of definition of the baud rate would not be as involved and complicated, and this is indeed the case. Labview itself is a graphical programming tool that is comprised of VIs (virtual instruments) that can be written to perform specific tasks. Similar to all programming languages, these parent VIs can encompass various other VIs, know as subvis (analogous to sub routines). Setting the baud rate in labview is a simple matter of defining this parameter in the VISA communication subvi.

Virtual Instrument Software Architecture (VISA) is the lower layer of functions in the Labview instrument driver VIs that communicates with the driver software, and can be used in the communication with other instruments. The baud rate is saved as a global variable and therefore can be passed to all VIs (opposed to local variable which cannot be passed outside it's parent VI). The advantage of saving the value as a global variable is that to change the baud rate throughout the entire program, the only value that requires adjustment is the value of this global variable. Figure 5.4(a) illustrates defining the baud rate as a global variable, while figure 5.4(b) illustrates the value stored in the global vari-

(a) Loading the global variable with the desired baud rate

(b) Setting the baud rate for the VISA vi
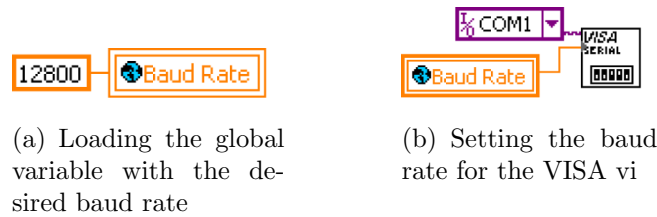
Figure 5.4: Example of labview code to adjust the baud rate. The value is stored in a global variable and cab be passed between VIs. This has the advantage that in order to change the value for all VIs only one adjustment has to be made.

able setting the baud rate for that particular VISA session.

This ensures that data transmitted and received to and from Labview (via VISA vis) is done so at a baud rate defined by the global variable named Baud Rate. The next section will deal with the transmittance and receiving of data for both platforms.

5.1.2 Data Flow

This section will discuss the management and control of data flow within the system. Once the baud rate is defined correctly for both devices, then uncorrupted data transfer between the two devices is possible. The following sections will deal with the appropriate adoption of the transmitted and received data, within both the μ-controller and Labview environment, and the core importance this implementation has in relation, to the correct operation and consequent measurement of the macular pigment optical density.

μ-controller serial port interrupt

The 8051 μ-controller has in built interrupts, which can be utilised to perform a number of different tasks. These interrupts are essentially, as the name implies, some event which interrupts the normal execution of the on chip program.

Interrupt	Flag	Interrupt procedure address in memory
External0	IE0	0003h
Timer 0	TF0	000Bh
External 1	IE1	0013h
Timer 1	TF1	001Bh
Serial Port	RI/TI	0023h

Table 5.4: 8051 Interrupts. Interrupts in bold are used in this project. Addresses are given in hex.

Implementation of interrupts in the program, increases the efficiency of program execution, as this strategy avoids the need of the program itself having to routinely check for

the occurrence an event. In this section the serial port interrupt will be discussed. The timer interrupt was referred to in a previous section, and will be discussed further under pulse width modulation.

An interrupt operates as follows, if an interrupt is detected (data to be read on serial port, timer overflow etc), the associated flag is HI, the normal program is interrupted and the code jumps to the procedure address in memory. Any code saved in this area of the memory is then executed, after which the program returns to normal execution. The interrupts on the μ-controller are listed in table 5.4, their flag bit[10] and interrupt procedure memory allocation are also listed.

Initially the interrupts have to be set up to operate correctly. This is done by loading the appropriate byte into the IE (interrupt enable) SFR. A table defining this particular SFR can be seen in the previous chapter. For this project we wish to enable timer0 and the serial port interrupt, these correspond to bit 1 and bit 4 respectively. In addition the global interrupt control must be enabled, which is located at bit 7 in the IE SFR. Essentially the value to load into the IE SFR, in binary, is 10010010. This can be seen in the assembly code extracted illustrated in figure 5.5.

```
;Interupts set up

;*********************************************************************************************************

ledstate:       MOV   IE,#%10010010       ;enable global interupts        (EA)
                                          ;enable timer0 interupt         (ET0)
                                          ;Serial interupt                (ES)

;*********************************************************************************************************
```

Figure 5.5: Initialising the interrupts used in the program.

When Labview sends a byte to the 8051, it is automatically saved in the SBUF register. On receiving the byte the RI[10] flag becomes HI and the interrupt process is initiated. Normal execution of the code on the μ-controller is interrupted and the code saved in memory location 0023h is executed. Figure 5.6 displays an extract from the code on the 8051, in particular the interrupt location. This performs a simple jump to the section labeled *Receive* in the code. This code is displayed in figure 5.7.

```
.Org   00Bh                    ;Timer0 interupt location
LJMP   LEDDim

.Org   0023h                   ;Serial Port interrupt
LJMP   Recieve
```

Figure 5.6: Initialising the timer0 and serial interrupts. Once a interrupt flag is detected the appropriate code is initiated. i.e when a serial interrupt is flagged the code jumps to the label *Recieve* (illustrated in figure 5.7)

---

[10]See figure 5.10 for physical address in memory.

Figure 5.7 essentially is the mode choice of the chip, and it is here where the different modes outlined in table 5.1 are determined. The code simply moves the received byte into the B register, clears the interrupt flag, clears the SBUF register and checks the byte and jumps to the appropriate area of the code for further instruction.

```
Recieve:        MOV   B, SBUF            ;Move byte into B,
                CLR RI                   ;can check bit
                CLR   SBUF               ;to determine mode
                JB    B.7, DIMGREEN
                JB    B.6, flash
                JB    B.5, Exposure_jump
                JB    B.4, DIMBLUE
                JB    B.3, IRjump
                JB    B.2, BLUECHOICE
                JB    B.1, flickchoice
                JB    B.0, CFFjump
                RETI
flickchoice:    JB B.2, FILTERTRIG       ;looks whether byte is
                LJMP HCFP_FLICKER        ;00000110 (trig for filter wheel)
```

Figure 5.7: When a serial interrupt is flagged by the 8051 the illustrated code is run. The desired mode is implemented depending on the byte recieved.

Similarly in order to transmit from the 8051 an interrupt is flagged. However, in this case the flagged bit is TI[10] and the transmitted byte is the value saved in the SBUF register. This is the basis of the handshaking strategy outlined in previous sections.

Labview communication

This section will briefly outline the control of transmitting and receiving data in Labview. An example of adjusting the intensity of the green LED is displayed in figure 5.8.
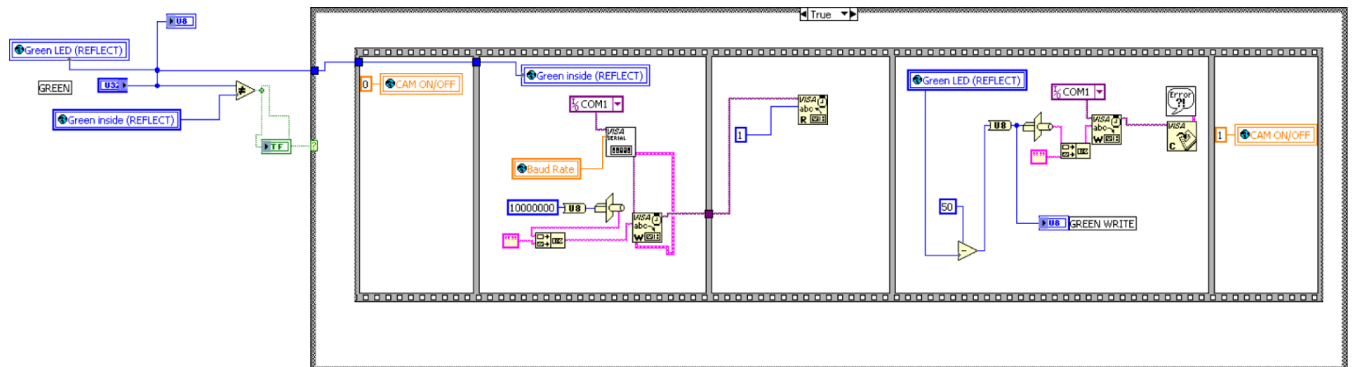
Figure 5.8: Typical example of communicating with the 8051 via Labview.

This example was chosen due to the fact that it illustrates the use of handshaking, and demonstrates the setting of the baud rate. This VI is controlled by a case structure (not shown in diagram) and is true when some front panel activity is detected, namely the VI is executed when the users adjusts the intensity of the green LED gauge (see chapter 6, figure 6.2). The code executes from left to right, and the content of each individual frame

in the sequence must be fully executed before advancing to the following frame.

Frame 1 loads the value 0 into the camera control global variable, which turns off the camera acquisition, while there is communication with the 8051[11]. Frame 2 is the setting up of the VISA VI for communication with the 8051. This initialises the correct communication port as well as setting the appropriate baud rate. Frame 2 also writes the identifying byte and sends it to the 8051. Frame 3 holds the program until the acknowledgment byte is received from the 8051. Once this bit is received the program executes frame 4. This sends the adjustment byte to the 8051. This byte is saved in the global VI *Green LED (REFLECT)* and is the value determined by the user on the front panel. Frame 5 simply turns the camera back on, and then returns to the main program. The speed of execution is limited by the baud rate and is in the μ-seconds. The other communication VIs written in Labview have a similar design, the difference being the identifying byte to distinguish the various mode choice.

Implementing dynamic control from front panel activity

The code presented in figure 5.8 also illustrates the method to automatically update the LED level when a change is detected on the front panel. The main code is included in a case structure and executes when a true value is detected. To avoid having a separate control to produce this true value, it is more desirable that a change on the slider on the front panel would automatically produce this true value, and thus execute the code. This is achieved by the use of global variables, namely *Green LED (REFLECT)* and *Green inside (REFLECT)*. This essentially holds the value of the desired LED level and the previous LED level. If the previous and desired level are different then a true value is produced and the code in the case structure is executed, and consequently the desired LED level is sent to the 8051. The same procedure is used to control the blue LED level, to achieve dynamic LED control in the subjective method and to implement correctly the yoked[12] adjustment of LED levels.

8051 implementation of received data

This section will outlined an example of the procedure of the 8051 once the byte is received and identified.

The example given is for the adjustment of the intensity of the green LED. The transmitting of the data from Labview is outlined in the previous section. The appropriate extract from the 8051 code is displayed in figure 5.9. This section of code is executed once called from the serial port interrupt (see figure 5.4). The code simply transmits back to Labview to acknowledge that it is ready to receive the adjustment byte, and waits for this byte to be sent from Labview. When the byte is received, the code loads this byte and checks to see if the byte is full power (all LO) for the LED or turn off the LED (all HI, neither case requires pulse width modulation (PWM)). If neither of these cases is true, the LED is adjusted to it's new value (via PWM). The operation of the LED is controlled via the flagging of various registers. The addresses of the various labels used throughout the code

---

[11]Control of the camera will be discussed later

[12]See chapter 3, or later section for explanation of yoked adjustment of LEDs.

```
;***********************************************************************
DIMGREEN:        clr TI                       ;clear transmit flag
                 clr GREENOFF                 ;reset IGNOREGREEN parameter
                 clr GREENFULL
                 MOV SBUF, #%00000001         ;load acknowledge byte
                 jnb     TI,$                 ;loop until transmitted
                 clr TI                       ;clear flag
                 jnb     RI,$                 ;wait for adjustment byte
                 MOV    R7, SBUF              ;move byte into R7
                 MOV GREENLEVEL, SBUF         ;move byte into greenlevel

                 CJNE R7,#50, TESTZERO        ;Test for LED OFF (All HI)
                 SETB GREENOFF                ;Flag LED OFF

TESTZERO:        CJNE R7, #0, NOTZERO         ;Test for LED ON (All LO)
                 SETB GREENFULL               ;Flag full power
                 sjmp NOTZERO
;***********************************************************************
NOTZERO:         clr SBUF                     ;Clear SBUF
                 clr RI                       ;Clear RI flag
                 reti                         ;exit routine

;***********************************************************************
```

Figure 5.9: Assembly language to adjust the intensity of the green LED using the handshaking method.

can be seen in the register file, which is called by the main program. This eases in the reading of the code and can be used to easily debug the program.

Figure 5.10 illustrates the register file that is called on by the main assembly language program. This file contains the physical address in memory for the labels used in the main program.

5.1.3   Control of motorised filter wheel

The inclusion of the motorised filter wheel in the device is to provide a user friendly, rapid method of switching between the various targets. Table 5.5 outlines the filter position and the target that it contains.

Filter wheel position	Target	Mode
1	0.5 degree (default)	HCFP
2	1 degree	HCFP
3	3 degrees	HCFP
4	Parafoveal (7 degrees)	HCFP
5	Fixation target	RE and AF
6	Clear	RE and AF

Table 5.5: Various targets and their position within the filter wheel

The software automatically switches to the appropriate filter position, depending on the mode required. This depends on two factors, (a) triggering the wheel the appropriate number of times via the 8051 and (b) calculating the appropriate number of times to trigger the the wheel to reach the desired position. The wheel can only be moved in a

Column (a):

```
.NOLIST
;      *** 8051 DEFINITIONS ***
;
;**************************************
;     8051 SFRs
;**************************************
P0      = $80   ;Port 0
SP      = $81   ;Stack Pointer
DPL     = $82   ;Data Pointer Low
DPH     = $83   ;Data Pointer High
PCON    = $87   ;Power Control
TCON    = $88   ;Timer Control
TMOD    = $89   ;Timer Mode
TL0     = $8A   ;Timer low 0
TL1     = $8B   ;Timer low 1
TH0     = $8C   ;Timer high 0
TH1     = $8D   ;Timer high 1
P1      = $90   ;Port 1
SCON    = $98   ;Serial Control
SBUF    = $99   ;Serial Buffer
P2      = $A0   ;Port 2
IE      = $A8   ;Interrupt Enable
P3      = $B0   ;Port 3
IP      = $B8   ;Interrupt Priority
PSW     = $D0   ;Program Status Word
ACC     = $E0   ;Accumulator
B       = $F0   ;B register
TR0     = $8c
EA      = $Af
ET0     = $A9
TF0     = $8D
ES      = $Ac
TI      = $99
RI      = $98
```

```
;**************************************
;  I/O port bit definitions
;**************************************
P0.0    = $80  ;Port 0
P0.1    = $81
P0.2    = $82
P0.3    = $83
P0.4    = $84
P0.5    = $85
P0.6    = $86
P0.7    = $87
BLUESTATE      = $85
IRSTATE        = $86
LEDCHOICE      = $87
FLICKSTATE     = $84
CFFSTATE       = $83
P1.0    = $90  ;Port 1
P1.1    = $91
P1.2    = $92
P1.3    = $93
P1.4    = $94
P1.5    = $95
P1.6    = $96
P1.7    = $97
P2.0    = $A0  ;Port 2
P2.1    = $A1
P2.2    = $A2
P2.3    = $A3
P2.4    = $A4
P2.5    = $A5
P2.6    = $A6
P2.7    = $A7
BLUE    = $A5
GREEN   = $A7
IR      = $A4
CAM     = $A0
FILTER  = $A1
P3.0    = $B0  ;Port 3
P3.1    = $B1
P3.2    = $B2
P3.3    = $B3
P3.4    = $B4
P3.5    = $B5
P3.6    = $B6
P3.7    = $B7
```

```
;**********************************************
;  Flags and 128 Bit addressable segment
;**********************************************
F0 = $D5      ;Flag 0 = PSW.5
F1 = $D1      ;Flag 1 = PSW.1
R0 = 00h
R1 = 01h
R2 = 02h
R3 = 03h
R4 = 04h
R5 = 05h
R6 = 06h
R7 = 07h
B0 = 08h
B1 = 09h
B2 = 0Ah
B3 = 0Bh
B4 = 0Ch
B5 = 0Dh
B6 = 0Eh
B7 = 0Fh
FLASHTRIG      = 08h
FLICKorFLASH = 09h
CFF_FLAG       = 0Ah
GREENOFF       = 0Bh
GREENFULL      = 0Ch
BLUEFULL       = 0Dh
GREENLEVEL  = 07h
.LIST
```

(a) Register file defining SFR memory locations

(b) Input and output memory location definitions

(c) Flags memory location definitions)

Figure 5.10: Extracts from the register file used to define memory locations referenced in the main program.

clockwise direction, and each trigger pulse[13] from the 8051 will advance the wheel by one position.

The number of trigger pulses, is the amount of times to trigger the wheel to get from the *current* position to the required (*AIM*) position. For example, if *Current* = 1 and *AIM* = 5, then *TRIG TIMES* = (5-1) = 4. This calculation is very straight forward when *Current* < *AIM*, however due to the fact that the wheel can only rotate in a clockwise direction, the calculation is a little more complicated when *Current* > *AIM*. ie if *Current* = 4 and if *AIM* = 3. Intuitively, it can be seen in order to return the wheel to position 4 from position 3, the wheel must be triggered 5 times. This can be viewed mathematically as 11 mod 6.

(a) Calculate required position and pass value to mod 6 subvi. This returns TRIG TIMES (The value to be sent to the 8051)

(b) Code to calculate *IN* modular 6
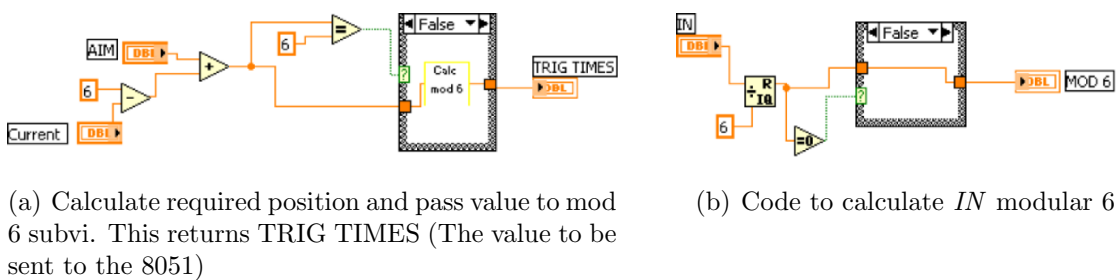
Figure 5.11: Labview code to calculate required position of filter wheel

Figure 5.11 illustrates the code used in this project to calculate filter positions. In order to find the required position, the current position ('current' in figure 5.11) of the wheel, and the required position (*AIM* in figure 5.11) must be known. As long as the value calculated in figure 5.11(a), is not equal to 6, then that value is passed to the subvi shown in figure 5.11(b). This calculates the modular 6 of this value, and thus returns the trigger value that must be sent to the 8051. In order for this method to remain accurate, the current position must be known at all times, this is the reason for the default position (position 1 in table 5.5). The design of the internal electronics in the filter wheel itself, defines this position as the default, and rotates automatically to this position on initially powering up. For this reason, on exiting the Labview program, the filter wheel is reset to this default position, and on starting up the Labview program, the starting position is defined as position 1 and required positions are calculated from this starting point. Full outline of the code required to carry this out can be found in the appendix.

Camera communication

The final area of data communication in the system is that of the control of the camera, and the acquired image information from the camera to the Labview interface. As outlined in chapter 4, the imaging camera used in this device, is the Retiga EXi. The camera is triggered via the 8051 controller and interfaced to the host PC via the firewire 1394 cable. The camera is allowed to run in two modes, free run and triggered mode, each of which will be outlined briefly in the following sections.

---

[13]Duration of pulse must be at least 1.0ms, with a max of 0.5 pulses per second.
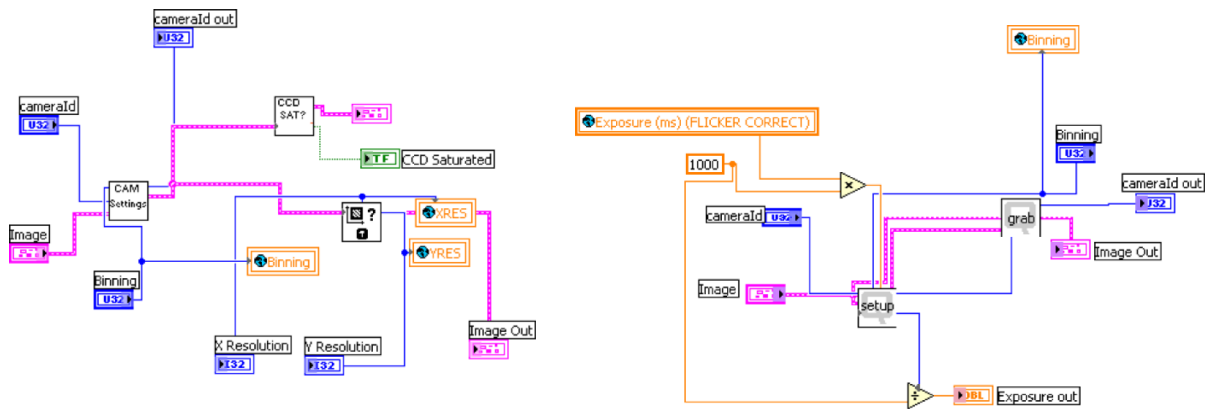
(a) Setting up of camera, Image in is defined as 12-bit, Camera ID identifies the retiga, Binning and resolution controlled by user and globally saved for further use, the two subvis in the diagram deals with saturation of the sensor and further camera settings ie run mode, exposure etc)

(b) Code to set up exposure for camera in free run mode. Included are subVIs provided by Qimaging.

Figure 5.12: Setting up the Retiga camera for correct exposure, binning and run mode. The values of the global variables in the code are user adjustable from the interface.

Free run mode

Free run mode is as the name suggests, where the camera is allowed to run, without any external influence. The various aspects of the running of the camera, such as the integration time, binning etc is inputted via the Labview subVI outlined in figure 5.13(a). The free run mode is easier to implement as it does not require any saving of images, as in trigger mode. The free run mode allows a live view of the retina on the labview front panel, which can aid in the alignment of the subject. When running in PWM[14], the exposure of the camera has to be adjusted to avoid flickering effects on the image caused by the finite overflow of the modulation. This correction will be outlined in a later section.

Triggered mode

Trigger mode is more difficult to implement than free run mode as there are a number of different factors to consider for a successful implementation of this mode. The goal of this mode is to provide 12 saved images, 6 blue and 6 green[15]. To achieve this goal, firstly the camera must be accurately triggered in time with each LED flash, and each subsequent image must be saved in memory. The triggering is achieved by the 8051 and electronic setup, both outlined previously, and correctly defining in Labview the appropriate triggering characteristics i.e camera is in triggering mode (Active LO). The code to achieve this is straight forward and can be found in the appendix, however, the code to save each of the images is a little more complex (figure 5.14) and will be outlined

---

[14]Pulse width modulation, outlined in a later section

[15]6 images of each were chosen to fit aesthetically on program screen. See figure 6.3(a)

here.
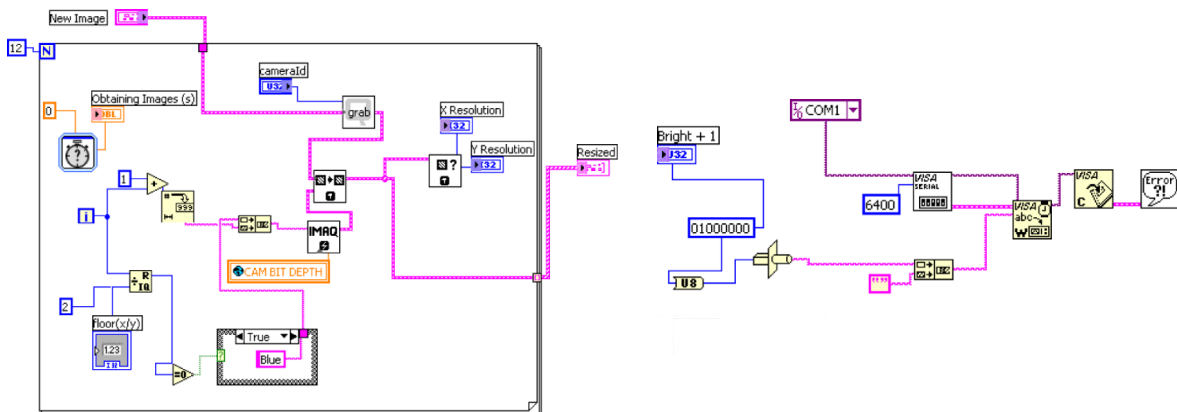
(a) The code is within a loop, each iteration of the loop produces a different image, which is uniquely saved according to its colour and loop number. The images are outputted as a 12 element array

(b) Code to communicate with the 8051 initialising the triggering routine. The byte 01000000 identifies the mode that the 8051 should run.

Figure 5.13: Setting up the retiga camera for triggered running and saving of the 12 captured images.

Each image is uniquely saved in a 2D array, it's size determined by the resolution of the image. In this project 13 images are acquired but only 12 images are saved. The first image is discarded, due to artifacts in the 8051 code which can lead to errors in the acquirement of first image for certain exposure times. The 12 saved images are bundled into a further array and saved for subsequent processing by Labview. The code outlined in figure 5.13(a) automatically names each image according to colour and sequence, which aids in retrieving the image at a later date. The loop value indicated in the code must match the loop value defined in assembly language, i.e if Labview expects 12 trigger events, then the 8051 must supply these 12 trigger events.

Image Choice

An important aspect for calculating the MPOD, in the reflectance and auto-fluorescence methods, is the quality of the acquired image. When the 12 images are obtained, an average of the blue and an average of the green images (see figure 5.14(a) for code) are calculated.

This reduces the noise in the image (readout/electronic noise and dark noise in camera), however, there are issues with individual image alignment. For example, this method works well for a static target, whereas with a real subject there will inter image variability, which will result in smearing of the average image. The ideal solution to this problem would be a subvi which automatically aligns each acquired image, and then calculates the average, unfortunately due to time constraints this was not possible. The solution was to allow the user to choose the image to work on. Essentially, the user has a choice of seven images for each colour (6 raw images and 1 average image), and then post process the choosen image to reduce the noise. This is achieved by saving each image in a global

90
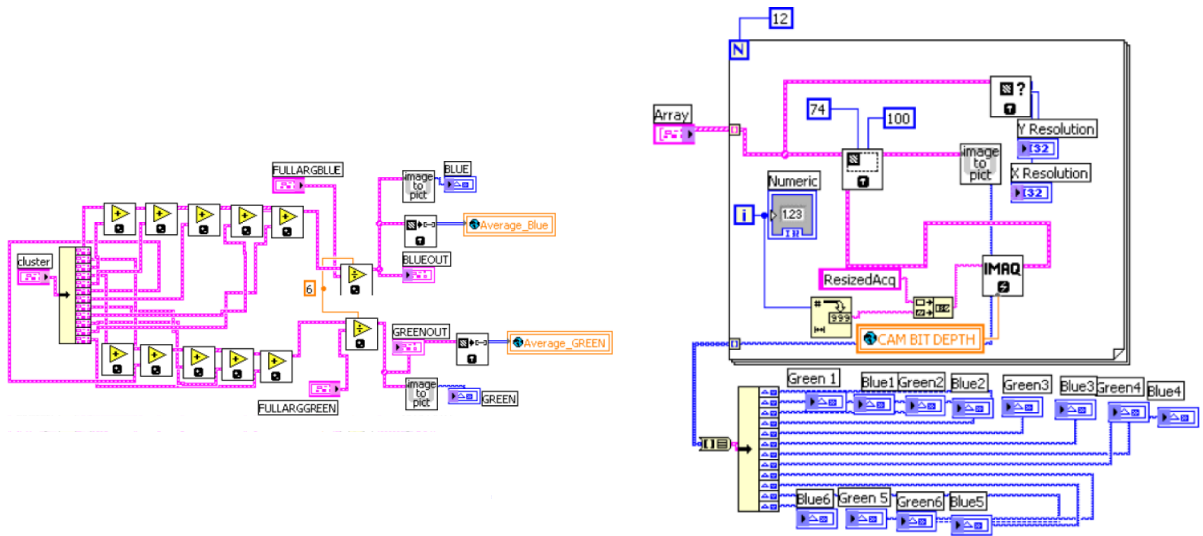
(a) Calculate the average green and blue image. Essentially calculate the average of six 2-D arrays and save the results as a 2-D array global variable.

(b) Extract each 2D image array from the array of images, convert to 12-bit image, resize and display on the front panel for subsequent choosing of image to work with.

Figure 5.14: Extracting each acquired image and calculating their averages.

variable and simply allow the user the option to pick which of these global variable to use, or alternatively continue with the default of using the average image. This is achieved as outlined in figure 5.15.
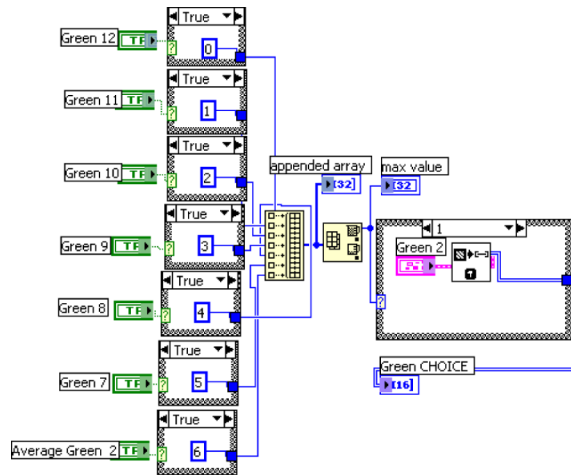
Figure 5.15: Allow user to choose which image to use. Choice is made by creating an array of identifying numbers, i.e. 1 for image 1, 2 for image 2 etc. Since only one image is chosen, it is possible to search the identifying array for the highest value. This is then used in the case structure to choose which image to save. This particular example is for green, a similar subvi is used for blue choice.

91

5.2 Pulse Width Modulation (PWM)

In order to provide a user friendly device, complete control of the system should be available using the Labview interface. In particular independent, dynamic control over the intensity of the two illumination LEDs would be an attractive feature. Essentially, what is required is to create a relationship between the Labview command and the intensity of the LED output at the cornea[16], real time estimate of the LED power can then be available without the need of a photometer, and light levels can be ensured to remain within safety limits (see appendix for ethical approval). The dynamic control of the LED brightness is also essential in the heterochromatic flicker photometry (HCFP) technique, as well as a method to flicker the LEDs at a variety of frequencies over a range of intensities. The technique employed in this project is pulse width modulation (PWM). Using the 8051 μ-controller, it is possible to independently control the current flowing through each LED and consequently control the individual brightness of each LED. The following sections will outline the technique of PWM and the code used to implement the procedure. The advantages and disadvantages of the technique will also be presented, in particular certain limitations of the technique will be highlighted.

5.2.1 Theory of PWM

Pulse width modulation (PWM) is the switching off and on of a circuit very rapidly, in order to adjust the behaviour of the particular circuit, i.e. speed of a motor or in this case the brightness of LEDs. Essentially the switching refers to the switching, and consequently the limiting, of the supply of current to the particular component, within the circuit.
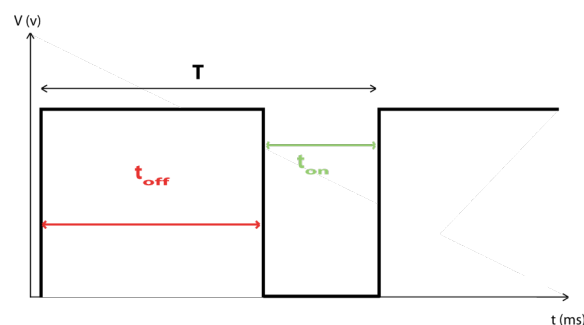
Figure 5.16: Single period in a PWM cycle for constant period T

However, the key to PWM is not changing the number of times the output switches on and off but rather the duty cycle of the signal, for a constant period. Figure 5.16 illustrates a single period in a PWM cycle. As mentioned in chapter 4, the LED driver circuit is active LO[17] therefore, in figure 5.16 the LED is on for t_{ON} and off for t_{OFF}. If t_{ON} is increased then t_{OFF} must be decreased in order to maintain a constant T, and vice versa. Figure

---

[16]See appendix for ethical approval application

[17]LEDs light up when LO signal present at relevant transistor base. See chapter 4 or figure 4.23.

5.26 demostrates the output for dim LED (5.17(a))and that of a bright LED(5.17(b)). Consequently, It is therefore possible to obtain a range of intensities by varying t_{ON} and t_{OFF}. The 8051 is coded to switch the LED at a constant rate T (well beyond the photoreceptors critical fusion frequency (CFF)[18], therefore no discernible flicker is observed), and also used to calculate t_{ON} and t_{OFF}, which are dependent on the input from the Labview interface. An outline of the assembly code written for this purpose follows, while inherent disadvantages associated with this method will also be outlined.

(a) LED mostly off   (b) LED mostly on
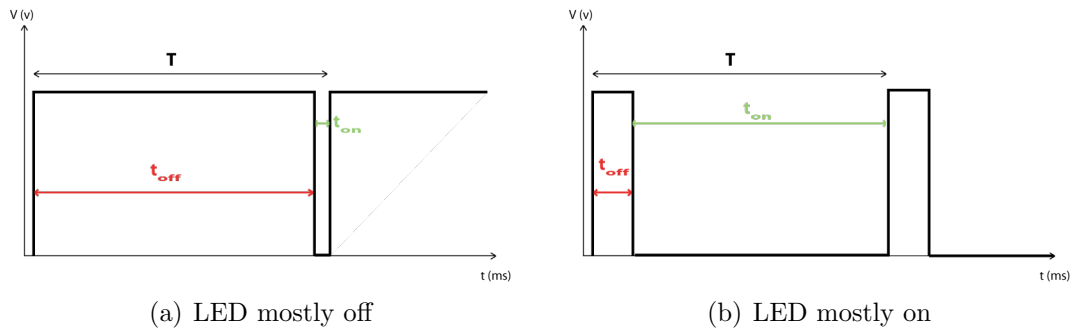
Figure 5.17: PWM to control the brightness of LEDs

Figure 5.26 illustrates the control of the HI and LO pulse of a constant period T, to achieve PWM. Again the key is modulation of the duty cycle for a constant T.

5.2.2 Method to implement PWM using 8051 micro-controller

To produce a constant period of T ($t_{ON} + t_{OFF}$), the timer interrupt can be used. Since timer1 is already in use for the calculation of the baud rate, timer0 will be utilised to implement the PWM method. The use of interrupts has been outlined in previous sections. Figure 5.18 illustrates a simple example of implementing PWM in assembly language, for controlling the brightness of a single LED.

Previously, it was explained how to set the timer up as a 8-bit timer mode[19], i.e. overflow at a value of 255. This mode executes an interrupt routine on each occasion the timer overflows, specifically each occasion timer0 reaches 255. The rate at which this overflow occurs, can be used to define t_{ON} and separately t_{OFF}, and consequently T. In order to achieve the full period T, two interrupts are required, one to define t_{ON} and one to define t_{OFF}.

In relation to the code illustrated in figure 5.18, an initial 8-bit[20] starting byte is sent to the 8051, called *LEDLEVEL*. This is the initial starting value from which the 8051 begins its count to 255. Initially t_{ON} is calculated, which is essentially the time it takes for timer1 to count from *LEDLEVEL* to 255. Once 255 is reached the overflow routine

---

[18]Critical fusion frequency, frequency threshold at which the photoreceptors can discern a flickering source

[19]See table 4.4

[20]Value between 0 and 255

```
PWM:              JNB CHOICE, T(HI)              ; If CHOICE is set then we just finished the T Low section
                                                 ; of the cycle so Jump to T(HI) to calculate T High
;*********************************************************************************************

T (LO):           clr CHOICE                     ; Make CHOICE=1 to indicate start of high section
                  CLR   LED                      ;Turn ON LED (Active LO)
                  MOV TH0, LEDLEVEL
                  reti


;*********************************************************************************************

T(HI):            SETB CHOICE                    ; Make CHOICE=0 to indicate start of low section
                  SETB LED                       ;Turn OFF LED (Active LO)
                  MOV A, #255                    ; Move 255 to A
                  CLR C                          ; Clear C (the carry bit) so it does not affect the subtraction
                  SUBB A, LEDLEVEL               ; Subtract R2 from A.  A = 255 - R7.
                  MOV TH0, A                     ; so the value loaded into TH0 + R7 = 255
                  reti
```

Figure 5.18: Simple example of implementing PWM in assembly language. This section of code will be called (interrupt will point to the label PWM) whenever timer0 (THO) overflows (reaches 255). The code is for one LED located in memory defined by LED, $CHOICE$ defines whether to calculate t_{ON} or t_{OFF} and $LEDLEVEL$ is the starting byte received from Labview.

is flagged, and the routine calculates t_{OFF}. On this occasion, the starting byte is defined by the following calculation, 255 - $LEDLEVEL$. Again, the overflow interrupt is flagged when 255 is reached, and this can be defined as t_{OFF}. The value stored in $CHOICE$, defines whether the calculation is for t_{ON} or t_{OFF}. Using this method it is possible to set up a constant period T, for a range of $LEDLEVEL$ values, so that $t_{ON} + t_{OFF} = 255$.

Calculation of overflow period, T

The overflow period T essentially depends on the XTAL speed of the chip. For the particular timer mode utilised in this project, each count of the timer is equal to 32 machine cycles. From the previous chapter the time for a single machine cycle was calculated,

$$1 \text{ cy} = 0.8138 \mu s \tag{5.4}$$

Since each count on the chip is equal to 32 machine cycles, it follows that the duration of each clock count is,

$$
\begin{aligned}
1 \text{ count} &= 32 \times 0.8138 \mu s \\
1 \text{ count} &= 26.0416 \mu s
\end{aligned}
\tag{5.5}
$$

Essentially the overflow period can be limited by the amount of counts available. Simply the maximum overflow period would consist of 255 distinct count values, which would also result in 255 levels of LED intensity. However this results in a overflow value of,

$$
\begin{aligned}
overflow &= 255 \times 26.0416 \mu s \\
overflow &= 6.64 ms
\end{aligned}
\tag{5.6}
$$

As will be outlined in later sections, this value can limit resolvable exposure and flicker frequencies. The most desirable overflow rate would be as little as possible. For this

reason count value of 50 was chosen. This limits the amount of distinct intensity values that can be resolved[21], however it does offer the advantage of greater temporal resolution and therefore more distinct exposure and flicker frequency values.

$$
\begin{aligned}
overflow &= 50 \times 26.0416\mu s \\
overflow &= 1.302ms
\end{aligned}
\tag{5.7}
$$

Whereas, figure 5.18 illustrates a very simple example of implementing PWM in assembly language, this particular project requires independent control over two LEDs, and appropriate triggering of the camera. As only one timer is used to implement the PWM, flags have to be used to achieve the various aspects outlined. This is possible due to the fact that the two LEDs are never on at the same time. The code used is illustrated in figure 5.19 and is based on the simple example of a single LED outlined in figure 5.18. The full code is included in the appendix.

The primary distinctions between this code and the simple example is the use of various flags to indicate the state of the program at a particular time. Further to the choice of whether to calculate t_{ON} or t_{OFF}, the particular LED currently in operation must be tracked, whether a camera trigger is required and whether mode running is flashing or flickering the LEDs. Another difference is the maximum overflow count is 50 as opposed to 255. For this reason all loaded values from Labview are initially added to the value 205. As outlined previously this results in a much quicker overflow rate, and while producing some restrictions, it does allow for overall a more versatile system. The result of this code can be seen in the next section, while some of the inferred restrictions will be outlined later.

---

[21]See sections on the potentiometer for solution to this problem

```
PWM:            JNB F0, LED_OFF              ; If F0 is set then we just finished the high section
                                            ; of the cycle so Jump to HIGH_DONE
;********************************************************************************************************
ON_LED:         clr F0                      ; Make F0=1 to indicate start of high section
                JB      LEDCHOICE, GREEN_ON  ;Decide which LED to set

BLUE_ON:        MOV A, #205
                ADD A, R2
                MOV TH0, A
                clr A
                JB      CFF_FLAG, IGNOREBLUE
                CLR     BLUE                ;SET Blue
                JNB FLASHTRIG, CAM_OFF
                CLR     CAM
                reti

GREEN_ON:       JB      GREENOFF, IGNOREGREEN  ;SET Green
                MOV A, #205
                ADD A, GREENLEVEL
                MOV TH0, A
                clr A
                CLR     GREEN
                JNB FLASHTRIG,  CAM_OFF
                CLR     CAM
                reti

IGNOREGREEN:    SETB GREEN

CAM_OFF:        SETB CAM                    ;If not flashing, CAM run in normal mode
                reti

IGNOREBLUE:     SETB BLUE
                reti                        ; Return from Interrupt to where the program came from
;********************************************************************************************************
LED_OFF:        SETB F0                     ; Make F0=0 to indicate start of low section
                JB      LEDCHOICE, GREEN_OFF  ;Decide which LED to set

BLUE_OFF:       JB BLUEFULL, FULLBLUE
                SETB   BLUE
                sjmp continueLO

FULLBLUE:       CLR BLUE
                SJMP continueLO

GREEN_OFF:      JB GREENOFF, continueLO
                JB GREENFULL, FULLGREEN
                SETB   GREEN                ; Turn off LED

continueLO:     JB      LEDCHOICE, GREEN_LO
                SJMP BLUE_LO

FULLGREEN:      CLR GREEN
                SJMP continueLO

BLUE_LO:        MOV A, #255                 ; Move FFH (255) to A
                CLR C                       ; Clear C (the carry bit) so it does not affect the subtraction
                SUBB A, R2                  ; Subtract R2 from A. A = 255 - R7.
                MOV TH0, A                  ; so the value loaded into TH0 + R7 = 255
                reti

GREEN_LO:       MOV A, #255
                CLR C
                SUBB A, GREENLEVEL
                MOV TH0, A
                reti
;********************************************************************************************************
;
```

Figure 5.19: The interrupt routine used in this project. This allows the independent control of the two LEDs, correct triggering of the camera and accurate control of single LED flickering (for CFF measurements)

Intensity of LEDs

Using the technique of pulse width modulation (PWM) it is possible to control the intensity of the LEDs utilised in the device. This ability to dynamically control the power output, and know the intensity of the LED at any time is a welcome attribute and aids greatly in the screening of subjects. This feature is achieved by sending the adjustment byte to the 8051, which is then used to adjust the duty cycle of the foundation overflow period T.
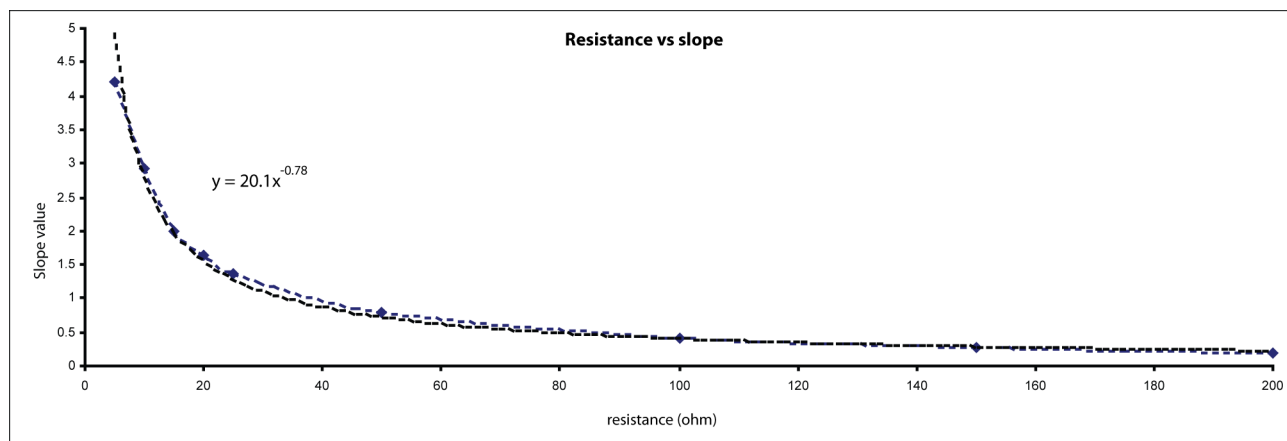
Figure 5.20: Effect of potentiometer resistance on the step size of intensity values (slope)
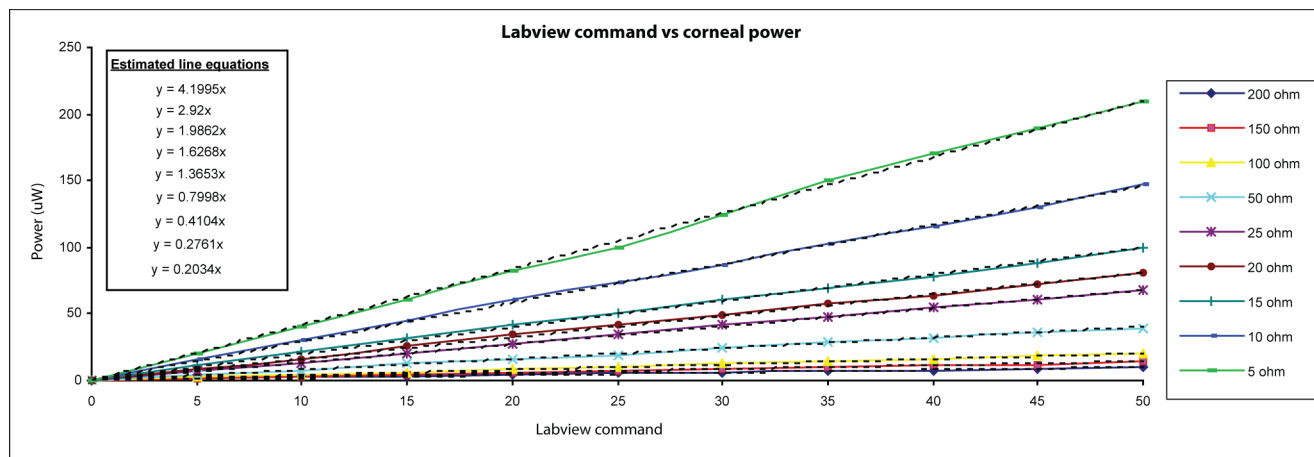
Figure 5.21: Power at the cornea as a function of labview command and start resistance (GREEN)

However, as was alluded to previously, it is important that this foundation period is as short as possible. In order to achieve this the count for overflow was reduced from 255 to 50. While this reduces significantly and successfully the overflow period, it also reduces the unique states of LED intensity, and therefore the intensity difference between adjacent states. To solve this problem a potentiometer was used to reduce the intensity steps

97

between each Labview command. This can also be stated as the sensitivity of adjustment of the LEDs. Chapter 4 illustrates in more detail the hardware setup for the device. Essentially the potentiometer limits the current through the LED and can be used to adjust the step size between each intensity level.
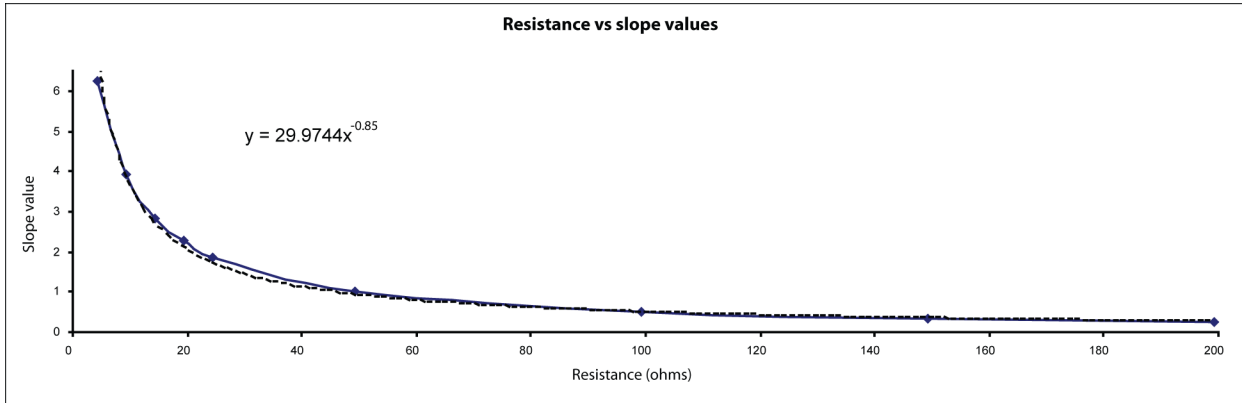
Figure 5.22: Effect of potentiometer resistance on the step size of blue LED intensity values (slope)
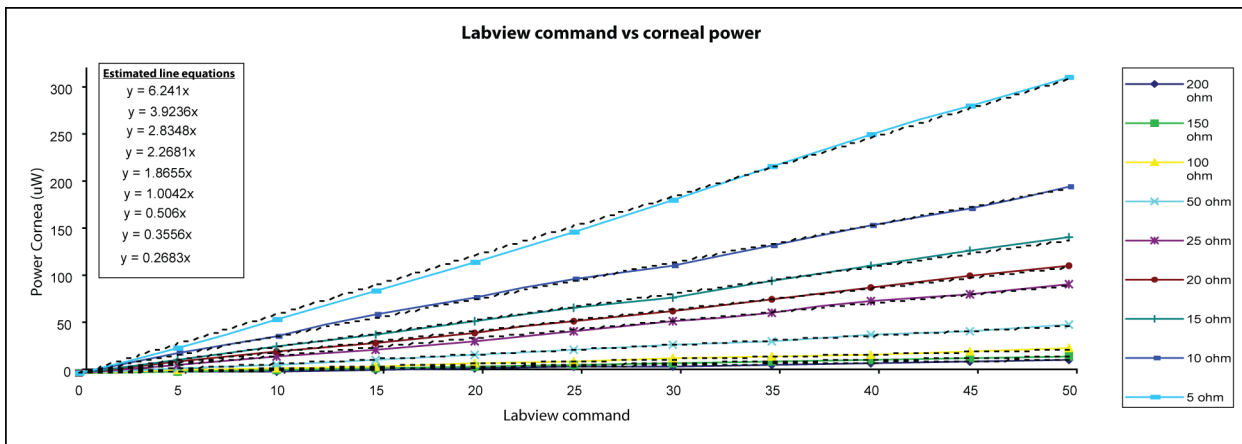
Figure 5.23: Power at the cornea as a function of labview command and start resistance (BLUE)

Figure 5.20 displays the slope values for various potentiometer resistance values for the green LED. Figure 5.22 displays the same results for the blue LED. The curve has being fitted to a power series and thus can be used to estimate the slope for a known resistance. Figure 5.21 displays the power[22] at the cornea for each Labview command. Therefore if we know the resistance across the potentiometer, and the Labview command we can accurately calculate the power of the LED on the cornea.

---

[22]Measured using two power meters. The 0220701 optical power meter system from Thorlabs using sensor head S120A and the Newport power meter , model 1815-C utilising sensor model number 818-SL.

98

The two graphs displayed in figure 5.20 and figure 5.21 refer to the result for the green LED. However the blue LED will display different attributes (heating considerations, lighting methods, individual component differences etc) and this is reflected in the the output of the LED. Using the potentiometer, it is possible to match the behaviour of the blue LED to that of the green LED (power at cornea for each Labview command). This will not overly effect the final result for the macular pigment optical density but presents an more attractive system where the behaviour of both LEDs are comparable.

Using known potentiometer resistance and the Labview command it is now possible to calculate the power of the LED at the cornea. This avoids having to recheck the power using a power meter and adds greatly to swift and safe measurement of subjects.
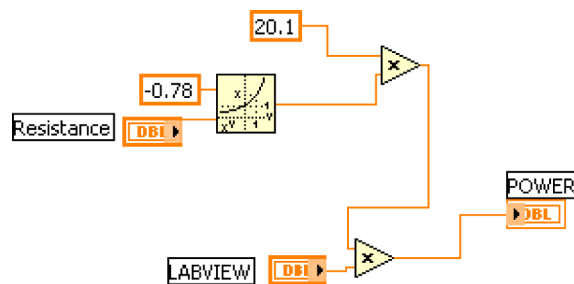
Figure 5.24: Labview calculation of power of led at the cornea. The inputs are the potentiometer resistance for the specific LED and the desired LED value. The power is calculated from the graph characteristics illustrated in previous graphs. This is for the green LED, a similar VI exists for the blue LED utilising the blue LED characteristics.

One disadvantage is the need to measure the potentiometer resistance manually. This value will rarely change but an attractive solution would be to measure dynamically the resistance using Labview (by means of an A to D converter). Unfortunately due to time constraints this solution was not pursued.

Implementing exposure while retaining PWM (examination of limitations)

Accurate implementation of the pulse width modulation (PWM) technique requires that two overflow interrupts are calculated, specifically t_{ON} and t_{OFF}. These two interrupts constitute the infrastructure from which it is possible to build pulses of desired exposure, while retaining the desired intensity (implementing PWM). Any exposure therefore is a multiple of the interrupts, t_{ON} and t_{OFF}, or simply the constant period T. Alternatively the temporal resolution of the LED exposure is restricted by T. For example figure 5.25 represents an exposure of 4*T ms (loop iteration of 8).

$$Exp = n \times T; \text{ n is positive even number} \tag{5.8}$$

The exposure of a pulse is established in two steps. Labview transmits a loop value to the 8051, depending on the desired exposure. This is easily done on the Labview interface
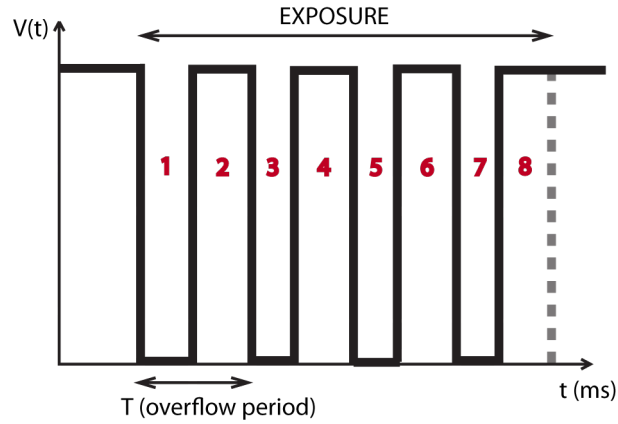
Figure 5.25: Method of building pulses of required exposure width from fundamental overflow period T thus retaining PWM.

by use of text labels (see table 5.6). Once the 8051 receives the loop value, and the flash command is detected, the 8051 will loop for the desired exposure, while retaining the desired intensity. Equation 5.9 displays the equation for calculation of a loop value for a desired exposure (EXP) for a specific overflow period (T). The value will be an odd number in this case due to the DJNZ command in assembly language. The command means decrement and jump if the value is not zero (jump to a label), otherwise execute the code following the command. Therefore the code following the command is not executed when the value is 0, therefore to execute the code following the command 8 times, a loop value of 9 must be loaded.

Equation 5.9 can be used as a generic estimate for the loop value for a number of different overflow values T. However, this equation doesn't consider other inherent delays that may be included in the delay and is specific to the on chip code such as transition between on and off, reading serial port values etc.

$$loop = \left(2 \times \lfloor \frac{EXP}{T} \rfloor\right) - 1 \tag{5.9}$$

A more robust estimate is given by equation 5.11. This is for an overflow value of 1.360 ms and is particular to the behaviour of the μ-controller used in this project.

$$loop = 1.468 \times EXP + 1.4667 \tag{5.10}$$

Table 5.6 lists the exposure desired exposure values and the loop value sent to the 8051μ-controller. Notice that the loop value is also a odd integer for the reasons outlined previously.

In order to achieve an adequate exposure resolution, the overflow time T must be a minimum. However, the limitations of PWM are far more critical with regards to the

100

```
;************************************************************************************************
;*                                   TIMER INTERUPT JUMP LOCATION                            *
;************************************************************************************************
LEDDim:              clr ET0
                     JNB FLASHTRIG, PWM              ;FLASHTRIG set implies flash, FLICKorFLASH decides
                                                     ;flicker or flash
                     JB SKIPR5, skipexp1             ;ensure 1 pass on each pulse
                     DJNZ R5, PWM                    ;exp1 value
                     JNB overflow, skipof
                     SETB SKIPR5

skipexp1:            CJNE R1, #0,  outloop           ;count loop 254 value
                     sjmp skipof                     ;254 loop finish;exit

outloop:             DJNZ ExpFULL1, PWM              ;loop max value of 254 R1 times
                     DEC R1                          ;dec r1 to indicate pass
                     MOV ExpFULL1, #254              ;reload expfull1 for next pass
                     sjmp skipexp1                   ;jump back to looping 254

skipof:              MOV TH0, #255
                     JB FLICKorFLASH, EXITLOOP
;************************************************************************************************
LOOPCOUNT:           DJNZ C6,DELAYLO                 ;R1 flash count, loop through 12 times, matched what
                     SJMP EXITSEQ                    ;labview expects
                                                     ;Jumps on 0! so to flash 12 load 13
;*************************************
;EXIT ROUTINE AFTER ALL FLASH COMPLETE
;*************************************
EXITSEQ:             CLR FLASHTRIG                   ;unflag LED pulsing
                     clr SKIPR5
                     SETB ET0                        ;restart Timer interupt
                     reti
;*****************************
;All off between ind. pulses
;*****************************

DELAYLO:             MOV P2, #%10100011              ;All off
                     MOV    R3,#150
LOOP1LO:             MOV    R4,#150                  ;ALL OFF TIME DELAY
LOOP2LO:             DJNZ   R4,LOOP2LO
                     DJNZ   R3,LOOP1LO
;*****************************
;reset parameters for remaining pulses
;*****************************
EXITLOOP:            CLR A
                     MOV    A,R6        ;reload exposure values
                     MOV    R5,A
                     CLR A
                     MOV    A,copyR1    ;reload loop value for 254 loop
                     MOV    R1,A
                     CLR A
                     MOV ExpFULL1, #254 ;reload expfull
                     CLR A
                     CLR SKIPR5
                     CPL LEDCHOICE      ;Complement LED choice, switch from G to B and vice vearsa
                     setb F0
                     SETB ET0
                     RETI
```

```
;************************************************
Exposure:            clr ET0                        ;turn off interrupt to ensure all data loaded
                     clr overflow
                     clr TI
                     MOV SBUF, #%00000001
                     jnb     TI,$
                     clr TI
                     jnb     RI,$
                     MOV   R5, SBUF                  ;exp1 from labview, remainder if expval>254
                     MOV   R6, SBUF                  ;need to keep copy of exp so can reload later
                     clr RI
                     clr SBUF
                     clr TI

                     MOV SBUF, #%00000001
                     jnb     TI,$
                     clr TI
                     jnb     RI,$
                     MOV   A, SBUF                   ;second value accounts for numbers >8bit
                     clr RI
                     JZ NOoverflow                   ;if 0 then expval<254 otherwise split
                                                     ;into divisor and remainder
                     MOV R1, A                       ;load into R1
                     MOV copyR1, A                   ;copy so can be reloaded
                     SETB overflow                   ;flag overflow loop
                     clr A

NOoverflow:          clr A
                     setB ET0
                     RETI
;************************************************
```

(a) Load and save loop value from labview

(b) Implement exposure value from saved loop value

Figure 5.26: 8051 implementation of attaining various exposure values while retaining PWM. Note also the use of overflow interrupts to indicate overflow of loop values and consequent splitting of the value (see later section)

Desired Exposure (ms) (Front panel label)	Loop value (value sent to the 8051)
50	75
75	111
100	149
125	185
150	221
175	259
200	295
225	331
250	369
500	731
750	1099
1000	1463

Table 5.6: Desired exposure and required loop values

heterochromatic flicker technique. This technique requires the LEDs to be flickered at high frequencies and will be discussed in later sections.

Exposure select (limits on free run preview)

As outlined previously, the use of PWM limits the temporal resolution of the LED output. This has an effect on the exposure of the camera, specifically on the preview window, when the camera is in freerun mode. In order to avoid image flickering, the exposure of the camera has to be a multiple of T (overflow time)[23]. In otherwords, the exposure of the camera must match that of the exposure of the LEDs. For simplicity the exposure times available to the user are 50ms, 100ms, 150ms, 200ms, however, in reality these exposure values are corrected to account for T, thus avoiding the flickering of the image in the preview window.

Figure 5.27 displays one of the cases in the code used to achieve this correction. The loop values stored in the global variable *Exposure*, are used to select a specific case in the case structure, the appropriate exposure value is then sent to the camera (via the global variable *Exposure(ms)(FLICKER CORRECT)*), so that the exposure value of the LEDS is matched to that of the exposure value of the camera.
Table 5.7 compares the desired and actual exposure values for the freerun mode. This illustrates one of the disadvantages of implementing PWM, and the importance of a small overflow period. This correction however, avoids flickering, and results in a more accurate representation of the image expected after acquirement[24].

---

[23]See section 5.3.2, specifically exposure and flicker restrictions

[24]Not required in triggering mode, as exposure values are set by the 8051, and as a result will match with those of the LED. Correction only required in freerun mode where exposure of the camera is independent of the 8051
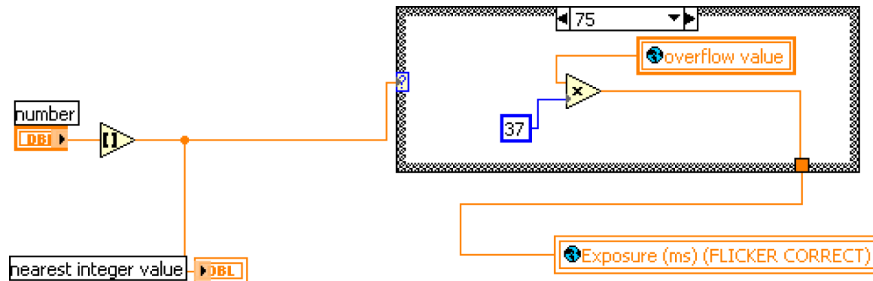
Figure 5.27: Correct the exposure value for preview to account for overflow restrictions from PWM. The exposure is limited to steps of the overflow period, and the camera is corrected as such. One case is illustrated, that of 50ms desired exposure, or 75 loop value. All 12 available exposure values have a similar correction procedure.

Desired Exposure (ms)	Actual Exposure (ms)
50	49
75	75.1
100	101.2
125	124
150	150.1
175	176.3
200	199.1
225	225.2
250	254.6

Table 5.7: Desired exposure and actual exposure values

Critical Fusion Frequency (CFF) measurement (overcoming XTAL limitations)

The critical fusion frequency (CFF) is the threshold frequency at which the photoreceptors can perceive a flashing stimuli, in otherwords, stimuli presented at a higher rate than CFF are perceived as continuous stimuli. This device can measure a subjects CFF, in order to more accurately, and more easily obtain heterochromatic flicker photometry (HCFP) readings. The 8051 can be coded to flicker the LED at various frequencies and thus measure the subjects CFF. For a 50% duty cycle, the relationship of t_{ON} to the flicker frequency can be seen in figure 5.28. As one will notice from the graph, the higher frequencies require t_{ON} values that are becoming closer and closer together.

$$
\begin{aligned}
loopval &= 2 \times \lfloor \frac{t_{ON}}{\lfloor T \rfloor} \rfloor + 1 \\
t_{ON} &= \frac{desiredfreq}{2}
\end{aligned}
\qquad (5.11)
$$

This problem of resolving t_{ON} to achieve these higher frequency values manifest for slow overflow times (T). Again this is due to the fact that the overflow period T, directly affects the temporal resolution of the system. The loop value required to achieve the desired frequency for a overflow period T is shown in equation 5.11.
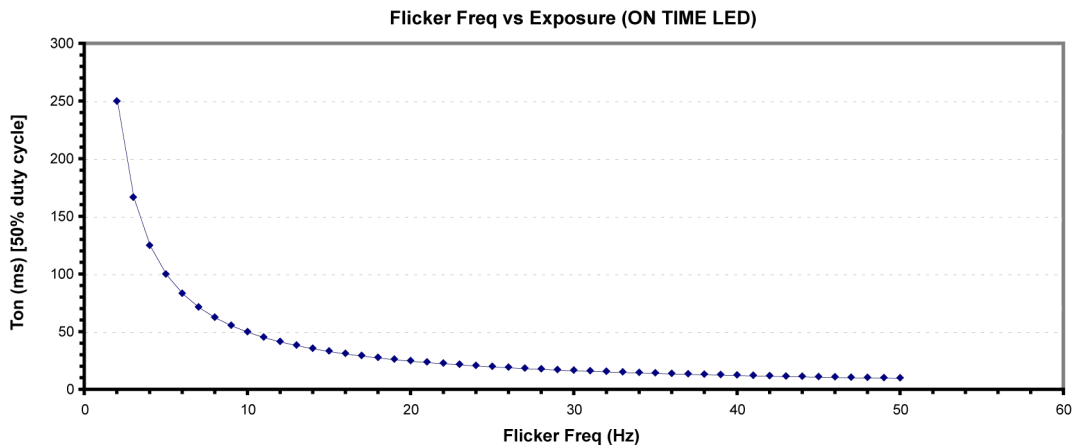
Figure 5.28: Flicker frequency as a function of LED on time (50% duty cycle).

Figure 5.29 illustrates the resolvable frequencies for different overflow periods for the 8051. A subjects CFF will depend on the luminance of the stimulus (see Ferry-Porter law in chapter 7). For this project the luminance level is such that the CFF values will vary approximately between 13 Hz and 24 Hz, and so this range should be resolvable. The red line in figure 5.29 represents the behaviour of the current system. Again this is not ideal as 20 Hz and 24 Hz are not resolvable[25], however, the performance is still an improvement

---

[25]May be a problem at higher luminance levels, as CFF is related to luminance of stimuli (see figure 7.6)
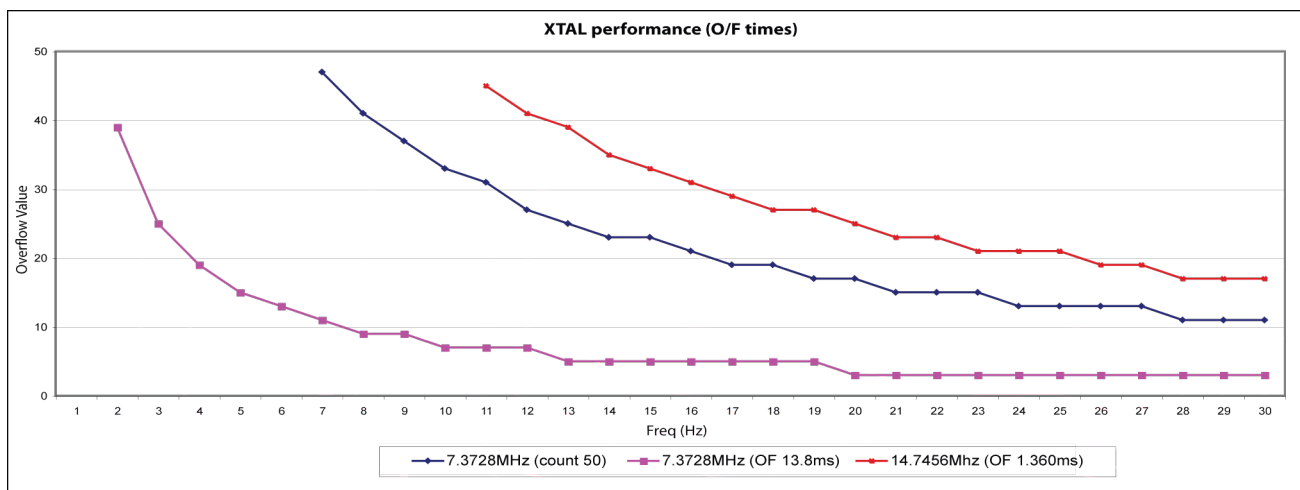
Figure 5.29: Comparison of different overflow rates and the restriction of frequency resolution for the 8051.

on slower XTALs[26] and satisfactory for this project. Table 5.8 displays a list of some of the frequencies available and their required loop value. For values greater than 254 the method of splitting the number is carried out, and appropriate flags indicate so on the 8051 (see later section).

Once a subjects CFF is measured, this information can be used to flicker alternately the blue and green LED, at a frequency equal to that of the subjects CFF. This has the advantage of suppressing the influence the short wavelength cones may have on the MPOD measurement and may improve the accuracy of reaching the minimum flicker point[27]. The improved accuracy arises from the fact that flicker is reduced to a minimum when the luminances are perceived equal (when presented at subjects CFF, the flicker arises from differences in luminances and not from the temporal effects (blue cones suppressed, so perception arises from middle and long wavelength cones)).

The distinguishing factor between CFF measurements and HCFP measurements is the use of two LEDs as opposed to single LED displaying 50% duty cycle. This is implemented in assembly language using the *FLICKorFLASH* flag.

Differentiation of flicker and flash of LEDs

As alluded to in figure 5.1 there is differences between flicker and flashing. Flickering of the LEDs is used in the reading of the subjects critical fusion flicker (CFF) and also in heterochromatic flicker photometry (HCFP) measurements. The flashing technique refers to the objective techniques of reflectance (RE) and auto-fluorescene (AF) and involves the use of the camera. Due to the finite readout speed of the camera an extra delay is required to ensure accurate and complete data read out to the host PC, for this reason

---

[26]For purple line, 8 to 9 Hz, 10 to 12 Hz, 13 to 19Hz and 20Hz + not resolvable.

[27]Point at which the perceived luminance of the blue and green stimuli are equal.

Desired Frequency (Hz) (Front panel label)	Loop value (value sent to the 8051)
2	368
5	149
10	75
15	49
19	39
21	37
22	35
23	33
25	31

Table 5.8: Selection of desired frequency and required loop values

the flash technique does not display 50% duty cycle. There occurs a period where both LEDs and camera are off (allows for camera read out[28]). In contrast the flicker method has no concerns with the camera and therefore displays 50% duty cycle (essentially for frequency measurements). These two methods are differentiated in code by their initial identifying byte. As the code is executed the flag *FLICKorFLASH* indicates whether the extra delay is required for camera readout. Further to this the *CFF_FLAG* indicates whether CFF or HCFP measurements are being carried out. The difference here being the participation of one or both the LEDs.

Splitting of 8-bit number to accomodate adequate time delay

The key to producing the desired exposure durations, delay loops, implementing flickering and flashing is timing, and in particular delays. However due to the timing set up (8-bit) the maximum count that the 8051 can handle is consequently 8-bit, namely 254. (0 to 254, 2^8 distinct states). For greater timing durations, due to the fast overflow, it is neccesary to load loop values which are greater than 254 (see table 5.6).
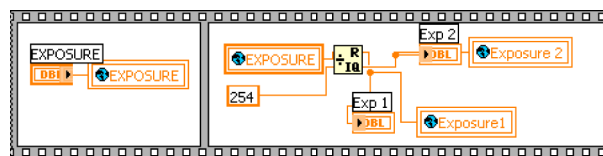
Figure 5.30: Labview VI to split the exposure loop value into two if the exposure loop value is greater than 254

To achieve the desired delay it is necessary to split the exposure loop value. Figure 5.30 displays the Labview code to carry out this task. If the exposure is greater than 254

---

[28]Readout time approximately 37ms which is constant for all exposures

then it is split into two exposure values, the quotient value and the remainder value, for the exposure divided by 254. These two values are then sent to the 8051 where the appropriate delay is then implemented. Figure 5.26 displays the assembly code used to implement such an occurrence in the 8051. Essentially a loop is set up to delay for the maximum value of 254. This loop value is the quotient value calculated in Labview. The delay dictated by the remainder value is also implemented to achieve the full overflow value desired. For value less then 254 just the remainder value is implemented. Using this method is is possible to achieve a vast range of exposures[29], and as the all off time is calculated using the same method, a number of duty cycles can also be easily achieved. The resolution is the overflow time T, which for this project is 1.36ms. The same method is employed to achieve the slower frequency values for the flicker technique.

LED intensity adjustment techniques

The basis and success of the heterochromatic flicker photometry (HCFP) technique, is the ability to adjust the intensity of a blue flickering LED to match that of a flickering green LED. The method at which this flicker match is made is vital to the accuracy of the final result. In this project the user has the choice to adjust the LED intensity by means of two methods, use of the mouse or use of the keyboard. This confronts the problem in previous designs, of subject learning of the position of minimum flicker match. This problem arose due to clearly defined start positions and end positions on a circular dial. These methods outlined for this project has no such detectable boundaries. Figure 5.31 illustrates the code for translating keyboard activity to LED adjustment values.

Figure 5.31: Labview VI to translate keyboard activity to LED adjustment values. The LED is adjusted using the up and down keys, while the sensitivity of the adjustment is controlled by the left and right keys.

Further to this two different adjustment schemes are available, that of normal and yoked adjustment. Normal adjustment is the method where the user is presented with an alternatively flickering green and blue LED, and is required to adjust the intensity of only the

---

[29]Loop values from 0 to $(254 \times 254) + 254$

Figure 5.32: Labview VI to change the adjustment scheme of the LEDs.

blue, to match the green LED which remains at a constant intensity. Yoked adjustment is a method where both LED intensities change dependent on each other. In other words, as the intensity of the blue LED is adjusted by a certain level, the green is automatically adjusted opposing the change, by the same[30] level. This method allows any perceived differences in luminance's to be far more perceivable than with just normal adjustment. Figure 5.32 displays the Labview code to implement the yoked method of adjustment for the LED.

5.3   Data analysis

The data analysis refers to the processing carried out on the data acquired from the system. The data for the objective methods are the images acquired by the imaging camera, while in the subjective method the subject feedback constitutes the data. In this chapter emphasis will be placed on the code, so screen shots will be of the block diagrams. The result of the code, and subsequent front panel screen shots will be presented in the results section in chapter 6.

5.3.1   Objective methods

The key to calculating the macular pigment optical density (MPOD) from the objective methods is applying equations 5.12 and equation 5.13 for the auto-fluorescence (AF) and the reflectance (RE) technique respectively[31].

$$D_{AF}(460) = \frac{1}{K_{mp}(\Lambda_1) - K_{mp}(\Lambda_2)} \times \left[\log \frac{I_P(\Lambda_1)}{I_P(\Lambda_2)} - \log \frac{I_F(\Lambda_1)}{I_F(\Lambda_2)} \right] \qquad (5.12)$$

$$D_{RE}(460) = \frac{0.5}{K_{mp}(\lambda_1) - K_{mp}(\lambda_2)} \times \left[\log \frac{I_P(\lambda_1)}{I_F(\lambda_1)} - \log \frac{I_P(\lambda_2)}{I_F(\lambda_2)} \right] \qquad (5.13)$$

---

[30]Same refers to the overflow value sent to the 8051. If the change in blue overflow value is +2 the change in the green overflow value sent to the 8051 is -2. The intensity produced is determined by the off resistance across the specific LED (see earlier sections for complete explanation of determining LED intensities).

[31]See chapter 3 for explanation of equations.

In order to apply these equations the macular region must be isolated from the surrounding parafoveal regions. Log difference images must be calculated for the acquired green and blue images. In addition the macular pigment peak density must be calculated[32] and finally the distribution of the pigment across the desired area of the retina. Filters are also applied in order to reduce noise. These processes will be briefly outlined in the following sections. Some features of the code will not be discussed, but may be referred to, however the full code can be seen in the appendix.

Macula area identification

In order to calculate the MPOD, the macular area must be isolated from the selected acquired images. The method of acquiring the images and calculating the image averages is outlined in previous sections. Since the distribution of the pigment varies among individuals [51], a generic extraction of a set area from the acquired image may lead to inaccuracies in calculating the MPOD. For this reason, the user is required to manually chose the macular region from a displayed blue image of the retina.

The code illustrated in figure 5.33, presents the user with the selected blue retinal image and requests that the macular region be defined. This is done intuitively, by presenting the user with a graphical tool (oval), which can be manipulated on the blue image, and used to select the desired area. The selected coordinates of the macular region are saved in a global variable. This information can then be used to extract the corresponding region from the corresponding green image, return the size of the extracted image (in mm and °'s), and utilised to extract regional information in regards to the parafoveal sections of the images.

The front panel activity and consequent result of this extraction can be seen in chapter 6.

Region extraction

The information gathered from the selection of the macular region can be used to divide the image into five distinct regions (see figure 6.4(b)). Each of these regions can now be extracted from the original image, and the information contained within each region can be used in the calculation of the MPOD.

The primary difficulty with accurate region extraction is the presence of the field stop in the selected images. Since the calculation of the MPOD depends on the average intensity values from each region (see figure 6.2, 6.1), from each image, the presence of the field stop will adversely bias the average calculation. Therefore it is necessary to extract the desired retinal information from the particular region, in each of the selected images. Figure 5.35 displays the code to isolate the retinal information from the field stop. The code displays each image region for the inputted image, calls the extraction subvi and returns the original histogram and the updated histogram containing just the retinal information. The

---

[32]Central 1° area of the fovea
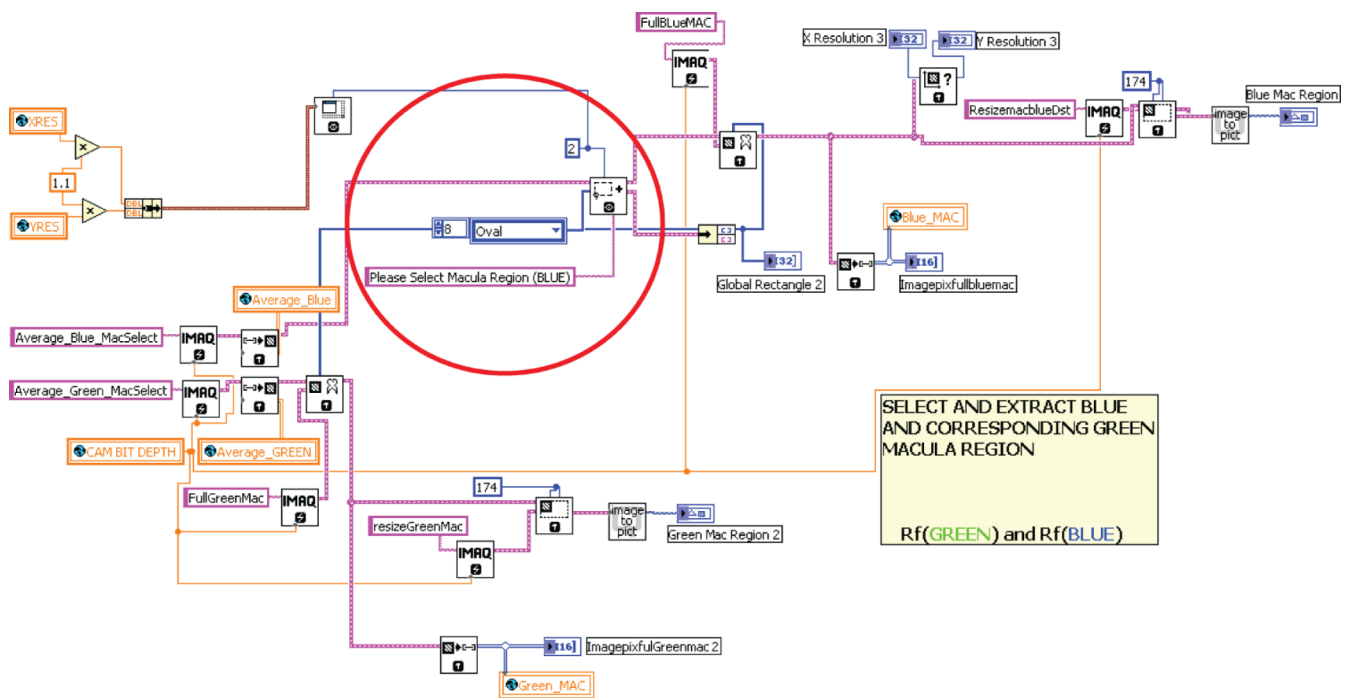
Figure 5.33: Code to extract the macular region. The user manually selects the region on the displayed blue image, the software automatically divides both images into five different regions. The code circled in red prompts the user to select macular region of displayed blue region. Using the inputted information the program displays on the front panel the extracted macular region of the blue and green images, then saves these regions as *Blue_MAC* and *Green_MAC* respectively. The coordinates of the macula is saved and used in a subsequent subvi to define the other regions of the image.
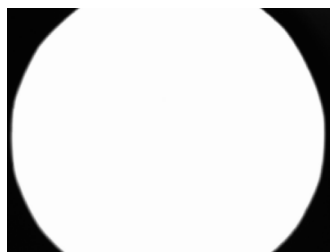
Figure 5.34: Image of the field stop in the system. Image obtained by saturating the retinal field.

subvi code is displayed in figure 5.36. This code simply converts the 2D image array into a 1D array and produces a histogram of these values. The histogram represents from left to right, low intensity values to higher intensity values. Since we know that the intensity value of the field stop is relatively low, it is possible to extract information higher than this threshold value, thus producing information independent of the field stop. The subvi then calculates the average intensity value of the particular region, ignoring the presence of the field stop.
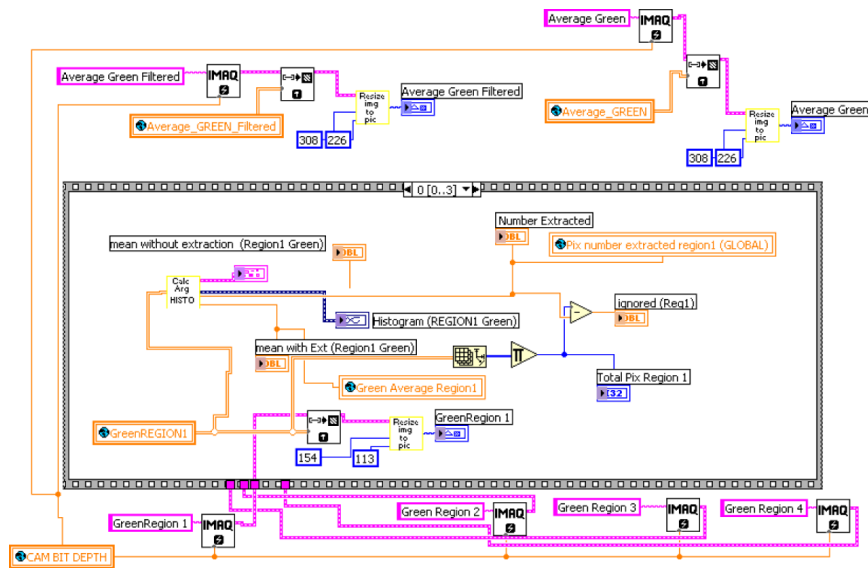
Figure 5.35: Code to extract the parafoveal regions. The subvi calcHistoarg is outlined in figure 5.36. The code is arranged in a stacked sequence therefore only one instance of the loop is displayed. A similar instance of the code exists for each particular region of both colours.

The input for this vi is the selected blue and corresponding green image. However, the image is first passed through a low pass gaussian filter to reduce the noise in the image, produced from electronic and readout noise of the camera.

Incorporation of the extinction coefficients

The extinction coefficient essentially is the fractional depletion of radiance per unit path length, for the particular radiation propagating through the particular medium. Figure 5.37 displays the calculation for the extinction coefficients for the two wavelengths in relation to the macular pigment. The data presented assumes maximum absorption of the pigment at 455nm, or in otherwords an extinction coefficent of 1, at this particular wavelength. The calculation for the two colours depends on the overlap between the LED emission spectrum and the pigments absorption spectrum. This is illustrated in the graphs presented in figure 5.37. The data used was originally measured by Brown *et al* using HPLC[33] on unfixed retinal tissue of a rhesus monkey. The data was averaged over the spectral distribution of each of the excitation lights to obtain the effective extinction

---

[33]High performance liquid chromatography
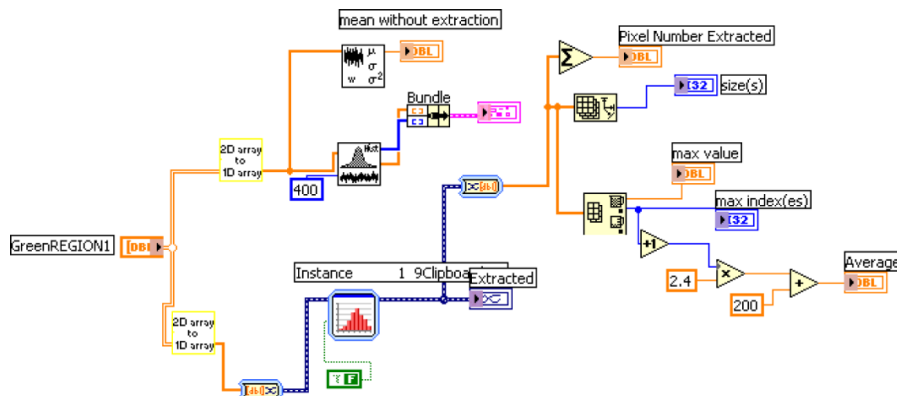
Figure 5.36: The subvi calcHistoarg. This produces a histogram of the inputted image and extracts the values produced by the retina. These values are then saved for further analysis and calculation.

coefficient for each LED. These values for the effective extinction coefficient of the green LED and the blue LED, 0.9137 and 0.0402 respectively, is incorporated in Labview via the VI illustrated in figure 5.38. This VI calculates the quotient outside the bracket outlined in the equations in equations 5.12 and 5.13.
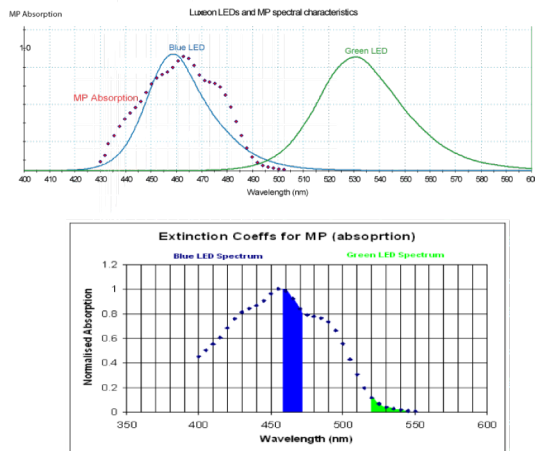
λ_1 (nm)	Extinction Coeff (Kmp(λ_1))	λ_2 (nm)	Extinction Coeff (Kmp(λ_2))
445	0.904	520	0.116
450	0.96	525	0.067
455	1	530	0.041
460	0.983	535	0.026
465	0.923	540	0.017
470	0.838	545	0.01
475	0.788	550	0.005
Average	0.9137	*Average*	0.0403
Correction RE	**0.572**	Correction AF	**1.145**

Figure 5.37: Illustration of the calculation of the extinction coefficients for the macular pigment. The values stated are meaured by Brown *et al* as quoted in [9]

Isolation of 1-degree and 4-degree area of macular region (MPOD peak calculation)

The peak MPOD refers to the density measured over the central 4° area of the pigment, biased towards the central 1° area. In order to carry out this calculation, it is necessary to isolate the desired areas from the calculated difference image.
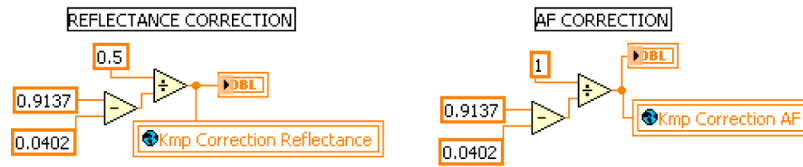
Figure 5.38: Code employed to implement the extinction coefficients for the green and blue wavelengths. The values for the extinction values are those calculated as illustrated in figure 5.37.
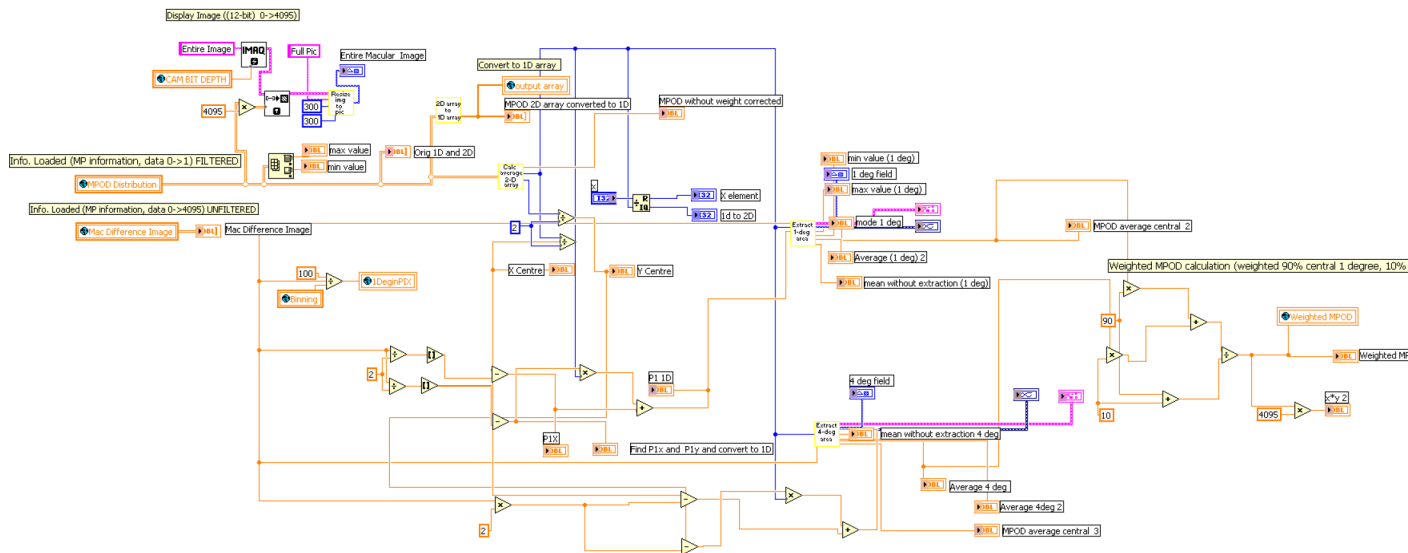
Figure 5.39: Main VI to extract 1 degree and 4 degree information from inputted image

The VI in figure 5.39 displays the main sub VI code to extract the two regions, central 1°
and 4°, and calculate the weighted average over the region. This VI contains two impor-
tant subvis to extract the two desired regions and calculate the averages. These subvis
can be seen in figure 5.40 and figure 5.41.
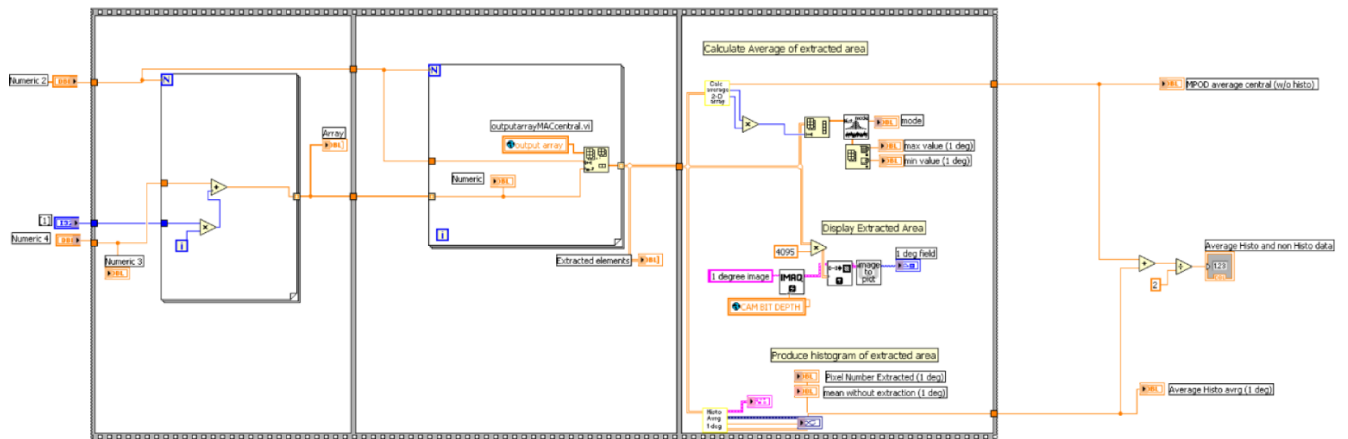
Figure 5.40: SUB VI to extract 1 degree information from inputted image
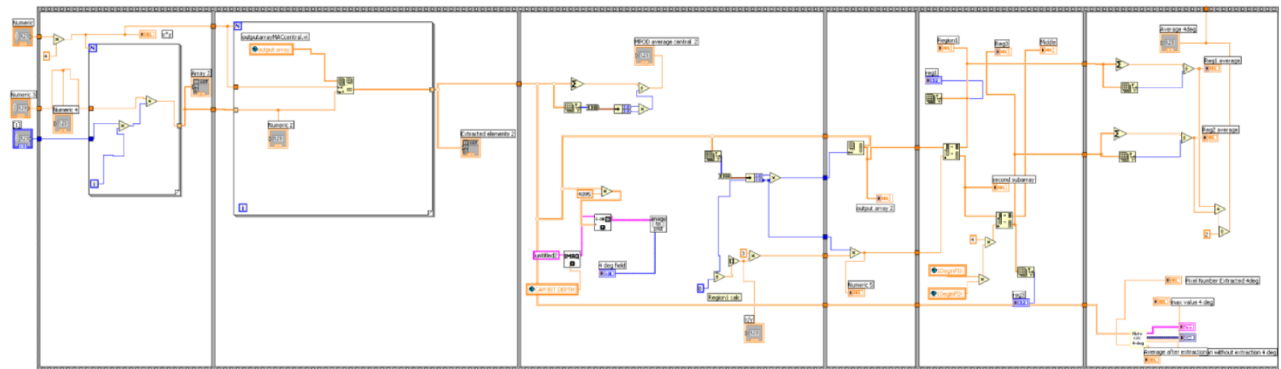
Figure 5.41: SUB VI to extract 4 degree information from inputted image

The important aspect of this VI is that accurate extraction must be carried out for varying
input image sizes. Therefore the extraction must be essentially independent of the image
size, ie must not be calculated as a percentage of the image, as the input image will vary
with subject. The size of extraction is therefore defined by individual pixels (corrected
for binning). The code converts the 2D image array into a 1D array and extracts the
appropriate sections of this array, depending on pixel information. The code recombines
these extracted sections to rebuild the 1° and 4° 2D array. The front panel activity, and
outcome of the Subvis illustrated in figure 5.40 and figure 5.41 can be seen in chapter 6.

The average values are calculated from these recombined arrays and saved in a global VI. The weighted average is then calculated and applied to the appropriate equation to calculate the peak MPOD.

MP distribution estimation

The macular pigment distribution is the calculation, and display of the pigment across the desired area of the retina.
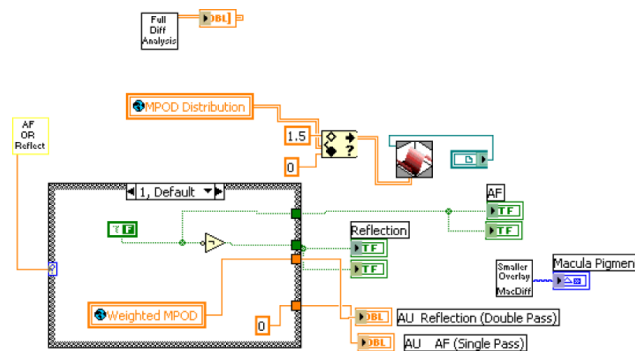
Figure 5.42: SUB VI to extract and display the MPOD distribution across the desired area of the retina.

The code displays both a 2D and 3D representation of the pigment distribution, and consequently the profile and pigment density on any area of the macula can be expressed. Figure 5.42 displays the code produce the 2D and 3D profiles. The input is a global VI which contains the MPOD at every pixel in the macula. This global vi is calculated in a previous VI.

For both the objective methods the camera characteristics, LED intensities, acquired images, the extracted data and MPOD information are all saved in the selected named files.

5.3.2 Subjective method

The subjective method employed in this project is the heterochromatic flicker photometry (HCFP) technique. The various methods to adjust the LED intensity and achieve accurate subject feedback is outlined in previous sections. Once the data are received the code saves the LED levels for each section of the retina in various global variables. Figure 5.43 displays the code to save the selected values.

Once the data have being acquired and saved the user decides which data to use in the calculation of the MPOD (Goal is to produce data which will produce coefficient of variation less than 20%, same method as Mellerio device [63]). For each retinal location a number of readings for the minimum flicker point are acquired. Due to the subjective
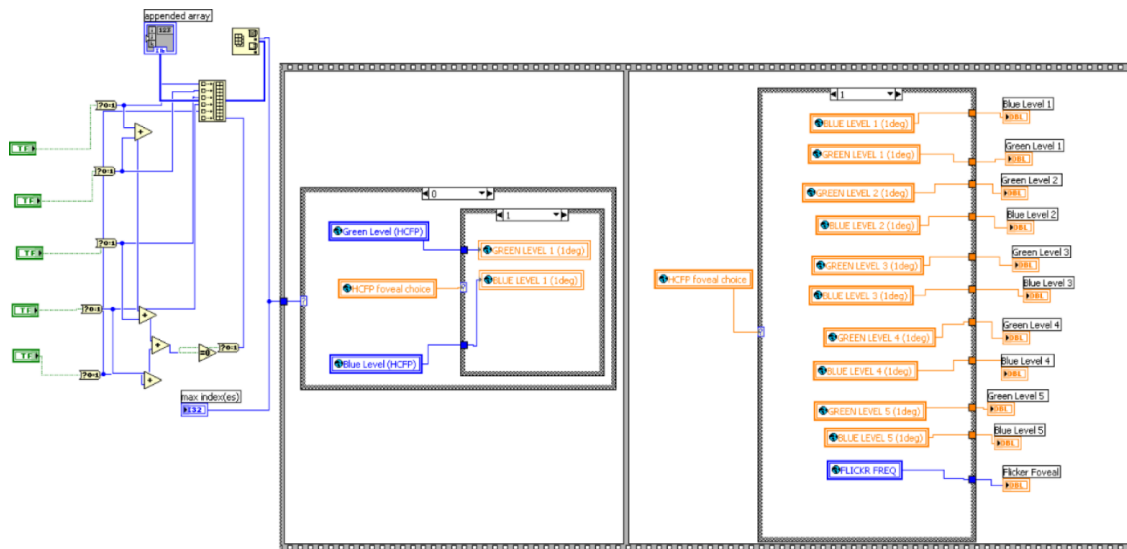
Figure 5.43: SUB VI to save levels of LED for minimum flicker point for various regions on the retina.

nature of the technique there will be some variation within the readings. Figure 5.44 displays the code which allows the user to select which values to use for each retinal location. The coefficient of variation is also displayed for the selected results and can be used to determine if the values are valid.
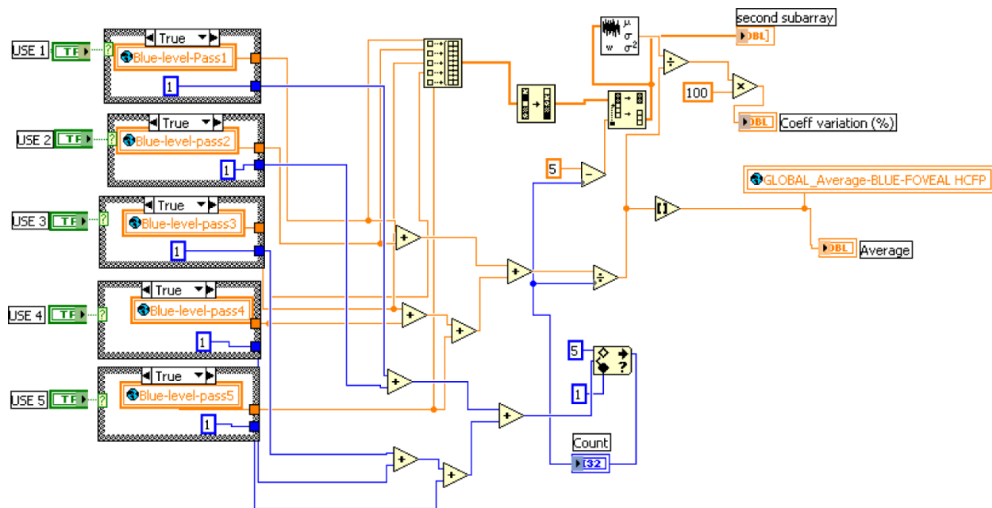
Figure 5.44: Subvi to display the acquired results for minimum flicker point. This is for the retinal location, and similar VIs exist for each location. The user has a choice of which values to use for calculation of the MPOD. The coefficient of variation of the chosen values is also calculated and displayed.

As outlined earlier certain designs and methods are utilised in this project in order to

116

reduce the variation of the subjective readings, however, some variation will still persist. These values are used to find a value for $I_P(460)$ and $I_F(460)$ for equation 5.14. The extinction coefficients $K_{mp}(460)$ and $K_{mp}(535)$ are outlined in a previous section.

$$D_{flick}(460) = \frac{-1}{K_{mp}(460) - K_{mp}(535)} \times \left[\log \frac{I_P(460)}{I_F(460)} \right] \qquad (5.14)$$

These values for each retinal location can then be used to display the distribution of the pigment across the retina. Chapter 6 will present the results of these calculations and display the interface to control the subjective technique.

5.4   Saving of Data

The acquired data and results are automatically saved by the Labview software. The folder path illustrated in figure 5.45 is automatically created on starting the software. The root folder is named by the date, time and optional user inputted name. Once the folder hierarchy has being created the appropriate images are saved in the appropriate folder.

The images are saved after each acquisition or calculation and are automatically overwritten if the operation is repeated. This can be avoided by renaming the root folder. The software also automatically creates a text file which contains the acquisition information, i.e. for the objective techniques, exposure, LED levels, image resolution, binning etc and CFF frequency, LED levels for the subjective techniques. The results for the macular pigment optical density from each technique are also saved in the corresponding folder.
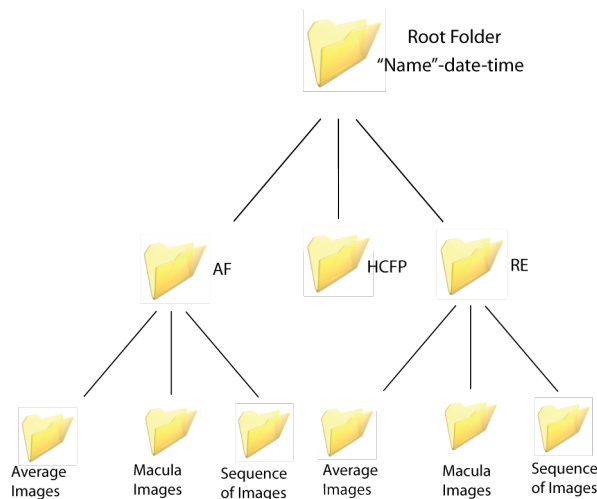
Figure 5.45: The folders are automatically created during acquisition. The appropriate images are saved in the appropriate folders, as well as acquisition information and results for all techniques are saved in a text file.

Chapter 6

Results : Device operation

This chapter of the thesis is dedicated to the operation of the device, and will illustrate the results of the cooperation between the Labview interface and 8051 μ-controller. The purpose is to calculate the macular pigment optical density (MPOD) for the three different techniques employed, essentially applying equations 6.1, 6.2 and 6.3. The chapter is divided into two main sections.

$$D_{AF}(460) \;=\; \frac{1}{K_{mp}(\Lambda_1) - K_{mp}(\Lambda_2)} \times \left[\log \frac{I_P(\Lambda_1)}{I_P(\Lambda_2)} - \log \frac{I_F(\Lambda_1)}{I_F(\Lambda_2)} \right] \qquad (6.1)$$

$$D_{RE}(460) \;=\; \frac{0.5}{K_{mp}(\lambda_1) - K_{mp}(\lambda_2)} \times \left[\log \frac{I_P(\lambda_1)}{I_F(\lambda_1)} - \log \frac{I_P(\lambda_2)}{I_F(\lambda_2)} \right] \qquad (6.2)$$

$$D_{flick}(460) \;=\; \frac{-1}{K_{mp}(460) - K_{mp}(535)} \times \left[\log \frac{I_P(460)}{I_F(460)} \right] \qquad (6.3)$$

The first section illustrates the user interface, by displaying the front panel of the labview code, and highlights the options available from each screen. The initial testing of the system, using specially designed test targets and examples from real eyes, will be presented. The two objective methods utilise comparable procedures on the acquired images, while the subjective method is the interpretation of subject feedback and as such the flicker method will be treated separately from the reflectance and auto-fluorescence methods.

The second section of the chapter will present the results of *in vivo* measurements on a small cross section of subjects. The intention is to demonstrate the ability of the instrument to measure the MPOD within a lab environment, examine repeatability of measurement, investigate the acquired results with an established instrument, and to divulge any potential difficulties that may arise in the screening of larger populations. The appendix includes extracts from the ethical approval application, which allows for the measurement of real subjects.

6.1 Target design

The purpose of the artificial target is to simulate the dimensions of a human retina, in order to test the behaviour of the device. The setup is a simple imaging lens, with the test target placed at its focal point. The dimensions of the target is determined by the imaging lens employed, and is essentially the scaling of, the known dimensions of the real retina, for the known overall refractive power of the eye. For the real eye the focal length[1] is approximated to be 16mm. The relationship between visual angle and spatial distance on the image plane for a imaging system is approximated by equation 6.4.

$$\frac{\pi}{180} \times \text{ Focal length} \cong 1° \text{ of visual angle} \tag{6.4}$$

The relationship for a real eye can be seen in equation 6.5 while that for the artificial test setup is illustrated in equation 6.6.

$$1° \text{ of visual angle (real eye)} \quad \cong \quad 288 \mu m \tag{6.5}$$

$$1° \text{ of visual angle (F = 25mm)} \quad \cong \quad 444 \mu m \tag{6.6}$$

The most common test target used in this project is illustrated in figure 6.1. The dimensions are such that it is equivalent to the real eye for a single lens of focal length of 25mm (chosen both due to similar curvature to cornea, and still retaining a satisfactory working distance between the lens and target).

(a) Test target used to test extraction and calculation of peak MPOD.

(b) Magnified image of the test target. The central cross represents a 1° area on the retina.
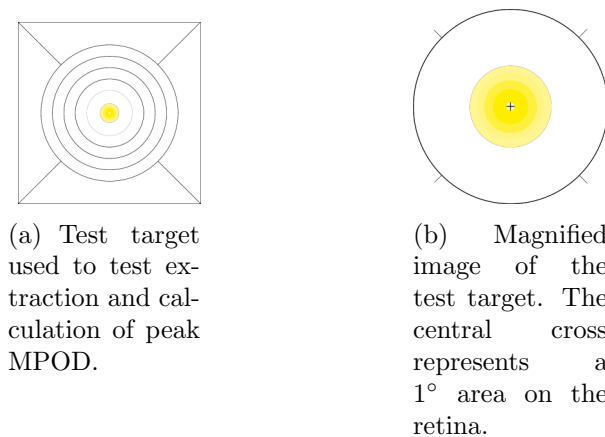
Figure 6.1: The test target used to test correct extraction of central 1° area of the retina

The design is such that the yellow area represents 5° on the retina, corresponding to typical macular pigment distribution, while the outer circle (figure 6.1(b)) represents approximately 15° (desired illumination area). The saturation of the yellow varies across the field[2], while the central 1° area is devoid of colour and consists of a small cross. This

---

[1]Power of cornea and lens focussed at infinity
[2]Symmetrically falls off from the centre

is to test accurate extraction of the central area by the program and is not representative of the macular pigment which one would expect to peak in this area.

While the test target set up is useful in the testing of many facets of the system[3] it is far from a perfect representation of the real eye. The reflection from the target is many orders of magnitude higher than from the real retina, the complex scattering from various layers of the real retina is not reproduced, the imperfections of the real cornea and lens, spectral behaviour coupled with the interplay of the tear film, is not simulated, the subject inter-variability is not accurately represented, movement of the eye due to various factors and basic difficulties with working with subjects cannot be duplicated with this technique. The target does allow the testing of the auto-fluorescence (AF) algorithm, but does not exhibit fluorescence. A fluorescent dye, which matches the characteristics of lipofuscin, may be used, but the greatest problem remains the low emission signal from the real eye. In order to test the device optics suitability for the AF method, testing was done on a real eye. The design of an accurate representation of the real retina is a big task and not necessary for this project. However in spite of these indiscretions, the use of a simple test target is still vital in the initial testing and alignment of the system.

6.2 Objective methods

The primary objective of this project is to measure the macular pigment optical density (MPOD) accurately, consistently, rapidly and easily. The design of the hardware is essential to its success, but also an intuitive control of the hardware, determines both the ease and speed of the interpretation of the acquired data, and consequently the quality of the final result. Labview was utilised to design the interface, and a tab based approach was implemented for navigation of the program, the rational for which will be illustrated in the following sections. The objective methods are the reflectance technique and auto-fluorescence technique. Both techniques employ the same navigational procedure in the interface, the only difference being a tick box to determine which equation is used for the final calculations.

6.2.1 Labview interface design

The techniques of reflectance (RE) and auto-fluorescence (AF) require that sufficient retinal information is acquired in order to apply the appropriate algorithms to extract the macular pigment optical density (MPOD). To acquire sufficient information the different aspects of the device all have to operate together, and this cooperation is controlled from a single interface.

Main set up screen

Figure 6.2 displays the set up screen for the RE and AF techniques. The main feature of this screen is a live view of the camera image. This view can be utilised to both align the subject, by adjustment of the stand and focussing of the camera, while the modification

---

[3]Tracking of retinal and corneal planes throughout system, resolution of system, behaviour of triggering of system, behaviour of extraction of specific regions etc.

of the intensity of the image, by adjustment of camera exposure, modification of LED intensity and binning of the camera can be refined.
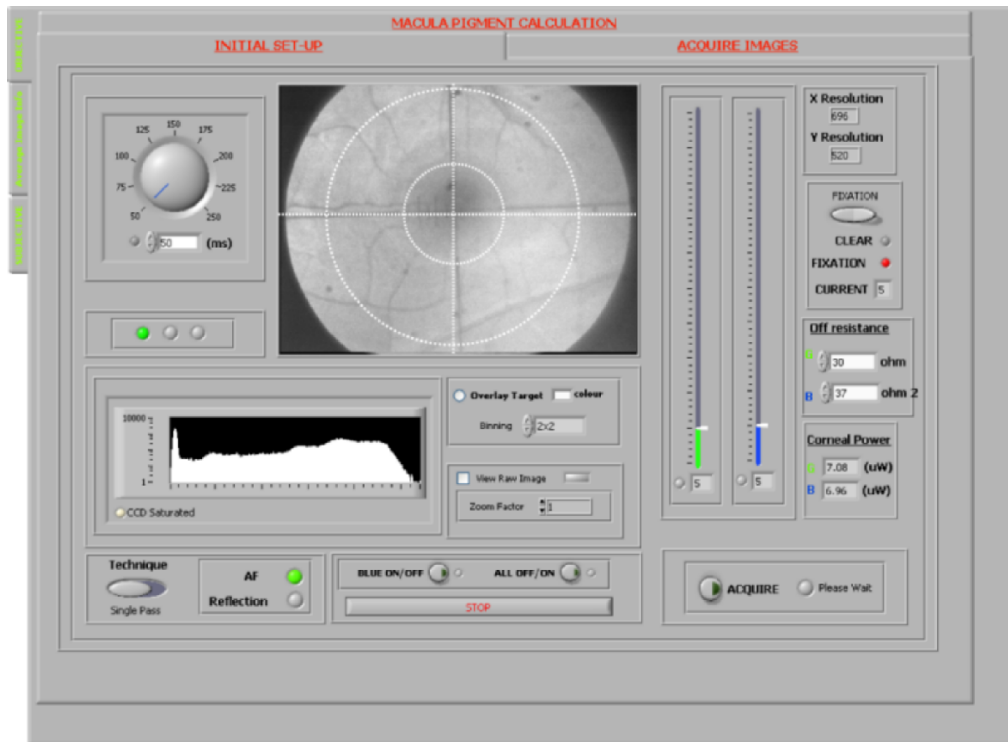
Figure 6.2: The front panel design to set up the measurement of MPOD using the RE and AF techniques. Control of full LED, filter wheel and camera behaviour is accessible from this screen.

A histogram of the image is useful in adjusting the intensity values of the image on the camera. This screen also allows switching of the illuminating LED, from green to blue, and allows switching of the retinal target. The power of each LED at the cornea is also displayed. As outlined in previous chapters this depends on the resistance of the potentiometer, as well as the labview command. The resistance value can be adjusted from this screen to ensure accurate readout of the LED power values. The manner in which these various factors can be adjusted is outlined in previous chapters.

Straightforward navigation through the different screens is feasible by use of a tab system. This not only offers an intuitive control system to the user, but also switching and calling of appropriate subvis within the code. This greatly enhances the speed and efficiency of the execution of the code.

Image acquisition and average

The next screen after acquisition of the images is displaying the acquired images. This screen allows the user to rename and save the acquired images and the averages of the acquired images.
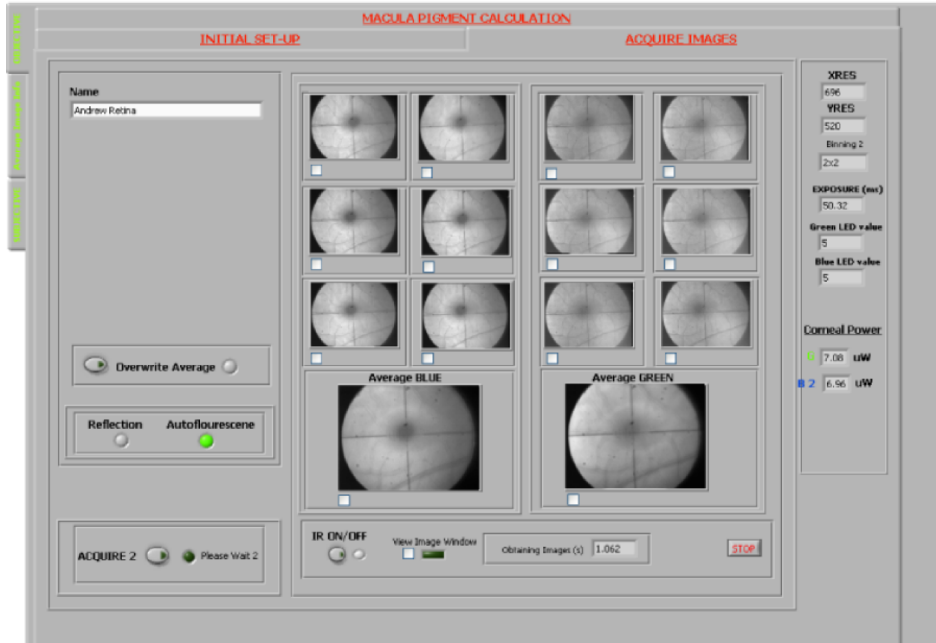
(a) The screen displaying the 6 blue and 6 green acquired images.
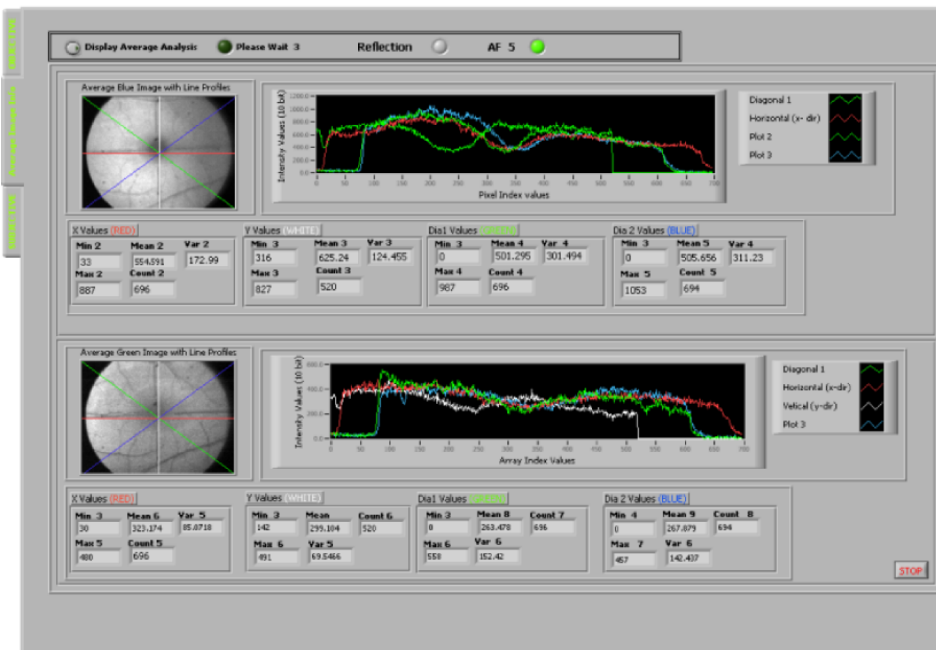
(b) Screen displaying a more in depth analysis of the average of the acquired green and blue imges

Figure 6.3: The acquired images and analysis of their averages.

Due to inevitable eye movement and method of adding the images together, each individual image will not be perfectly aligned, therefore the average image will appear smeared. The ideal solution to this is a Labview subvi to align the images and then calculate the average, however due to time constraints this was not accomplished (see chapter 7). The next solution was to present the user the choice to overwrite the calculated average with a selected individual image. The user can do this by ticking a box under the desired image. This screen also provides information on image resolution, individual LED powers, resistance values, actual exposure and binning, all of which is saved in an accompanying information file to the images. If so desired the user can analysis further the selected average images. A line profile is provided vertically, horizontally and diagonally through the image.

The screens in figure 6.3 display the result for a real eye. The correct flashing and triggering for the blue LED can be seen with a clearly identifiable macular region on the blue images. Smearing on the average image indicates eye movement and consequently it can be inferred that correct triggering and saving of time lapsed individual images has occurred[4].

Isolation of macular area

As outlined in the previous chapter in order to calculate the macular pigment optical density it is necessary to isolate the macular region from the surrounding parafoveal regions. Information from these regions in both colours can now be used to calculate the MPOD. The front panel screen presented to the user to manually isolate the macular region can be seen in figure 6.4(a). Since the MPOD distribution varies among individuals the most satisfactory method to select this region is to manually chose the desired area. The outcome of the selection and subsequent division of the image into 5 distinct regions can be seen in figure 6.4(b). The advantage of obtaining 5 distinct regions is that information can be extracted for each region so any heterogeneous illumination of the retina can be easily recognised. This information may then be used to correct the final calculation of the MPOD distribution[5]. A full analysis screen is also available to inspect each of the regions individually (not shown here).

Figure 6.5 illustrates the extraction of the yellow pigment for the test target and for a real eye. The two images displayed on the left of each panel represent the selected/average acquired images. The two images on the right side displays the extracted macular region (as selected manually as in figure 6.4(a)). The central image displays the result of applying the appropriate equation to the two extracted images, and essentially displays an image of the macular pigment distributed across the extracted area. As is evident from the test target screen the calibration displays that the correct area is extracted ($10°$). The central cross is quite clear, as is the distribution of yellow saturation across the selected area. This method utilising the test target was used to calibrate the system for equivalent distance calculations on the retina.

---

[4]The correct triggering sequence has being tested using test targets and deemed to be sufficient.

[5]Not implemented in this project due to time constraints.
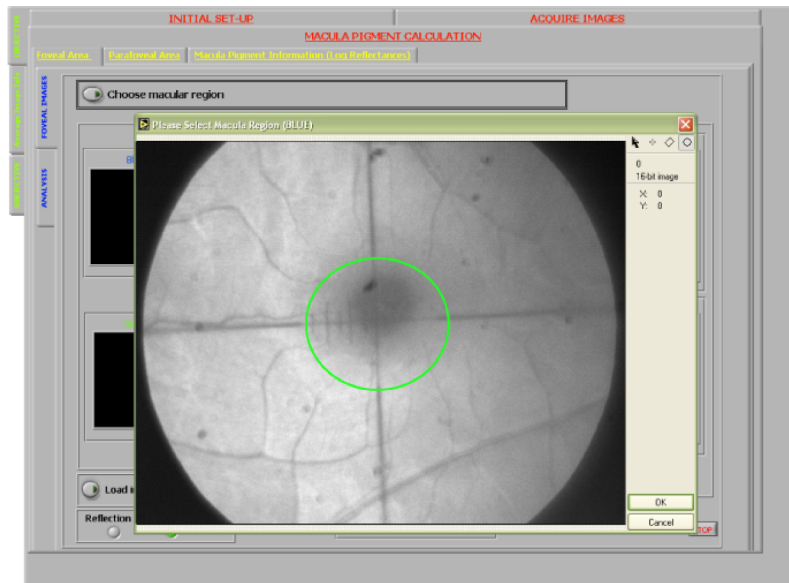
(a) The screen presented to the user requiring selection of the macular region. The green oval can be manipulated to accurately define the desired area of interest.
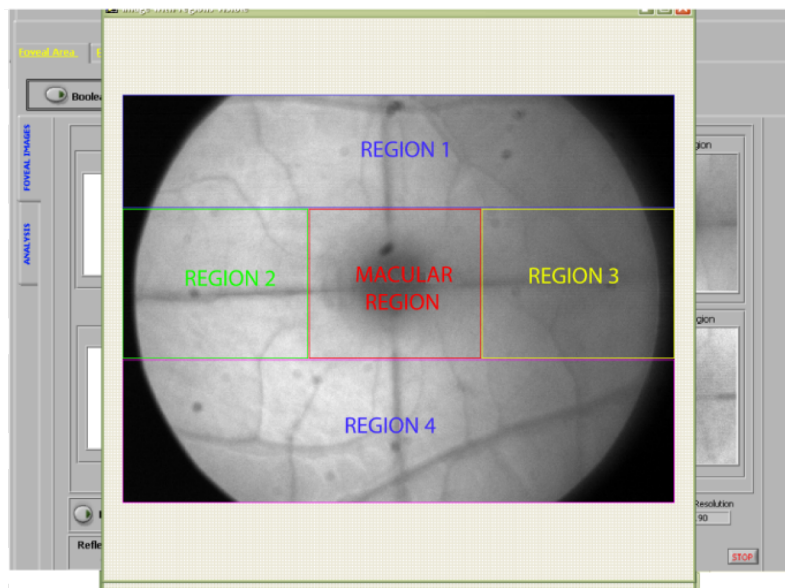
(b) Display of the five regions associated with the calculation of MPOD. The image is a blue reflective image and the central darker area representing the macular pigment can be clearly seen.

Figure 6.4: Manual selection of macular region utilising an intuitive graphical method and subsequent extraction and display of the various image regions.
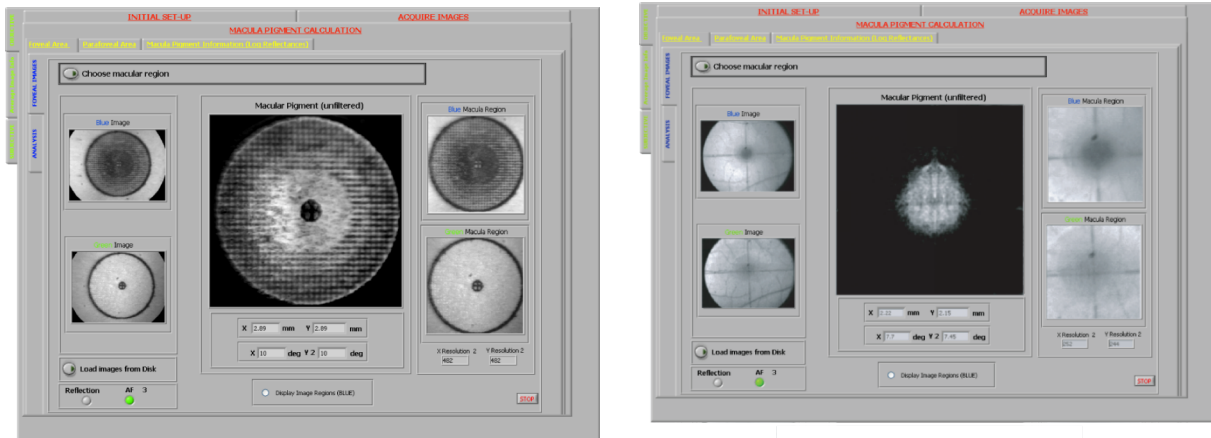
(a) Illustration of image extraction of the test target illustrated in figure 6.1

(b) Illustration of difference image on real subject

Figure 6.5: The difference image for (a) test target and (b) real subject.

This screen also allows the user to load previously obtained images. This allows for recalculation of the macular pigment at a later date, the idea being that a number of subjects can be tested very rapidly, and their automatically saved images can be processed at a later time.

Extraction of regions

As outlined previously, the information gathered from the selection of the macular region can be used to divide the image into five distinct regions (see figure 6.4(b)). Each of these regions can now be extracted from the original image, and the information contained within each region can be used in the calculation of the MPOD.
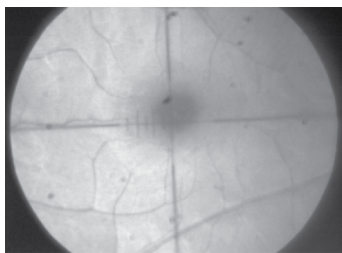
(a) Example of typical image and field stop
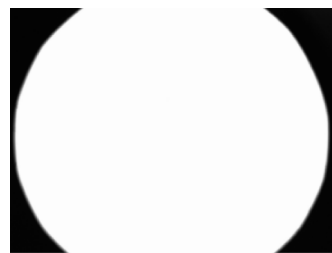
(b) Image of the field stop in the system. Image obtained by saturating the retinal field.

Figure 6.6: Example of acquired image, and highlighting the isolation of the field stop.

As outlined in the previous chapter, the primary difficulty with accurate region extraction is the presence of the field stop in the selected images. Therefore it is necessary to extract

the desired retinal information from the particular region, in each of the selected images. Figure 6.7 displays the extracted regions, and their histograms of before and after isolation of the retinal area. Chapter 5 outlines the code to produce the images and values outlined in the figure. This is a subvi and is not displayed on the front panel, and unless requested is hidden from view from the user.

The two input images are first passed through a low pass gaussian filter to reduce the noise in the image[6]. Both the raw and processed image for each colour is displayed in figure 6.7. Each region has being resized to fit a generic sized box. Therefore the aspect of the image may not be true to the image extracted. However a option exists to view the image in its native resolution.

Understanding regional information

Regional information is not only essential in calculating the MPOD (as required by equations outlined in figures 6.1 and 6.2) but can also be used to examine homogenous illumination across the retina. If large disparities occurs between the average intensity, of each of the regions (for the same image) then it can be inferred that there is not homogenous illumination across this area of the retina. As a result, inaccuracies in the calculation of the peak MPOD and distribution of the pigment across the macular region may occur.

Disparities between the average value for region 1 and region 4 (see figure 6.4(b) for location of regions) would indicate heterogeneous illumination in the vertical direction, while correspondingly, disparities between the average value for region 2 and region 3 would indicate heterogeneous illumination in the vertical direction. This can be corrected by either realigning the subject, by software, or a combination of both.

MPOD calculation : noise considerations

The method of calculation of the MPOD is dependent on the mode employed by the user. The objective techniques employ the same program path, differing only for the single and double path considerations (see equations 6.1 and 6.2).
The values to be extracted from the processed data are the peak macular pigment optical density and the macular pigment optical density distribution. The peak MPOD refers to the density measured over the central $4°$ area of the pigment, biased towards the central $1°$ area. The extraction of these regions will take place on the calculated difference image (see figure 6.5 and figure 6.8). However as is evident from the display of the difference image (figure 6.5(b), figure 6.8(a)) in spite of initial processing, a detrimental amount of noise still exists in the image. Due to the presence of the noise certain pixels in the image will have lower values than their neighbours, and thus will affect any average value that will be extracted from the data. This can be reduced by reapplying the low pass filter to the image.

Figure 6.8 displays the result of reapplying the low pass gaussian filter to a difference image from a real eye. On this occasion the user has control over the kernel of the filter,

---

[6]Manifests from electronic and readout noise of the camera.
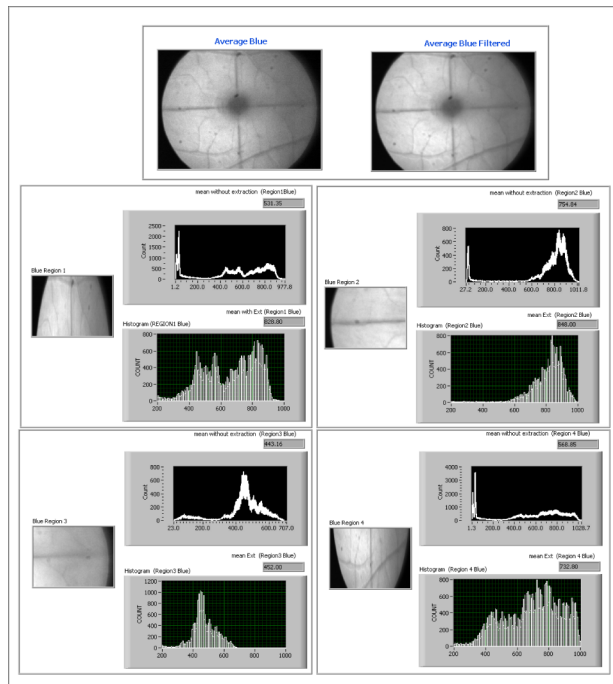
(a) Isolation of Blue parafoveal information from field stop.
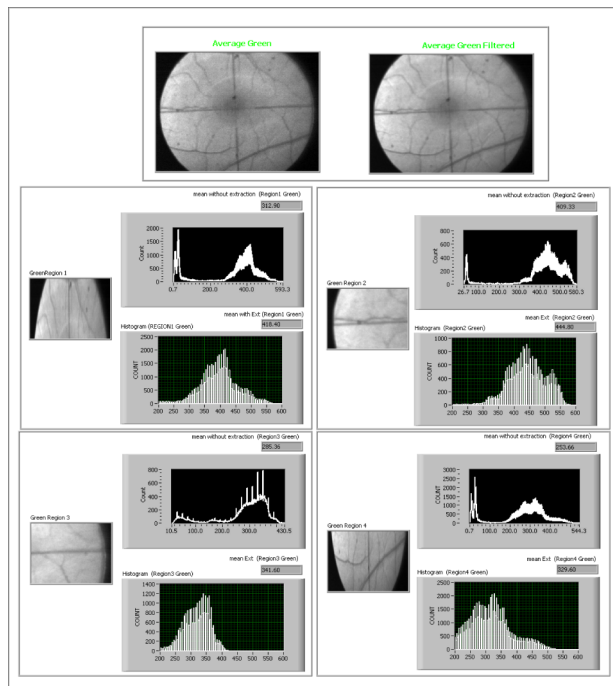
(b) Isolation of Green parafoveal information from field stop.

Figure 6.7: Illustration of the isolation of the retinal information from the field stop. Each extracted image region is displayed. The accompanying histograms represent the full image information (Top histogram) and the extracted retinal information (Bottom histogram). The two images for each colour are the raw image (left) and a processed image(right) to reduce the noise. The processed image is passed to the vi for analysis.

(a) Unfiltered   (b) Filtered
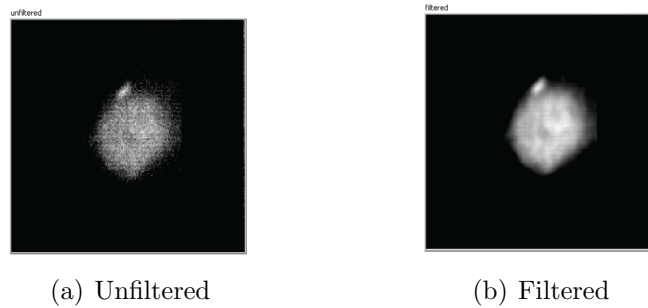
Figure 6.8: The effect of a low pass gaussian filter on the difference image.

as it is fully adjustable from the front panel. The subvi to isolate, and hence calculate the average intensity of a 4° area and average intensity of the central 1° area is automatically called. An outline of this procedure can be seen in the previous chapter, and the result of such is illustrated in the following section.

Isolation of 1-degree and 4-degree area of macula region (MPOD peak calculation)

As previously outlined the peak MPOD refers to the density measured over the central 4° area of the pigment, biased towards the central 1° area. In order to carry out this calculation, it is necessary to isolate the desired areas from the calculated difference image.

For the purpose of testing the correct behaviour of the software, the test target illustrated in figure 6.1 is used to demonstrate the appropriate extraction. The central cross represents a 1° area on the retina[7]. The varying yellow saturation across the central area of the target represents the varying MPOD across the real retina. The central greater area of saturation covers an area of approximately 4°.

Before any extraction is carried out the inputted difference image is processed for noise (outlined in previous section). Therefore the difference image illustrated in 6.9 loses some detail (central cross no longer visible etc), and appears more blurred than the actual acquired image displayed in figure 6.5(a).

Figure 6.9 also displays the results for extracting the central 1° area and 4° area on the target. From inspection it can be seen that the software is successful in the desired extraction. A histogram, and subsequent average value is also returned for each of the areas. The desired areas are automatically isolated by the software and can do so, no matter the size of the macular region, camera binning etc. The key to correct extraction is knowledge of the pixel relationship to retinal dimension. Again this screen is a subvi, and unless requested by the user is hidden from view and is automatically carried out in the background, to produce the final result screen.

---

[7]Using equivalent lens of focal length 25mm
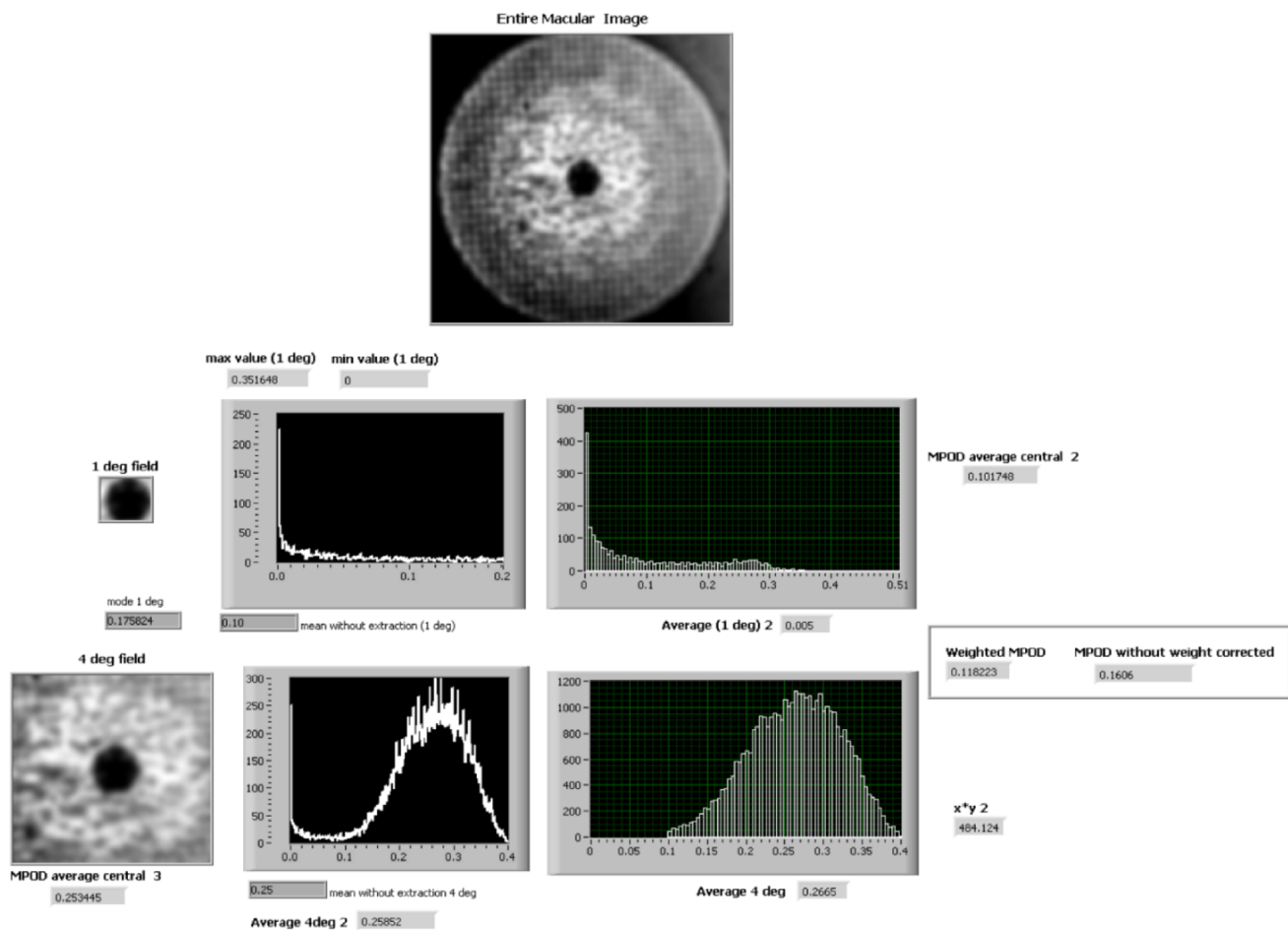
Figure 6.9: Illustration of extraction of the desired areas of the image. This is produced as a result of the code illustrated in the previous chapter. This information is hidden from the users front view and only the weighted averages are passed to the front panel. The correct extraction of the 1° can be seen and the average intensity value of this area is also produced. Similarly the corresponding results for the 4° area of the retina can be seen.

Result Screen (Peak MP and MP distribution)

The final screen presented to the user is that of the result for the peak macular pigment optical density, and that for the distribution of the pigment across the desired area of the retina.
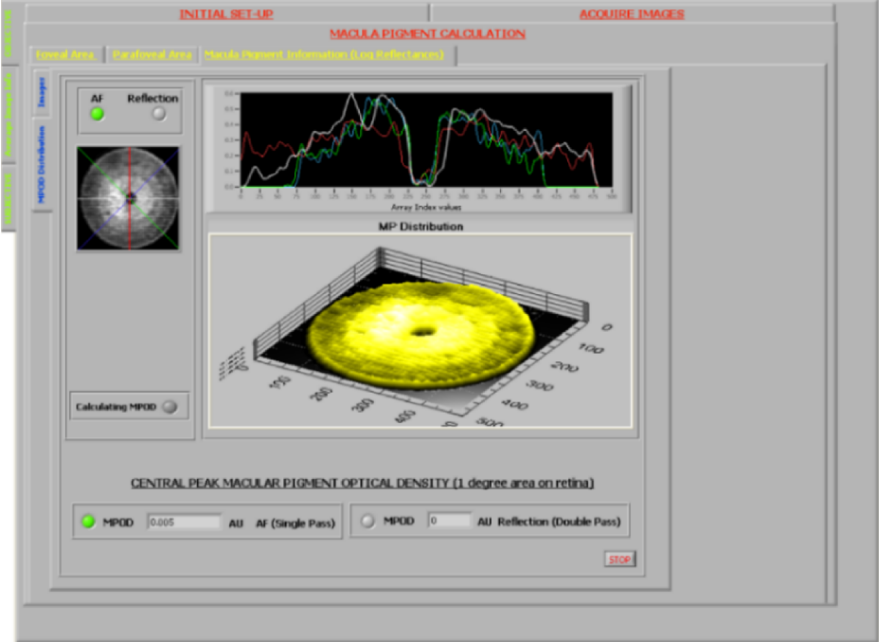
(a) Illustration of last screen on artificial test target illustrated in figure 6.1
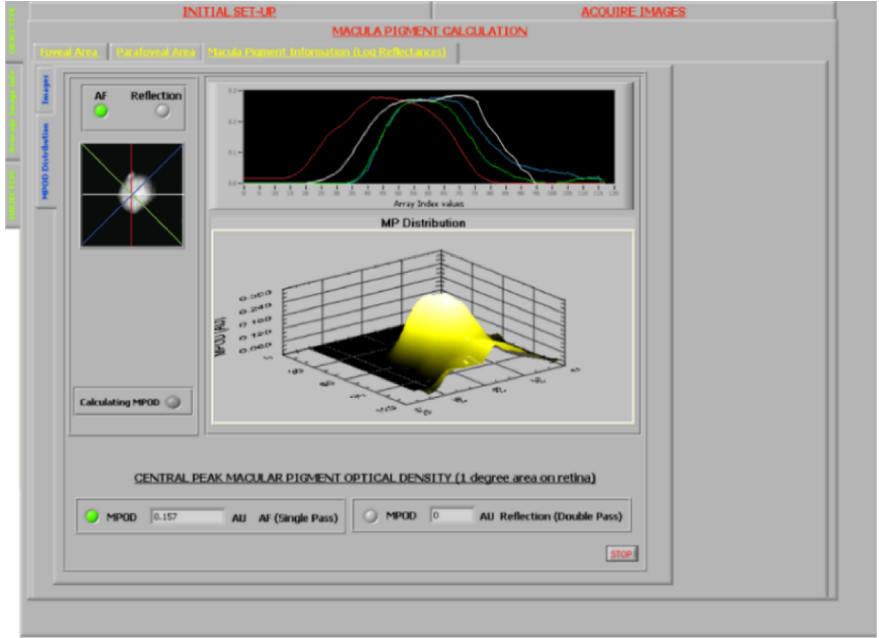
(b) Illustration of last screen on real subject

Figure 6.10: The final screen displaying the MPOD peak result and a 2D and 3D representation of the MPOD distribution.

Figure 6.10 present the results for the test target and also for a real eye. An illustration of the difference image is presented, and a line profile of the image is displayed. The profile is the vertical, horizontal and both diagonals and is colour coded to the line graph for ease of interpretation. This graph can be used to determine the symmetry of the pigment distribution, and determine whether the peak value is actually located at the central area. The screen also present to the user a 3d representation of the pigment. This graphic is fully adjustable by the user, i.e. can be rotated in any directed and can be zoomed into and out from, and again can be used to examine the characteristics of the pigment distribution.

Figure 6.10(a) displays the behaviour of this analysis on a target of known dimensions. The central 1° is very clear both from the 2d and 3d representation, and the varying distribution is also apparent. The symmetric design of the target is also reproduced, while the small peak value is indicative of the absence of the simulated pigment in this central 1° area.

6.3   Subjective method

The technique of heterochromatic flicker photometry is utilised for the subjective measurements of the macular pigment optical density (MPOD) and distribution of the MPOD across the retina. The code to produce the following screens, and analysis is outlined in the previous chapters. The following results is for a single subject and the emphasis of this section is on the design of the user interface. The result for a cross section of subjects will be presented in section 6.4. In contrast to the objective techniques the operation of the device is determined by subject feedback, and as such it is not possible to design a test target.

6.3.1   Labview interface design

Figure 6.11 illustrates the main setup and control screen for the subjective method. This is navigated from the objective screens by selection of the appropriate tab. As indicated in an earlier section, this tab system not only allows navigation of the code but is also used to switch certain subVIs. In this case the switching of the tab disables all subVIs associated with the objective techniques. For example, the subVI dictated the control and operation of the camera, which is redundant in this method, is switched off. This adds greatly to the speed of operation of the code, and particularly the communication between the interface and 8051 μ-controller.

Due to the nature of this technique, it is the slowest of all to obtain a measurement of the macular pigment density and distribution. For this reason all the desired features are located on a single screen. The screen is designed in a manner that the initial options associated with setting up of the subject is located together, the subject participation is positioned together and the gathering of the results are located together. These features will be briefly outlined in the following sections.
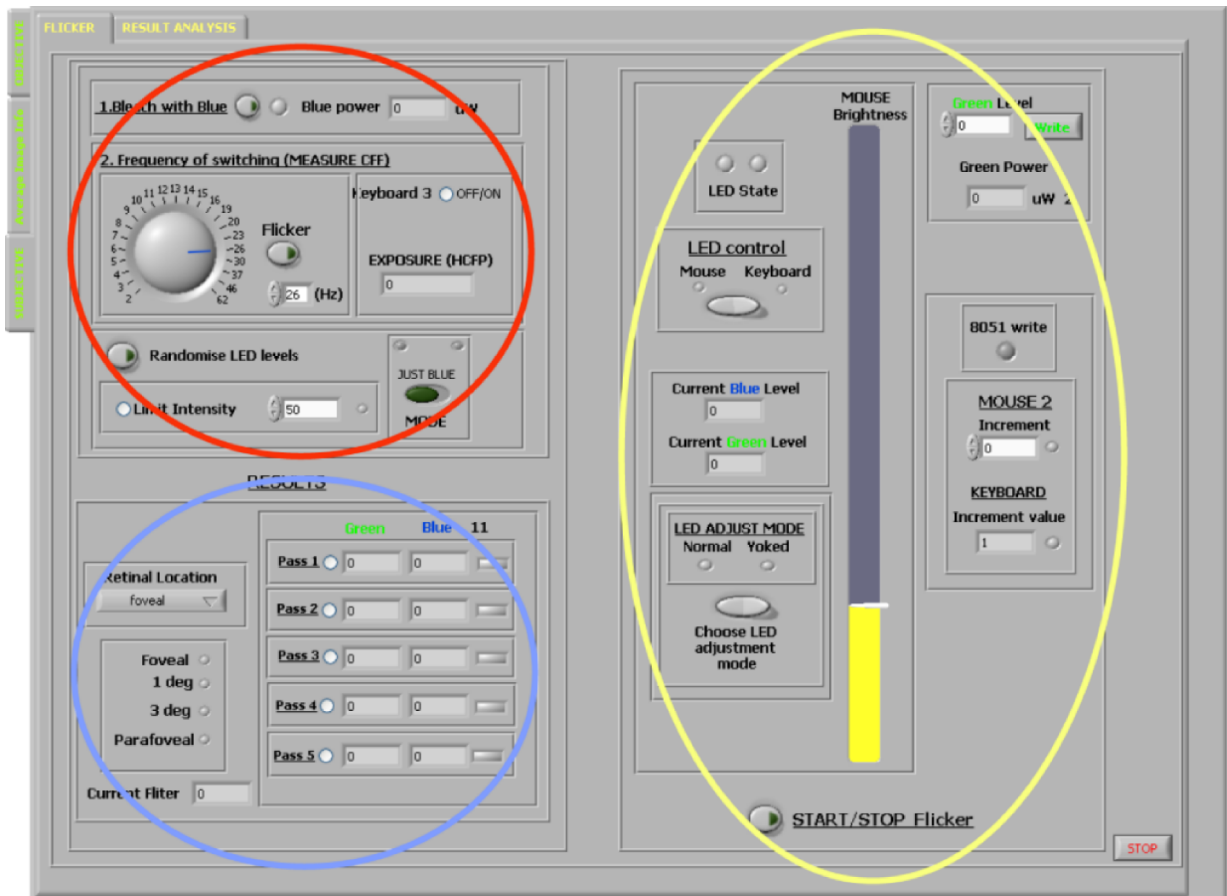
Figure 6.11: Front panel for controlling the HCFP technique. The panel is divided into three sections for ease of use. The red circle is the initial setting up the device, the yellow represents the adjustment of LED intensity and the blue indicates the gathering of the results for the different areas of the retina.

Optimising the device for the subject.

The initial setting up of the device for measurement on a subject includes bleaching of the blue cones, the ability to randomise LED levels and measurement of the subject's critical flicker fusion frequency (CFF)[8]. The control for these factors can be seen circled in red displayed in figure 6.11. Bleaching of the blue cones is simply exposing the retina to blue light[9]. The ability to randomise the initial LED intensity values can lead to avoiding subject learning of the minimum flicker point, also the option to limit the LED intensity[10] is available as is the choice of single LED or both LEDs to randomise. Arguably the more important aspect of optimising the device for the subject is the measurement of the subject's CFF. As outlined in previous chapters the CFF is the threshold frequency at which a subject can distinguish a flickering stimuli. Therefore if two different stimuli are flickered alternately at the subject's CFF, the primary factor which will cause the stimuli to appear to flicker is differences in perceived luminances of the source. Subsequently, if the subject adjusts the intensities of the stimuli until they are perceived as being of equal intensity, then very little flicker will be observed by the subject. This aids greatly in finding the point at which the blue and green LED are perceived as equal in luminance.

The CFF point is measured by flashing the green LED at a number of different frequencies[11]. The frequency can be adjusted by the user, or alternatively by the subject. Once the CFF is calculated it is automatically saved in the info file associated with the specific subject.

Estimating the minimum flicker point.

The primary consideration of the HCFP method is the adjustment by the subject[12] of the luminance of a blue LED, which alternately flickers with a green LED, until the minimum flicker point is reached, i.e perceived luminances of both LEDs are equal. The section controlling the various options associated with the LED adjustment can be seen circled in yellow on figure 6.11. The subject can adjust the intensity of the LED using either the mouse or keyboard control. Both these methods are devoid of any reference points, therefore any subject learning of the minimum flicker point is not possible. Access to the sensitivity of the adjustment is also possible from this screen, where the step size of the adjustment is fully controllable.

The mode in which the LEDs are adjusted can be changed on this screen. The two LED adjustment modes are normal and yoked method. This has being outlined in previous chapters, but essentially the yoked method aids in the identification of the minimum flicker point, as perceived differences in luminances are greater than in normal mode.

---

[8]photoreceptors ability to resolve temporal detail

[9]A additional blue filter can be used to match the LED to peak absorption of blue cones (445nm), used in combination with CFF to negate the influence of the short wavelength cones.

[10]To remain within the subjects CFF values (see figure 7.6), higher luminances requires higher CFF values.

[11]50% duty cycle.

[12]Either by mouse or keyboard. LED luminance dictated by method of PWM (see chapter 5)

Acquisition of results.

The section of the screen circled in blue displays the accumulation of the results for the different areas of the retina. The user can adjust which area of the retina to measure by the drop down box. This triggers the filter wheel to appropriate filter. Figure 6.12 displays the mask on the retina for each of the desired areas of illumination.

| (a) 1 degree | (b) 3 degree | (c) 4 degree | (d) Peripheral |
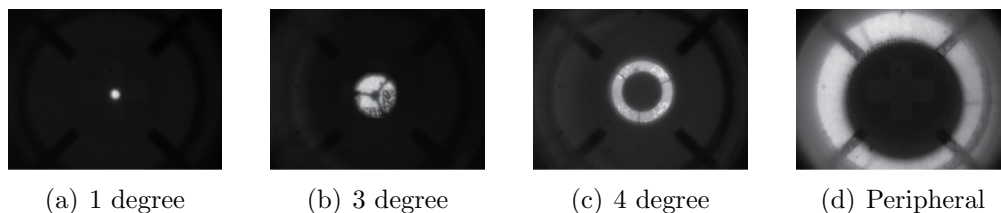
Figure 6.12: HCFP retinal illumination. The subject is expected to fixate on the central portion of the mask. This can lead to difficulty. See chapter 7 for discussion on redesign of the targets to include central fixation point.

The values for each retinal point are automatically saved. A maximum of 5 readings can be taken at each point[13] and the average value can be calculated. The result screen is displayed in figure 6.13. Each value for the flicker point, for each area of the retina is automatically displayed and used in calculation of the average flicker point for each area of the retina. The user can chose to omit any abnormal points from the calculation (depending essentially minimising the coefficient of variation for those points which is displayed).

This screen also displays the peak macular pigment optical density as well as a 2D representation of the pigment distribution across the macula. However, it should be emphasised that this is not a completely true representation of the distribution of the pigment. The value for each measurement of the pigment (1 degree area of retina to the peripheral retina) is the average value over that desired area of the retina. This assumes certain symmetry to the pigment profile. This assumption is adequate for the majority of subjects. However, if any anomalies in the pigment distribution are suspected, the objective techniques can be utilised to detect and produce a more accurate representation.

The screen in figure 6.13 illustrates the results calculated for the normal adjustment of the LEDs i.e. constant green level. Access to yoked calculation is available by means of the tab, as this method uses a different method for calculation of the MPOD due to not having a constant green LED level. The file details are also displayed. This is the name of the text file that is saved containing the various information associated with the particular subject. This includes the LED levels, the CFF frequency and the macular pigment density calculated at each area of the retina. The file name is a user defined name (subject name) automatically appended to the date, and time of the reading.

---

[13]In total 20 values are saved
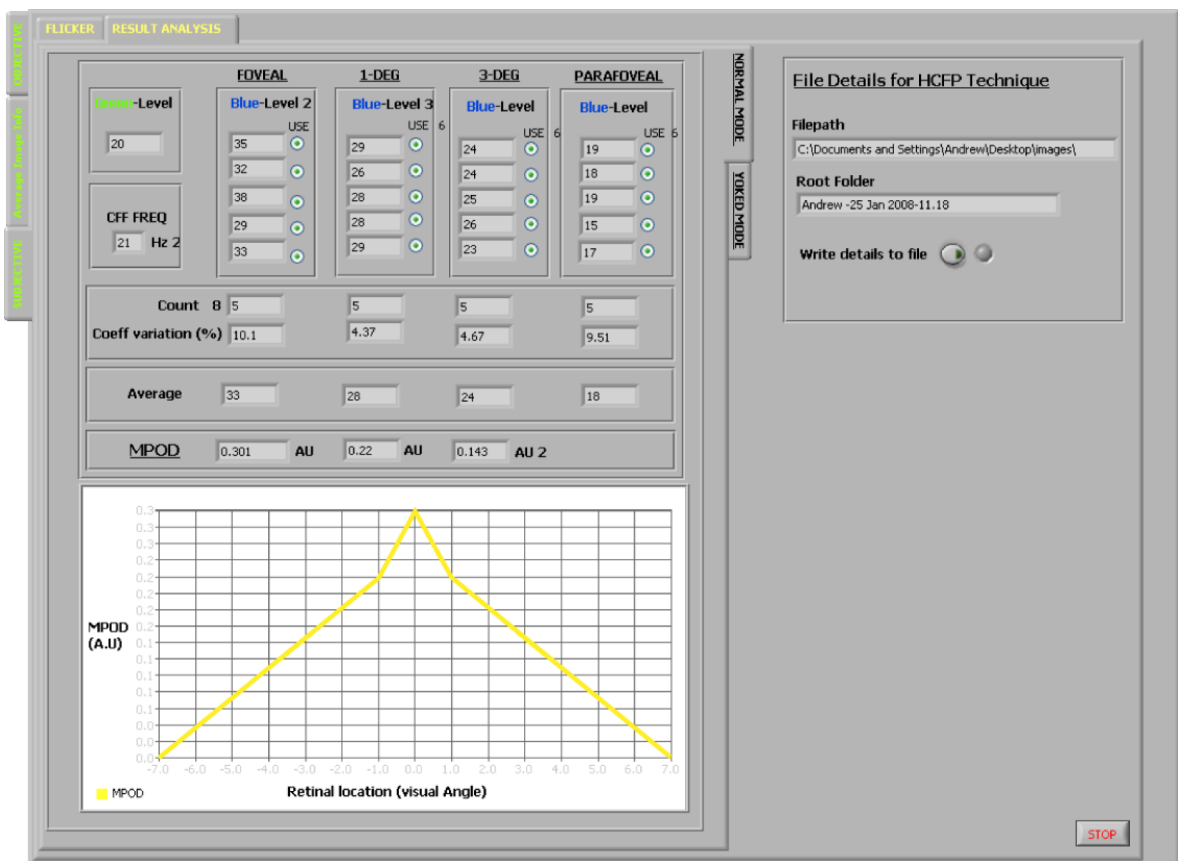
Figure 6.13: Screen for interpretation of the results from the HCFP technique. It should be noted that the method of calculating the macular pigment optical density over each desired area of the retina assumes a certain symmetry in the pigments distribution across the retina.

6.4 Real eyes

The following section will present the results from the investigation of human eyes using the device. The primary aim is to demonstrate the capability of the system to attain a result for pigment levels and not a definite study on the pigment. A comparison with an established device (Maculometer described in chapter 3) is included for reference.

6.4.1 Subjective methods

The technique of heterochromatic flicker photometry (HCFP) was utilised to measure the macular pigment optical density (MPOD) of each subject on three different eccentricities across the retina. The method has being described in previous sections. All results were obtained using the device software[14], however for the convenience of space the final results have being exported to an external program, and plotted on a single graph. Figure 6.14 displays the pigment distribution for 11 subjects across 7° on the retina.
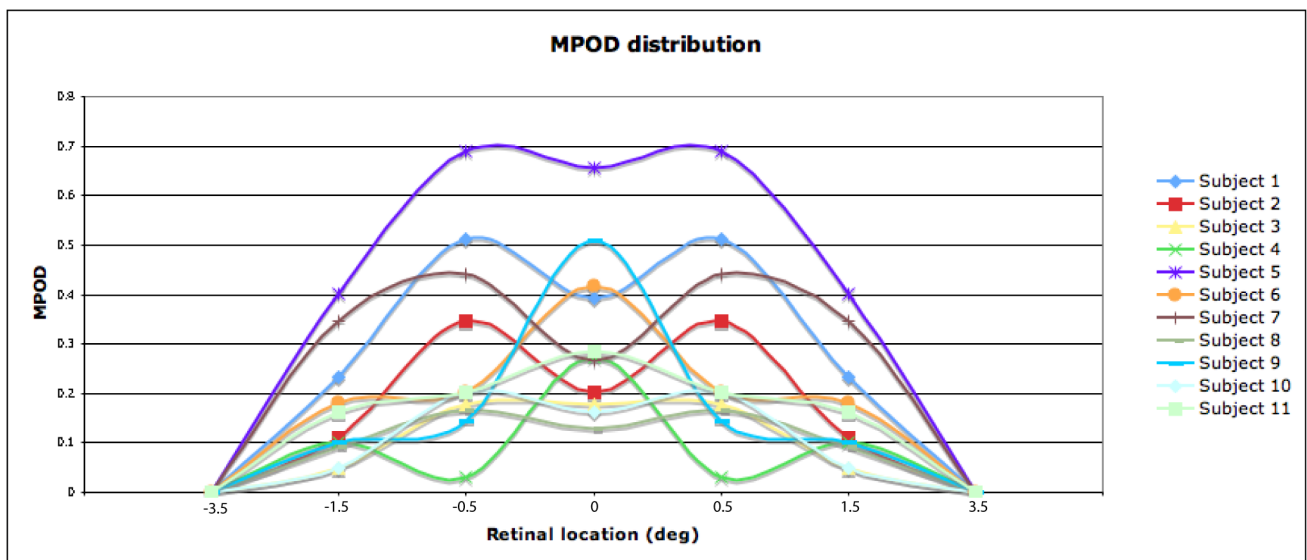
Figure 6.14: Macular pigment distribution using subjective method for a number of subjects. The symmetry is assumed and as such each point is the average pigment value over that particular eccentricity.

The results display the common distribution curve of the macular pigment, mostly peaking in the central vision and falling with increased eccentricity. There is the expected variation of pigment readings within the subject population, with overall average of 0.24 AU. This value is consistent with various other studies, however in this case a far greater number is required for any real conclusions to be reached. Various subjects display density peaks at 3° eccentricity and as such demonstrate a ring-like structure to the macular pigment. This has also being noted in previous studies by Berendschot *et al* [71]. It should be stated that the x-axis is not entirely linear so the shape of the curve is not truly representable of the actual pigment distribution. Also due to the design of the mask there is a certain

---

[14]All subjects produced results page similar to figure 1.13

symmetry assumed at each eccentricity, consequently each mask is calculating the average pigment reading across that particular area of the retina. In fact the amount of ring like behaviour is greater than expected (expect 10% of population to display ring like properties [71]) and may suggest a redesign of the mask is required.

CFF measurements

The ability of this device to measure the subjects critical fusion of flicker (CFF) is yet to be fully investigated and suggested work is outlined in the following chapter. The primary consideration in regards to the subjects CFF is its relation to the intensity of the illuminating source, essentially applying the Ferry-Porter law which states that the CFF is proportional to the logarithm of the luminance of flickering stimulus (L) i.e. CFF = a logL + b. However, for this project a low intensity green illuminating light was used to measure the CFF. Across the 11 subjects the average CFF was 19 Hz for corneal power of 5μW (approximately 3.2 mLumen).

Comparison with established techniques

The macular pigment optical density (MPOD) was measured for each of the 11 subjects using the system constructed for this thesis, and separately using the established Mellerio device which was outlined in chapter 3.
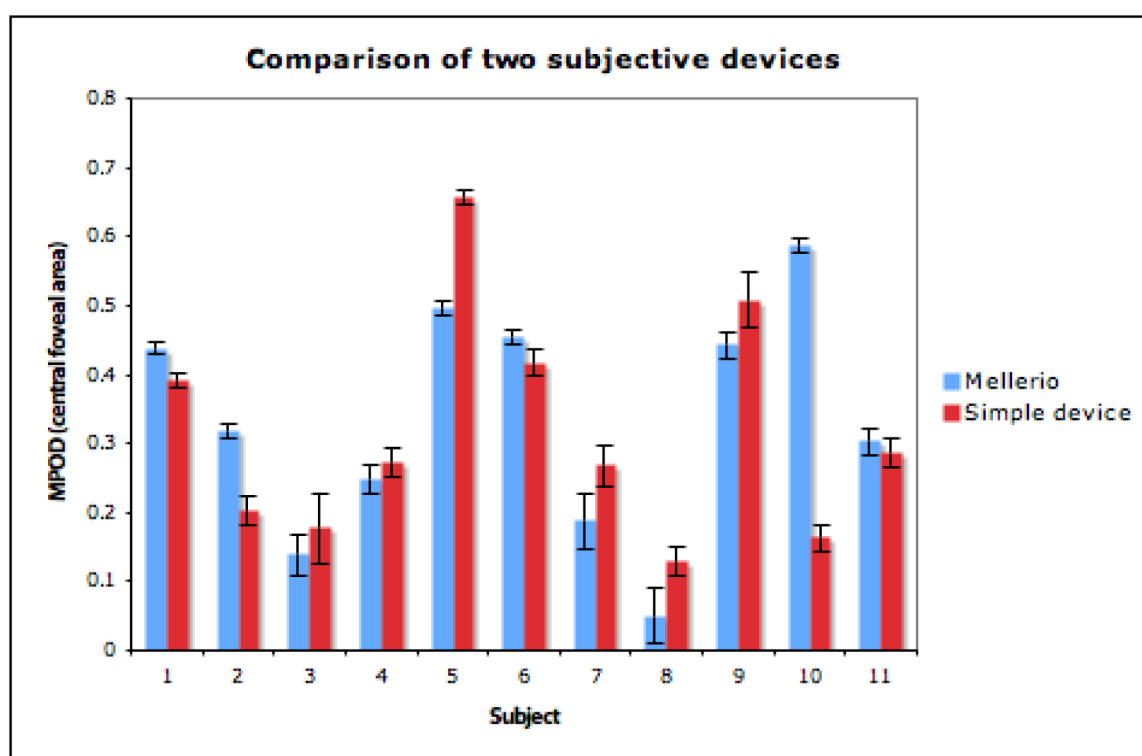
Figure 6.15: Graph illustrating the same 11 subjects comparing their pigment reading using this device and the established Mellerio device. The results for this device are taken as the central foveal area. The errors are standard errors of the mean.

Complete comparison is not possible due to the differing measuring strategies utilised, as the Mellerio device measures the pigment just over the foveal area, where as the system described in this thesis measures a distribution of the pigment across the retina. The result presented, as measured by this new device, is only for the central fovea area (1° area). As outlined earlier some subjects displayed higher pigment values in more eccentric areas of the macular compared to the central foveal area (see figure 6.14). The more eccentric values were not considered in figure 6.15, and may account for some of the lower values obtained using the new system compared to those as measured by the Mellerio device.

The error bars in figure 6.15 are the standard error of each subject's flicker measurements (at each subject's minimum flicker point). The standard errors are found for 3 to 6 separate measurements[15], and therefore themselves contain a certain error. Furthermore, for the Mellerio device an assumption is made in the propagation of the error (this assumption was that the calibration calculation[16], namely converting DVM (Digital Voltmeter) measurements to normalised luminance levels, was linear in nature, over the subjects measurement range). It is clear from figure 6.15 that subjects 2, 5 and 10 display significant differences in the measurement of the optical density of the macular pigment. Subject 2 and 10 display higher values for the Mellerio device, while subject 5 displayed a higher value for the simple device. These subjects have also displayed ring-like structure in the distribution of the macular pigment, however the more likely reason for the significant difference in their pigment measurement is difficulty with a particular device, in particular correctly identifying the minimum flicker point. Figure 6.20 displays a comparison of the subjective methods with the objective reflectance measurements. For subject 5, the reflection measurement and the Mellerio measurement are quite similar (0.45 AU and 0.49 AU respectively), which may suggest that the subject had difficultly correctly performing the subjective measurements on the new device. In contrast, subject 10 displays similar readings for the reflection and subjective method using the new device (0.11 AU and 0.16 AU respectively), while the reading from the Mellerio device displays a significant difference. This may suggest difficulty in using the Mellerio device to obtain minimum flicker point. This simple example displays the difficulty with subjective methods for the measurement of macular pigment optical density. The method of obtaining minimum flicker point must be refined to produce more consistent and accurate measurements.

The subjects displaying ring-like structure are subject 1, subject 2, subject 5, subject 7 and subject 10. All of these, except subject 5 and subject 7, display lower pigment values for the new device compared to the Mellerio device. Subject 5 displays slight ring-like properties i.e. foveal reading is 0.66 AU and 3° is 0.69 AU (as mentioned previously, difference in readings likely due to difficulties in correctly identifying minimum flicker point). Subject 7 also displays a ring like structure, with readings of 0.27 AU and 0.44 AU for their foveal and 3° reading respectivity. This trend of certain subjects with higher pigment readings outside the central foveal region, may account for the Mellerio device measuring lower values, compared to that of the new device.

---

[15]Exact amount is subject dependent

[16]Calculation carried out on Excel worksheet supplied with Mellerio device.

6.4.2   Objective methods

The primary objective method is the reflectance technique and the results presented in this section will deal predominantly with this technique. The results presented are taken from result screens produced by the software (as in figure 6.10) but for the purpose of space only the extracted macular images, and subsequent difference image, will be presented here, and not a screenshot of the software.

Reflection results : difference image

Figure 6.18 displays a series of extracted macular images and their corresponding difference images for a number of subjects. The procedure to obtain these images are as described in previous sections (passing the acquired images, with user defined macular region, to the subvi described in figure 6.7, and produce the difference image by applying equation 6.2). The extracted images and calculated difference image are saved automatically, as described in chapter 5.

All the images are native 12-bit tiff images (calculations to produce difference image are carried out on the native 12-bit green and blue images). In order to display the images outside the Labview program, the bit depth is decreased to 8-bit in all three images, and converted to .png[17]. This conversion has caused certain artifacts to appear in the displayed images, however, for the purpose of illustration this is unimportant, and has no effects on the numerical calculation.

All results display some form of difference between the blue and green image (essentially a representation of the macular pigment), however for certain subjects, the software seems to have over-estimated the extent of pigment distribution (namely subject 8, subject 9 and subject 11). This over estimation of the pigment could be due to heterogeneous illumination in the images, and failure of the software to account for this. Improvement of the image quality, by increasing the blue wavelength and inclusion of red probing light (see final chapter), may improve this situation[18].

In contrast to over estimation of the pigment, subject 3 appears to display an underestimation of the pigment distribution. This was the oldest subject in the study and as expected the quality of the blue image was quite low, and as such may have affected the overall estimation of the pigment distribution. The subject displayed a larger pigment distribution in their subjective measurements and this should be repeatable in the reflectance measurements. Further investigation of the algorithm to produce the difference image, and amendments to the hardware may reveal a solution to the problem of producing adequate images for a larger cross section of subjects[19].

Some difference images also demonstrate a slight ring like property, namely subject 1, subject 2, subject 5, subject 7 and subject 10. Interestedly these subjects also produced

---

[17]Exported from Abode Illustrator.

[18]Subject 3, 8 and 11 are older subjects and as such influence of lens on blue image may be playing a greater role.

[19]See chapter 7.
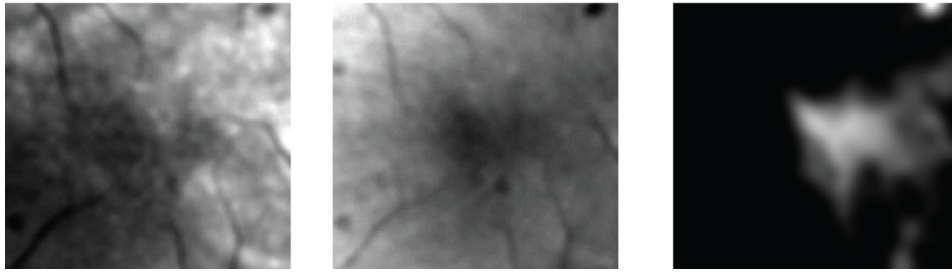
Figure 6.16: Macular images and their difference image for subject 12. Subject has very little retinal pigmentation and found subjective method difficult to complete and as such only reflectance measurements included in this thesis.

ring like properties in their subjective measurements. However, it should be noted that this may be a result of the colour depth conversion and further investigation is required to confirm any correlation. Subject 8 also produced ring like structure to the pigment in their subjective measurements but no evidence exists in their objective difference image.

Subject 12 also displays some interesting properties. This subject has not been included in the overall results, figure 6.15 and figure 6.20, but is mentioned here for the sake of completeness. Figure 6.17 displays the full retinal image of subject 12, from which the macular images and subsequent difference image are displayed in figure 6.16. The subject is young (25 yrs), thus the good quality blue image (figure 6.17(b)), however, has very little macular pigment (very little darkening in the macular region of the blue image.). This lack of pigment is also evident from the subjects subjective readings, where the subject demonstrated great difficulty in acquiring consistency in their measurements, and thus reaching a confident final result. Consequently, the subject's subjective reading has not be included in this thesis, however, it may highlight certain conditions in which a subject may be more suited to one technique over another.
Investigation of the green image (figure 6.17(a)) reveals very little overall retinal pigmentation, as it seems that the green light is in fact reflecting from the choroid, deep in the retina. This is evident from the out of focus larger blood vessels slightly noticeable in the image. The software has still produced a difference image for the subject, which does not display the usual properties of pigment distribution. These unusual cases must also be further investigated to establish the accuracy of the system.

Reflection results : analysis of difference image

Analysis of the difference images was carried out using the system software. Figure 6.19 displays the result screen for a single subject (subject 7 in figure 6.18, brown line in figure 6.14). This screen displays the distribution of the pigment as well as the peak density as calculated by the software. Due to constraints of space this screen will not be presented for all subjects, but the relative information from this screen will be extracted and presented as the final result.

For the majority of subjects the pigment estimation using the reflection technique is ap-
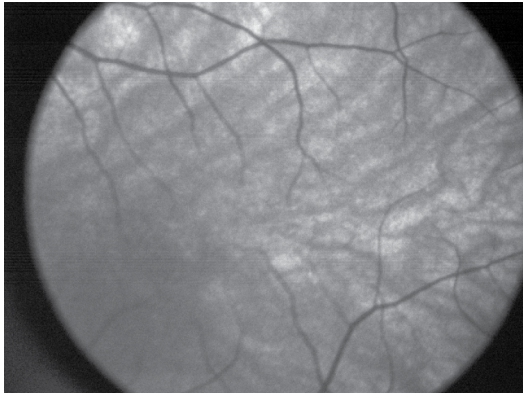
(a) Green Image indicating high reflection from the choroid
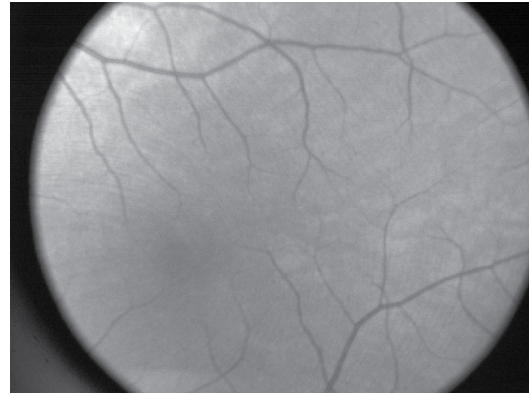
(b) Blue Image displaying lower retinal penetration and little presence of the macular pigment.

Figure 6.17: Full retinal image of subject 12, displaying low general retinal pigmentation and highlighting potential difficulties in measuring MPOD for special cases.

proximately a factor of 2 lower, than those determined by the same device using the subjective method (see figure 6.20). It is still unknown whether this difference is due to the double pass nature of the reflectance technique, or due to a lack of compete knowledge of the influence of the lens on scattering the illumination light, and on the exact reflectance location of the two illumination wavelengths. This disparity between the pigment result, using reflectance and flicker techniques, is consistent with Delori's observation in [9], however further work is required to determine the exact root of this discrepancy.

The MP peak density is underestimated for those subjects displaying ring like properties to their pigment distribution. This is due to the nature of the program in calculating the peak density. The software automatically extracts the central 1° and performs analysis on this area. For the case of subjects with ring like properties this central area is lower than an area at greater eccentricity. Examination of the distribution profile, presented in the final screen for each subject, will give a more complete representation for the pigment. Amendment to the software is recommended to account for this oversight in estimating the peak density for a subject, whose peak density is not located within the central portion of the pigment distribution.

Subject 1

Subject 2

Subject 3

4°

Subject 4
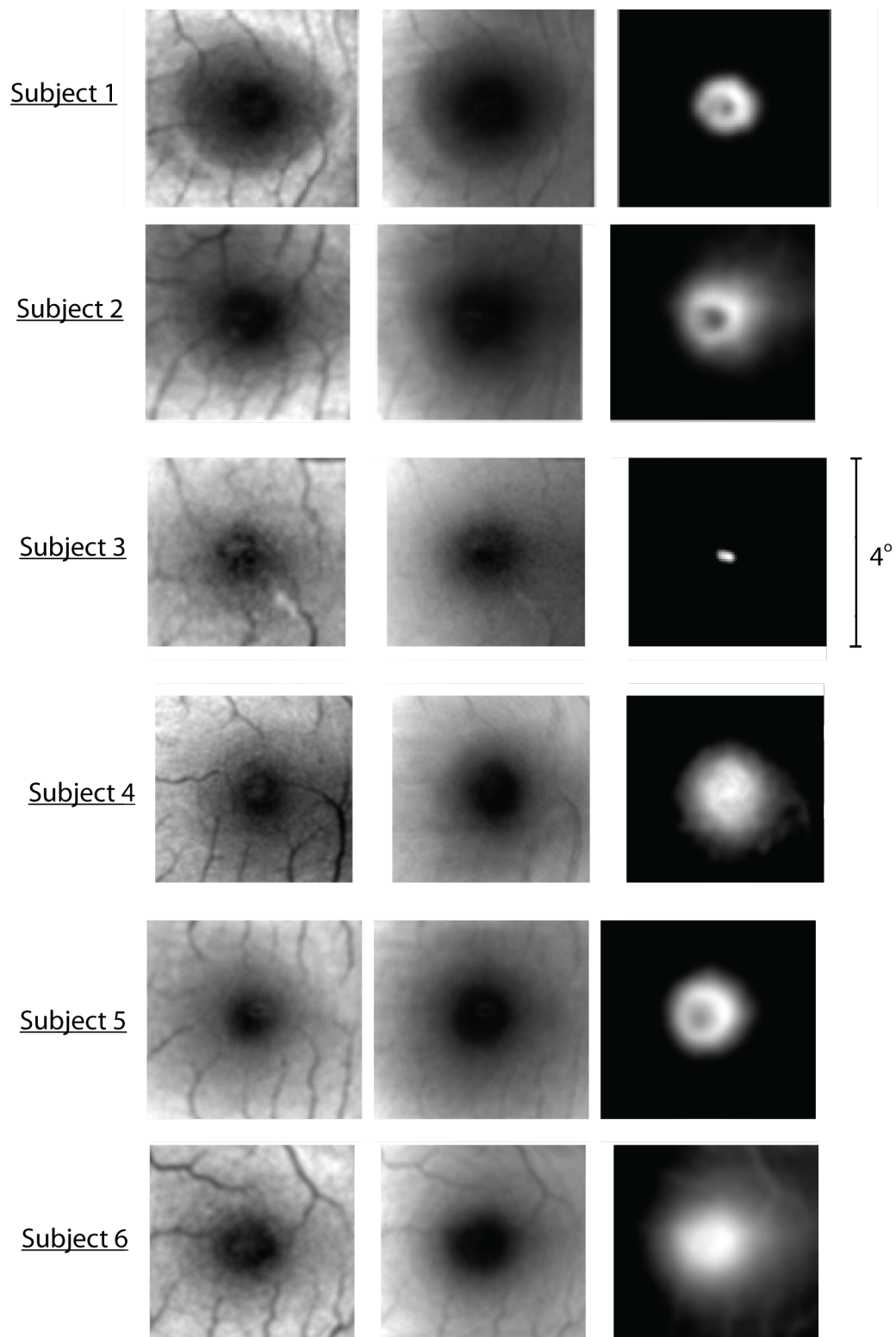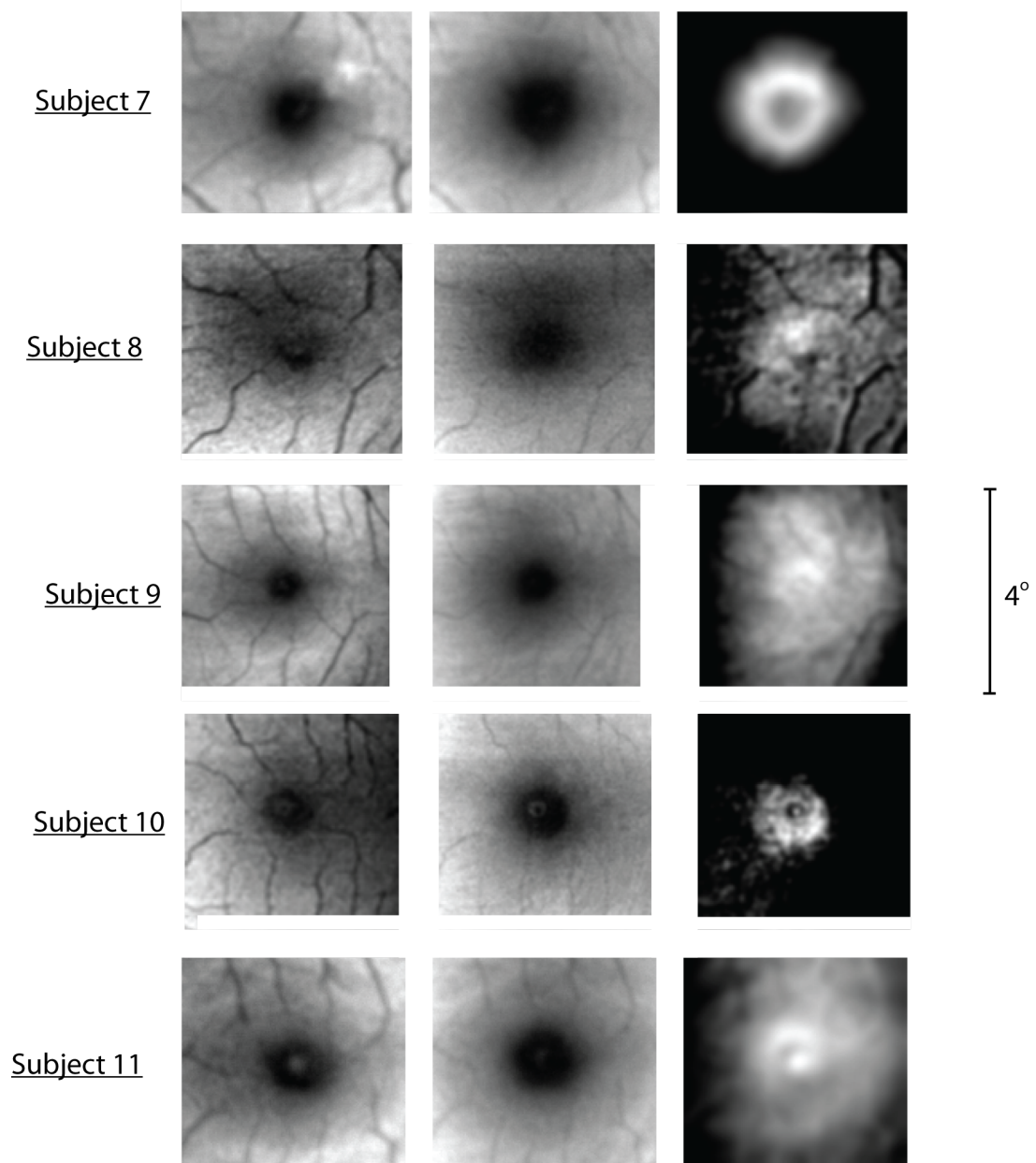
Subject 5

Subject 6

Figure 6.18: Macular images and their difference image. The order is green, blue and difference image from left to right. Certain subjects display anomalies in their difference image and requires more investigation into software. Each image represents approximately 4° on the retina.
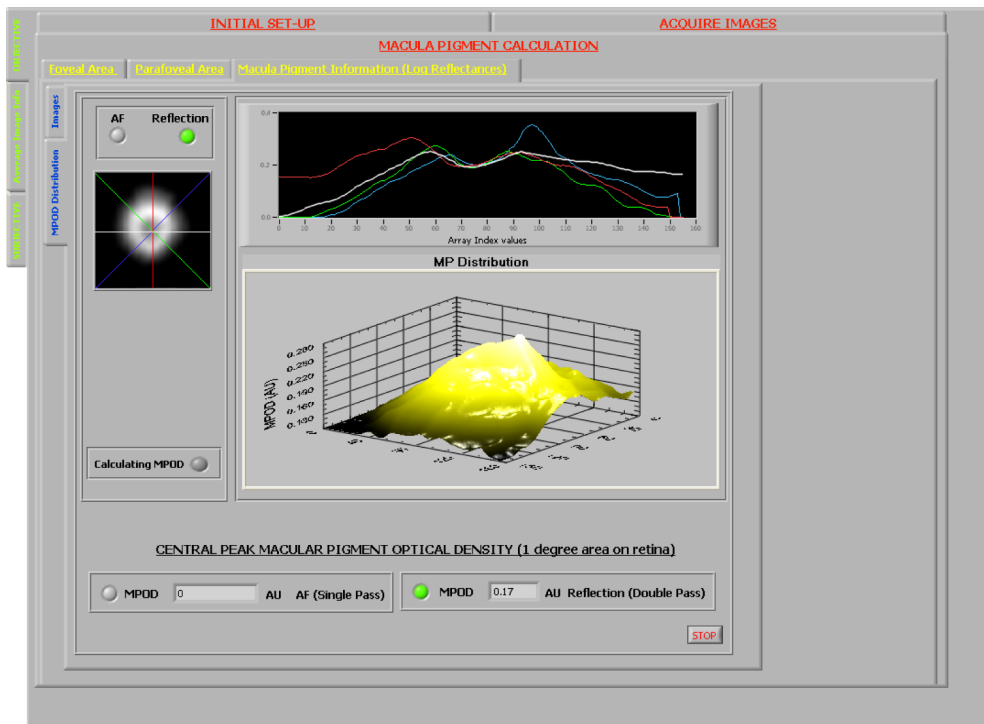
Figure 6.19: The final result screen for reflectance technique. This displays the result for subject 7.

Comparison with established technique and inter-device correspondence

The results compared in this section are the MPOD measured using the flicker technique, as implemented by the Mellerio device (blue bar) and the device described in this thesis (red bar), and the results for the MPOD as measured by the reflectance technique (yellow bar). The results for each technique were exported to an external program to produce the graph displayed in figure 6.20.

As in figure 6.14, the subjective results presented for the new device is the central foveal readings, therefore for subjects with ring like properties to their pigment distribution, the central foveal area will be lower than more eccentric locations. For example subject 7 has central reading of 0.268 AU and a reading of 0.441 AU at 3° as measured subjectively. The result quoted is 0.268 AU where a truer representation may be closer to 0.441 AU. For the same subject the reflectance results can be seen in figure 6.19. The peak density (value over 1°) is 0.17 AU, but the maximum value reached is located at approximately 3° and is approximately 0.3 AU. The value quoted for the Mellerio device is the averaged pigment value over 1° and as such does not measure any peaking outside this area, and as such underestimates the real pigment value across the retina.

The error represented in the figure is calculated in the same manner as outlined earlier referring to figure 6.15.
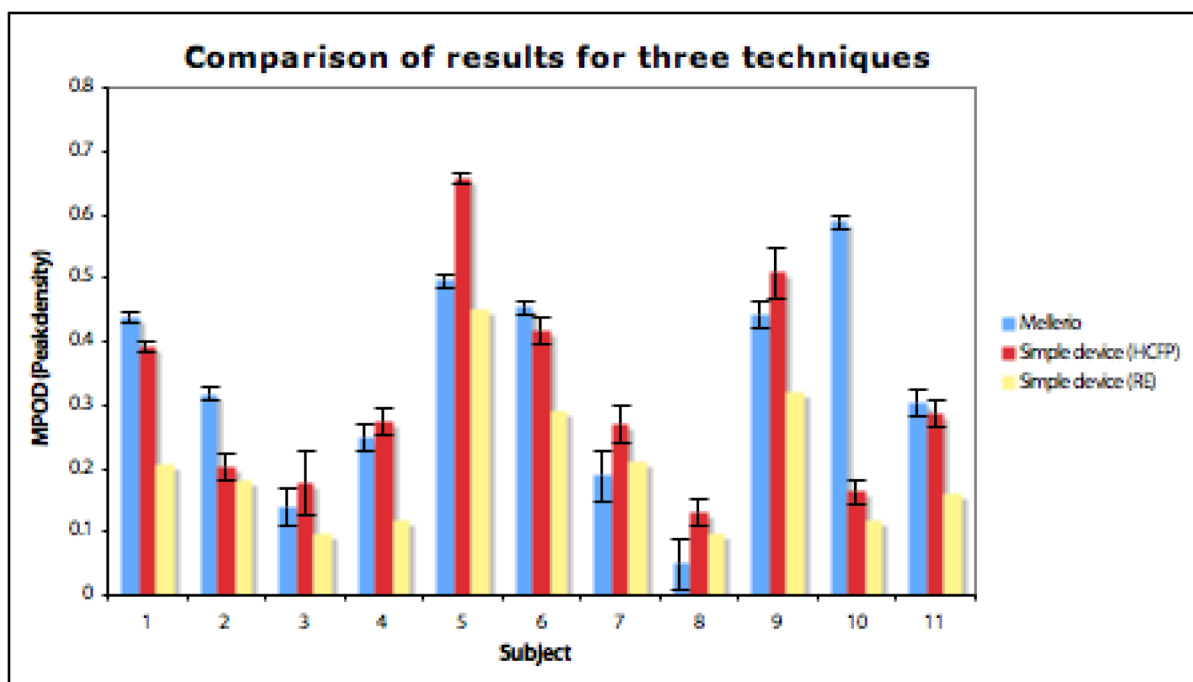
Figure 6.20: Comparison of 3 techniques. Two subjective techniques utilising different instruments and one objective reflectance technique.

Auto-fluorescence

The technique of auto-fluorescence has not been included in this thesis. This is due to the difficulty in acquiring fluorescence images of adequate quality to carry out the necessary analysis. A number of factors may play a role in acquiring sufficient quality images. The majority of the subjects used to test the system are relatively young (only 3 subjects over 30 and 1 subject over 50) and therefore would have very little accumulation of lipofuscin. In addition the optical design of the imaging arm was biased towards the green, blue region of the spectrum and so imaging in the red may not produce the same quality. Further investigation of the quality and characteristics of the red filter is required and if necessary a new filter must be purchased to ensure maximum image quality. The sensitivity of the CCD chip is not biased towards the red part of the spectrum and this may also be a factor in the difficulty in acquiring red images. The initial intensities of the blue and green illumination light must also be examined. A full analysis of the safety levels within the eye must be carried out, and greater illuminating intensities can be examined. A full investigation of the spectral content of the fluorescence images using a quality spectrometer is required.

Chapter 7

Conclusion

The objective of this project was to interpret the presence of the macular pigment on the human retina, culminating in the design and construction of a simple, easy to use device, to measure accurately and consistently the optical density of this pigment *in vivo*. The ultimate goal is to confront the problems experienced with previous devices and techniques [72]. The device presented in this thesis, utilises a novel approach of combining the three most popular techniques[1] for measuring the macular pigment optical density (MPOD) *in vivo* in one dedicated instrument, managed via a Labview interface which offers an easy to use intuitive user-interface. The strategy of utilising an independent control system, specifically the 8051 μ-controller governed by the Labview interface, ensures a robust and thorough procedure for the management of all aspects of the system. The versatile nature of the design preserves the feature of adaptability, essential for the uncomplicated addition of any further elements, or the upgrading of existing elements, within the system.

The paramount expression of a desirable clinical instrument is one that can generate commercial interest, and consequently demonstrate success, and potentially become a leading device, in its specific area of activity. The evolution of this system to achieve commercial status requires refinement of various elements and features of the system. A complete investigation of the macular pigment and this new device, requires that these possible amendments be discussed. The potential improvements of the current system will be presented, and the policy influencing these developments will be outlined, in the following sections. These suggested enhancements will be divided into software changes and hardware changes.

7.1 Software considerations

Software considerations refer to suggested developments that can be made to the software in terms of improving the ease of use of the system, via the strategy of increasing the automation of the examination procedure. Software amendments refer both to the control and to the interface software, and to the refinement of the interaction between the two platforms. This can improve the speed of subject examination, and importantly may improve the accuracy and consistency of results.

---

[1]See chapter 3

7.1.1 Accurate alignment of images

The primary purpose of acquiring several blue images and green images[2] is to calculate the average image for both colours, and subsequently obtain a less noisy final representative image for the two colours. On examination of the image sequence, certain movement of the eye can be distinguished between each acquired image. Figure 7.1 illustrates a sequence of reflectance images, numbered in order of their acquisition. The exposure for each image is 100ms with readout period of approximately 10ms between images. The sequence was obtained with the use of a head rest, and without the use of a fixation target. The border colour of each image indicates the image colour. The average image for each colour sequence is also displayed. The displacement of the retinal image between each of the successive acquired images can be seen, and consequently the smearing of the average image is quite clear. Certain precautions can be implemented to reduce the amount of eye movement, such as placing of a fixation target within the system, larger binning, faster camera exposure etc, however, the movement is subject dependent and cannot be completely avoided.
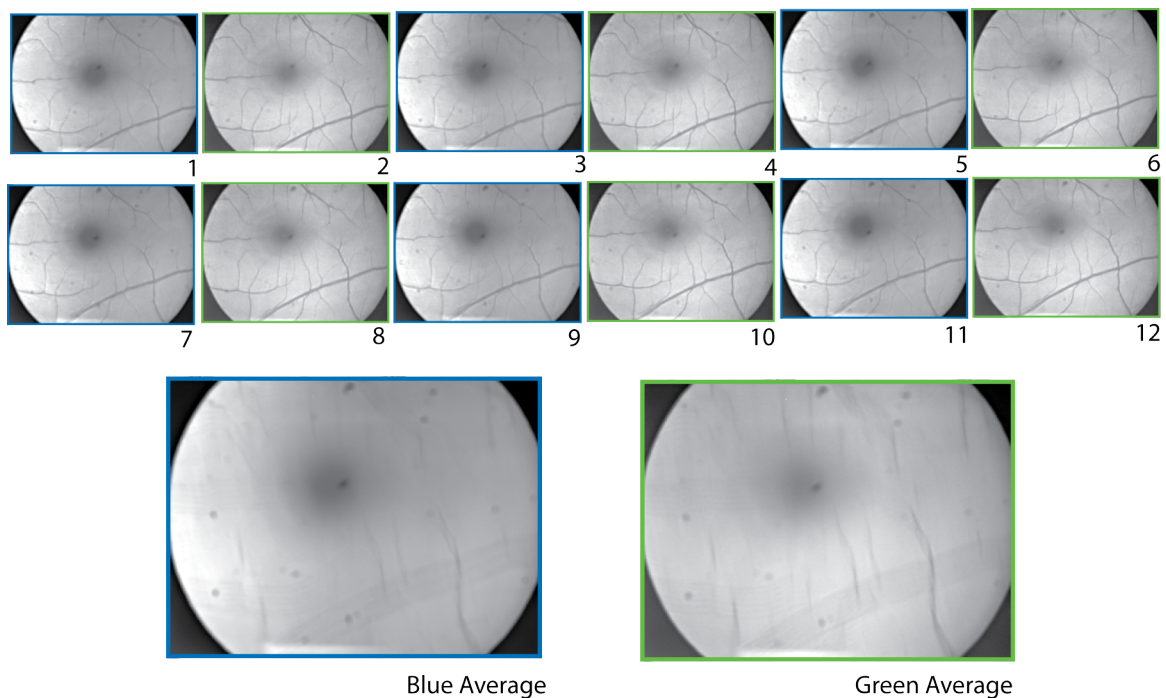
Figure 7.1: Illustration of the problem of averaging misaligned images. The sequence of the acquired images can be seen above and the retinal movement is quite noticeable. Due to this unavoidable movement of the eye the details in the final averaged image appears smeared.

The current strategy employed in calculating the average is a simple addition of each corresponding pixel in the image sequence (6 acquired images of the same colour), and dividing the final result by the number of images added. This method does reduce the presence of any random noise which appears in each individual image from appearing

---

[2]Only applicable to objective techniques; reflection (RE) and auto-fluorescence (AF)

in the final average image. However, the problem with the method is that it does not consider any inter image displacement within the sequence, and as such the corresponding pixels within the sequence may not represent the same point on the retina. This leads to smearing of the image detail in the final average image, and can lead to inaccuracies in the calculation of the pigment peak density and pigment distribution.

The images displayed in figure 7.1 are that for a subject who had relatively good fixation, however the smearing of the detail is still quite discernible. The ideal solution to this problem of smearing is to automatically align the images in software before calculating the average, so that each corresponding pixel in the image sequence, represent the same point on the retina. The images can be aligned using common features in each of the images. For this area of the retina the arcade vessels would be ideal candidates as they are relatively large, easily recognisable and present in all the images. This strategy can be implemented in software by initially having a reference image, i.e. the first image in each colour sequence, and by use of a cross correlation routine (written in Labview), align each successive image to this original reference image. Once the images are properly aligned, the average can then be calculated, and a less noisy, less smeared final average image can be produced.

This method of aligning the images can also be used to align the chosen blue and green image. The software currently allows the user to define the macular area on the blue image, and automatically extracts the same area on the green image. This assumes a certain symmetry between the two images, however this is not always the case and as a result a different area of the retina is extracted on the green image compared to that of the blue. So for a complete solution not only should the images of the same colour be aligned, but also that of the two chosen images to ensure the same area of the retina is eventually extracted.

Algorithm for pigment extraction

Chapter 6 presented the results for a range of subjects and highlighted certain conditions where further investigation into the performance of the extraction algorithm is required. There were certain subjects, whose pigment distribution was misrepresented. This was due to either low quality retinal images, or some inherent unavoidable characteristic of their retina. A more robust evaluation is required, and intensive testing is necessary to obtain a satisfactory and trust worthy algorithm to produce accurate and consistent results for the MPOD.

Further investigation in the optical density of the lens may also be of benefit to the system. This will require certain amendments to the control software and to the analysis software. Further algorithms to extract the lens information must be tested, again with the objective of measuring the MPOD accurately and consistently.

Ergonometric amendments

Ergonometric amendments refer to changes, that does not effect the actual macular pigment result, but may enhance the experience of the user, and add to the ease of use of the

system. These include various changes to the front panel, to aid in the navigation and use of the program. Such changes include the addition of help files, and more prompting from the program, to aid the user. Redesign of the front panel requires user feedback, and as such requires a greater number of users to run the program and provide feedback on their experience. The addition of a more complete result page, including images, and MPOD results in one complete document would be an attractive feature and an improvement on the current system. For large scale studies, and investigation of repeat examinations a dynamic database would be a very desirable feature. This database can be stored remotely and accessed via the interface, and automatically updated on each examination. Trials with various different users would be recommended and their feedback would influence the desired amendments.

7.2 Hardware considerations

The hardware considerations refer to the refinement of the hardware utilised in the project, with the objective of producing a more robust, easy to use, more consistent system capable of more rapid and more accurate examination of the macular pigment optical density (MPOD). The changes outlined in the following sections include amendments to the optical setup, the 8051 μ-controller and the electrical driver.

7.2.1 Adjustable retinal plane

The number of relevant retinal planes in the system depends on the examination technique employed. The objective techniques utilise the entire system (imaging arm and illumination arm) and as such there are 4 conjugate retinal planes, while the subjective technique is just concerned with the illumination arm, consequently there are 2 associated retinal planes[3]. The primary factor influencing the position of the retinal planes within the system is the optical position of the retina itself, which is dictated by the subjects refractive power (whether subject is myopic, hyper-myopic)[4] and if the subject has undergone dilation[5]. These factors will alter the position of the relevant retinal focus points within the system.

For the objective techniques the subject's pupil is dilated, not only does this enlarge the pupil but the subjects accommodative power is frozen[5]. The retinal plane in the illumintion pass contains the fixation target and must be adjusted until focussed on the subject's retina. Similarly within the imaging pass the position of the imaging camera must be adjusted until the subject's retina is sharply focussed. The current system depends on the subject feedback for the correct position for the illumination retinal plane, and on the examiner's discretion for the retinal image on the camera. Both these planes are adjusted manually. An alternative method would be to automate this procedure with addition of a motorised stage which can be controlled from the 8051 and Labview. Sharpness algorithms may be implemented to find automatically the sharpest image of

---

[3]Including the retina, see figure 4.2

[4]System is designed to examine subjects without any corrective spectacles.

[5]Using Tropicamide; note that the freezing of accommodation does not last as long as pupil dilation.

the retina, or the current method may be improved upon by controlling the camera focus remotely from the labview interface.

For the subjective technique, no dilation is required, nor is the imaging pass utilised. The retinal plane in the illumination contains the various masks for the subjective technique and must be focused on the retina. However, due to the dilation of the pupil for the objective techniques, the position of this plane in the illumination pass will differ for the objective techniques and the subjective technique. There will be also inter subject variability, due to differing refractive errors between subjects eyes[6], in the position of this retinal plane. As suggested for the objective techniques, an automated method for the refocussing of this plane would add to ease of use of the system and may aid in rapid examination of subjects.

7.2.2 Design of the adjustment terminal for LEDs

The adjustment terminal refers to the unit that the subject alters to change the LED intensities in the subjective method for the measurement of the macular pigment optical density (heterochromatic flicker photometry). The design of this piece of hardware is vital, to aid the subject in reaching accurately and consistently the minimum flicker point[7].

The current system uses either the computer mouse, or arrow keys on a keyboard for the altering the LED intensities. These devices have the advantage of not having any defined start/end points and therefore can avoid the problem of subject learning (outlined in previous chapters). However these components are the same keyboard and mouse that the examiner uses to navigate through the program and conduct the examination. An independent dedicated device should be designed and constructed for this method. The design of the component must consider the large cross section of people that may potentially use the system and as such the component must be easy to use and comfortable for a large cross section of subjects displaying varying levels of dexterity. The ideal candidate for the component would be some dedicated wireless device that can communicate with Labview, and thus adjust LED levels via the 8051, that does not require great dexterity to use.

Various unrelated devices exist for people with limited manual dexterity (adapted mouse, customised joysticks, touch screen devices etc) and any design of this component may benefit from further investigation into these devices.

Fixation strategy for subjective method

The primary problem with the subjective technique is the requirement of the measurement of the parafoveal regions of the retina, which depend on the subject to fixate centrally, and adjust the flickering in their peripheral vision. The various regions of the retina are examined using a number of different masks, which are imaged on the retina (see figure 6.12).

---

[6]Non-emmetropes are examined without corrective spectacles (due to problems regarding reflections. Contact lenses can be used).

[7]See chapter 3 for full explanation of the procedure.

Figure 7.2: Example of the proposed redesign of the illumination targets for the subjective techniques. The simple addition of a filtered hole highlighting the desired point of fixation.

Since there is no clearly defined point for the subject to fixate on this may lead to inaccuracies as the subjects gaze may drift during examination. The obvious solution is to create some point of interest on where the subject is instructed to fixate. An important consideration of the design of this point is that it does not interfere with the spectral properties of the macular pigment or with the flickering LEDs, and that it is small enough not to interfere with the mask dimensions. The obvious choice must be an illuminated point in the red part of the spectrum. This can be achieved by introducing a red laser into the system, essentially highlighting the point of fixation. This may require a redesign of the optical setup in order to produce a adequate sized spot on the mask. Therefore a more attractive method would be to drill a small hole (approximately 0.25mm) in the masks and place a red filter over this hole. The flickering LEDs can be essentially used as the illumintion source, and the filter ensures that the macular pigment will have no effect on this point.

Unfortunately this will not produce a perfect illumination point, due to differences in the red spectral content between the two LEDs, and also the construction of these targets will also require precise engineering. However this will still offer the subject a target to remain fixated on.

Electronic design

The design of the electronics is established and proven to work. However a more detailed examination of the interpretation of the 8051 output signal by the electronic driver, and subsequent reaction of the LEDs may benefit from a more detailed analysis. This essentially means that the output square wave from the 8051 μ-controller should be reproduced as closely as possible by the output of the electronic driver. Perfect duplication of the signal is not possible due to the physical delays with the transistor, and reaction of the LEDs but a more accurate representation may be possible. This can be achieved by examining any potential stray capacitances and isolating the driver in its own insulted compartment. The construction and subsequent upgrading of the system to a dedicated IC[8] board may also improve the performance of the system.

---

[8] Integrated circuit.

8051 μ-controller upgrade

The upgrading of the μ-controller is essential in moving the system forward. The current system utilises[9] certain methods to run the chip at desired speeds, however a faster chip would be a more desirable permanent solution. A faster chip will result in a greater temporal resolution for the system, while retaining the possibility of pulse width modulation. The system will also have a greater number of distinct LED intensities and may reduce the need of the potentiometer within the driver setup. Currently the chip has two on board timers and these need to be shared among three time dependent resources (baud rate, green and blue PWM). Upgrade of the 8051 chip, with extra on-board timers will be of further benefit to the system and would greatly simplify the code required and allow more features for the device itself.

Another addition to the system which would aid in ease of use and speed of examination would be a strategy to automatically read the resistance across the potentiometer. This could be possible with a analogue to digital converter, which would read the resistance value and pass this to Labview. The software can then interpret this value and return accurately and dynamically the value of the LED intensity at the cornea.

Investigation of shifting blue LED to longer wavelength

The success of the system in accurately calculating the macular pigment optical density (MPOD) objectively, is ultimately limited by the quality of retinal image acquired.
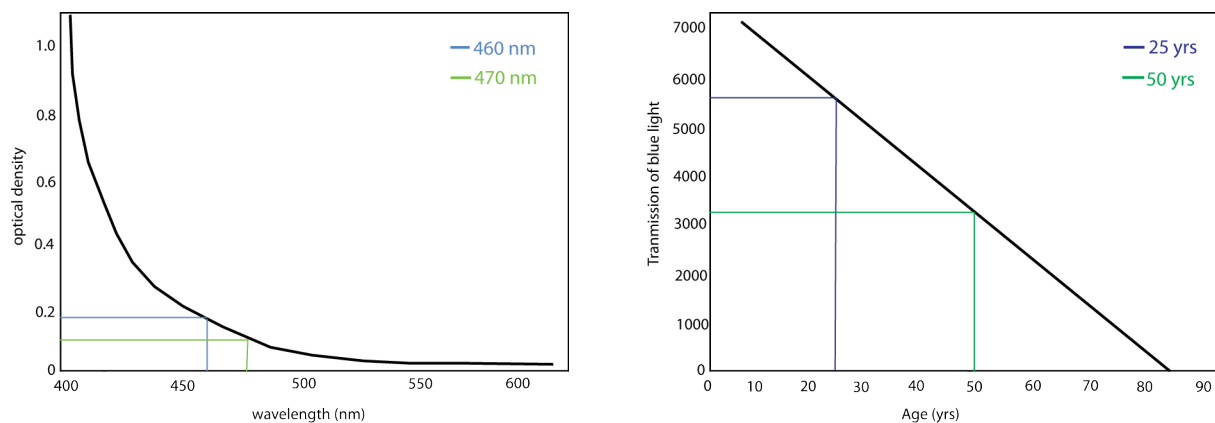
(a) The absorption spectrum of a typical healthy lens. The graph has being adapted from [73]

(b) Influence of age on lens transmision for blue light (400nm to 500nm). The graph is a simplified version of data presented in [74]

Figure 7.3: Illustration of effect of lens on blue image and influence of age on transmission of blue light by the lens.

Reflectance images are simply acquired by illuminating the retina and detecting the reflected light. Illumination of the retina is achieved by sending light though the pupil, the cornea and lens. For the reflectance measurements the light will traverse through these

---

[9]See chapter 5 for full explanation of the limitations of the chip.

components twice, and as such the influence of these components on the illuminating and subsequent reflected light must be at a minimum. Figure 7.3(a) displays the absorption spectrum of the lens, which by far has the greatest influence[10] on light entering and exiting the eye. The lens has an optical density of approximately 0.2 at 455nm the wavelength used in this system. The decrease in optical density by shifting to a longer wavelength is also illustrated in figure 7.3(a)[11]. An approximate shift of 10nm results in almost halving the optical density of the lens, and potentially an improvement in the retinal image quality.

(a) Older subject blue image

(b) Older subject green image

(c) Younger subject blue image

(d) Younger subject green image
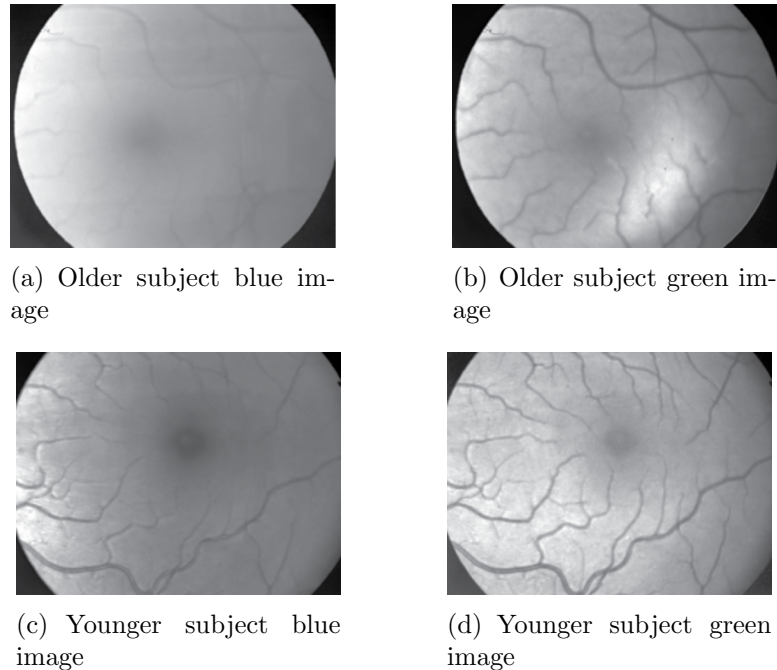
Figure 7.4: Illustration of effect of lens on blue image, and influence of age on imaging quality. The older subject is subject 3 and the younger subject is subject 10 from chapter 6. The two sets of images are of equal binning (2X2) and exposure (100ms)

The influence of the lens also increases with age and as such the quality of the blue image is decreased to a more detrimental extend. Figure 7.3(b) displays the influence of age on transmission of blue light by the lens. It is evident from the graph that the transmission almost halves when the age is doubled. It can be inferred that by decreasing the optical density of the lens, by increasing the wavelength, that the aging effect of the lens may also be reduced.

Figure 7.4 displays the results from an older subject (55 yrs) and also that of a typical younger subject (25 yrs). For both subjects, the decline in quality of the blue image is very noticeable when compared to the equivalent green image. However the decline in quality between the blue image for the young eye and for the older eye is very apparent.

---

[10]Regarding scattering and absorption and not optical power.

[11]Transmission of blue light is calculated from the integration of the transmission spectra of the anterior segment of the human eye from 400nm to 500nm. Refer to [74] for a more complete explanation.

There may be alignment issues etc., but the greatest influence on the image quality is the aged lens inducing more scatter and absorbing to a greater extend. There is even a discernible reduction in quality between the green images, but not to the same extend as the blue images.

The possibility of increasing the quality of the blue images, for a large cross section of subjects, should be investigated. Illumination of a slightly smaller field[12] may also reduce the influence of the lens and again is another factor to be considered. However, the shifting of the blue LED may also effect the fluorescence of lipofuscin. This should also be investigated.

Measurement of the crystalline lens optical density

A full appreciation of the influence that the crystalline lens may be exerting on the illuminating, and subsequent reflected light, could be of great benefit in the final calculation of the macular pigment optical density (MPOD). Figure 7.5 displays the absorption spectrum of the macular pigment (MP), oxygenated hemoglobin (HbO_2) and the crystalline lens. The figure also includes the new proposed blue illuminating wavelength (470 nm, see previous section), the green illuminating wavelength (530nm) and introduces a new red probing light (650nm).
The absorption of HbO_2 is similar at the blue and green wavelength[13], while the influence of the MP is only an issue in the macular region of the retina. The additional red probing wavelength displays zero influence by the MP, HbO_2 or the lens, therefore a baseline measurement, common to all subjects, can be obtained using this wavelength. This extra source may be introduced into the system by inclusion of a further dichroic, to reflect the red and transmit the green and blue. Additional investigation should be carried out into spectral bandwidth of all sources (and correct using extinction coefficients where necessary) and also examination of variations in retinal reflectors [76].

Analysis of the reflectance of the three wavelengths, from the peripheral area of the retina[14], can be used to estimate the optical density of the crystalline lens. If successful a far greater section of subjects may be accessible for MPOD readings, namely older subjects and cataract sufferers.

7.3   Future Experiments

Future experiments are planned investigations that will demonstrate the systems potential, and highlight further issues that need to be confronted. These experiments do not include the testing of the suggested amendments highlighted in the previous sections.

---

[12]illuminate 10° as opposed to 15°, and image 7° as opposed to 10°.

[13]Discrepancies can be corrected by inclusion of extinction coefficients.

[14]7°, devoid of MP and mayor blood vessels.
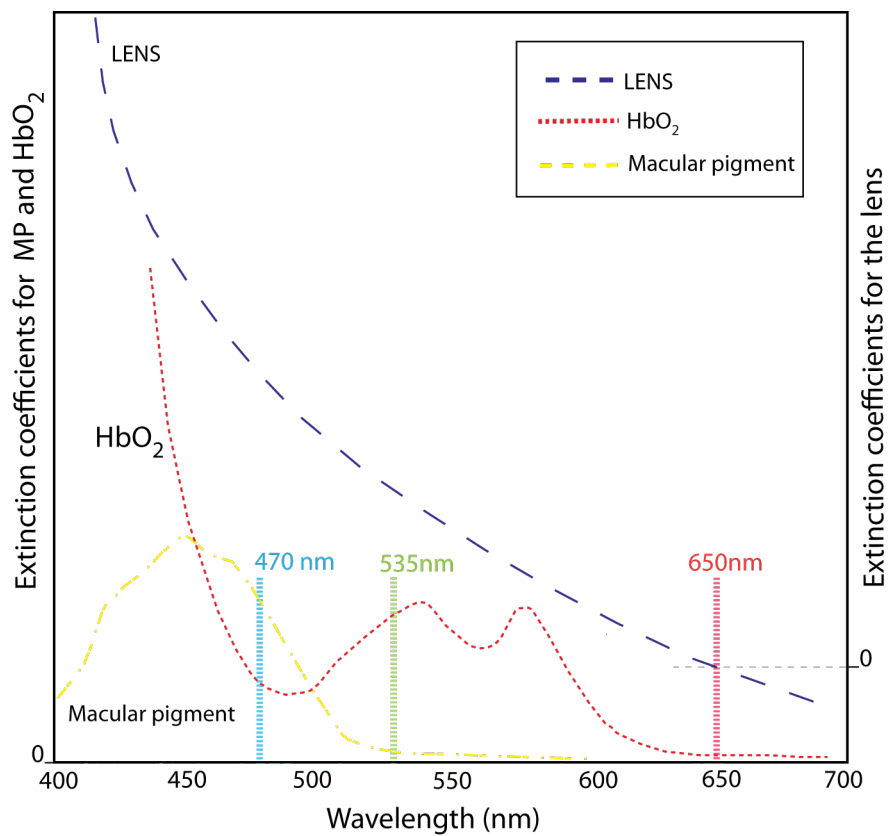
Figure 7.5: Extinction spectra of the macular pigment, oxygenated hemoglobin (HbO$_2$) and the crystalline lens. Included is the proposed wavelengths to extract information for the optical density of the lens. Extinction spectra adapted and simplified from [75]

7.3.1 Investigation of CFF

The success of the subjective method in measuring the macular pigment optical density (MPOD) is the ability of the user to accurately adjust the levels of the LEDs in order to account solely for the influence of the macular pigment.
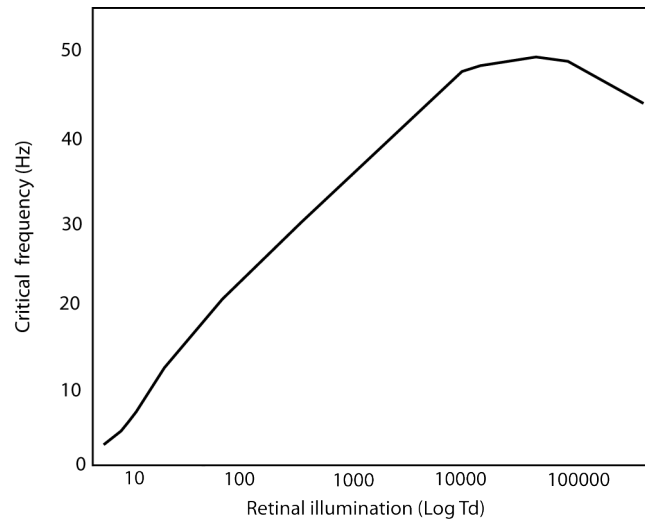
Figure 7.6: CFF at the fovea over a range of illuminations. Adapted and simplified from [77]

The CFF of the photoreceptors has being mentioned in previous sections but what is required is a full analysis and investigation of the process for both colours, at differing areas of the retina, and for differing luminance values. Figure 7.6 illustrates the influence of light intensity on the CFF value. This characteristic curve can be reproduced using this system, and investigation of altering the frequency of flash with alternating intensity values should be investigated. For example it could be possible to measure the subjects CFF at maximum level (labview overflow of 50) and their CFF at minimum level (Labview overflow of 1), and assuming the Ferry-Porter Law[15] holds for the range of intensity values, then the frequency can be automatically and dynamically adjusted.

The Broca-Sulzer effect could also be investigated. This effect is where flickering stimuli appear to be brighter than they actually are. This usually occurs for high frequency flicker (>50Hz) and must be considered for any flickering that may be used in this range. In addition, any wavelength dependent variability must also be investigated.

7.3.2 Validation of the device

Validation of the device can be achieved by reproducing spectral absorption curves for each of the techniques used to measure the MPOD. These curves should match the extinction spectra of macular pigment as measured *ex vivo*, and displayed in full in figure 7.7.

---

[15]CFF is proportional to the logarithm of the luminance of flickering stimulus (L) i.e. CFF = a logL + b; represented by the linear portion of graph in figure 7.6
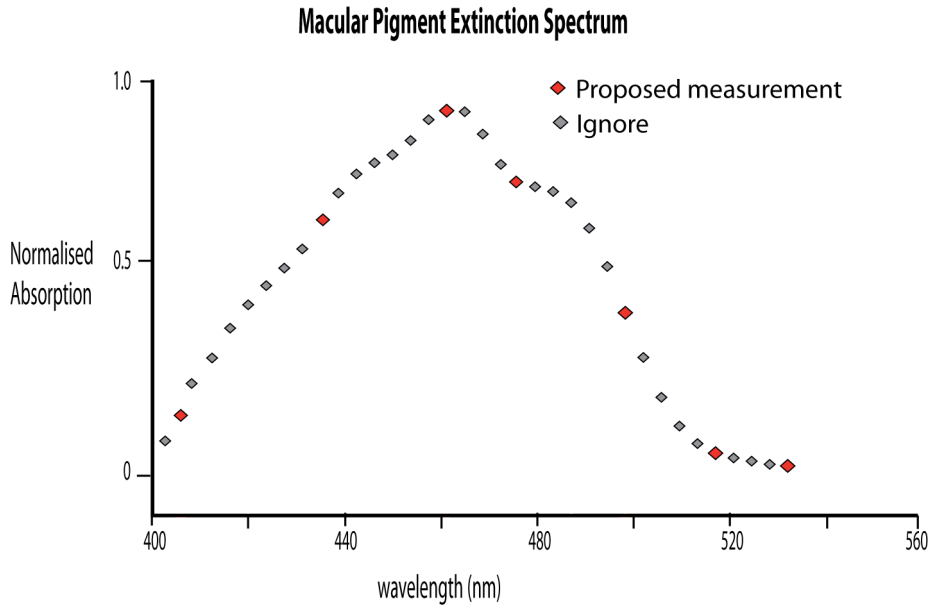
Figure 7.7: Extinction spectrum of the MP as measured by Brown (taken from data in [9])

Due to the design of the device the full spectral analysis would not be easily performance[16]. The method proposed would be to use the LEDs currently in the system in combination with carefully select filters, to achieve the spectral band required. Figure 7.7 displays proposed spectral locations (in red) to measure the macular pigment density, which correspond to recognised features on the ex vivo measurement. The success of this method depends on the performance of the filters used, and their ability to narrow the spectral spread and match the peak wavelength of the LEDs to the desired wavelength. A reproduction of the absorption spectrum of the macular pigment would validate the device an confirm the successful measurement of the macular pigment optical density.

---

[16]Without having to replace current LEDs

Appendix A

Carotenoid content of common fruit and vegetables

Table A.1: Dietary sources of carotenoids (mol%)

	Xanthophylls			Carotenes			
	L and Z	L	Z	Cryptoxanthin	Lycopene	α-carotene	β-carotene
Egg Yolk	89	54	35	4	0	0	0
Maize (Corn)	86	60	25	5	0	0	0
Kiwi	54	54	0	0	0	0	8
Zucchini squash	52	47	5	24	0	0	5
Pumpkin	49	0	0	0	0	0	21
Spinach	47	47	0	19	4	0	16
Orange pepper	45	8	37	22	0	8	21
Yellow squash	44	44	0	0	0	28	9
Cucumber	42	38	4	38	0	0	4
Pea	41	41	0	21	0	0	5
Green pepper	39	36	3	20	0	0	12
Red Grape	37	33	4	29	0	1	6
Butternut squash	37	37	0	34	0	5	0
Orange Juice	35	15	20	25	0	3	8
Honeydew	35	17	18	0	0	0	48
Celery (stalks, Leaves)	34	32	2	40	1	13	0
Green grapes	31	25	7	52	0	0	7
Brussels sprouts	29	27	2	39	0	0	11
Spring onions	29	27	3	35	4	0	0
Green beans	25	22	3	42	0	1	5
Orange	22	7	15	12	11	8	11
Broccoli	22	22	0	49	0	0	27
Apple (red delicious)	20	19	1	23	13	5	17
Mango	18	2	16	4	6	0	20
Green lettuce	15	15	0	26	0	16	0
Tomato juice	13	11	2	2	57	12	16
Peach	13	5	8	8	0	10	50
Yellow pepper	12	12	0	1	0	1	0
Nectarine	11	6	6	23	0	0	48
Red pepper	7	7	0	2	8	24	3
Tomato (fruit)	6	6	0	0	82	0	12
Carrots	2	2	0	0	0	43	55
Cantaloupe	1	1	0	0	3	0	87
Dried apricots	1	1	0	9	0	0	87
Green kidney beans	0	0	0	28	0	0	0

Appendix B

Labview

B.1   List of global variables and their function

B.2 List of custom written VIs and their function

Global variable	Function
AIM-FILTER-position	Holds AIM position for filter wheel
Average_BLUE_Array	Hold average blue image values
Average_BLUE_Array	Hold average blue image values
Average_BLUE_Filtered	Hold average filtered blue image values
Average_GREEN_Array	Hold average green image values
Average_GREEN_Filtered	Hold average filtered green image values
blue1	Hold value of blue image 1
blue2	Hold value of blue image 2
blue3	Hold value of blue image 3
blue4	Hold value of blue image 4
blue5	Hold value of blue image 5
blue6	Hold value of blue image 6
Blue Average Region 1	Hold average value of region 1 of average blue
Blue Average Region 2	Hold average value of region 2 of average blue
Blue Average Region 3	Hold average value of region 3 of average blue
Blue Average Region 4	Hold average value of region 4 of average blue
BLUE LEVEL 1 (1deg)	Hold value of blue led for $1°$ area (pass1)
BLUE LEVEL 1 (3deg)	Hold value of blue led for $3°$ area (pass1)
BLUE LEVEL 2 (1deg)	Hold value of blue led for $1°$ area (pass2)
BLUE LEVEL 2 (3deg)	Hold value of blue led for $3°$ area (pass2)
BLUE LEVEL 3 (1deg)	Hold value of blue led for $1°$ area (pass3)
BLUE LEVEL 3 (3deg)	Hold value of blue led for $3°$ area (pass3)
BLUE LEVEL 4 (1deg)	Hold value of blue led for $1°$ area (pass4)
BLUE LEVEL 4 (3deg)	Hold value of blue led for $3°$ area (pass4)
BLUE LEVEL 5 (1deg)	Hold value of blue led for $1°$ area (pass5)
BLUE LEVEL 5 (3deg)	Hold value of blue led for $3°$ area (pass5)
Blue Ohm	Hold value of potentiometer value limiting blue LED
BLUE_ID	Hold current condition of blue led (objective techniques)
BLUE_Level_HCFP	Hold blue level (subjective technique)
Blue_LEVEL_inside_(HCFP)	Hold value blue for auto change of blue level
Blue_MAC	Hold values of blue macular region (2d array)
Blue_MAC	Hold values of filtered blue macular region (2d array)
BlueLEDvalue	Hold value of blue LED value
Blue-level-Pass1	Hold value of blue level pass 1 (Subjective)
Blue-level-Pass1-Para	Hold value of blue level pass 1 parafoveal region(Subjective)
Blue-level-pass2	Hold value of blue level pass 2 (Subjective)
Blue-level-Pass2-Para	Hold value of blue level pass 2 parafoveal region(Subjective)

Global variable	Function
Blue-level-pass3	Hold value of blue level pass 3
Blue-level-Pass3-Para	Hold value of blue level pass 3 parafoveal region
Blue-level-pass4	Hold value of blue level pass 4
Blue-level-Pass4-Para	Hold value of blue level pass 4 parafoveal region
Blue-level-pass5	Hold value of blue level pass 5
Blue-level-Pass5-Para	Hold value of blue level pass 5 parafoveal region
BlueRegion1	Hold values of region 1 of average blue (2D)
BlueRegion2	Hold values of region 2 of average blue (2D)
BlueRegion3	Hold values of region 3 of average blue (2D)
BlueRegion4	Hold values of region 4 of average blue (2D)
BOTH-SINGLE RAND HCFP	Flag to randomise single or both LEDs
CAM BIT DEPTH	Hold value of image bit depth (12 bit default)
Cam ON-OFF	Flag operation of camera (0 Off, 1 On)
Corneal Power BLUE	Hold value of blue LED power
Corneal Power Green	Hold value of green LED power
Current Filter	Hold value of current filter position
exposgobal	Hold value of exposure (Objective)
exposure1(if bigger than 254)	Hold exposure 1 of split exposure
exposure2 (if bigger than 254)	Hold exposure 2 of split exposure
EXPOSURE (HCFP)	Hold value of exposure (Subjective)
Exposure-Reset_Reflect	Reset exposure values when switching to techniques
filepath	Hold filepath for saving images and subject information
Flickerfreq	Hold value for the flicker frequency (Subjective method)
Flickerfreq1	Split value of flicker value if greater than 254
Flickerfreq2	Split value of flicker value if greater than 254
GLOBAL_Average-BLUE-1-deg HCFP	Average blue value for $1°$ (Subjective)
GLOBAL_Average-BLUE-2-deg HCFP	Average blue value for $2°$ (Subjective)
GLOBAL_Average-BLUE-3-deg HCFP	Average blue value for $3°$ (Subjective)
GLOBAL_Average-BLUE-PARAFOVEAL HCFP	Average blue value for parafoveal (Subjective)
Global_BAUD-RATE	Hold value of baud rate
Global-Average-BLUE-FOVEAL HCFP	Average blue value for $1°$ (Subjective)
GlobalRectangle	Hold value of extraction rectangle

Global variable	Function
green1	Hold values for green 1 image (2D)
green2	Hold values for green 1 image (2D)
green3	Hold values for green 1 image (2D)
green4	Hold values for green 1 image (2D)
green5	Hold values for green 1 image (2D)
green6	Hold values for green 1 image (2D)
Green Average Region1	Hold value of region 1 of average green
Green Average Region2	Hold value of region 2 of average green
Green Average Region3	Hold value of region 3 of average green
Green Average Region4	Hold value of region 4 of average green
Green inside (REFLECT)	Hold value of green level (For auto adjust of LED value)
Green LED (REFLECT)	Hold value of green LED level
GREEN LEVEL 1 (1deg)	Hold value of green LED for 1° (Pass 1)
GREEN LEVEL 1 (3deg)	Hold value of green LED for 3° (Pass 1)
GREEN LEVEL 2 (1deg)	Hold value of green LED for 1° (Pass 2)
GREEN LEVEL 2 (3deg)	Hold value of green LED for 3° (Pass 2)
GREEN LEVEL 3 (1deg)	Hold value of green LED for 1° (Pass 3)
GREEN LEVEL 3 (3deg)	Hold value of green LED for 3° (Pass 3)
GREEN LEVEL 4 (1deg)	Hold value of green LED for 1° (Pass 4)
GREEN LEVEL 4 (3deg)	Hold value of green LED for 3° (Pass 4)
GREEN LEVEL 5 (1deg)	Hold value of green LED for 1° (Pass 5)
GREEN LEVEL 5 (3deg)	Hold value of green LED for 3° (Pass 5)
Green_LED_Level_HCFP	Hold value of green LED level (Subjective)
Green_MAC	Hold value of green macular region (2D)
Green_MAC_Filtered	Hold value of filtered green macular region (2D)
Green_Ohm	Hold value of potentiometer value limiting green LED
greenLEDvalue	Hold value of green LED
Green-level-Pass1	Green Led intensity (Pass 1 of subjective technique)
Green-level-Pass1-Para	Green Led intensity parafoveal (Pass 1 of subjective technique)
Green-level-Pass2	Green Led intensity (Pass 2 of subjective technique)
Green-level-Pass2	Green Led intensity parafoveal (Pass 2 of subjective technique)
Green-level-Pass3	Green Led intensity (Pass 3 of subjective technique)
Green-level-Pass3-Para	Green Led intensity parafoveal (Pass 3 of subjective technique)
Green-level-Pass4	Green Led intensity (Pass 4 of subjective technique)
Green-level-Pass4-Para	Green Led intensity parafoveal (Pass 4 of subjective technique)
Green-level-Pass5	Green Led intensity (Pass 5 of subjective technique)
Green-level-Pass5-Para	Green Led intensity parafoveal (Pass 5 of subjective technique)

Global variable	Function
GreenREGION1	Hold value of green region 1 (2D)
GreenREGION2	Hold value of green region 2 (2D)
GreenREGION3	Hold value of green region 3 (2D)
GreenREGION4	Hold value of green region 4 (2D)
HCFP foveal choice	Hold value of desired area of retina (Subjective)
HCFP-Exposure_FLAG	Flag request to change exposure value (Subjective)
imageDEGREES	Hold value of image size in visual angle
imageinMM	Hold value of image size in mm
imageloadstatus	Indicates request for loading new image
IMAGENAME	Hold image name (Subject name)
Increment value (HCFP)	Hold value of LED adjustment step (Subjective)
Initial_Blue-HCFP-YOKED	Hold value of original blue value
IR_ID	Hold condition of LEDs i.e. Normal or all off
kmp_correction_AF	Hold extinction coefficient for AF technique
kmp_correction_Reflectance	Hold extinction coefficient for RE technique
Limit_LED-Bright_HCFP-Y-N	Flag request to limit LED intensity in randomise process
LOG(FOV)-LOG(PARA)_HCFP	Hold value of LOG(FOV)-LOG(PARA)
LOG-FOV-HCFP-1	Hold value of LOG(FOV) pass 1 (Subjective)
LOG-FOV-HCFP-2	Hold value of LOG(FOV) pass 2 (Subjective)
LOG-FOV-HCFP-3	Hold value of LOG(FOV) pass 3 (Subjective)
LOG-FOV-HCFP-4	Hold value of LOG(FOV) pass 4 (Subjective)
LOG-FOV-HCFP-5	Hold value of LOG(FOV) pass 5 (Subjective)
LOG-FOV-HCFP-AVERAGE	Hold average value of LOG(FOV)
LogMacRatio	Hold value of log difference for macular region
LOG-PARA-HCFP-1	Hold value of parafoveal region pass 1 (Subjective)
LOG-PARA-HCFP-2	Hold value of parafoveal region pass 2 (Subjective)
LOG-PARA-HCFP-3	Hold value of parafoveal region pass 3 (Subjective)
LOG-PARA-HCFP-4	Hold value of parafoveal region pass 4 (Subjective)
LOG-PARA-HCFP-5	Hold value of parafoveal region pass 5 (Subjective)
LOG-PARA-HCFP-AVERAGE	Hold average value of parafovel region (Subjective)
macdifferenceImage	Hold log difference image for macular region (2D)
Mouse Keyboard control	Flag request for mouse or keyboard control
MPOD Distribution	Hold values for pigment distribution (2D) (Objective)
MPOD Distribution (HCFP)	Hold values for pigment distribution (2D) (Subjective)
outputarrayMACcentral	Value for central $1°$ of macular region (2D)
overflow-Value	Hold overflow value for exposure value greater than 254
Pix number extracted region1 (GLOBAL)	Pixel count for region 1
Pix number extracted region2 (GLOBAL)	Pixel count for region 2
Pix number extracted region3 (GLOBAL)	Pixel count for region 3
Pix number extracted region4 (GLOBAL)	Pixel count for region 4

Global variable	Function
Plus-Minus-HCFP-YOKED	Flag whether to increase or decrease LED value (Yoked method)
Raw_view_ID	Flag request to view live RAW image
Reflect-OR-AF	Flag choice of RE or AF method
Rf-RpDISPLAY	Array containing displayed Log diff image data
RpB	Hold average value of parafoveal blue image
RpG	Hold average value of parafoveal green image
Upper_Limit_HCFP	Hold value of upper limit for restricted randomise value
weighted_MPOD	Hold value for calculated weighted pigment
Write_GREEN-HCFP-sep	Flags request to write new green LED intensity
XRES	Hold value of x resolution of image
YOKED-NORMAL-HCFP	Flag LED adjustment mode (Subjective)
YRES	Hold value of y resolution of image

B.3   Labview Code

Custom written VI name	Function
1-deg_avrg_BLUE-HCFP	Calculates average value 1° for subjective measurements
2D_to_1D_array	Convert 2D array to 1D array
3-deg_avrg_BLUE-HCFP	Calculates average value 3° for subjective measurements
8051_write-indicate	Lights indicator on front panel when writing to 8051
acquiredimageinfo	Save parameters associated with selected image in external file
AF_OR_REFLECT	Tracks choice of objective measurement
auto-filter-change-HCFP	Automatically change filer position to subjective position
auto-filter-change-REAF	Automatically change filer position to objective position
Average_2D-array_return array size	Return size of average image
avrg6images	Calculate the average from 6 acquired images
BLUE_ON	Control switching of blue LED
Calc_Histo_Average_Blue	Produce histogram of blue average
Calc_Histo_Average_Green	Produce histogram of green average
CalC_region_averages_Histogram	Produce histogram of regions
calc_Trig_val_FILTER	Calculate trigger value to send to filter wheel for desired mask
CAMsettings	Set up the camera for the desired user settings
CAM-SETUP	Set up the camera for objective methods
CCDsat	Calculate if CCD chip becomes saturated (pix value >4095 (12 bit))
CFF-control	Control the flicker frequency for CFF measurement
comm_filter_8051	Communicate with 8051 for filter wheel control
control_show_img_regions	display the selected image regions
convert-ledleveltopower	Convert Led level to power at the cornea
DIMLEDS	Dim the LEDs (Implement PWM)
display12images	Display the 12 acquired images
DisplayBlueReg1	Display blue region 1
DisplayBlueReg2	Display blue region 2
DisplayBlueReg3	Display blue region 3
DisplayBlueReg4	Display blue region 4
displayCorrectedImage	Display noise corrected image
displayfront-live	Display live view of retina on front panel
DisplayGreenRegion1	Display green region 1
DisplayGreenRegion2	Display green region 2
DisplayGreenRegion3	Display green region 3
DisplayGreenRegion4	Display green region 4
displayLOGDIFFregions	Display the log difference for the image regions
displayMACDIFF	Display the log difference for the image macular region
distancecalc	Calibrate pixel number to distance across retina
distancedisplay	Display calibrated image distances
EXP1andEXP2_greater8bit	Calculate EXP1 and EXP2 for loop values greater than 254

Exposure correct overflow value	Calculate correction in exposure due to XTAL speed
exposuresetup	Set up exposure of camera for free run and triggered mode
Ext-LED-control	Control operation of LEDs in system
Extract1deg	Extract 1° from image
Extract4deg	Extract 4° from image
Extract_Parafoveal_Regions	Extract pavafoveal regions from selected images
Filter postion calc RE AF	Calculate filter position for objective techniques
filtertrig	Trigger the filter wheel
flicker_control	Control of LED adjustment method (yoked or normal)
flicker_freq_Control	Control of flickering frequency
FullDiffAnalysis	Display analysis of difference image
grabimage	Sends command to trigger camera and grab 12 images
Green-adjust_HCFP	Writes new green LED level to 8051 for subjective method
HCFP_CHOOSE_FOVEAL	Choose retina area (Subjective)
HCFP_display_results	Display results for subjective method
HCFP_FLASH	Initiate dual flashing of LEDs (Subjective)
HCFP-average_BLUE_FOVEAL	Calculate average blue for foveal region (Subjective)
HCFP-average_BLUE_PARAFOVEAL	Calculate average blue for parafoveal region (Subjective)
histo-avrg-calc-1deg_area	Produce histogram of 1° area of average image
histo-avrg-calc-4deg_area	Produce histogram of 4° area of average image
imagechoice	Overwrite average image with selected images
imageselectl_BLUE	Choose blue image
imageselect_GREEN	Select acquired green image to overwrite average green
IMGS-to-Global_Arrays	Saveimages as global array
infosave	Save information associated with acquired image
ircontrol	Switching LEDs all off
Keypress_translate-(HCFP)	Translate keypress to adjustment values
Keypress_Exposure_HCFP	Translate keypress to adjustment values for flicker frequency
Keypress_HCFP	Translate keypress to adjustment values for LED intensities
kmp_correction	Apply extinction coefficients to values
LED-adjust-mode	Determines desired mode of led adjustment (normal, yoked)
LED-POWER-CALC	Displays LED power, depending on off resistance and Labview
lineanalavrg	Produces line analysis of average images (4 lines)
LogBminusLogG	Calculates log difference between each pixel for green and blue
Logdiffanalysis	Produces analysis of difference image
LogpL1L2	Calculates log difference of parafoveal regions
LOOP_EXP_OF	Calculates overflow value for exposure values greater than 254
manselectmac	Displays blue image and request manual selection of macular area
MOD6	Calculate modular 6 value for correct filter position
MPOD	Main program to control MPOD calculation

MPODcalc	Calculate MPOD (objective methods)
MPOD_HCFP	Calculate MPOD (Subjective method)
overlaylinesonimage	Display image with lines overlaid to demonstrate line analysis
overlayMACregions	Display line overlay on selected macular regions
overlaytarget	Overlay target reticule on live view image
parabluedisplay	Display parafoveal regions of blue image
paraGREENdisplay	Display parafoveal regions of green image
pararegions	Extract parafoveal regions from selected images
Power Calculation (BLUE)	Calculate power of blue LED
Power Calculation (GREEN)	Calculate power of green LED
random_LED_value	Randomise the LED values (Subjective method)
randomise1or2LEDs	Determines to randomise single or both LEDs (User input)
Reset_FILTER	Reset filter to default position 1 (on program exit)
Reset_HCFP	Resets all parameters for subjective measurements
Reset_Reflect	Resets all parameters for objective measurements
Reset-LEDS	Resets LED values
Resize_image_to_picture	Resizes image to on screen display
resizearvgs	Resizes average images to on screen display
Retinal Location1_filter	Return filter wheel to position 1
save_light_levels_HCFP	Save the light levels in external file (Subjective method)
savearg	Save selected average images in external file (convert to 8bit jpeg)
SaveChosenImage	Save selected images in external file
saveimgs	Save the acquired images in an external file
SaveMacRegions	Save the macular regions in an external file
SaveMacRegions_Corrected	Save noise corrected macular regions in external file
Show-BlueandGreenREGs-1-4	Display regions of selected images (Auto resized)
split- 8 bit number	Split exposure value for number greater than 254 (Objective)
split- 8 bit number (FLICKER)	Split exposure value for number greater than 254 (Subjective)
Start POS filter	Move filter wheel to position 1
STOP	Exit program
view_RAW_image	Display live retinal image in its native resolution
Write_BLUE-HCFP	Write desired blue LED level to 8051 (Subjective)
Write_GREEN-HCFP	Write desired green LED level to 8051 (Subjective)
Write-Flicker_greater bit	Write split 8 bit number to 8051

Table B.1: List of Labview VIs used in the Labview program and their function

Appendix C

8051 μ-controller

C.1   Variables and their function.

Variable name	Address in memory (Hex)	Function
RI	$98	Receive interrupt flag
TI	$99	Transmit interrupt flag
CFFSTATE	$83	Indicates state of CFF
FLICKSTATE	$84	Indicates state of flicker
BLUESTATE	$85	Indicates state of blue LED
IRSTATE	$86	Indicates state of LEDs (All off)
LEDCHOICE	$87	Indicates active LED
IRSTATE	$86	Indicates state of LEDs (All off)
CAM	$A0	Output of CAM pulse
FILTER	$A1	Output of Filter pulse
BLUE	$A5	Control of Blue LED pulse
GREEN	$A7	Control of Green LED pulse
CHOICE	$D5	Indicates state of PWM modification
FLASHTRIG	$08	Controls triggering of flash
FLICKorFLASH	$09	Differentiates between flicking and flashing
CFF_FLAG	$0A	Initiate CFF measurements
GREENOFF	$0B	Indicates request for green LED off
GREENFULL	$0C	Indicates request for green LED full
BLUEFULL	$0D	Indicates request for green LED full
GREENLEVEL	$07	Hold level for green LED intensity
overflow	$10	Indicate loop for larger exposure values (greater than 254)
C6	$16	Flash count for obtaining 12 images
copyR1L	$17	Copy of original flash count value. Used to reload C6 at later
SKIPR5	$18	Used in loop values greater than 254.
ExpFULL1	$19	Used in loop values greater than 254.
ExpFULL2	$19	Copy of ExpFULL1 to reload for next run.

Table C.1: List of variables, their function and physical address

C.2   Register File

C.3 Assembly code

Appendix D

Glossary

Table D.1: Glossary of terms used throughout the thesis

Abbreviation	Meaning
AF	Auto-fluorescence
AMD	Age related macular degeneration
Ar	Argon
BMI	Body mass index
BNC	Bayonet nut connection
CCD	Charge coupled device
CFF	Critical fusion frequency
CMOS	Complementary metal-oxide semiconductors
CNVM	Choroidal neovascular membrane
DFLT	Diode focal laser treatment
DM	Dichroic mirror
EDCC	Eye disease case-control
EXP	Exposure
F	Foveal
HCFP	Heterochromatic flicker photometry
HPLC	High performance liquid chromatography
IR	Infrared
I/O	Input/Output
L	Lutein
L	Long (refers to long wavelength sensitive cone, i.e. red)
LED	Light emitting diode
M	Medium (refers to medium wavelength sensitive cone, i.e. green)
MP	Macular pigment
MPOD	Macular pigment optical density
MP	Macular pigment
OCT	Optical coherence topography
OD	Optical density
P	Parafoveal
PC	Personal computer
PDT	Photodynamic therapy
PM	Pellicle beamsplitter
PWM	Pulse width modulation
RE	Reflection
RPE	Retinal Pigment Epithelium
ROI	Reactive oxygen intermediates

Abbreviation	Meaning
S	Short (refers to short wavelength sensitive cone, i.e. blue)
SFR	Special functions register
SLO	Scanning laser ophthalmoscope
SPDT	Single pole double throw
TASM	Turbo Assembler
TTL	Time to live
VEGF	Vascular endothelial growth factor
VI	Virtual instrument
VISA	Virtual instrument software architecture
Z	Zeaxanthin

Appendix E

Selected extracts from ethical approval application

Bibliography

[1] T. Young. The Bakerian lecture on the mechanism of the eye. *Phil. Trans.*, 91:23–88, 1801.

[2] H. Helmholtz. Translated version of handbuch der physiologischen optik. *Physiological optics, Optical Society of America*, 1:160–203, 416–443, 1924.

[3] F. Buzzi. Nuove sperienze fatte sulli occhio umano. *Opuscoli Scetti Sulle Scienze e Sulle Arti*, 5, 1782.

[4] E. Home. An account of the orifice in the retina of the human eye, discovered by professor soemmering: to which are added proofs of this appearance being extended to the eyes of other animals. *Philos Trans R Soc Lond*, 2, 1798.

[5] S. Soemmering. De foramina centrali limbo luteo cincto retinae humanae. *Comment Soc Reg Sci Goetting*, 13, 1799.

[6] J.C Maxwell. On the unequal sensibility of the foramen centrale to light of different colours. *Report of the British Association*, 1856.

[7] M. Schultze. Uber den gelben fleck der retina, seinen einflussauf normales sehen und auf farbenblindheit (on the yellow spot of the retina: it's influene on normal vision and on colour blindness. *Von Cohen & Sohn, Bonn*, pages 1–5, 1866.

[8] G. Wald. Human vision and the spectrum. *Science*, 101:653–658, 1945.

[9] F.C. Delori, D.G. Goger, B.R. Hammond, D.Max Snodderly, and S.A. Burns. Macular pigment density measured by autofluorescence spectrometry: comparison with reflectometry and heterochromatic flicker photometry. *J. Opt. Soc. Am. A*, 18(6):1212–1230, 2001.

[10] R.A Bone, J.T Landrum, L. Fernandez, and SL. Taris. Analysis of the macular pigment by HPLC : retinal distribution and age study. *Invest. Ophthalmol. Vis. Sci.*, 29:843–849, 1988.

[11] Paul L.Kaufman and Albert Alm. *Physiology of the Eye*. Mosby tenth Edition, 11830 Westline Industrial Drive, St Louis, Missouri, 1992.

[12] Y Otake, M Miyao, S Ishihara, M Kashiwamata, T Kondo, H Sakakibara, and S Yamada. An experimental study on the objective measurements of accommodative amplitude under binocular and natural viewing conditions. *J. Exp. Med*, 170:93–102, 1993.

[13] Y Imanishi, K Palczewski, SB Sires, and EJ Seibel. Methods for assessing a physiological state of a mammalian retina. *United States Patent 20050159662*, 10/926780, 2004.

[14] Alfredo Dubra Suarez, 2004. A Shearing Interferometer for the Evaluation of Human Tear Film Topography. PhD thesis, Imperial College, London.

[15] David H. Hubel. Eye, brain and vision. *Scientific American Library*, 1988.

[16] J.K Bowmaker and H.J.A Dartnall. Visual pigments of rods and cones in a human retina. *J. Physiol.*, 298:501–511, 1980.

[17] Eric R. Kandel, James H. Schwartz, and Thomas M. Jessell. *Principles of Neural Science*. McGraw-Hill Education, Fourth Edition, 2000.

[18] LJ. Rizzolo. Polarity and the development of the outer blood-retinal barrier. *Histol. Histopath*, 12:1057–67, 1997.

[19] CJ Kennedy, PE Rakoczy, and IJ Constable. Lipofuscin of the retinal pigment epithelium: a review. *Eye*, 9:763, 1995.

[20] N.M. Haralampus-Grynaviski, L.E. Lamb, C.M.R. Clancy, C. Skumatz, J.M. Burke, T. Sarna, and J.D. Simon. Spectroscopic and morphological studies of human retinal lipofuscin granules. *PNAS*, 100:3179–3184, 2003.

[21] S. Ben-Shabat, C.A. Parish, M. Hashimoto, J. Liu, K. Nakanishi, and J.R. Sparrow. Fluorescent pigments of the retinal pigment epithelium and age-related macular degeneration. *Bioorganic and Medicinal Chemistry letters*, 11:1533–1540, 2001.

[22] L. Feeney-Burns, E.S Hilderbrand, and S Eldridge. Aging human rpe: morphometric analysis of macular, equatorial, and peripheral cells . *Invest Ophthalmol Vis Sci.*, 25:195–200, 1984.

[23] R.A Bone, J.T Landrum, G.W Hime, A. Cains, and J. Zamor. Stereochemistry of the human macular carotenoids. *Invest. Ophthalmol. Vis. Sci.*, 34:2033–2040, 1993.

[24] S. Liaaen-Jensen. *Isolation, reactions. In Carotenoids.* Basel/Stuttgart:Birkhauser, 1971.

[25] O. Sommerburg, J.E Keunen, A.C Bird, and F.J Kuijk. Fruit and vegetables that are sources for lutein and zeaxanthin: the macular pigment in human eyes. *Br. J. Ophthalmol*, 82:907–910, 1998.

[26] F. Khachik, F.F de Moura, D.Y Zhao, C.P Aebischer, and P.S Bernstein. Transformations of selected carotenoids in plasma, liver, and ocular tissues of humans and in nonprimate animal models. *Invest. Ophthalmol. Vis. Sci.*, 43:3383–3392, 2002.

[27] M.R Malinow, L. Feeney-Burns, L.H Peterson, M.L Klein, and M. Neuringer. Diet related macular anomalies in monkeys. *Invest. Ophthalmol. Vis. Sci.*, 19:857–863, 1980.

[28] R.A Bone, J.T Landrum, L.H Guerra, and C.A Ruiz. Lutein and zeaxanthin dietary supplements raise macular pigment density and serum concentrations of these carotenoids in humans. *J. Nutr.*, 133:992–998, 2003.

[29] B.R Hammond jr., E.J Johnson, R.M Russel, N.I Krinsky K.J Yeum, and R.B Edwards. Dietary modification of human macular pigment density. *Invest. Ophthalmol. Vis. Sci.*, 38:1795–1801, 1997.

[30] A.Jeffery Whitehead, Julie A. Mares, and Ronald P. Danis. Macular pigment. a review of current knowledge. *Arch Ophthalmol*, 124:1038–1045, 2006.

[31] Norman I. Kinsky, John T. Landrum, and Richard A. Bone. Biologic mechanisms of the protective role of lutein and zeaxanthin in the eye. *Annu. Rev. Nutr.*, 23(2):171–201, 2003.

[32] K. Ruddock. Evidence for macula pigmentation from colour matching data. *Vision Res.*, 3:417–429, 1963.

[33] G Wyszecki and W.S Stiles. Colour science: concepts and methods, quantitive data and formulae., 1982.

[34] P.L Pease, A.J Adams, and E. Nuccio. Optical density of human macular pigment. *Vision Res*, 27:705–710, 1987.

[35] R.A Bone, J.T Landrum, and A. Cains. Optical density spectra of the macular pigment in vivo and in vitro. *Vision Res*, 32:105–110, 1992.

[36] R.A Bone. Computer enhanced resolutionas an aid to identifying the macular pigment. *Vision Res.*, 16:1191–1192, 1976.

[37] Nigel P. Davies and Antony B. Morland. Macular pigments: their characteristics and putative role. *Progress in Retinal and Eye Research*, 23:533–559, 2004.

[38] John Nolan, Orla O'Donovan, and Stephan Beatty. The role of macular pigment in the defence against AMD. *AMD*, pages 39–41, 2003.

[39] R.E Anderson, L.M Rapp, and R.D Wiegand. Lipid peroxidation and retinal degeneration. *Curr. Eye. Res.*, 3:223–227, 1984.

[40] W.T Ham Jr., J.J Ruffolo Jr, H.A Mueller, A.M Clarke, and M.E Moon. Histologic analysis of photochemical lesions produced in rhesus retina by short-wavelength light. *Invest. Ophthalmol. Vis. Sci.*, 17:1029–1035, 1978.

[41] WK Noell. Possible mechanisms of photoreceptor damage by light in mammalian eyes. *Vision Res.*, 12:1163–71, 1980.

[42] EG Faktorovich, RH Steinberg, D Yasumura, MT Matthes, and MM LaVail. Basic fibroblast growth factor and local injury protect photoreceptors from light damage in the rat. *J Neurosci.*, 9:3554–67, 1992.

[43] LN Thibos. Calculation of the influence of lateral chromatic aberration on image quality across the visual field. *J Opt Soc Am A.*, 8:1673–80, 1987.

[44] VM Reading and RA Weale RA. Macular pigment and chromatic aberration. *J Opt Soc Am A.*, 2:231–4, 1974.

[45] D. Max Snodderly, PK Brown, FC Delori, and JD Auran. The macular pigment. absorbance spectra, localization, and discrimination from other yellow pigments in primate retinas. *Invest. Ophthalmol. Vis. Sci.*, 25:660–673, 1984.

[46] W.Haidinger. Ueber das directe erkennen des polarisirten lichts und der lage der polarisationsebene. *Annalen der Physik*, 139:29–39, 1844.

[47] H. Helmholtz. *Handbuch der Physiologischen Optik. Leopold Voss, Hamburg.*, 1866.

[48] R.A. Bone and J.T. Landrum. Macular pigment in henle fiber membranes: A model for haidingers brushes. *Vision Research*, 24(2):103–108, 1982.

[49] R.A Bone and J.T Landrum. Dichroism of lutein: a possible basis for haidinger's brushes. *Appl. Opt.*, 22:775–776, 1983.

[50] A. Stanworth and E. J. Naylor. Polarized light studies of the cornea i. the isolated cornea. *Journal of Experimental Biology*, 30:160–163, 1953.

[51] B.R.Hammond jr., B.R. Wooten, and D. Max Snodderly. Individual variations in the spatial profile of human macular pigment. *J. Opt. Soc. Am. A*, 14(6):1187–1196, 1997.

[52] G. Haegerstom-Portnoy. Short-wavelength-sensitive-cone sensitivity loss with aging: a protective role for the macular pigment? *J. Opt. Soc. Am*, 5:2140–2144, 1988.

[53] I Barbazetto, A Burdan, N.M Bressler, S.B Bressler, L. Haynes, and A.D Kapetanios. Photodynamic therapy of subfoveal choroidal neovascularization with verteporfin; fluorescein angiographic guidelines for evaluation and treatment - tap and vip report. *Arch. Ophthalmol.*, 121:1253–1268, 2003.

[54] P. van Wijngaarden and SH Qureshi. Inhibitors of vascular endothelial growth factor (vegf) in the management of neovascular age-related macular degeneration: a review of current practice. *Clin Exp Optom.*, 5:427–37, 2008.

[55] Gragoudas ES, Adamis AP, Cunningham ET Jr, Feinsod M, and Guyer DR. Pegaptanib for neovascular age-related macular degeneration. *N Engl J Med.*, 351:2805–2816, 2004.

[56] Seddon JM, Ajani UA, Sperduto RD, Hiller R, Blair N, Burton TC, Farber MD, Gragoudas ES, Haller J, Miller DT, Yannuzzi LA, and Willett W. Dietary carotenoids, vitamins a, c and e and advanced age-related macular degeneration. *J. Am. Med. Assoc.*, 272:1413–1320, 1994.

[57] J.T. Landrum, R.A. Bone, and MD Kilburn. The macular pigment: A possible role in protection from age-related macular degeneration, in advances in pharmacology. *Sies H, ed., Academic Press, London*, 38:537–556, 1996.

[58] EDCC Study Group. Antioxidant status and neovascular age-related macular degeneration. Eye Disease Case-Control Study Group. *Arch Ophthalmol.*, 1:104–9, 1993.

[59] S Beatty, H Koh, M Phil, D Henson, and M Boulton. The role of oxidative stress in the pathogenesis of agerelated macular degeneration. *Surv. Ophthalmol*, 45:115–134, 2000.

[60] K. Ruddock. The effect of age upon colour vision. changes with age in light transmission of the ocular media. *Vision Res.*, 5:47–58, 1965.

[61] J.D. Moreland and J Kerr. Optimization of stimuli for tritanomaloscopy. *Mod. Probl. Ophthalmol.*, 19:162–166, 1978.

[62] J.S Werner, S.K Donnelly, and R. Kliegl. Aging and the human macular pigment density. appended with translations from the work of max schultze and ewald hering. *Vision Res.*, 27:257–268, 1987.

[63] J. Mellerio, F.J.G.M van Kuijk S.Ahmadi-Lari, D. Pauleikhoff, A.C Bird, and J. Marshall. A portable instrument for measuring macular pigment with central fixation. *Current Eye Research*, 25(1):37–47, 2002.

[64] A. Peters. Structural changes that occur during normal aging of primate cerebral hemispheres. *Neurosci. Biobeh.*, 26:733–741, 2002.

[65] BR Wooten, BR Hammond jr, RI land, and DM Snodderly. A practical method for measuring macular pigment optical density . *Invest. Ophthalmol. Vis. Sci.*, 40:2481–2489, 1999.

[66] E. Loane, J.Stack, S. Beatty, and J.M Nolan. Measurement of Macular Pigment Optical Density using two different heterochromatic flicker photometers. *Current Eye Research*, 32:555–564, 2007.

[67] W Gellermann, IV Ermakov, RW McClane, and PS Bernstein. Raman imaging of human macular pigments . *Optics Letters*, 27:833–835, 2002.

[68] W Gellermann, IV Ermakov, MR Ermakova, RW McClane, DY Zhao, and PS Bernstein. In vivo resonant raman measurement of macular carotenoid pigments in the young and aging human retina. *J. Opt. Soc. Am. A*, 19:1172–1180, 2002.

[69] L.A. Castaneda-Escobar and D.Malacara-Hernández. A new design of a fundus camera for the human eye using the hartmann test. *Proc. of SPIE*, 5622:132–133, 2004.

[70] Craig Steiner. The 8051/8052 microcontroller: Architecture, assembly language, and hardware interfacing.

[71] Tos TJM Berendschot and Dirk van Norren. Macular pigment shows ringlike structures. *Investigate Ophthalmology and Visual Science*, 47:709–714, 2006.

[72] Stephan Beatty, Frederik J. G. M van Kuijk, and Usha Chakravarthy. Macular pigment and age-related macular degeneration: Longitudinal data and better techniques of measurement are needed. *Investigate Ophthalmology and Visual Science*, 49:843–845, 2008.

[73] Tos TJM Berendschot, Peter Jaap DeLint, and Dirk van Norren. Fundus reflectance - historical and present ideas. *Progress in Retinal and Eye Research*, 22:171–200, 2003.

[74] James Dillon, Lei Zheng, John C. Merriam, and Elizabeth R. Gaillard. Transmission of light to the aging human retina:possible implications for age related macular degeneration. *Experimental Eye Research*, 79:753–759, 2004.

[75] F.C Delori and S.A Burns. Fundus reflectance and the measurement of crystalline lens density. *J. Opt. Soc. Am. A*, 13:215–226, 1996.

[76] F.C Delori and K.P Pflibsen. Spectral reflectance of the human ocular fundus. *Appl. Opt.*, 28:1061–1077, 1989.

[77] Christopher Tyler and Russell D. Hamer. Eccentricity and the ferry-porter law. *J. Opt. Soc. Am. A*, 10:2085–2087, 1993.